

REPORT DOCUMENTATION PAGE

Form Approved
OMB No. 0704-0188

Public reporting burden for this collection of information is estimated to average 1 hour per response, including the time for reviewing instructions, searching existing data sources, gathering and maintaining the data needed, and completing and reviewing the collection of information. Send comments regarding this burden estimate or any other aspect of this collection of information, including suggestions for reducing this burden, to Washington Headquarters Services, Directorate for Information Operations and Reports, 1215 Jefferson Davis Highway, Suite 1204, Arlington, VA 22202-4302, and to the Office of Management and Budget, Paperwork Reduction Project (0704-0188), Washington, DC 20503.

1. AGENCY USE ONLY (Leave blank)	2. REPORT DATE Sept. 30, 1996	3. REPORT TYPE AND DATES COVERED Technical 1/1/96 - 9/30/96
----------------------------------	----------------------------------	--

4. TITLE AND SUBTITLE Some Structural Features of a Turbulent Wing-Body Junction Vortical Flow	5. FUNDING NUMBERS N00014-94-1-0092
---	--

6. AUTHOR(S) M. Semih Olcmen and R. L. Simpson

7. PERFORMING ORGANIZATION NAME(S) AND ADDRESS(ES) Dept. of Aerospace and Ocean Engineering Virginia Polytechnic Institute and State University Blacksburg, VA 24061-0203	8. PERFORMING ORGANIZATION REPORT NUMBER VPI-AOE-238
--	---

9. SPONSORING/MONITORING AGENCY NAME(S) AND ADDRESS(ES) Office of Naval Research 800 N. Quincy St. Arlington, VA 22217	10. SPONSORING/MONITORING AGENCY REPORT NUMBER
---	--

11. SUPPLEMENTARY NOTES

19970219 026

12a. DISTRIBUTION / AVAILABILITY STATEMENT Unlimited	12b. DISTRIBUTION CODE
---	------------------------

13. ABSTRACT (Maximum 200 words) The horse-shoe vortex that forms around a wing-wall junction is experimentally investigated. Laser-Doppler velocimeter measurements of mean velocity and higher order statistics including the third order products are reported for 15 measurement stations in one plane to the side of the junction of a 3:2 elliptical nose, NACA 0020 tail wing and a wall. The approach Reynolds number of the air flow based on momentum thickness is ≈ 5940 . The outer layer vortical structure on the down-wash or wing side results in a thin boundary layer and lower turbulence intensity due to the redirected free-stream. Lateral pressure-gradients cause separation on the uplifting side of the vortex on the wall. Bimodal histograms of the w fluctuating velocity occur under the vortex core near the wall. A vortical structure with higher vorticity concentration and opposite sense to the large vortical structure is located below the large vortical structure. High normal stress values are obtained at the wing-wall junction. In this wing-wall junction region a vortical structure of the same rotation sense of the large outer layer vortex forms. Triple products describe the diffusion processes for this type of a flow. In such a flow the shear-stress angle (SSA) highly lags the flow-gradient angle (FGA) and the turbulent structure highly lags the mean flow. The turbulence diffusion is highly altered due to the presence of the large outer layer vortical structure.
--

14. SUBJECT TERMS Three-Dimensional Flow Turbulence Structure	15. NUMBER OF PAGES 104
	16. PRICE CODE

17. SECURITY CLASSIFICATION OF REPORT unclassified	18. SECURITY CLASSIFICATION OF THIS PAGE unclassified	19. SECURITY CLASSIFICATION OF ABSTRACT unclassified	20. LIMITATION OF ABSTRACT unlimited
---	--	---	---

ABSTRACT

The horse-shoe vortex that forms around a wing-wall junction is experimentally investigated. Laser-Doppler velocimeter measurements of mean velocity and higher order statistics including the third order products are reported for 15 measurement stations in one plane to the side of the junction of a 3:2 elliptical nose, NACA 0020 tail wing and a wall. The approach Reynolds number of the air flow based on momentum thickness is ≈ 5940 . The outer layer vortical structure on the down-wash or wing side results in a thin boundary layer and lower turbulence intensity due to the redirected free-stream. Lateral pressure-gradients cause separation on the uplifting side of the vortex on the wall. Bimodal histograms of the w fluctuating velocity occur under the vortex core near the wall. A vortical structure with higher vorticity concentration and opposite sense to the large vortical structure is located below the large vortical structure. High normal stress values are obtained at the wing-wall junction. In this wing-wall junction region a vortical structure of the same rotation sense of the large outer layer vortex forms. Triple products describe the diffusion processes for this type of a flow. In such a flow the shear-stress angle (SSA) highly lags the flow-gradient angle (FGA) and the turbulent structure highly lags the mean flow. The turbulence diffusion is highly altered due to the presence of the large outer layer vortical structure.

TABLE OF CONTENTS

ABSTRACT	i
Nomenclature	iii
List of Tables	v
<i>CHAPTER I - INTRODUCTION</i>	1
<i>CHAPTER II - RESULTS AND DISCUSSION</i>	3
II-1. Mean Velocities	3
II-2. Normal Stresses	4
II-2. Shear Stresses	4
<i>CHAPTER III - PROBABILITY DENSITY FUNCTIONS OF u, v, w FLUCTUATIONS AT THE STATIONS SURROUNDING THE VORTEX CORE</i>	6
III-1. $s/t = -0.247$	6
III-2. $s/t = -0.291$	6
III-3. $s/t = -0.336$	7
III-4. $s/t = -0.368$	7
<i>CHAPTER IV - TRIPLE PRODUCTS</i>	8
<i>CHAPTER V - DERIVED QUANTITIES</i>	12
V-1. Flow Angle	12
V-2. Flow Gradient Angle	12
V-3. Shear Stress Angle	12
V-4. $(\partial W / \partial y) / (t / U_{ref})$	12
V-5. TKE / U_{ref}^2	13
V-6. V_{q^2} / U_{ref}	13
V-7. $\overline{uv} / \overline{u^2}$	13
V-8. Skewness of u	13
V-9. Skewness of v	14
V-10. Skewness of w	14
V-11. Shear Stress Magnitude	14
V-12. Townsend's Structural Parameter A_1	15
V-13. $\frac{\overline{u^2} + \overline{w^2}}{v^2}$ Structural Parameter	15
V-14. Rotta's T Parameter	15

<i>CHAPTER VI - VARIATION IN FLOW PHYSICS AT SELECTED LOCATIONS</i>	16
VI-1. Separation Location	16
VI-2. Stations Surrounding the Vortex Core	17
VI-3. Near the Wing/Wall Junction	18
 <i>CHAPTER VII - CONCLUSIONS</i>	21
REFERENCES	23
 TABLES	25
 <i>APPENDIX A: Line Plots of Flow Variables Products and some Structural Parameters</i> ...	51

NOMENCLATURE

C_p	static pressure coefficient
$(\partial C_p / \partial x)_{FS}$	static pressure coefficient gradient
C_{ij}	$\frac{\partial \overline{u_i u_j}}{\partial t} + U_j \frac{\partial \overline{u_i u_j}}{\partial x_j}$, Reynolds' stress convection tensor
FA	$\arctan(W/U)$, flow angle
FGA	$\arctan(\frac{\partial W / \partial y}{\partial U / \partial y})$, flow gradient angle
p	fluctuating pressure component
P_{ijk1} production	$\overline{u_i u_j} (\overline{u_k u_m})_{,m} + \overline{u_j u_k} (\overline{u_i u_m})_{,m} + \overline{u_k u_i} (\overline{u_j u_m})_{,m}$, triple product transport tensor
P_{ijk2} production	$-(\overline{u_i u_j u_m} U_{k,m} + \overline{u_k u_i u_m} U_{j,m} + \overline{u_j u_k u_m} U_{i,m})$, triple product transport tensor
PR_{ij}	$-(\overline{u_i u_j} \frac{\partial U_j}{\partial x_i} + \overline{u_j u_i} \frac{\partial U_i}{\partial x_j})$, Reynolds' stress production tensor
PD_{ij}	$-\frac{1}{\rho} (\frac{\partial (\overline{p u_i})}{\partial x_i} + \frac{\partial (\overline{p u_j})}{\partial x_j})$, Reynolds' stress pressure diffusion tensor
Re_θ	Reynolds number based on momentum thickness
S_{ij}	rate-of-strain tensor
SSA	$\arctan(\frac{\overline{vw}}{\overline{uv}})$, shear stress angle
TD_{ij}	$-\frac{\partial (\overline{u_i u_j u_i})}{\partial x_i}$, Reynolds' stress turbulent-diffusion tensor
TKE	$(\overline{u^2} + \overline{v^2} + \overline{w^2})/2 = (\overline{u_i u_i})/2$, Turbulent kinetic energy
U_θ	velocity magnitude at the boundary layer edge
U_i	mean velocity components
$\overline{u_i u_j}$	Reynolds stress tensor. $i=1, 2, 3; j=1, 2, 3$.
$\overline{u_i u_j u_k}$	triple velocity correlation tensor
U^+	$\frac{U}{u_\tau}$, nondimensional mean velocity
u_τ	$\sqrt{\tau_w / \rho}$, skin friction velocity

VD_{ij}	$\nu \frac{\partial^2 \overline{u_i u_j}}{\partial x_l^2}$, Reynolds' stress viscous diffusion tensor
x_{TC}, y_{TC}, z_{TC}	tunnel coordinates
$y^+ = y u_\tau / \nu$	wall-law variable
β_{FS}	flow angle at the boundary layer edge
β_{WC}	wall-stress direction
δ_{ij}	Dirac delta function. $\delta_{ij} = 1$ if $i=j$, $\delta_{ij} = 0$ if $i \neq j$.
δ	boundary layer thickness
ε_{ij}	$-2\nu \frac{\partial \overline{u_i} \partial \overline{u_j}}{\partial x_l \partial x_l}$, Reynolds' stress viscous dissipation tensor
ε	$\varepsilon_{ii}/2$, dissipation of turbulent kinetic energy
θ	$\int_0^\infty (1 - \frac{U}{U_e}) \frac{U}{U_e} dy$, momentum thickness
ν	kinematic viscosity
ρ	density
σ	standard deviation
τ	$\sqrt{(-\rho \overline{uv})^2 + (-\rho \overline{vw})^2}$, shear stress magnitude in the flow
τ_w	wall shear stress
Φ_{ij}	$\frac{p}{\rho} (\frac{\partial \overline{u_i}}{\partial x_j} + \frac{\partial \overline{u_j}}{\partial x_i})$, Reynolds' stress pressure-strain tensor
Ω_{ij}	vorticity tensor
d_{ijk}	$-[\overline{u_i u_j u_k u_m} + (\overline{p/\rho}) \overline{u_j u_k} \delta_{im} + (\overline{p/\rho}) \overline{u_k u_i} \delta_{jm} + (\overline{p/\rho}) \overline{u_i u_j} \delta_{km} - \nu (\overline{u_i u_j u_k})_{,m}]_{,m}$, triple product transport diffusion tensor
ϕ_{ijk} interaction	$(\overline{p/\rho}) [(\overline{u_i u_j})_{,k} + (\overline{u_k u_i})_{,j} + (\overline{u_j u_k})_{,i}]$, triple product transport pressure tensor
ε_{ijk} dissipation tensor	$2\nu (\overline{u_k u_{i,m} u_{j,m}} + \overline{u_j u_{k,m} u_{i,m}} + \overline{u_i u_{j,m} u_{k,m}})$, triple product transport

LIST OF TABLES

Table 1. Laser-Doppler Velocimeter Locations and Flow Parameters 25

Table 2. 21:1 odds $\pm 2\sigma$ Uncertainties in Measured Quantities 26

Table 3. Some Length Scales Obtained From LDV Data in 22.4° Line Coordinates 27

CHAPTER I. INTRODUCTION

Wing-body junction flows have been the subject of many studies in the past. The flow at the nose of the wing has aperiodic (bimodal) double-peaked fluctuating velocity histograms with very large Reynolds stress values compared to the approaching boundary layer values (Devenport and Simpson, 1990a). Shinpaugh and Simpson (1995) used a scanning LDV and a pressure transducer to further investigate this velocity and the pressure field simultaneously.

Martinuzzi and Tropea (1993) studied flow around several rectangular shaped obstacles to show the flow phenomena around the obstacles in a fully developed air channel. The approach boundary layer separates due to the adverse pressure gradient in this region and rolls in towards the floor, generating backflow. The flow visualization water tunnel studies of Khan et al. (1995) and Kim (1991) also show these characteristics and describe the time development of the motion. The vortical flow is stretched around the wing and is reoriented by the wing, which results in vortical flow along the sides of the wing-body junction.

The 3-D TBL of the pressure-driven type has been the subject of many papers. Reviews of recent experimental data were done by Anderson and Eaton (1989), Flack and Johnston (1994), Schwarz and Bradshaw (1992), and Ölgmen and Simpson (1992, 1993). DNS studies of Spalart (1989) and Moin et al. (1992) also show the capability of CFD in explaining the flow physics at low Reynolds numbers. Three-dimensional boundary layer/vortex interaction, which is relevant to the work undertaken here, was studied by Eaton's group (Eaton, 1995).

In the present study the detailed mean flow, Reynolds stress and triple product characteristics of a wing/body junction flow in one plane at the side of a NACA 0020 tail; 3:2 elliptical nose wing (maximum thickness $t = 7.17$ cm) are presented. Figure 1 shows the measurement locations and the coordinate axes used in the present study. All the data, unless otherwise specified, are presented in a coordinate system where $x_{22.4}$ is perpendicular to the plane of measurements "s" is in the plane of the measurements with positive axis towards the wing and y axis is perpendicular to the wall. Table 1 gives the flow characteristics at the measurement locations.

This flow is extremely well documented and detailed references can be found in the work by Simpson (1995, 1996) and Ölgmen and Simpson (1995a, 1996e). Mc Mahon, Merati and Yoo (1987), Mc Mahon, Hubbart and Kubendran (1982), and Dickinson (1986) made measurements with a similar model at other Reynolds numbers to report the flow field around and in the wake of the wing using hot-wire probes. The work undertaken here is similar to the work of Devenport and Simpson (1992) and of Fleming et al. (1993) and of the previously mentioned researchers. Fleming et al. (1993) made measurements at several planes along the side and in the wake of the wing and described the global flow characteristics of the junction vortex in comparison to the data of McMahon (1987) and Devenport and Simpson (1990b). The work of Devenport and Simpson (1992) gives the general characteristics of the mean flow and Reynolds' stresses at five

different planes around the nose and side of the wing using LDV. They further used their data to evaluate some turbulence models. In contrast to the body of existing experimental data this flow has not yet been extensively studied computationally. Sung and Yang (1988) showed that simple algebraic eddy viscosity models did not perform well for such a flow.

The present study differs from these previous studies with more detailed and more accurate near wall information of not only of the mean flow and Reynolds stresses but also of the triple products. The approach flow conditions, static pressure distribution on the wall were previously presented (Ölçmen and Simpson, 1990, 1995a). The five-component laser-Doppler velocimeter used for the measurements and the data reduction techniques were previously discussed (Ölçmen and Simpson, 1995a, b). The effective probe volume had a diameter of 30 microns. The probe volume could traverse as close as 50 microns to the wall and the wall could be found with an uncertainty of ± 10 microns. The data acquisition and reduction are described here very briefly. The coincident three velocity components in the optical coordinate system were transformed to the tunnel coordinates. The skirts of the histograms of the velocity were interactively cleaned of the noise using a parabola fitting routine to the logarithm of the histograms. The inverse-velocity-magnitude bias-corrected histograms calculated using the cleaned data were used to extract the mean velocity and higher order terms. Table 2 gives 21:1 uncertainties calculated using two separate data sets measured at one of the measurement locations and using Chauvenet's criterion to define the uncertainty.

In the following sections selected data are presented and the differences in flow characteristics at selected locations due to different flow conditions are explained. Remaining quantities can be found in the report by Ölçmen and Simpson (1996d). That report includes the mean velocity, Reynolds' stress, all triple product contour plots, discussion of the bimodal nature of the fluctuating velocity probability density distributions and contour plots of some derived quantities such as: skewnesses for different velocity components, turbulent kinetic energy, longitudinal vorticity distribution, $\overline{uv}/\overline{u^2}$, shear stress magnitude, Townsend's structural parameter a_1 , $(\overline{u^2} + \overline{w^2})/\overline{v^2}$, and velocity magnitude. The transport equation balance for the selected locations in this flow were reported by Ölçmen and Simpson (1996a, b), and the evaluation of some of the existing pressure-strain and of the turbulent-diffusion models for the same stations of the previous work were reported by Ölçmen and Simpson (1996a,c and 1997).

CHAPTER II. RESULTS AND DISCUSSION

In this section the mean velocity at 15 locations that lie in a plane perpendicular to the wing and the wall which passes through station 5 (Ölçmen and Simpson, 1995a) are presented. The $x_{22.4}$ axis perpendicular to this plane lies at 22.4 degrees with respect to the tunnel coordinates and the centerline of the wing (Fig. 1).

II-1. MEAN VELOCITIES

The approaching 2-D turbulent boundary layer (TBL) on the wall separates from the wall along and around the symmetry line of the wing due to the adverse pressure gradients generated by the presence of the wing. The separated shear layer further rolls in towards the wall-wing junction carrying the high speed free-stream fluid and generates a high vorticity flow zone which is non-periodic in time. The vorticity within the approach 2-D TBL and the vorticity generated within the nose section of the wing are stretched around the wing-wall junction and their direction is reoriented along the wing contour. The corkscrew motion of the large rotational region shapes the structure of the entire wing-wall junction flow. The outer layer large vortical structure core is located at $\log_{10}(y/t) \approx -1.1$ and $s/t \approx -0.32$.

The high speed free-stream fluid directed towards the wall by the outer layer vortex results in high streamwise U velocity components in the zone between the vortex core and the wing and faster moving fluid as the wing is approached (Fig. 2). (The boundary layer on the wing is not studied here). The $\partial U / \partial z$ of the flow is positive which results in acceleration in the $+s$ direction.

Near the wall $\partial U / \partial y$ also increases towards the wing. In a region between the vortex core and the wing $\partial U / \partial y$ is approximately zero where a law-of-the-wall for the U component would not hold. The boundary layer on the wall becomes thinner compared to the layer thickness at Station 5, which is the station farthest away from the wing presented in this study. The free-stream fluid directed towards the wall also results in high negative V velocity components closer to the wing and away from the wall (Fig. 3). Positive V velocities are observed in the uplifting side of the vortex. The rolling motion within the measurement plane at locations closer to the wall redirects the flow away from the wing parallel to the floor.

This flow has high speed negative W velocity components faster than the outer layer positive W free stream velocity component (Fig. 4). The lateral pressure gradient $\partial C_p / \partial s$ values obtained on the wall in the plane of the measurements are tabulated in Table 1 and show adverse pressure gradients in the $-s$ direction. The high speed W velocity energizes the near wall flow, although the adverse lateral pressure gradients shape the lateral boundary layer away from the wing. The near wall low momentum fluid affected by the lateral pressure gradients separates at $s/t \approx -0.54$ as shown by the convergence of the stream lines. Near the wing and the wall

intersection, the W velocities change sign and become positive.

II-2. NORMAL STRESSES

High speed free-stream flow directed towards the wall by the large outer layer vortex also carries the low level turbulence of the free-stream flow. This results in low turbulence levels between the vortex core and the wing (Figures 5, 6 and 7). In this region the $(-\overline{uv}\frac{\partial U}{\partial y})$, the largest $\overline{u^2}$ transport equation production term is small since $\frac{\partial U}{\partial y}$ is small. The $\overline{u^2}$ maximum is at a location close to the wing and wall intersection (Fig. 5). High u fluctuations are partly due to redirection of the large instantaneous negative V velocity component to instantaneous W and instantaneous U velocity components. The v fluctuations are suppressed due to the presence of the wall and w fluctuations are suppressed due to the presence of the wing near the intersection. High $\overline{u^2}$ values are also located in the vicinity of the vortex core, between the vortex core and the wall, and near the wall below the vortex core. Below the rotational separation region $\overline{u^2}$ values are as low as at Station 5.

Maximum $\overline{v^2}$ normal stress location is right below the vortex core (Fig.6) and high $\overline{v^2}$ values are confined to a region surrounding the vortex core. The $\overline{v^2}$ near the wall is not effected by the outer layer vortex. Both at the wall-wing junction and also near the separation location $\overline{v^2}$ values are low.

The $\overline{w^2}$ normal stress maximum is at a location close to the wall below the vortex core (Fig. 7). The $\overline{w^2}$ maximum is 5/3 times larger than the $\overline{u^2}$ maximum. Large $\overline{w^2}$ values are due to non periodic meandering of the vortex core which will be discussed later in this section. Similar to the $\overline{v^2}$ normal stress the $\overline{w^2}$ normal stress is also not affected by the large scale mean flow motion at the wing/wall junction. The lowest $\overline{w^2}$ is located at Station 5. The $\overline{w^2}$ values around separation location are close to Station 5 values.

II-3. SHEAR STRESSES

The velocity correlations \overline{uv} , \overline{uw} and \overline{vw} are large negative values both when the two of the fluctuating velocities are highly correlated with opposite signs and also when seldom occurring large opposite signed fluctuating velocity couple outweigh the Reynolds' averaged mean value towards large negative numbers. Small magnitude \overline{uv} values are located at the uplifting side of mean vortical flow (Fig. 8). This region is far away from large $\overline{u^2}$ regions but closer to the maximum $\overline{v^2}$ location. At the locations where the u and v fluctuations are large either they are not of the opposite sign or they are not well correlated. At regions where \overline{uv} magnitude is small, the $\overline{u^2}$ values are as high as the maximum value at Station 5, however much smaller than the

values at the wing-wall junction and than the values below the vortex core. At the same region $\overline{v^2}$ values are twice as large of the $\overline{u^2}$. The \overline{uv} shear stress magnitude is much smaller at the locations where $\overline{u^2}$ contours show maxima. Positive \overline{uv} values are located near the wing closer to layer edge. In the downwash side of the large outer vortical flow \overline{uv} shear stress magnitudes are smaller than that of at Station 5. High speed low fluctuation free-stream fluid redirected by the vortex towards the wall in this region results in less correlated u and v fluctuating velocities. Around the separation location the \overline{uv} stress values are as low as at Station 5.

Maximum value of the \overline{uw} stress is obtained below the vortex core near the uplifting side of the vortex (Fig. 9). This location is closer to the wall than the \overline{uv} stress contours show a minimum. Another maximum occurs very close to the wing/wall intersection. Minimum values of the \overline{uw} stress are obtained in the downwash side of the outer vortical flow. These locations roughly correspond to the locations where $\overline{u^2}$ normal stress is large.

The \overline{uv} and \overline{vw} stress minimum locations are in close proximity to one another and they are located at the uplifting side of the outer layer vortical flow (Fig. 10). The \overline{vw} stress changes sign as the wall is approached and shows a local maximum near the wall and a separate local maximum closer to the wing. The \overline{vw} stress magnitude is slightly increased compared to Station 5 values.

CHAPTER III. PROBABILITY DENSITY FUNCTIONS OF u , v , w FLUCTUATIONS AT THE STATIONS SURROUNDING THE VORTEX CORE

Inverse-instantaneous-velocity-magnitude bias-corrected probability density functions (pdf) of the u , v , w fluctuating velocities are presented in Figures 11 to 14. The pdfs were calculated at stations $s/t = -0.247$, -0.291 , -0.336 , and at $s/t = -0.368$. The selected stations encompass the vortex core located at $s/t = -0.32$, $\log_{10}(y/t) \approx -1.1$. The pdfs show the probability of finding a fluctuating velocity in a certain velocity range. The mean value of a pdf is zero. The pdfs were calculated at selected stations and at all y locations and equal probability contours were generated. The probability values above 0.01 are not included in the contour plots to increase the resolution of the plots. Probability at large positive or negative fluctuating velocity ranges at fixed y location indicates that the pdfs are skewed towards positive or negative side. The most probable velocity range is the range where most of the fluctuations are clustered. The width of the pdf of a certain fluctuating velocity at a fixed y location is an indicator of the magnitude of the normal stress computed with that fluctuating velocity. The wider the pdf the larger the normal stress.

III-1. $s/t = -0.247$

The u fluctuating velocity pdfs show that the large negative fluctuations occur in the $\log_{10}(y/t) \approx -2.7$ to -2.3 range. Most probable velocity range is larger than zero (Fig. 11a). Very near the wall the most probable range is less than zero. Away from the wall around $\log_{10}(y/t) \approx -1.1$ the large positive and negative fluctuations are observed.

The v fluctuating velocities at this station show both large positive and negative fluctuations in the $\log_{10}(y/t) \approx -1.5$ to -1.0 range with larger positive values (Fig. 11b).

The w fluctuations in the $\log_{10}(y/t) \approx -2.7$ to -2.0 range show equal probability velocity ranges separated with lower probability velocity ranges (Fig. 11c). The positive seldom large w fluctuations skew the pdfs towards positive side and the most probable velocity range is negative. This indicates that instantaneous velocity prefers two states or it indicates the meandering of the flow between two states. The pdfs around $\log_{10}(y/t) \approx -1.1$ also show that large positive w fluctuations occur in this region and the most probable velocity ranges are negative.

III-2. $s/t = -0.291$

The u fluctuation pdfs in the $\log_{10}(y/t) \approx -2.7$ to -2.4 range show that large negative u

fluctuations skew the pdfs to the negative side (Fig. 12a). Around $\log_{10}(y/t) \approx -1.1$ both large positive and negative fluctuations are observed.

The v fluctuations are spread across a large velocity range in the $\log_{10}(y/t) \approx -1.5$ to -0.8 range (Fig. 12b). The positive v fluctuations are larger than the negative v fluctuation magnitudes. The most probable values in this range are negative. Large positive v fluctuations indicate seldom upwards motion of the instantaneous flow with respect to the mean flow which might be related to the non-periodic stretching and re-accumulation of the vorticity at the wall/wing junction at the nose of the wing.

The w pdfs at this station show clear bimodal pdfs near the wall in the $\log_{10}(y/t) \approx -2.7$ to -1.6 range (Fig. 12c). The large positive and negative fluctuations in this range are not accompanied by large v fluctuations. This indicates that the meandering of the vortex between two preferred states demonstrates itself with large variations of the u and w fluctuations. The w fluctuations around $\log_{10}(y/t) \approx -1.1$ are in a wider velocity range than that are observed at $s/t = -0.247$. The pdfs are not bimodal. This indicates that the instantaneous flow below the vortex core appears to have preferred directions. The outer layer vortex appears to be not affected by the large bimodality of the near wall flow.

III-3. $s/t = -0.336$

The u fluctuating velocity pdfs at this station also show large positive and negative fluctuations in the $\log_{10}(y/t) \approx -2.8$ to -2.0 range and also in the $\log_{10}(y/t) \approx -1.4$ to -0.8 range similar to the other station pdfs discussed (Fig. 13a). Weak bimodality of the pdf at $\log_{10}(y/t) \approx -2.4$ is an indication of the meandering of the flow in the y - s plane around this region.

The v fluctuation pdf positive values at $\log_{10}(y/t) \approx -1.5$ to -0.8 range are smaller in magnitude than the values obtained at station $s/t = -0.291$ in the same range (Fig. 13b). Positive v fluctuation values are larger than the negative v fluctuation magnitudes. These two stations are both in the vicinity of the vortex core and V/U_{ref} values at $\log_{10}(y/t) \approx -1.1$ for both stations are close to zero. The non-periodic stretching of the vortex to a narrower cork-screw motion along the wall and wing junction contour is believed to cause the large negative v fluctuations. The following expansion of the vortex into a larger domain after the re-accumulation of the vorticity around the nose of the wing is believed to cause the large positive v fluctuations.

The w pdf bimodality at this station is confined to $\log_{10}(y/t) \approx -2.2$ to -1.3 region indicating the extent of the bimodal flow (Fig. 13c). The bimodal region moves away from the wall.

III-4. $s/t = -0.368$

The bimodal region further moves away from the wall and is confined to $\log_{10}(y/t) \approx -1.7$ to -1.3 region (Figures 14a, 14b, 14c). The u and v pdfs are similar to the other station distributions with reduced magnitudes of the fluctuations.

CHAPTER IV. TRIPLE PRODUCTS

The signs of the Reynolds averaged triple products indicate the direction of the average transfer of the u^2 , v^2 , w^2 momentum along the coordinate axes. The sign of a triple product depends on the instantaneous flow characteristics. As an example the conditions under which the $\overline{u^2 v}$ is positive are listed below:

- a) The $\overline{u^2 v}$ is positive when most of the large u fluctuations occur together with average magnitude positive v fluctuations.
- b) The $\overline{u^2 v}$ is positive when most of the large positive v fluctuations occur together with average magnitude u fluctuations.
- c) The $\overline{u^2 v}$ is positive when large u and large positive v fluctuations seldom occur together and outweigh the seldom occurring large u and large negative v fluctuations.
- d) Small u and small positive v fluctuations outweigh the small u and small negative v fluctuations.

The following discussion on the triple products is based on the similar line of thought applied to the other triple products.

The $\overline{u^2 v}$ in close vicinity of the vortex core is large and positive with a local maximum located at the uplifting side of the large vortical flow (Fig. 15). The minimum is below the vortex core at $\log_{10}(y/t) \approx -1.4$. Both at these locations the $\overline{v^2}$ values are also large. Within the vicinity of the vortex core the $\overline{u^2}$ value is on the order of half of the $\overline{v^2}$. Another local maximum is located near the wall below the minimum $\overline{u^2 v}$ region at $\log_{10}(y/t) \approx -2.1$ and extends towards the wing. In this region $\overline{v^2}$ values are small but $\overline{u^2}$ values are large. The large positive v fluctuations occur with average magnitude u fluctuations in the vicinity of the vortex core except right below the vortex core. Right below the vortex core large negative v fluctuations occur with the average magnitude u fluctuations. Nearer the wall large u fluctuations occur together with average magnitude positive v fluctuations. The flow that is uprising encounters the lateral low turbulence free-stream flow and results in positive v fluctuations. On the other hand the mean velocity on the downward side directed towards the wall is low turbulent free-stream flow. The positive v fluctuations in that region may be due to the free-stream velocity that is aperiodically flowing in the plane parallel to the wall thus causing a positive v fluctuation on the average mean V velocity. Another explanation may be the meandering of the vortex core in the plane of the measurements, but this motion is not very clear from the histograms of the w fluctuations. The minimum right below the vortex core is believed to be due to the fluctuations caused by the instantaneous vortex structure that is directed in to this region. The maximum near the wall is below $y^+ \approx 60$ ($\log_{10}(y/t) \approx -$

2.1). This region is where $\overline{v^2}$ is low and it is close to the $\overline{u^2}$ maximum location.

The maximum $\overline{u^2 w}$ is located close to the regions where $\overline{u^2}$ values show a peak (Fig. 16). The transfer of u^2 momentum in the Reynolds average sense is with positive w velocity. Negative peak values are observed at the wing/wall junction and at the uplifting side of the vortical flow. The u fluctuations and positive w fluctuations correlate well in this region. The structures persist in their original direction and directionally lag the mean flow as tabulated in Table 1. β_w in Table 1 shows the x wall coordinate direction with respect to the 22.4° line.

Large positive $\overline{u^3}$ values are located very near the wall and the large negative $\overline{u^3}$ values are located above these regions (Fig. 17). The minimum value magnitude is twice as large as the maximum value magnitude. The positive value indicates an occasional higher speed fluid reaching very close to the wall resulting in sweeps (+ u , - v). The low momentum fluid lifted up by these sweeps result in slower speed fluctuations causing ejections (- u , + v). The positive and negative $\overline{u^3}$ magnitudes are close to one another at the wing and wall junction. High $\overline{u^3}$ gradient near the wing-wall junction indicates high diffusion rates in this region.

The $\overline{u^2 v}$, $\overline{u^3}$ and $\overline{u^2 w}$ triple products together explain the u^2 momentum transfer in the average (Figures 15, 16 and 17). The $\overline{u^3}$ triple product indicates that the near wall $\overline{u^2}$ transfer is with a + u transport velocity and away from the wall it is with a - u longitudinal transport velocity. The $\overline{u^2 v}$ triple product indicates that the momentum transfer of $\overline{u^2}$ except near the wall and below the vortex core is with + v transport velocity. In the Reynolds average sense the u^2 momentum is carried towards the wall in the near wall region and in the region below the vortex core but carried away from the wall within the vicinity of the vortex core and the locations where ejection motions are dominant. The $\overline{u^2 w}$ triple product shows that the $\overline{u^2}$ momentum is carried towards the wing at the locations where ejections are dominant. These locations are in the vicinity of the vortex core and below the vortex core. The $\overline{u^2}$ momentum is carried away from the wing at locations very near the wing-wall intersection and at the uplifting side of the large outer vortical structure.

The negative u fluctuations and v fluctuations appear to be well correlated in the region surrounding the vortex core as indicated by the $\overline{uv^2}$ (Fig. 18). The $\overline{v^2}$ is also large in this region. The region extends close to the wall.

The triple product $\overline{v^3}$ shows that in the vicinity of the vortex core positive v fluctuations are dominant (Fig. 19). The maximum value is obtained at the downwash side of the vortical motion. Large $\overline{v^3}$ may be due to intermittent nature of the vortex and meandering of the vortex location. The instantaneous flow parallel to the wall results in a positive v fluctuation on the mean velocity when the vortex is instantaneously stretched and confined to a smaller area.

The negative w fluctuations and v fluctuations are well correlated in the vicinity of the vortex core as shown in the $\overline{v^2 w}$ figure (Fig. 20), especially below the vortex core and on the uplifting side of the vortex. At the downward motion section of the vortex the + w fluctuations are

well correlated with the v fluctuations. The minimum value magnitude of the triple product is twice as large as the maximum value. The flow below the vortex core away from the wing is opposed by an adverse pressure gradient at $s/t=-0.3$.

The $\overline{v^2}$ momentum transfer in $x_{22.4}$ direction on the uplifting side of the large vortical flow is with a negative u transport velocity. In the same region. Lateral and vertical momentum transfer is both away from the wing and the wall. However on the downward motion side of the vortex the $\overline{v^2}$ momentum is transferred towards the wing and longitudinal transfer is with the negative u transport velocity. The vertical $\overline{v^2}$ momentum transfer is with a larger transport velocity than in the uplifting region.

The triple product $\overline{uw^2}$ shows that in the vicinity of the vortex core and at the uplifting side of the vortex core negative u fluctuations are more correlated with the w fluctuations (Fig. 21). Below the vortex core closer to the wall high positive values are surrounded by large negative values. Near the wall $\overline{uw^2}$ values at locations $\Delta s/t=-0.4$ and closer to the wing near wall $\overline{uw^2}$ values are positive. In this region sweep motion $(+u, -v)$ is dominant. Near the separation line the $\overline{uw^2}$ triple product is small and positive.

The w fluctuations are more correlated with the positive v fluctuations. The $\overline{vw^2}$ triple product negative values are an order of magnitude smaller than the positive maximum value (Fig. 22). High positive values are located around the uplifting region of the vortex. The small negative values are observed in the near wall region below the vortex core and in the outer edge of the downward side of the vortex.

The $\overline{w^3}$ triple product maximum and the minimum peak locations are located below the vortex core (Fig. 23). Large negative $\overline{w^3}$ are located at the uplifting side of the vortex and large positive values are observed at the downward side of the vortex. Positive $\overline{w^3}$ values show the seldom but strong positive w fluctuations are dominant and the w^2 momentum is carried with a positive lateral transport velocity in the positive s direction. The elevated values are believed to be due to the meandering of the vortex core.

The triple products $\overline{uw^2}$, $\overline{vw^2}$ and $\overline{w^3}$ together describe the transfer of the $\overline{w^2}$ momentum (Figures 21, 22 and 23). The $\overline{uw^2}$ shows that while the $\overline{w^2}$ momentum is transferred with positive u transport velocity in a column below the vortex core $\overline{w^2}$ momentum is transported with negative u velocity around this column and in the vicinity of the vortex core. The $\overline{vw^2}$ values show that in the vicinity of the vortex core and at the uplifting side of the large outer vertical motion momentum is carried away from the wall. This region is also where negative u fluctuations are dominant. The $\overline{w^2}$ momentum carried away from the wall is transported with negative u transport velocity. The $\overline{w^3}$ triple product on the other hand shows that the momentum is transferred both towards the wing and away from the wing due to the meandering of the instantaneous vortex structure.

The triple product \overline{uvw} (Fig. 24) is positive when seldom but positive fluctuations occur

simultaneously such that the average value is tipped towards the positive or when two of the fluctuating velocities have seldom but strong negative fluctuations provided that the third fluctuating velocity is simultaneously positive and strong. The \overline{uvw} is positive in the uplifting side of the vortex and largest negative values occur beneath the vortex. Large positive \overline{uvw} values are also located near the wall. Large negative values indicate that large seldom negative fluctuations or two positive and one negative strong fluctuations occur together. The $\overline{w^3}$ triple product is positive at the regions where \overline{uvw} is large.

CHAPTER V. DERIVED QUANTITIES

V-1. FLOW ANGLE

The flow angle is defined with respect to the $x_{22.4}$ axis. A positive flow angle shows a fluid motion towards the wing (Fig. 25). The maximum flow angle is at the boundary layer edge of station 5. The large vortex structure results in positive flow angles above the vortex core and negative flow angles below the vortex core. Near the wall/wing junction, positive flow angles are observed. The minimum value is located between a vertical line passing through the vortex core and the wing near the wall. The flow angles are of opposite signs on each side of the separation zone, indicating that the flow is merging towards a region from both sides.

V-2. FLOW GRADIENT ANGLE

Flow gradient angle (FGA) values show large variations between -114° and 90° with respect to the $x_{22.4}$ line (Fig. 26). A minimum value is obtained away from the vortex core, wing and the wall, and it is located below the vortex at $s/t = -0.35$, $\log_{10}(y/t) \approx -1.6$. The FGA shows large gradients between $\log_{10}(y/t) \approx -1.6$ and -2.2 . Positive FGA values are located in the zone between the vortex and the wing. Sharp variations are also observed near the wing.

V-3. SHEAR STRESS ANGLE

The shear stress angle (SSA) has large positive values beneath the vortex and large negative values near the wall in the $x_{22.4}$ -s plane of the measurements (Fig. 27). Negative and positive values greater than 90° indicate a region where $-\overline{uv}$ shear stress is negative. A positive SSA shows a $-\overline{vw} > 0$ and negative SSA indicate a $-\overline{vw} < 0$. The plot shows that very near the wall at the separation location, the $-\overline{uv}$ shear stress is negative. In such a flow the SSA lags highly behind the FGA. Large variations by the FGA are not followed by the SSA.

V-4. $(\partial W / \partial y) t / U_{ref}$

The vorticity component in the $x_{22.4}$ direction is $(\partial W / \partial y - \partial V / \partial s)$ (Fig. 28). In the figure the larger of the components $\partial W / \partial y$ is presented. The figure shows that large outer layer vortex has positive vorticity with a small magnitude. Vorticity is the rotation of the fluid particles along an axis and does not necessarily imply a large structural rotation. Maximum negative vorticity is located very near the wall close to the wing wall junction. It appears that the large outer layer vortex

generates a near wall vortex with the opposite sense of rotation. At the wall/wing junction the vorticity values reach to their positive peak with the same sense of vorticity of the outer region vortex and are caused by the large negative vorticity region near the wall. The vorticity values around the rotational separation zone are negative.

V-5. TKE/U_{ref}^2

The turbulent kinetic energy is defined as:

$$TKE = \frac{\overline{U^2} + \overline{V^2} + \overline{W^2}}{2}$$

Figure 29 shows that the TKE is very large in the region below the core. In this complex flow the TKE levels are very large away from the wall. In a 3-D turbulent boundary layer flow TKE maximum value is usually at $y^+ \approx 25$. Large TKE values are due to large $\overline{w^2}$ values. In the vicinity of the rotational separation region TKE values are higher than at Station 5.

V-6. V_{q^2}/U_{ref}

V_{q^2} is defined as the transport velocity of the turbulent kinetic energy:

$$V_{q^2} = \frac{\overline{U^2 V} + \overline{V^3} + \overline{V^2 W}}{\overline{U^2} + \overline{V^2} + \overline{W^2}}$$

The ratio defines a Reynolds average sense perpendicular velocity component that the TKE is transported (Fig. 30). The velocity is observed to be positive in general. Large positive values are located in the vicinity of the vortex core both on the uplifting and downwash side of the vortex. The TKE is transported away from the wall in these regions. Large negative values are located at the downward side of the vortex. This indicates that the TKE generation is maximum away but close to the wall and the TKE is transported in both directions around this region.

V-7. $\overline{uv}/\overline{u^2}$

The structural parameter shows that the contours define plateaus near the wall region below $\log_{10}(y/t) \approx -2$ indicating that the $\overline{u^2}$ is the correct scaling parameter for the \overline{uv} near the wall even in highly complicated flows (Fig. 31). This information can be used to deduce the \overline{uv} information near the wall from measured $\overline{u^2}$ data. However the coefficient values are not high indicating that the u and v fluctuating velocities are not very well correlated.

V-8. SKEWNESS OF u

Skewness of the u fluctuating velocity is defined as:

$$S_u = \frac{\overline{u^3}}{(\overline{u^2})^{3/2}}$$

The quantity shows the skewing of the probability density functions due to seldom but strong fluctuations (Fig. 32). The skewness of a Gaussian pdf is zero. The S_u is larger than zero near the wall indicating that the seldom but strong positive u fluctuations occur in this region. These are due to the sweeps which are directed towards the wall originating from a region of high momentum away from the wall. Large negative values near the wing are due to the large vortical flow generated near the wing reorienting itself due to the presence of the wing and the wall. In the vicinity of the vortex core negative u fluctuations dominate the flow.

V-9. SKEWNESS OF v

Large positive skewness values are located above the vortex core with the maximum values located at the uplifting side of the vortex (Fig. 33). Large negative values are located at the downward side of the vortex. This shows that the seldom but strong v fluctuations occur at the uplifting side and above the vortex core. The flow on the downwash side is occasionally with a fast instantaneous velocity. In general the S_v is larger than zero. Negative values are located near the wall and away from the vortex core and in the vicinity of the rotational separation region. Negative S_v in this region shows that the flow occasionally moves upwards with a fast instantaneous velocity.

V-10. SKEWNESS OF w

Skewness of w fluctuations S_w shows that large positive values are located below the vortex core all the way to the wall (Fig. 34). On the contrary to the intuitive reasoning the skewness in this region is positive. The positive values indicate that occasional strong $+w$ fluctuations occur below the vortex core region. This may be due to chaotic meandering of the vortex zone. Between this zone and the wing negative S_w indicates occasional strong $-w$ fluctuations. Large positive values show that the occasional large positive and small negative fluctuations are caused by the flow entrained by the vortex. The negative values located under the vortex core near the wall is also believed to be due to large chaotic meandering of the vortex structure. Negative S_w values surround the separation region and near the wall to indicate that the redirected flow generates seldom but strong $-w$ fluctuations. Near wall values on the left-hand side of the separation are small but positive.

V-11. SHEAR STRESS MAGNITUDE

Shear stress magnitude is highly elevated in the return and uplifting side of the vortex (Fig. 35). The fluctuations become more correlated in these regions since $-w$ and $+v$ fluctuations describe the instantaneous motion of the fluid redirected by the vortex in this region. The $-u$ and $+v$ fluctuations are also large in these regions. The separation region is observed to have the

lowest shear stress magnitude but larger than Station 5 values.

V-12. TOWNSEND'S STRUCTURAL PARAMETER, A_1

Townsend's structural parameter is defined as:

$$A_1 = \frac{\sqrt{(-\overline{UV})^2 + (-\overline{VW})^2}}{\overline{U^2} + \overline{V^2} + \overline{W^2}}$$

The A_1 structural parameter increases from very small values near the wall to large values at the outer region (Fig. 36). The downward side of the vortex core region is observed to have small values due to small shear stresses in this region since the free-stream fluctuations are close to the isotropic distribution. However large values are observed on the uplifting side of the vortex.

V-13. $\frac{\overline{U^2} + \overline{W^2}}{\overline{V^2}}$ STRUCTURAL PARAMETER

The values are close to 1 in most part of the layers. This value is the half of the isotropic distribution value (Fig. 37). This shows that $\overline{V^2}$ fluctuations are in general much higher than the isotropic value away from the wall which is due to large vortical motion energizing the whole domain studied. Near the wall region especially close to the wall/wing junction the values are much larger than 2 which is mainly due to very high u fluctuations dominating the region.

V-14. ROTTA'S T

Rotta's T anisotropy constant is defined as:

$$T = \frac{\tan(SSA - FA)}{\tan(FGA - FA)}$$

The eddy viscosity ratio T is relative to the local flow angle and is co-ordinate system independent about the y -axis. T is not a constant at any y for these data according to Fig. 17. T is about constant in the outer layer with $T \approx 0.4$ to 0.5 . Wherever $FGA = FA$, the data show T approaching large negative or positive values. Below $\log_{10}(y/t)$ of about -1.5 , this is a poor eddy-viscosity ratio model.

CHAPTER VI. VARIATION IN FLOW PHYSICS AT SELECTED LOCATIONS

VI-1. SEPARATION LOCATION

In this section the profiles of flow quantities measured at stations 5, A, B and C are used to describe the flow around a three-dimensional separation region. Mean secondary flow streamlines in the plane of the measurements around $s/t \approx -0.58$ show a region where the secondary streamlines merge. The streamlines diverging away from the wall join to this rotational region which indicates separation of the flow from the floor around $s/t \approx -0.54$. The vorticity of the region is opposite to that of the large outer layer vortex.

Within the surrounding of the rotational separation region the mean velocity magnitude is small since the region is close to the wall. Compared to station 5 skin friction velocity $u_\tau = 1.15$ m/sec on the wall, u_τ decreases to 1.094 m/sec at station A, to 1.002 m/sec at station B, and to 1.048 m/sec at station C. The W mean velocity minima values decrease at stations A, B and C, and the minima locations shift up in the layers. Station A appears to be the station closest to where the rotational separation region away from the wall occurs. The oil flow visualization on the floor shows that station C is closer to the separation on the wall where the streamlines start to converge.

The $\overline{u^2}$ normal stress (Fig. 5) at $\log_{10}(y/t) \approx -2.5$ increases 14% by station C with a larger increase nearer the wall. The $\overline{w^2}$ normal stress (Fig. 7) steeply increases near the wall proceeding from station 5 to station C. The monotonic increase show a 100% increase at station C compared to that at station 5 at $\log_{10}(y/t) \approx -1.5$. The $\overline{v^2}$ peak value is also increased proceeding towards the wing (Fig. 6). The peak value in the outer layer is doubled. The \overline{uv} (Fig. 8) and \overline{vw} (Fig. 10) stress minimum and maximum value magnitudes increase within this zone. The u and w and the v and w fluctuations are more correlated within the separation region compared to Station 5.

The transport of the $\overline{u^2}$ momentum both with positive and negative u, v, w fluctuations is increased. The maxima and minima value magnitudes of $\overline{u^2v}$ (Fig. 15), $\overline{u^2w}$ (Fig. 16) and $\overline{u^3}$ (Fig. 17) increase. The increase in magnitudes at the same y/t locations away from wall depicts larger diffusion for the transport of the $\overline{u^2}$ normal stress ($TD = -\frac{\partial}{\partial x_i}(\overline{u^2 u_i})$), largest term

$TD \approx -\frac{\partial \overline{u^2 v}}{\partial y}$). The $\overline{v^2}$ momentum is transported increasingly with negative u and w transport

velocities and transported increasingly with positive v transport velocity. Diffusion of $\overline{v^2}$ is increased ($TD = -\frac{\partial}{\partial x_i}(\overline{v^2 u_i})$, largest term $= -\frac{\partial}{\partial y}(\overline{v^3})$ (Fig 19)). The $\overline{uw^2}$ minima and maxima values increase, $\overline{vw^2}$ (Fig. 22) is positive and maxima values increase, $\overline{w^3}$ become increasingly negative. These observations show that $\overline{w^2}$ is increasingly transported away from the wall and the wing. The longitudinal transport of $\overline{w^2}$ is increased both with positive and negative u fluctuations.

VI-2. STATIONS SURROUNDING THE VORTEX CORE

The stations discussed in this section are TB, TC, R and S which encompass the vortex core of the outer layer vortex. Even though the streamlines indicate a rotating structure in the outer layer, the vorticity of the flow in this region is actually small. However, the circulation is large since it covers a large area. The near wall flow affected by this large structure shows a large vorticity region in a very narrow region near the wall with the opposite sense of rotation to that of the large vortex. The vortex core is located at $\log_{10}(y/t) \approx -1.1$. Below the vortex core, U mean velocity profiles (Fig. 2) show regions where $\partial U / \partial y$ is zero or even negative which indicates the largest gradient term using boundary layer approximations is nearly zero for such a flow. The maximum V velocities (Fig. 3) are observed near the vortex core and W mean velocities (Fig. 4) change sign above the vortex core. The regions where $\partial U / \partial y = 0$ (between $\log_{10}(y/t) \approx -2$ to -1.25) shows that the production of $\overline{u^2}$ and \overline{uv} stresses are small. In these regions $\overline{u^2}$ normal stress values decrease proceeding from station TB to station S. The dominant normal stress near the vortex core is $\overline{v^2}$ with values larger than near wall $\overline{u^2}$ values. The maximum value of the $\overline{w^2}$ near the wall is much larger than the other normal stresses due to aperiodic motion of the near wall flow to generate bimodal w fluctuating velocity histograms. The w' fluctuations reach $0.23 U_{ref}$ at $\log_{10}(y/t) \approx -2$ and v' fluctuations are as high as $0.19 U_{ref}$ at $\log_{10}(y/t) \approx -1.15$. The $\overline{w^2}$ and $\overline{v^2}$ stresses decrease on both sides of the vortex core.

The \overline{uv} correlation obtains the largest values within the measurement plane at station TB with values on the order of 3.5 larger than at station 5. However the values rapidly decrease by station S. The locations where $\partial U / \partial y = 0$ also corresponds to the locations where $-\overline{v^2} \frac{\partial U}{\partial y}$ which is the largest \overline{uv} production term is approximately zero. In this region $-\overline{uv} \frac{\partial V}{\partial y}$ production term becomes important. The \overline{uw} stress (Fig. 9) on the uplifting and on the downwash side of the vortex show different features. On the uplifting side the positive maximum is located in between two minima.

Positive \overline{uw} correlation denotes the $-(\rho \overline{uw})$ stress slowing down the flow to rotate along

the -y axis and a negative \overline{uw} correlation denotes a stress slowing down the flow to rotate along the +y axis. On the downwash side of the vortex, the near wall flow encounters stresses slowing down the flow towards the vortex. The \overline{vw} correlation reaches a minimum value at station TB within the measurement plane and increases on both sides of this station. The maximum value is reached at station R. Negative \overline{vw} results in a rolling motion along the $+x_{22.4}$ axis; this stress is the magnitude of the resistance of the fluid to a motion along the +s axis.

The $\overline{u^3}$ (Fig. 17) is positive very near the wall at all stations of this zone and above $\log_{10}(y/t) \approx -2.5$ the values are negative. Within the same near wall region $\overline{u^2v}$ (Fig. 15) values are negative indicating that sweep type motions ($u > 0, v < 0$) are dominant in this region. Above the near wall region $\overline{u^3}$ is negative throughout the layers. Except at stations on each side of the vortex core (TC and R) the $\overline{u^2v}$ is positive above this near wall region. The $\overline{u^2}$ momentum in this region is carried away from the wall with negative u transport velocity. The $\overline{u^2w}$ (Fig. 16) value becomes positive proceeding from station TB towards station S and the maximum value increases, indicating $\overline{u^2}$ momentum transport with a positive w transport velocity nearer the wing side of the vortex core.

The transport of $\overline{v^2}$ is with a positive w transport velocity as depicted by $\overline{v^2w}$ (Fig. 20). Near the vortex core at stations TB, TC and R it is with negative w transport velocity. Transport velocity is practically zero above the vortex core. The transport of $\overline{v^2}$ similar to that of the $\overline{u^2}$ is with negative u transport velocity as shown by $\overline{uv^2}$. At the downwash side the value becomes positive below the vortex core. The $\overline{v^3}$ indicates that the $\overline{v^2}$ transport is away from the wall. The $\overline{v^2}$ momentum is transported away from the wall and wing with a negative u transport velocity.

The $\overline{w^3}$ (Fig. 23) shows that transport of w^2 is with negative w transport velocity on the uplifting side of the vortex and with positive w transport velocity on the downwash side of the vortex. Transport velocities at different stations change sign many times. The $\overline{w^2}$ momentum is also transported away from the wall in a large part of the layer similar to that of the u^2 and v^2 momentum transport. The v transport velocity of $\overline{w^2}$ decreases below the vortex core. The transport of $\overline{w^2}$ in the longitudinal direction is with a negative u transport velocity at station TB however the value becomes positive and large positive at stations TC and R and at station S it is with a large negative u transport velocity. The $\overline{w^2}$ momentum transport is strongly affected by the vortex motion and responds rather quickly in such a short spatial variation.

VI-3. NEAR THE WING/WALL JUNCTION

In this section the flow physics near the wing/wall junction is described. The measurement stations used in this section are stations T through X. The mean U velocity accelerates as the wing is approached. Near the wall, the velocity gradient is increased. The region with constant

U velocity extends a longer range than around the vortex core. The V vertical velocity decreases with the minimum at station X. The W velocity minima values increase and the maxima values decrease as the wing is approached. At station X closest to the wing the W component changes sign near the wall.

The near wall $\overline{u^2}$ normal stress values continuously increase as the wing is approached. However the values above $\log_{10}(y/t) \approx -2$ continuously decrease till station W to reach values below the $\overline{u^2}$ normal stress obtained at station 5. At station X the values abruptly increase. The $\overline{v^2}$ and $\overline{w^2}$ normal stresses are reduced till station W throughout the layers. The values of the normal stresses at station W are relatively higher than at station 5. At station X values increase. The decrease of the normal stresses within this zone is due to the strong acceleration of the flow and also due to the free stream low turbulence fluid carried close to the wall by the large outer region vortex. However, at station X the effect of the wing/wall junction is felt. The turbulent kinetic energy of the flow away from the wall is lower at locations where all normal stresses are reduced.

The \overline{uv} stress values at stations T and U are comparable to the values at station 5. At station W the \overline{uv} stress magnitude is decreased above $\log_{10}(y/t) \approx -2.25$ with values close to zero. Near wall values are as large as the values at station 5. The \overline{vw} stress resembles a wave motion with increasing and decreasing values above and below zero values. The \overline{vw} stress magnitude decreases as the wing is approached. At station X the \overline{vw} stress once more increases. The \overline{uw} stress also show a wavy character with the maximum magnitude value located nearer the wall. The reduction of this magnitude at station U compared to that of T is followed by an increase which results in values an order of magnitude larger at station W than that at station 5. The \overline{uw} stress changes sign near the wall at station X. The increase of the maximum $-\overline{uw}$ causes increase resistance to a rotation along the +y axis.

As indicated by the $\overline{u^2v}$, $\overline{u^2w}$ and $\overline{u^3}$ triple products, the near wall Reynolds averaged transport of $\overline{u^2}$ momentum is towards the wall and away from the wing with positive longitudinal transport velocity. Away from the wall $\overline{u^2}$ transport is away from the wall towards the wing with negative longitudinal transport velocity. Near the wall sweep motions are dominant where positive large u fluctuations occur with large negative v fluctuations. Above this region ejection events ($u < 0, v > 0$) become dominant. All three triple products approach zero above $\log_{10}(y/t) \approx -2.0$ as the wing is approached. The triple products at station X do not follow the trends of the profiles of stations T through W, especially above $\log_{10}(y/t) \approx -2.0$. The $\overline{u^2v}$ is larger than near the wall in this region, the $\overline{u^2w}$ becomes negative and the $\overline{u^3}$ is negative.

The $\overline{v^2}$ momentum transfer near the wall is with positive longitudinal velocity and above $\log_{10}(y/t) \approx -2.5$ it is with negative longitudinal velocity. The lateral Reynolds average sense transport velocity of $\overline{v^2}$ momentum changes sign within the layers many times. At station X while

the near wall $\overline{v^2}$ momentum is transported towards the wall above $\log_{10}(y/t) \approx -1.5$ it is transported away from the wall. The vertical transport velocity of the $\overline{v^2}$ momentum also shows a wave type variation in the layers. At stations V and W the Reynolds averaged transport velocity is positive throughout the layers at station X near wall magnitude of this transport velocity is increased however in the outer region it becomes negative.

The $\overline{uw^2}$, $\overline{vw^2}$ and $\overline{w^3}$ triple products describe the transport of $\overline{w^2}$. The transport of $\overline{w^2}$ near the wall is with positive longitudinal velocity, above $\log_{10}(y/t) \approx -2.5$ it is with negative longitudinal velocity. In this region negative large occasional u fluctuations tip the average towards negative values. Transport velocity minimum location shifts up in the layer at station X. The vertical transport of $\overline{w^2}$ is with positive transport velocity and in the outer region it is towards the wall. The lateral transport shows wavy character of the transport with negative, positive transport velocities throughout the layer.

CHAPTER VII. CONCLUSIONS

In the present work structural features of a complex three-dimensional flow in a wing-wall junction were studied. The flow is complex not only due to three-dimensionality of the boundary layer on the wall but also due to the large vortical structure present in the outer layer and due to the separation of the 3-D TBL affected by the adverse lateral pressure-gradients. The analysis is further challenging due to the aperiodic motion of the vortex which generates large $\overline{w^2}$ normal stresses.

The large vortical structure in the outer region brings high speed free-stream fluid very close to the wall, which results in thinning of the boundary layer near the wing. Adverse lateral pressure gradients result in a 3-D separation zone. The flow very near the wing has positive flow angle with respect to $x_{22.4}$. The outer layer vortical flow has small vorticity along the $+x_{22.4}$. The high vorticity region is concentrated in a region near the wall between the wing and the vortex center with a vorticity along the $-x_{22.4}$ axis. At the wing/wall junction a region with vorticity along the $+x_{22.4}$ axis is observed.

The $\overline{u^2}$ normal stress is higher in the region between the vortex core and the wall than the other regions of the flow. The maximum $\overline{u^2}$ is very near the wing/wall junction. The $\overline{v^2}$ maximum occurs below the vortex core and large $\overline{v^2}$ values occur around the vortex core. The $\overline{w^2}$ is very large compared to $\overline{u^2}$ and $\overline{v^2}$ normal stresses, especially in the region between the vortex core and the wall. Bimodal w fluctuation histograms are observed at four measurement stations, two on each side of the vortex core. The turbulent kinetic energy of the flow increases to 5 to 6 times to that of the station 5 value at the stations in a region below the vortex core.

Both the \overline{uv} and the \overline{vw} stresses reach their maximum values on the uplifting side of the vortex core. The \overline{uw} stress maxima are located near the wall below the vortex core closer to the wing and at the wing/wall junction. Near the vortex core and the separation region the flow is along the $x_{22.4}$ axis. The inrush of the free-stream flow towards the wall/wing junction generates flow away from the wing with flow angles as high as -23.5° with respect to $x_{22.4}$ axis. The shear stress angle severely lags behind the flow gradient angles. Where there are severe FGA variations, the SSA response in the outer layer is not followed in the inner regions. Due to small $\partial U/\partial y$ values observed throughout the layers the FGA are very large.

Diffusion processes are highly altered by the outer layer vortex effects on the inner layer flow. Large triple product magnitudes are observed surrounding the vortex core, below the vortex core, within the region between the vortex core and wing nearer the wall and near the wing/wall junction.

ACKNOWLEDGEMENTS

The authors are grateful for the support of the Office of Naval Research Grant N00014-94-1-0092, Dr. L.P. Purtell, Program Manager.

REFERENCES

Anderson, S.C., and Eaton, J.K., 1989, "Reynolds stress development in a pressure-driven three-dimensional turbulent boundary layer", *J. of Fluid Mech.*, vol. 202, pp. 263-294.

Devenport, W.J., Simpson, R.L., 1990a, "A time-dependent and time-averaged turbulence structure near the nose of a wing-body junction", *J. of Fluid Mech.*, vol. 210, pp. 23-55.

Devenport, W.J., Simpson, R.L., 1990b, "An experimental investigation of the flow past an idealized wing-body junction:final report", VPI&SU report, VPI-AOE-172.

Devenport, W.J., Simpson, R.L., 1992, "Flow past a wing-body junction- Experimental evaluation of turbulence models", *AIAA J.*, vol. 30, number 4, April, pp. 873-882.

Eaton, J.K., 1995, "Effects of mean flow three dimensionality on turbulent boundary-layer structure", *AIAA J.*, vol. 33, number 11, November, pp. 2020-2025.

Fleming, J., Simpson, R.L., Devenport, W.J., 1993, "An experimental study of a turbulent wing-body junction and wake flow", *Exp. in Fluids*, vol. 14, pp. 366-378.

Ha, S.M., and Simpson, R.L., 1993, "An experimental study of coherent structures in a three dimensional turbulent boundary layer", Report VPI-AOE-205, submitted to DTIC.

Khan, M.J., Ahmed, A., Tropper, J.R., 1995, "Dynamics of the juncture vortex", *AIAA J.*, vol. 33, number 7, July, pp. 1273-1279.

Kim, S., Walker, D.A., and Simpson, R.L., 1991, "Observation and measurement of flow structures in the stagnation region of a wing-body junction", Report VPI-E-91-20; submitted to DTIC.

Lewis, D.J., Simpson, R.L., and Diller, T., 1994, "Time resolved surface heat flux measurements in the wing/body junction vortex", *AIAA J., Thermophysics and Heat Transfer*, vol. 8, pp. 656-663.

Mansour, N.N., Kim, J., and Moin, P., 1988, "Reynolds-stress and dissipation-rate budgets in a turbulent channel flow", *J. of Fluid Mech.*, vol. 194, pp. 15-44.

Mansour, N.N., Kim, J., Moin, P., 1989, "Near-wall k-epsilon turbulence modelling", *AIAA J.*, vol. 27, no. 8, pp. 1068-1073.

Martinuzzi, R., Tropea, C., 1993, "The flow around surface-mounted, prismatic obstacles placed in a fully developed channel flow", *J. of Fluids Eng.*, vol. 115, pp. 85-92, March.

McMahon, H.M., Hubbart, J., Kubendran, L., 1982, "Mean velocities and Reynolds stresses in a juncture flow", NASA Contractor report 3605.

McMahon, H.M., Merati, P., Yoo, K.M., 1987, "Mean velocities and Reynolds stresses in the juncture flow and in the shear layer downstream of an appendage", Georgia Tech Report, GITAER 87-4, Atlanta, Georgia, 30332.

Moin, P., Shih, T.H., Driver, D., Mansour, N.N., 1990, "Direct numerical simulation of a three-dimensional turbulent boundary layer", *Phys. of Fluids A*, vol. 2, no. 10, pp. 1846-1853.

Ölçmen, M.S., 1990, *An experimental study of a three-dimensional pressure-driven*

turbulent boundary layer, Ph.D. Dissertation, Virginia Tech, AOE Dept; submitted to DTIC.

Ölçmen, M.S., and Simpson, R.L., 1995a, "An experimental study of a three-dimensional pressure-driven turbulent boundary layer", *J. of Fluid Mech.*, vol. 290, pp. 225-262.

Ölçmen, M.S., and Simpson, R.L., 1995b, "A five-velocity-component laser-Doppler velocimeter for measurements of a three-dimensional turbulent boundary layer", *Meas. Sci. and Tech.*, vol. 6, pp. 702-716.

Ölçmen, M.S., and Simpson, R.L., 1996a, "Experimental evaluation of pressure-strain models in complex 3-D turbulent flow near a wing/body junction", VPI&SU Report, VPI-AOE-228; submitted to DTIC.

Ölçmen, M.S., and Simpson, R.L., 1996b, "Experimental transport-rate budgets in complex 3-D turbulent flow near a wing/body junction", 27th AIAA Fluid Dynamics Conference, June 17-20, New Orleans, LA; submitted to *J. of Fluid Mech.*

Ölçmen, M.S., and Simpson, R.L., 1996c, "Theoretical and experimental pressure-strain comparison in a pressure-driven three-dimensional turbulent boundary layer", 1st AIAA Theoretical Fluid Mechanics Meeting, June 17-20, New Orleans, LA; submitted to *J. of Fluid Mech.*

Ölçmen, M.S., and Simpson, R.L., 1996d, "Some structural features of a turbulent wing-body junction vortical flow", VPI&SU Report, VPI-AOE-238; submitted to DTIC.

Ölçmen, M.S., and Simpson, R.L., 1996e, "Higher order turbulence results for a three-dimensional pressure-driven turbulent boundary layer", VPI&SU Report, VPI-AOE-237; submitted to DTIC.

Ölçmen, M.S., and Simpson, R.L., 1997, "Experimental evaluation of turbulent diffusion models in complex 3-D flow near a wing/body junction", 35th Aerospace Sciences Meeting & Exhibit, Jan 6-10, Reno, NV, paper 97-0650.

Schwarz, W.R., and Bradshaw, P., 1994, "Term-by-term tests of stress-transport turbulence models in a three-dimensional boundary layer", *Phys. of Fluids* 6 (2), pp. 986-999.

Schwarz, W.R., and Bradshaw, P., 1994, "Turbulence structural changes for a three-dimensional turbulent boundary layer in a 30° bend", *J. of Fluid Mech.*, vol. 272, pp. 183-209.

Shinpaugh, K.A., and Simpson, R.L., 1995, "A rapidly scanning two-velocity-component laser-Doppler velocimeter", *Meas. Sci. and Tech.*, vol 6., pp. 690-701.

Simpson, R.L., 1995, "Three-dimensional turbulent boundary layers and separation", AIAA paper 95-0226.

Simpson, R.L., 1996, "Aspects of Turbulent Boundary Layer Separation", *Progress in Aerospace Sciences*, Nov.

Spalart, P.R., 1989, "Theoretical and numerical study of a three-dimensional turbulent boundary layer", *J. of Fluid Mech.*, vol. 205, pp. 319-340.

Sung, Chao-Ho, and Yang, Cheng-I, 1988, "Validation of turbulent horseshoe vortex flows", 17th symposium on Naval Hydrodynamics, 29 August-2 September, The Hague, Netherlands.

TABLE 1. LASER-DOPPLER VELOCIMETER LOCATIONS AND FLOW PARAMETERS.										
Stations	X (mm)	Z (cm)	U_e (m/sec)	U_t (m/sec)	β_w (degree) in 22.4°	β_{FS} (degree) in 22.4°	δ (mm)	s/t	$(\partial C_p / \partial x)$ (1/m) in 22.4°	$(\partial C_p / \partial z)$ (1/m) in 22.4°
Station 5	6.60	-7.47	29.54	1.15	2.7	14.7	40	-0.6774	-5.551	-3.471
A	8.79	-6.94	29.74	1.094	2.276	13.12	39.6	-0.589	-6.402	-5.195
B	9.98	-6.64	29.94	1.002	-0.647	12.53	39.9	-0.545	-7.025	-5.994
C	11.2	-6.35	30.2	1.048	-1.195	12.02	39.3	-0.501	-7.701	-6.671
D	12.42	-6.06	30.45	1.093	-2.409	11.41	39.2	-0.456	-8.249	-7.983
E	13.61	-5.77	30.65	1.132	-3.184	10.88	40.3	-0.412	-8.782	-9.488
TB	14.83	-5.47	31.82	1.163	-3.858	9.83	39.7	-0.368	-9.754	-10.455
TC	15.7	-5.26	32.27	1.188	-7.074	9.29	40.9	-0.336	-10.884	-9.813
R	16.92	-4.97	32.58	1.297	-15.583	8.21	39.2	-0.291	-11.654	-10.579
S	18.11	-4.67	33.15	1.362	-20.741	7.09	40.3	-0.247	-12.193	-5.293
T	19.33	-4.38	33.72	1.413	-18.914	5.77	38.9	-0.203	-14.54	-4.502
U	20.55	-4.09	34.85	1.320	-13.539	4.24	39.3	-0.159	-15.129	-5.093
V	21.74	-3.79	36.29	1.454	-10.943	2.82	38.4	-0.114	-13.134	-8.909
W	22.96	-3.50	37.56	1.656	-10.888	1.02	28.6	-0.070	1.456	-0.949
X	24.26	-3.18	40.42	1.917	10.752	-0.17	20.6	-0.023	1.472	-0.933

Maximum thickness of the wing (t) = 7.17 cm, Nominal reference velocity (U_{ref}) = 27.5m/sec, Reynolds number based on momentum thickness at 0.75 chord upstream of the wing on the tunnel centerline (Re_θ) = 5936. Wing chord length = 30.48 cm.

TABLE 2. 21:1 ODDS $\pm 2\sigma$ UNCERTAINTIES OF MEAN VELOCITIES, REYNOLDS' STRESSES AND TRIPLE PRODUCTS.			
Term	Uncertainty $\times 10^{-3}$	Term	Uncertainty $\times 10^{-6}$
U/U_{ref}	5.64	$\overline{U^2 V}/U_{ref}^3$	4.54
V/U_{ref}	1.25	$\overline{U^2 W}/U_{ref}^3$	7.97
W/U_{ref}	3.7	$\overline{V^2 W}/U_{ref}^3$	2.82
$\overline{U^2}/U_{ref}^2$	0.09	$\overline{UV^2}/U_{ref}^3$	3.04
$\overline{V^2}/U_{ref}^2$	0.0581	$\overline{UW^2}/U_{ref}^3$	9.13
$\overline{W^2}/U_{ref}^2$	0.01017	$\overline{VW^2}/U_{ref}^3$	2.93
\overline{UV}/U_{ref}^2	0.0363	\overline{UVW}/U_{ref}^3	2.77
\overline{UW}/U_{ref}^2	0.0537	$\overline{U^3}/U_{ref}^3$	14.06
\overline{VW}/U_{ref}^2	0.0276	$\overline{V^3}/U_{ref}^3$	2.38
		$\overline{W^3}/U_{ref}^3$	23.47

TABLE 3. SOME LENGTH SCALES OBTAINED FROM LDV DATA IN 22.4° LINE COORDINATES								
stations	δ (mm)	δ_1 (mm)	δ_2 (mm)	δ_3 (mm)	δ_4 (mm)	δ_5 (mm)	δ_6 (mm)	δ_7 (mm)
Station 5	40.0	6.17	5.26	4.85	-7.86	0.79	-7.07	-1.68
A	39.6	6.02	5.27	4.7	-6.9	0.57	-6.32	-1.38
B	39.9	5.95	5.26	4.64	-6.47	0.49	-5.98	-1.29
C	39.3	5.81	5.16	4.55	-6.08	0.41	-5.67	-1.21
D	39.2	5.71	5.09	4.48	-5.76	0.34	-5.42	-1.14
E	40.3	5.71	5.1	4.47	-5.35	0.27	-5.08	-1.11
TB	39.7	5.51	4.94	4.33	-4.74	0.17	-4.57	-1.02
TC	40.9	5.37	4.79	4.26	-4.49	0.14	-4.36	-1.02
R	39.2	5.01	4.42	3.99	-3.9	0.01	-3.89	-1.00
S	40.3	4.64	4.14	3.77	-3.22	-0.03	-3.26	-0.85
T	38.9	4.04	3.69	3.36	-2.53	-0.05	-2.59	-0.61
U	39.3	3.72	3.49	3.13	-1.78	-0.06	-1.84	-0.39
V	38.4	3.46	3.33	2.94	-1.20	-0.06	-1.25	-0.23
W	28.6	2.46	2.42	2.11	-0.31	-0.07	-0.38	-0.08
X	20.6	1.82	1.78	1.44	0.76	-0.09	0.67	-0.07

U_e =Velocity magnitude at the layer edge.

$\delta = y$ where $\sqrt{U^2+W^2}/U_e=0.995$ = Boundary Layer Thickness

$\delta_1 = \int_0^{\infty} (1 - \frac{U}{U_e}) dy$ = Streamwise Displacement Thickness

$\delta_2 = \int_0^{\infty} (1 - \frac{\sqrt{U^2+W^2}}{U_e}) dy$ = Magnitude Displacement Thickness

$\delta_3 = \int_0^{\infty} (1 - \frac{U}{U_e}) \frac{U}{U_e} dy$ = Streamwise Momentum Thickness

$\delta_4 = \int_0^{\infty} (-\frac{W}{U_e}) dy$ = Lateral Displacement Thickness

$\delta_5 = \int_0^{\infty} \frac{W}{U_e} (1 - \frac{U}{U_e}) dy$ = Lateral Momentum Thickness

$\delta_6 = \int_0^{\infty} -\frac{WU}{U_e^2} dy$ = Cross Product Momentum Thickness

$\delta_7 = \int_0^{\infty} -\frac{W^2}{U_e^2} dy$ = Crossflow Momentum Thickness

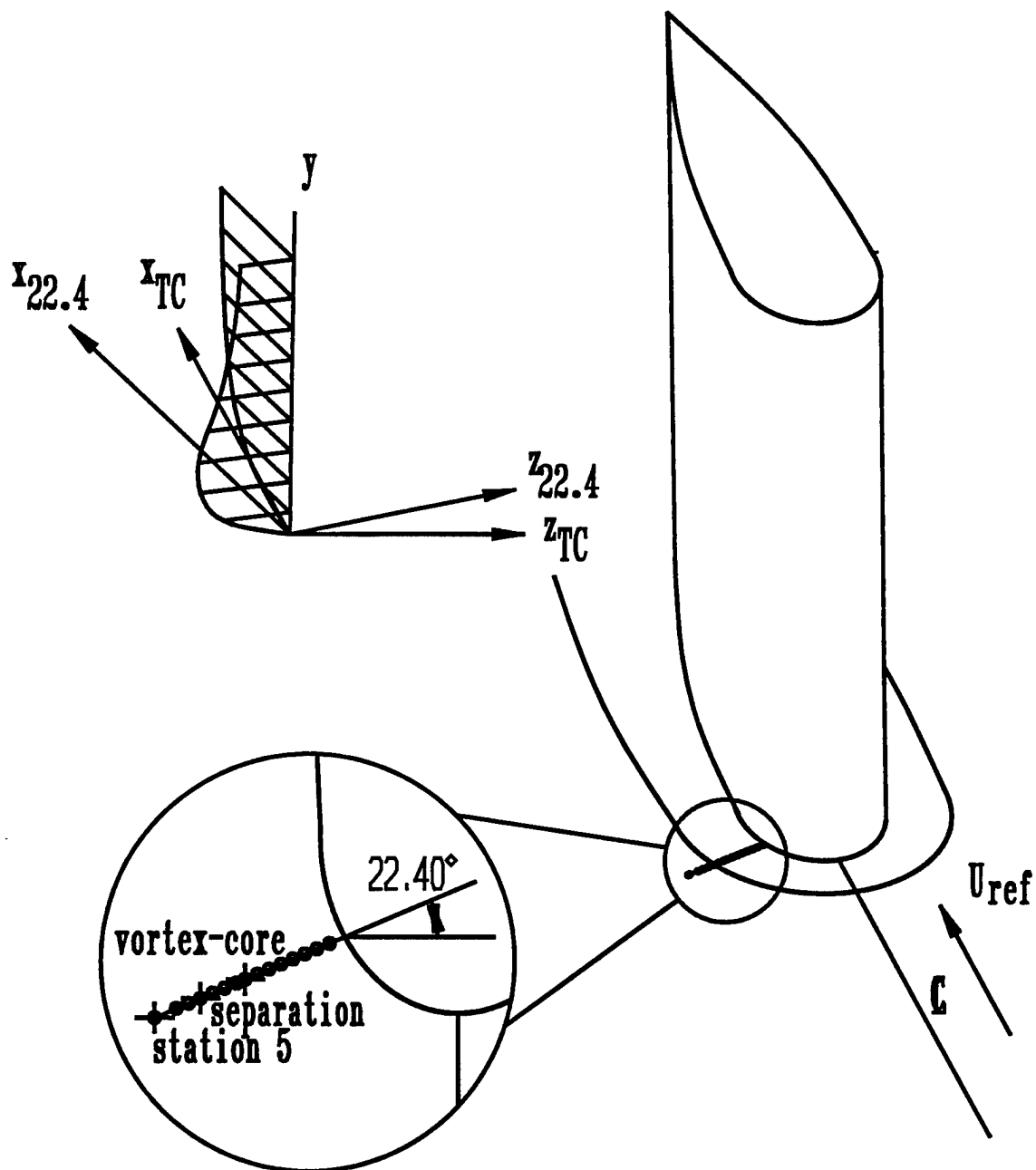


Figure 1. Measurement locations and definitions of coordinate systems. "s" direction same as " $z_{22.4}$ ".

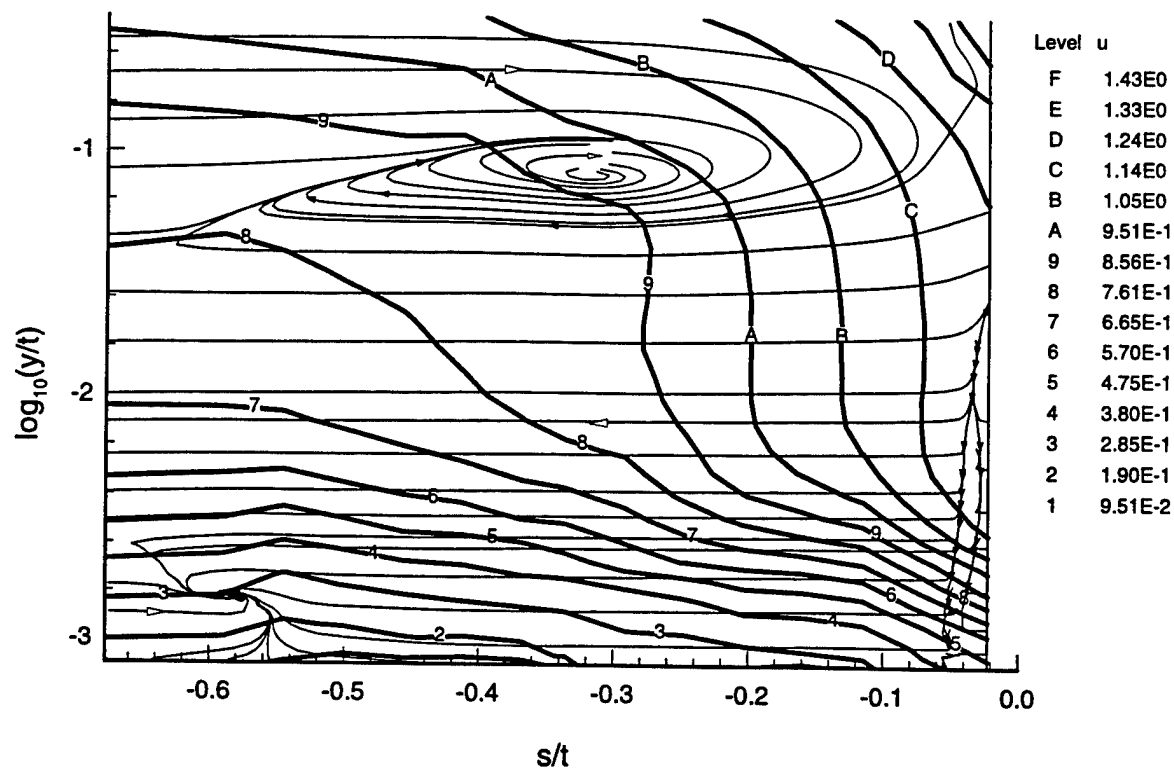


Figure 2. U/U_{ref} velocity magnitude contours and secondary flow streamlines.

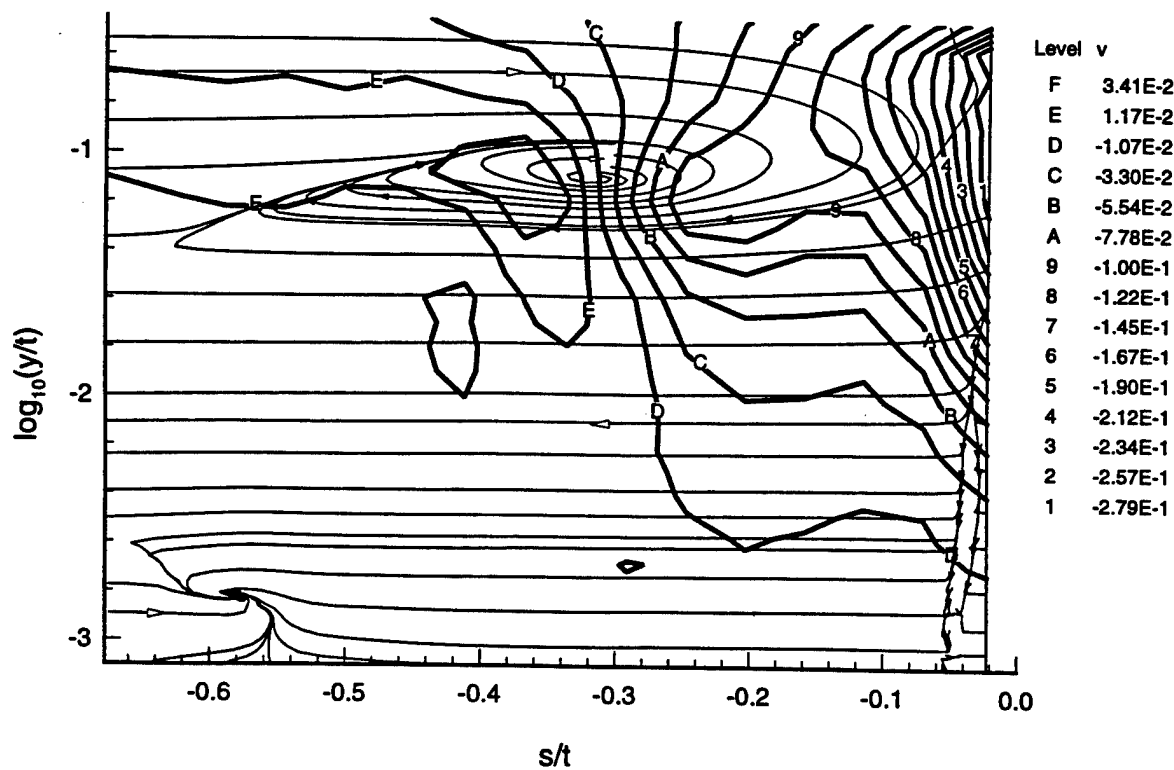


Figure 3. V/U_{ref} velocity magnitude contours and secondary flow streamlines.

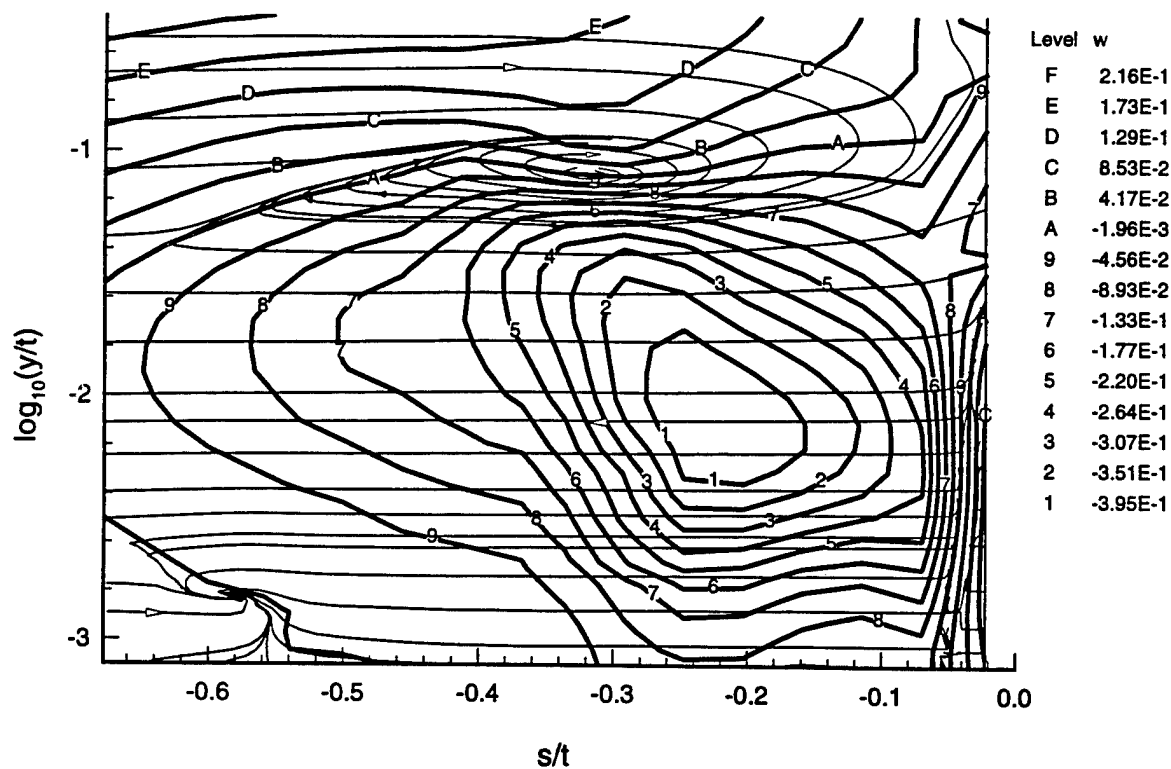


Figure 4. W/U_{ref} velocity magnitude contours and secondary flow streamlines.

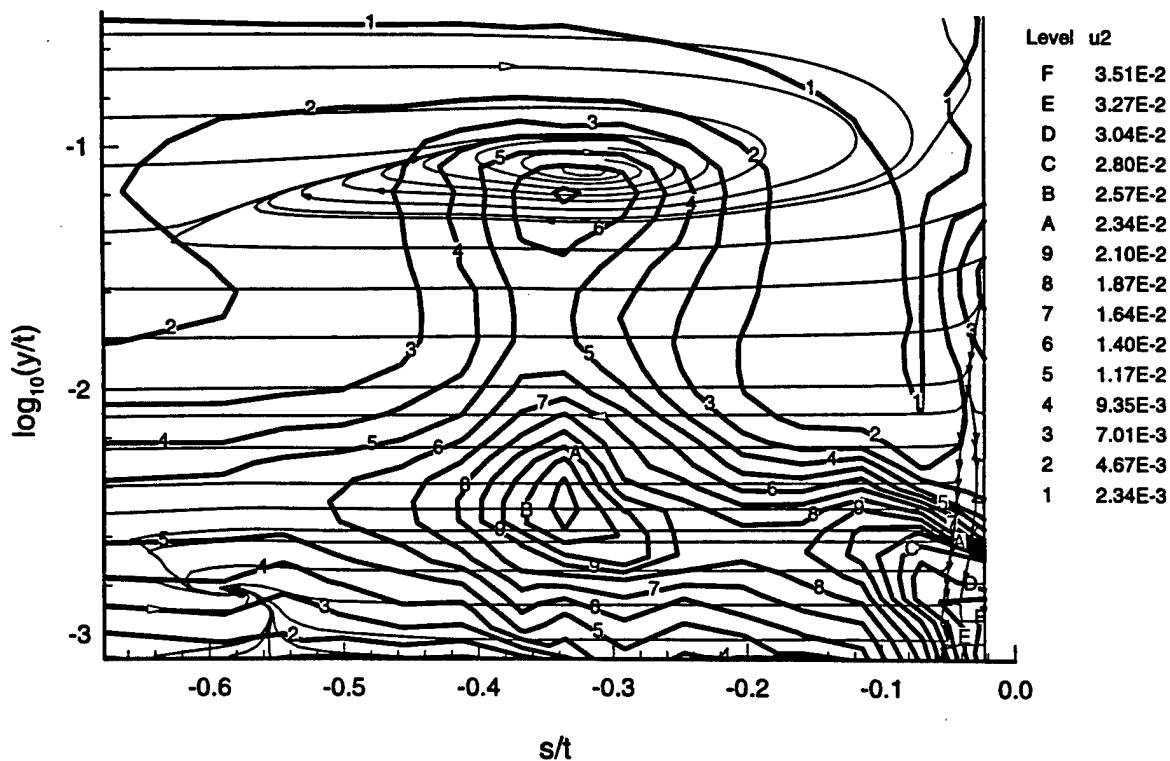


Figure 5. $\overline{U^2}/U_{ref}^2$ normal stress contours and secondary flow streamlines.

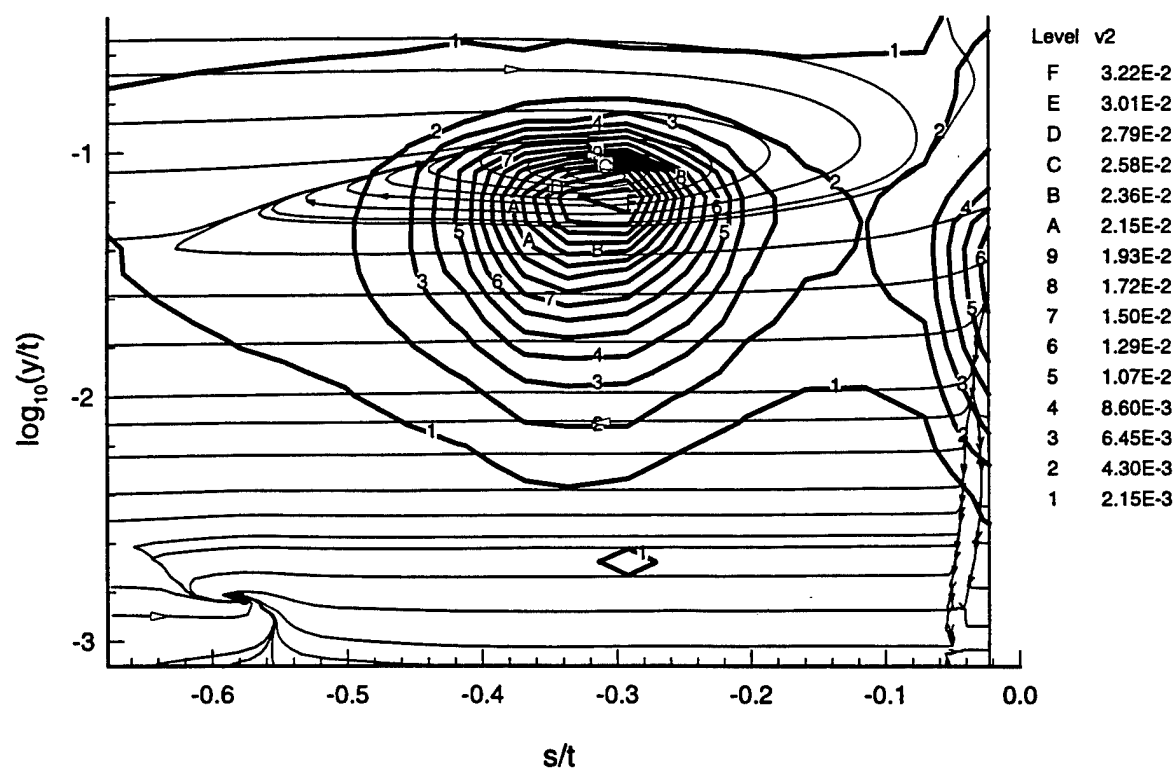


Figure 6. $\overline{v^2}/U_{ref}^2$ normal stress contours and secondary flow streamlines.

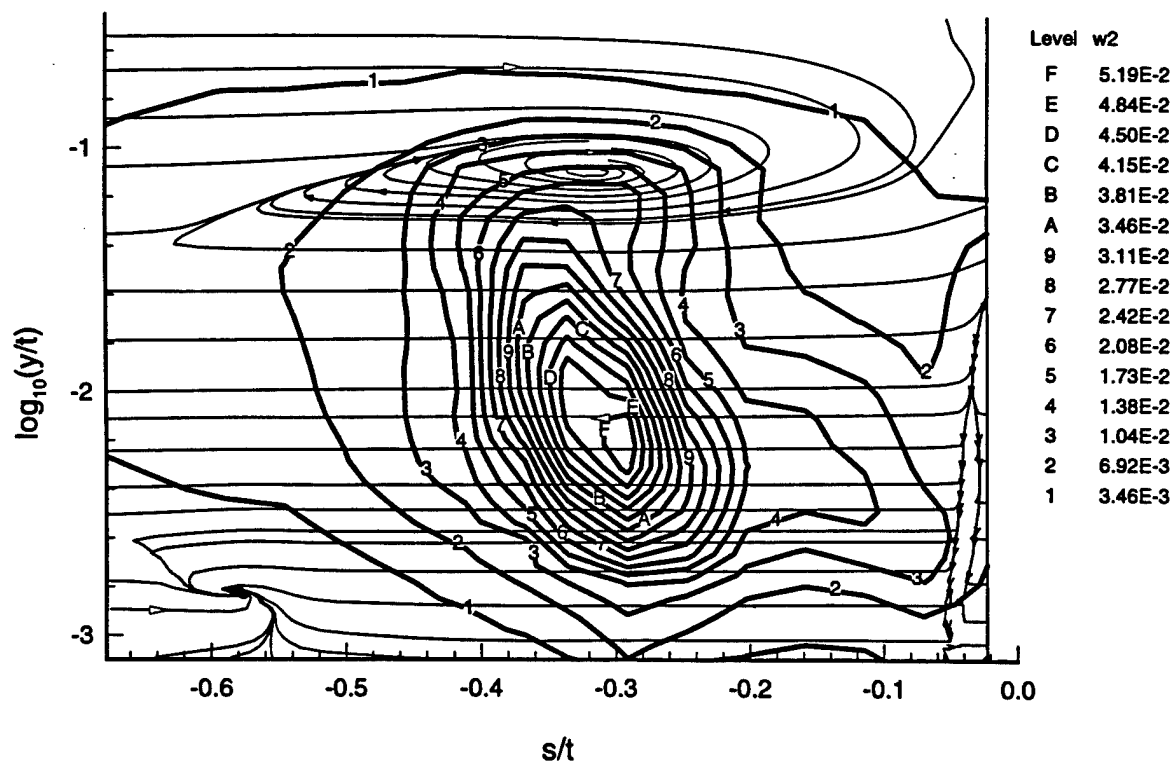


Figure 7. $\overline{w^2}/U_{ref}^2$ normal stress contours and secondary flow streamlines.

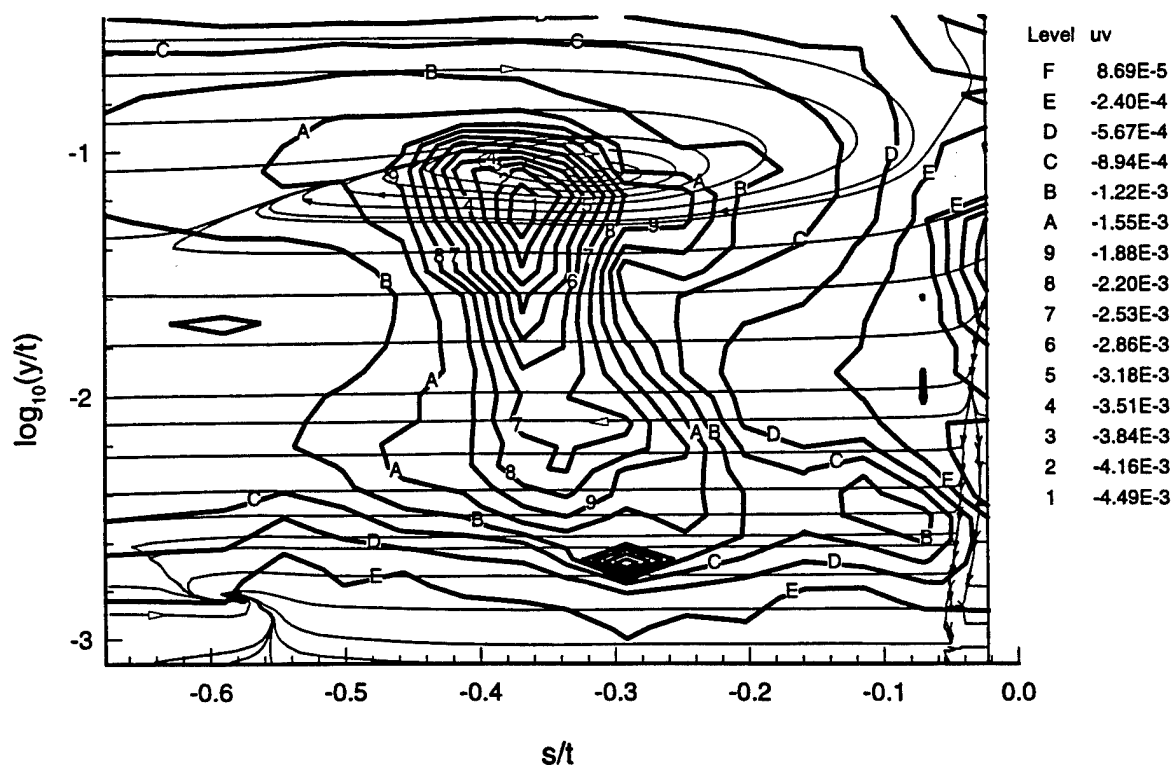


Figure 8. \overline{uv}/U_{ref}^2 shear stress contours and secondary flow streamlines.

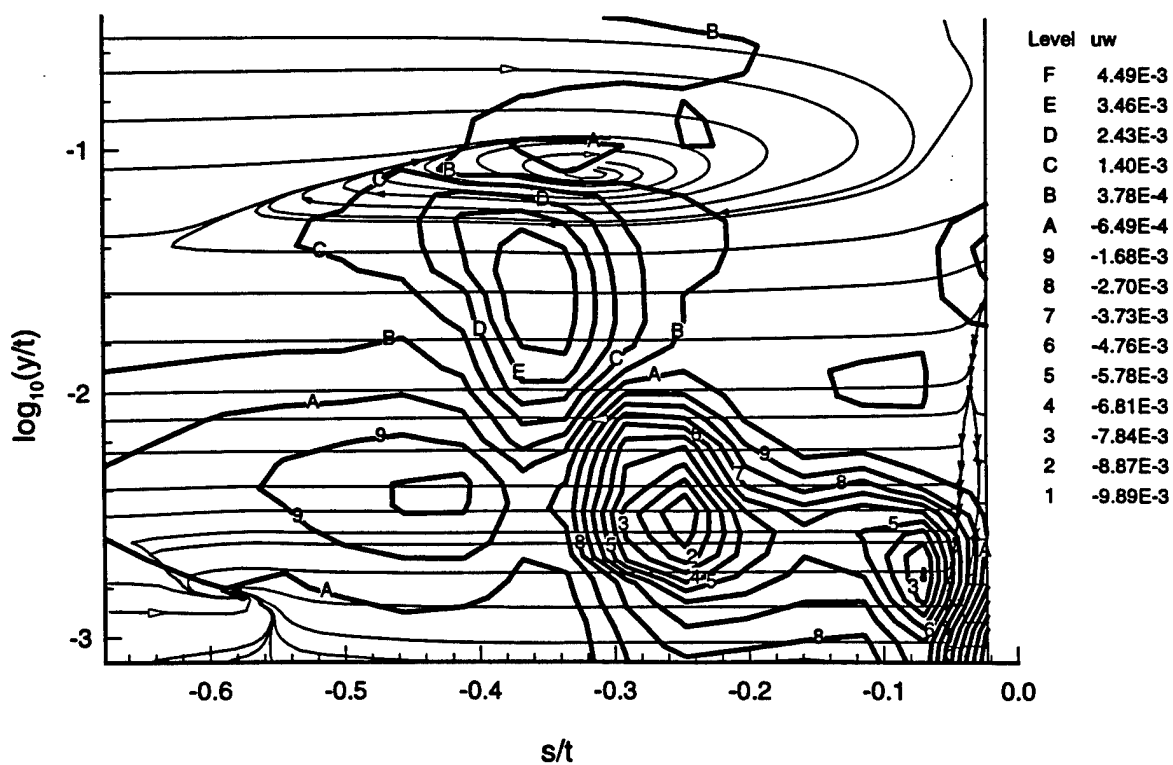


Figure 9. \overline{uw}/U_{ref}^2 shear stress contours and secondary flow streamlines.

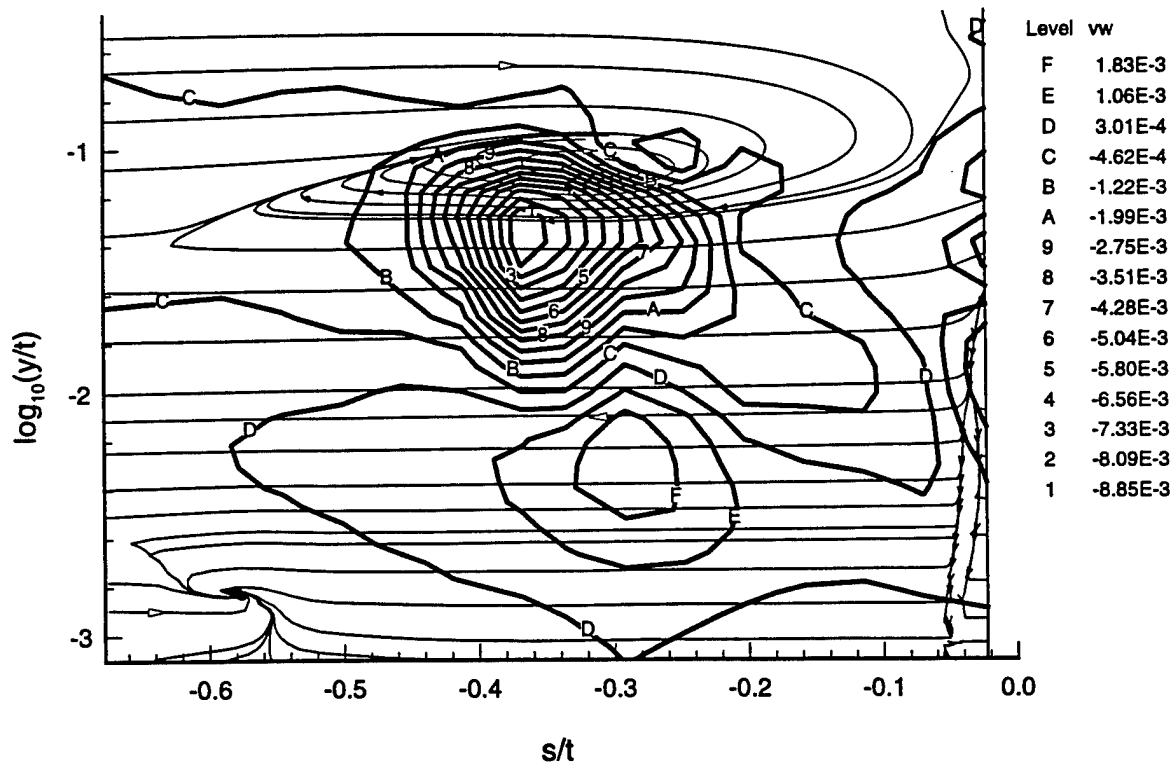


Figure 10. \overline{vw}/U_{ref}^2 shear stress contours and secondary flow streamlines.

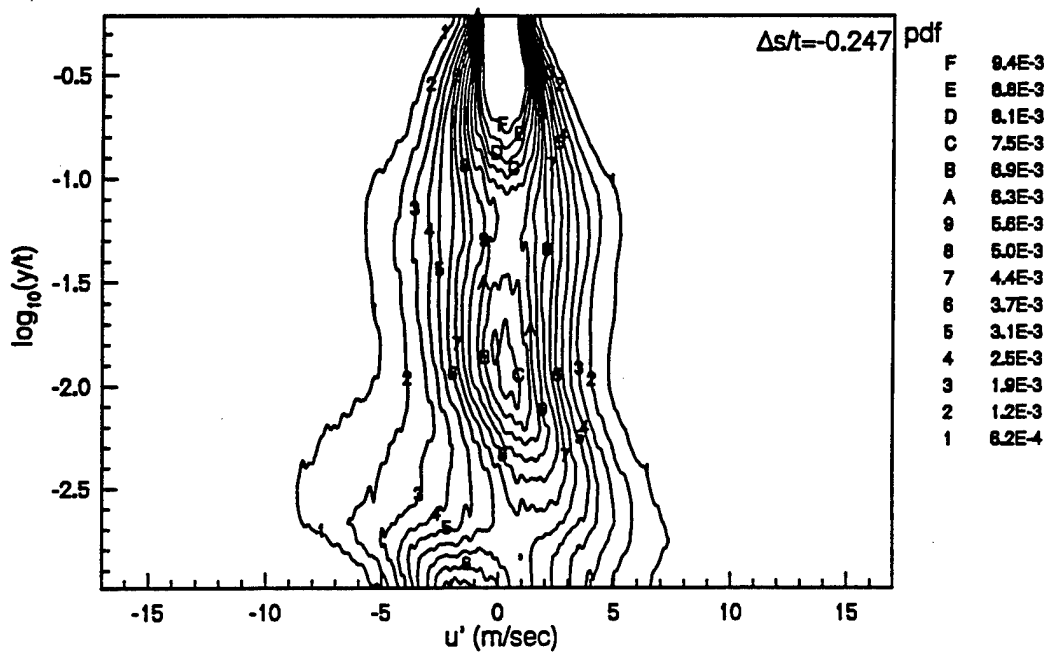


Figure 11a. Probability density function of u fluctuating velocity at $s/t = -0.247$.

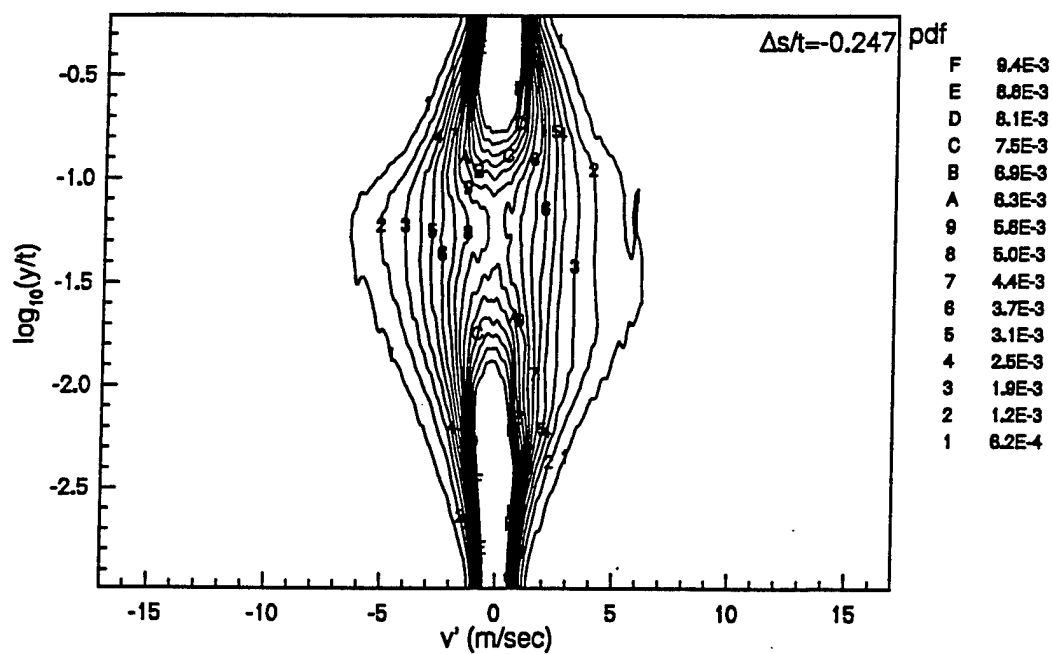


Figure 11b. Probability density function of v fluctuating velocity at $s/t = -0.247$.

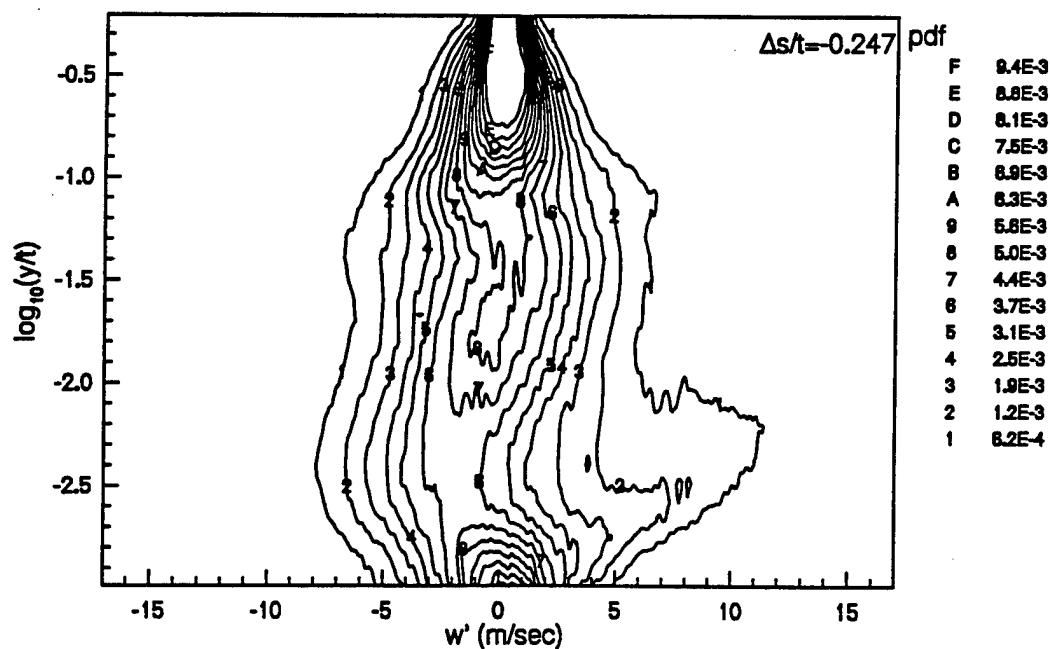


Figure 11c. Probability density function of w fluctuating velocity at $s/t = -0.247$.

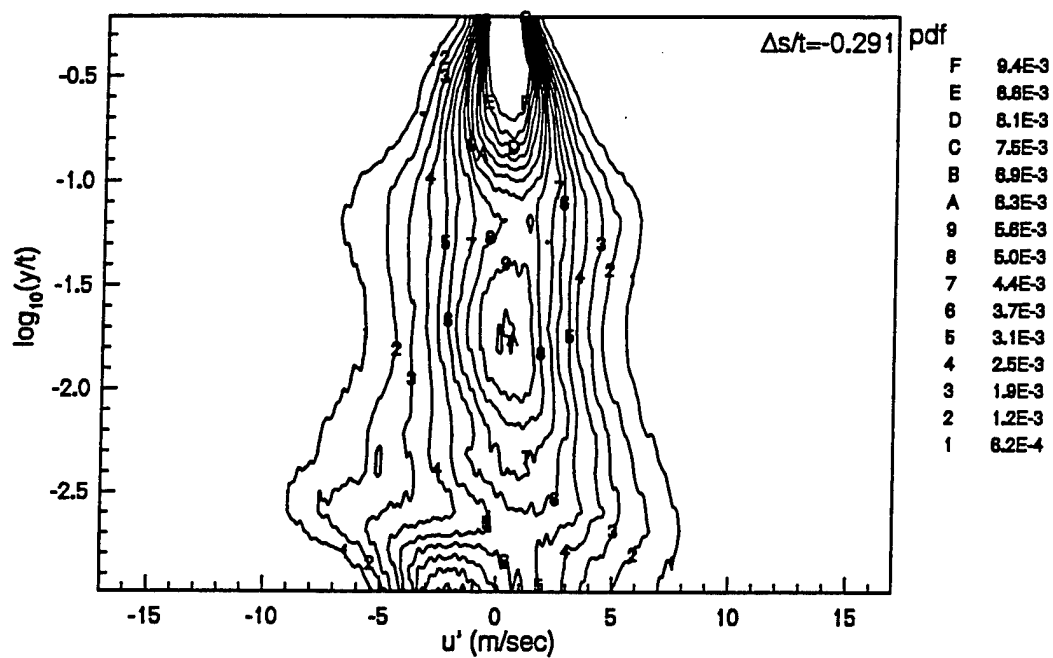


Figure 12a. Probability density function of u fluctuating velocity at $s/t = -0.291$.

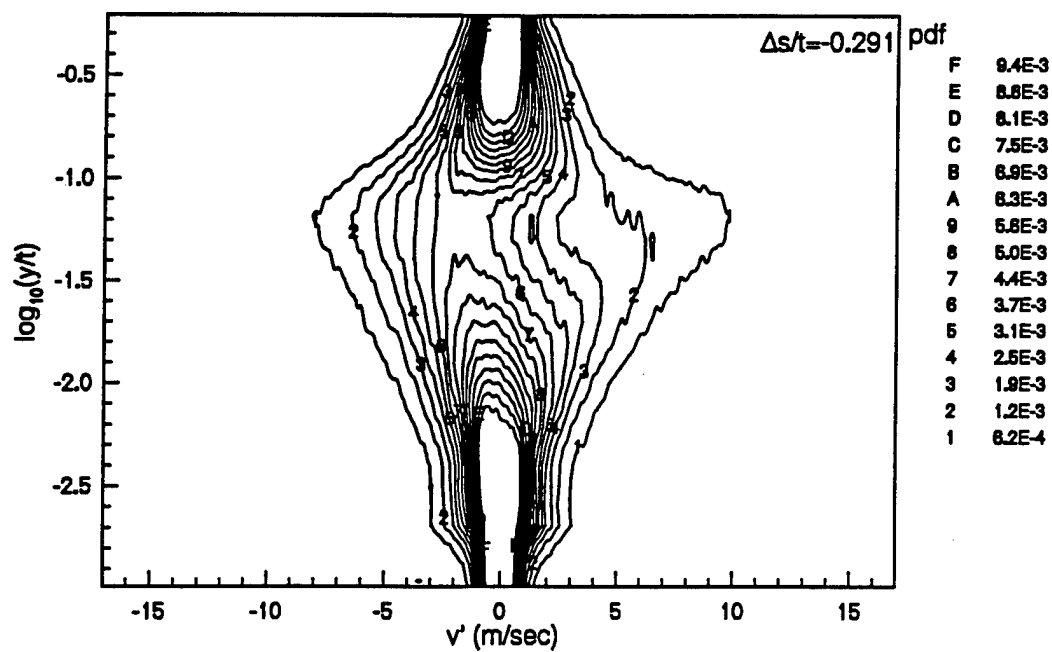


Figure 12b. Probability density function of v fluctuating velocity at $s/t = -0.291$.

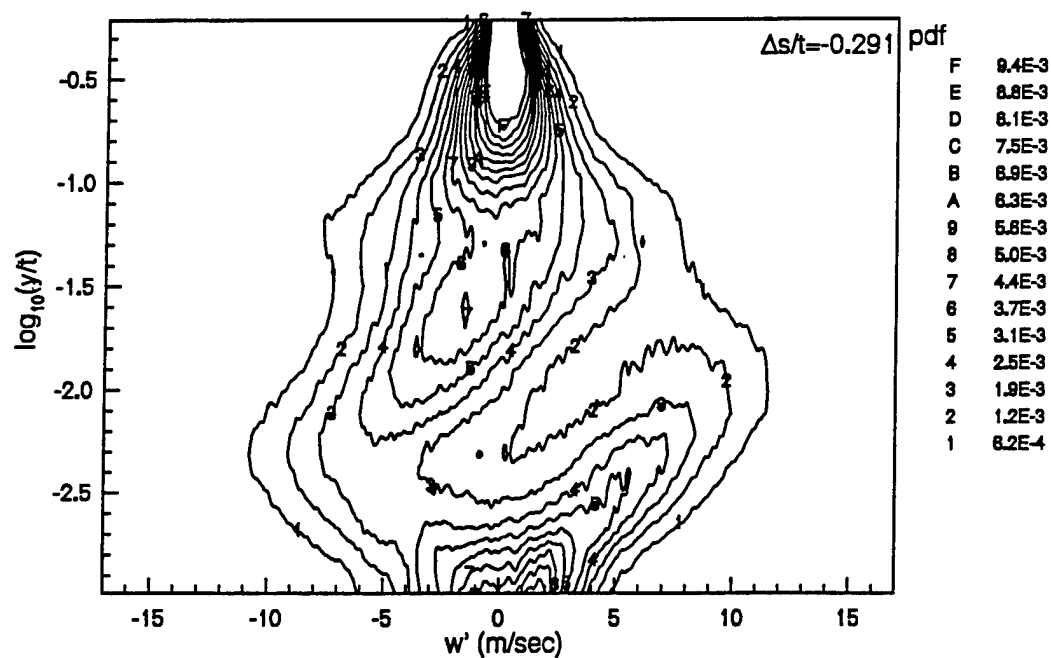


Figure 12c. Probability density function of w fluctuating velocity at $s/t = -0.291$.

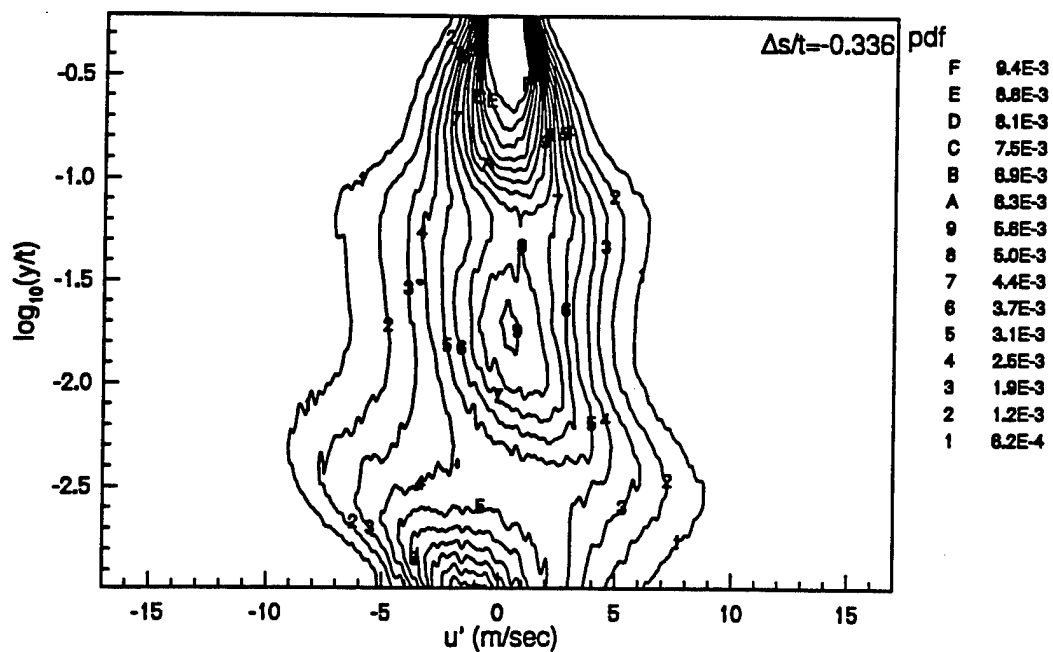


Figure 13a. Probability density function of u fluctuating velocity at $s/t = -0.336$.

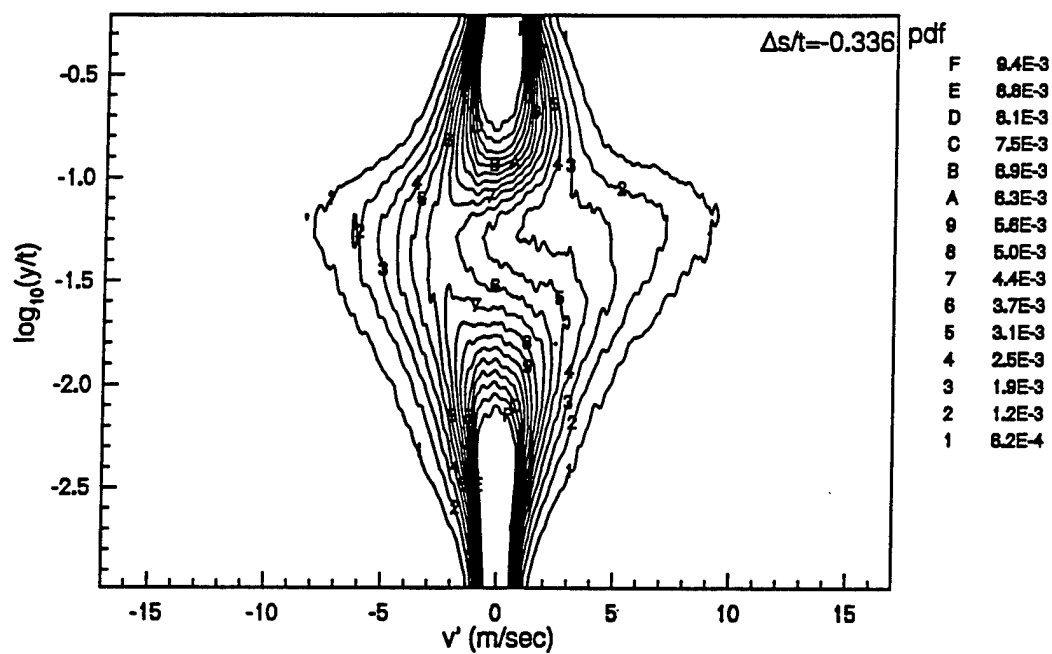


Figure 13b. Probability density function of v fluctuating velocity at $s/t = -0.336$.

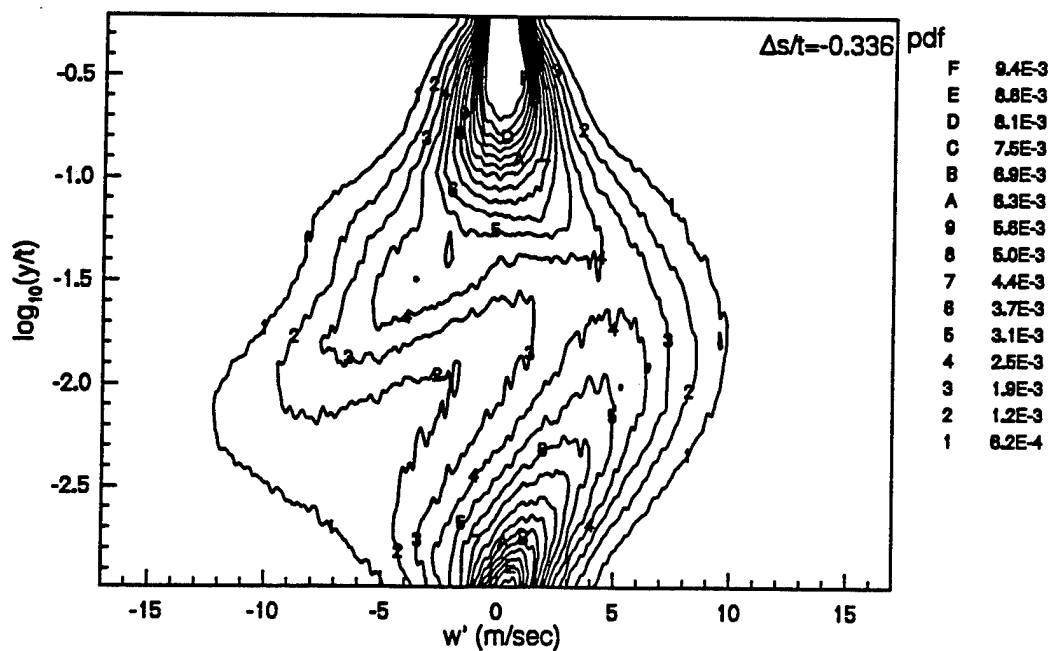


Figure 13c. Probability density function of w fluctuating velocity at $s/t = -0.336$.

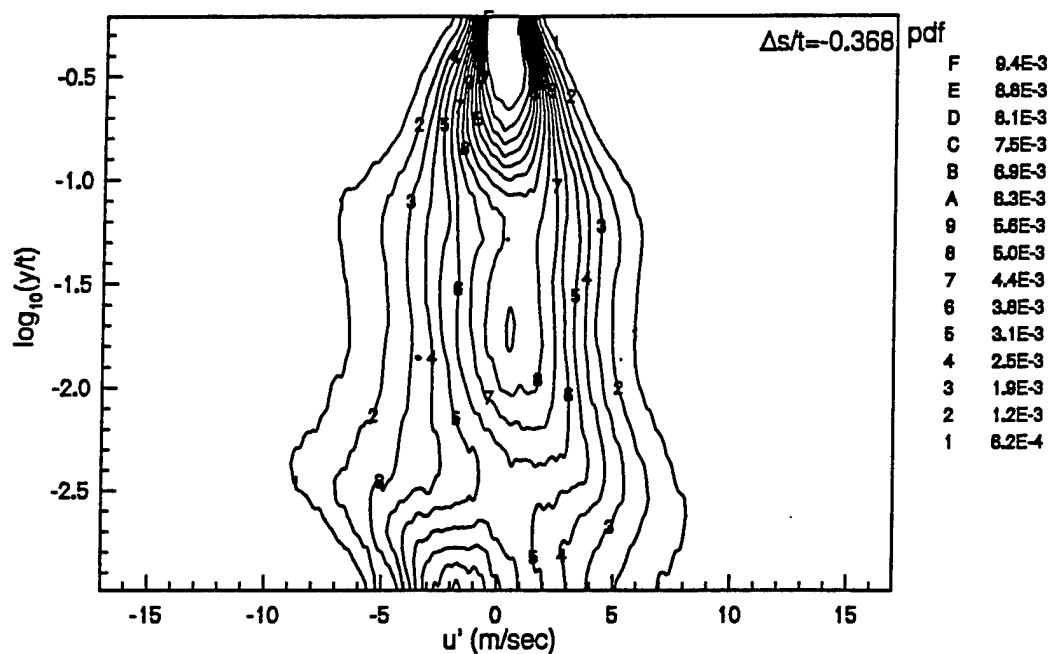


Figure 14a. Probability density function of u fluctuating velocity at $s/t = -0.368$.

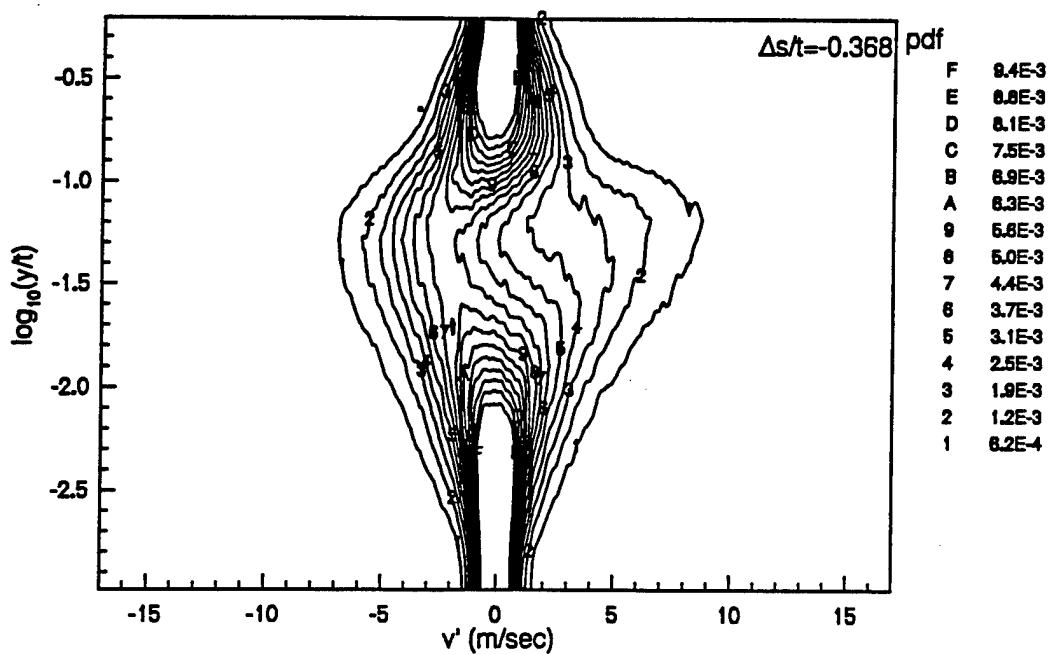


Figure 14b. Probability density function of v fluctuating velocity at $s/t = -0.368$.

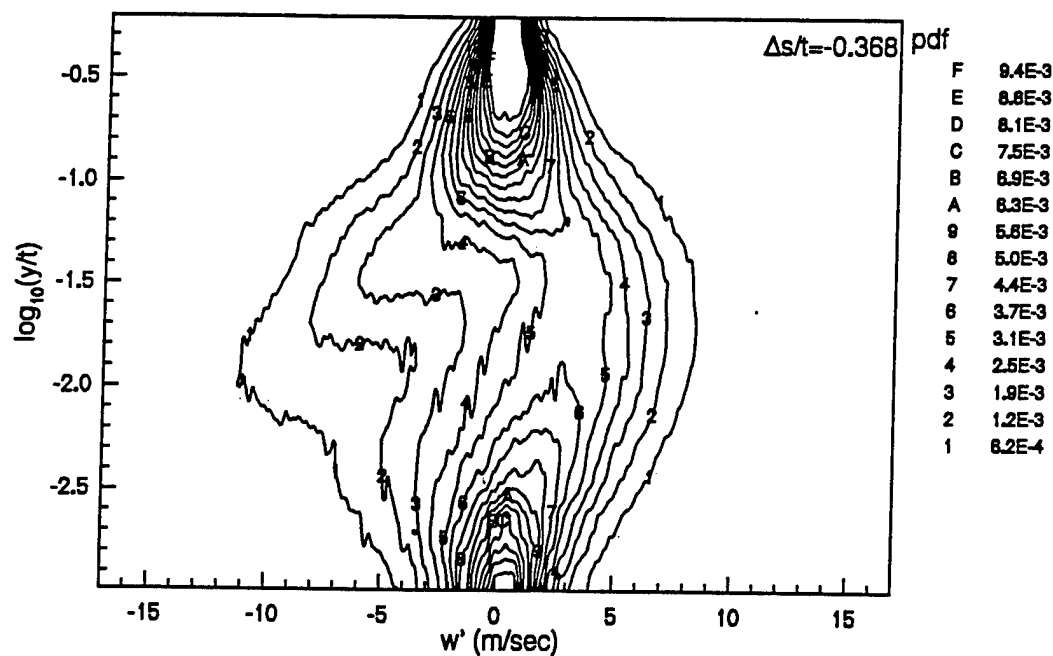


Figure 14c. Probability density function of w fluctuating velocity at $s/t = -0.368$.

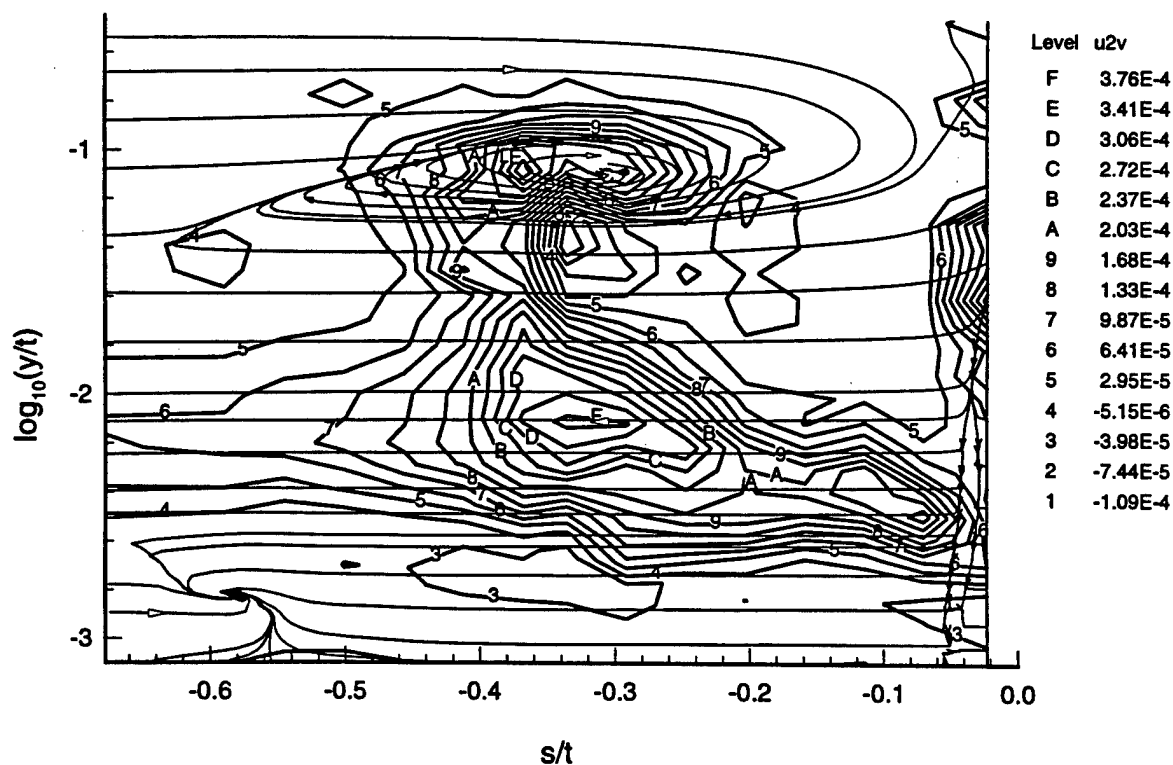


Figure 15. $\overline{U^2v} / U_{ref}^3$ triple product contours and secondary flow streamlines.

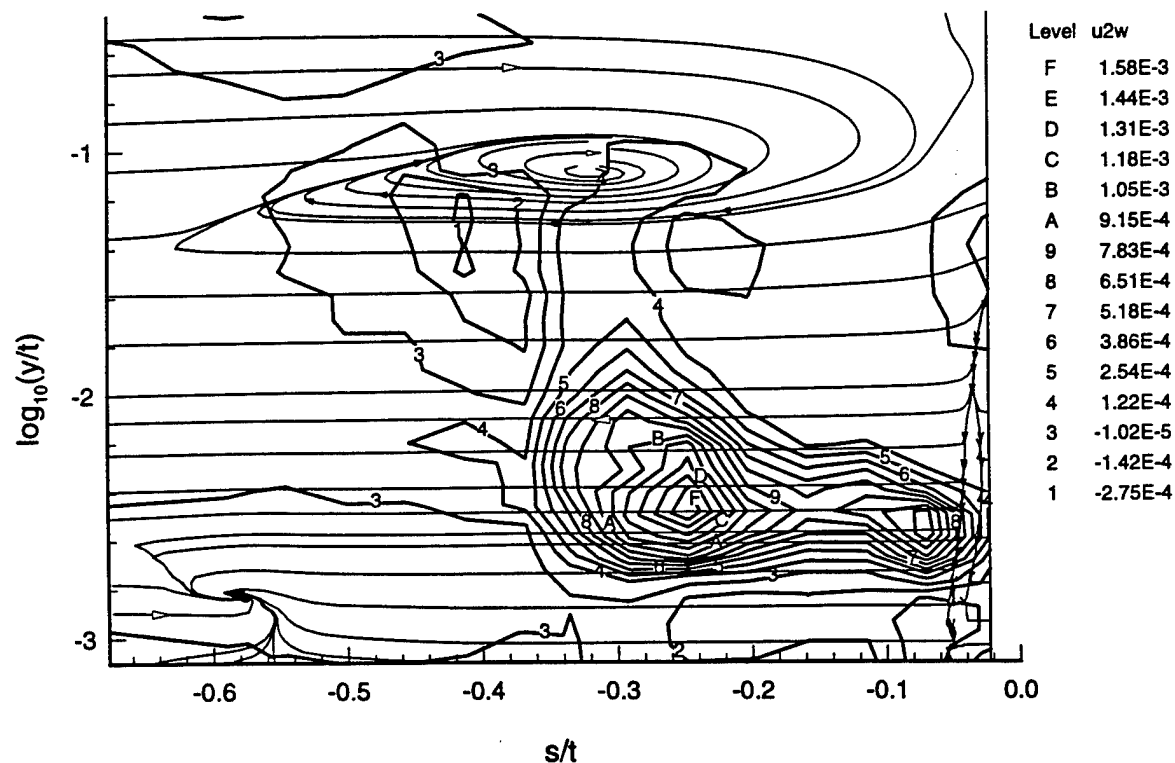


Figure 16. $\overline{u^2 w} / U_{ref}^3$ triple product contours and secondary flow streamlines.

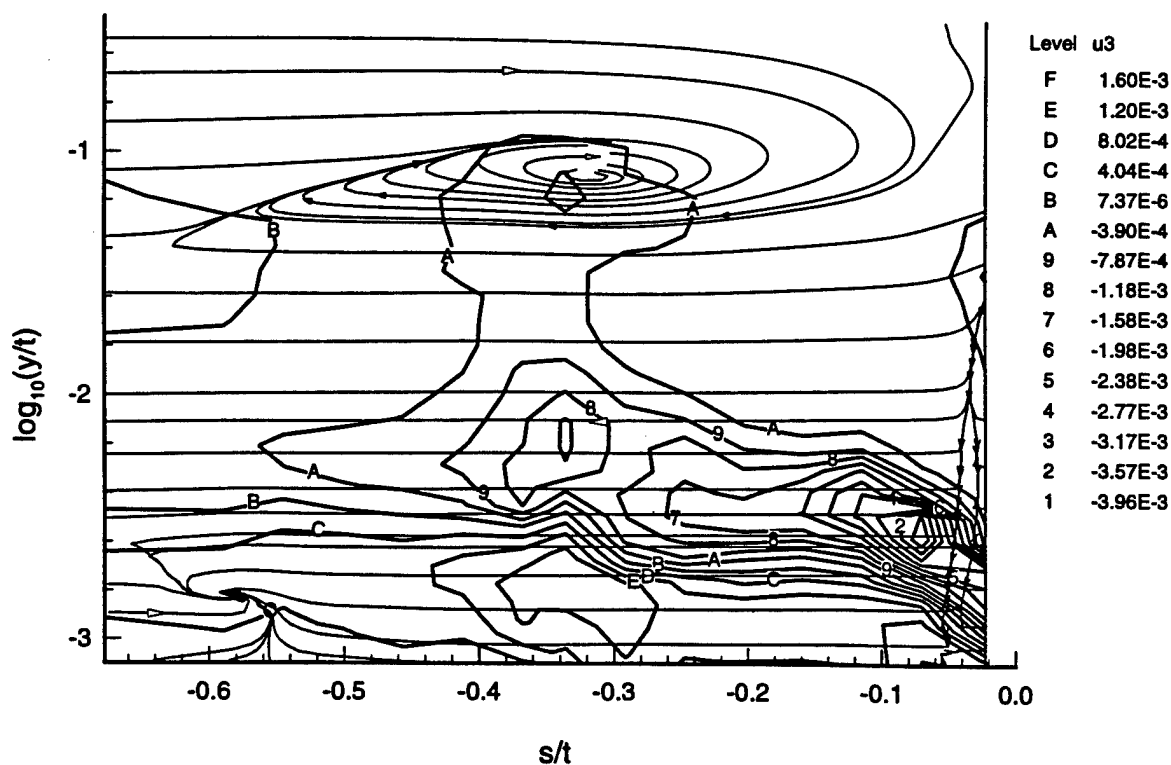


Figure 17. $\overline{u^3} / U_{ref}^3$ triple product contours and secondary flow streamlines.

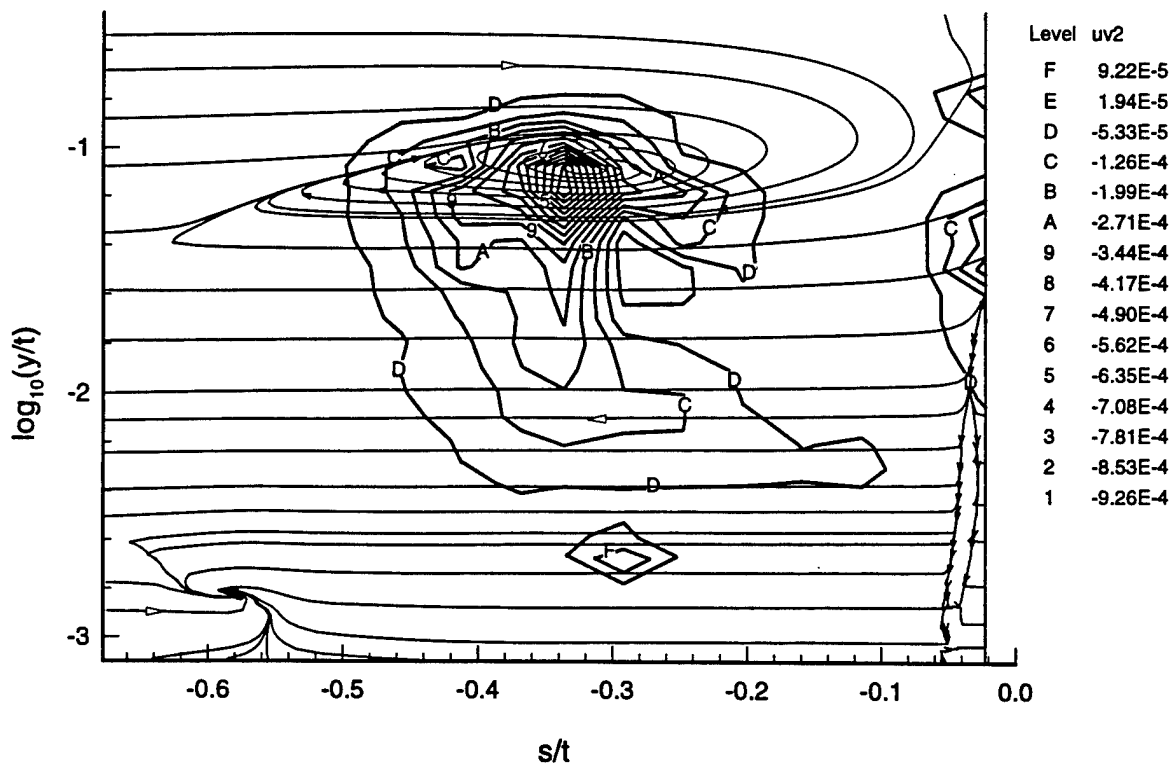


Figure 18. $\overline{uv^2}/U_{ref}^3$ triple product contours and secondary flow streamlines.

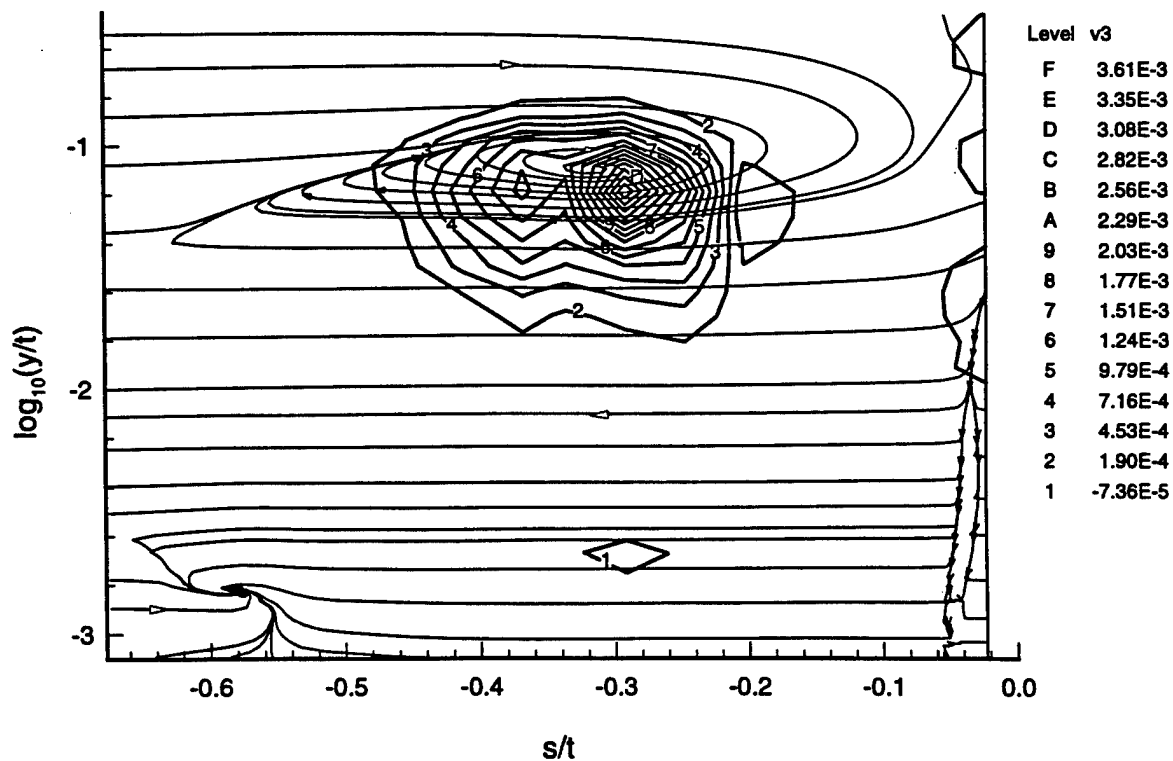


Figure 19. $\overline{v^3}/U_{ref}^3$ triple product contours and secondary flow streamlines.

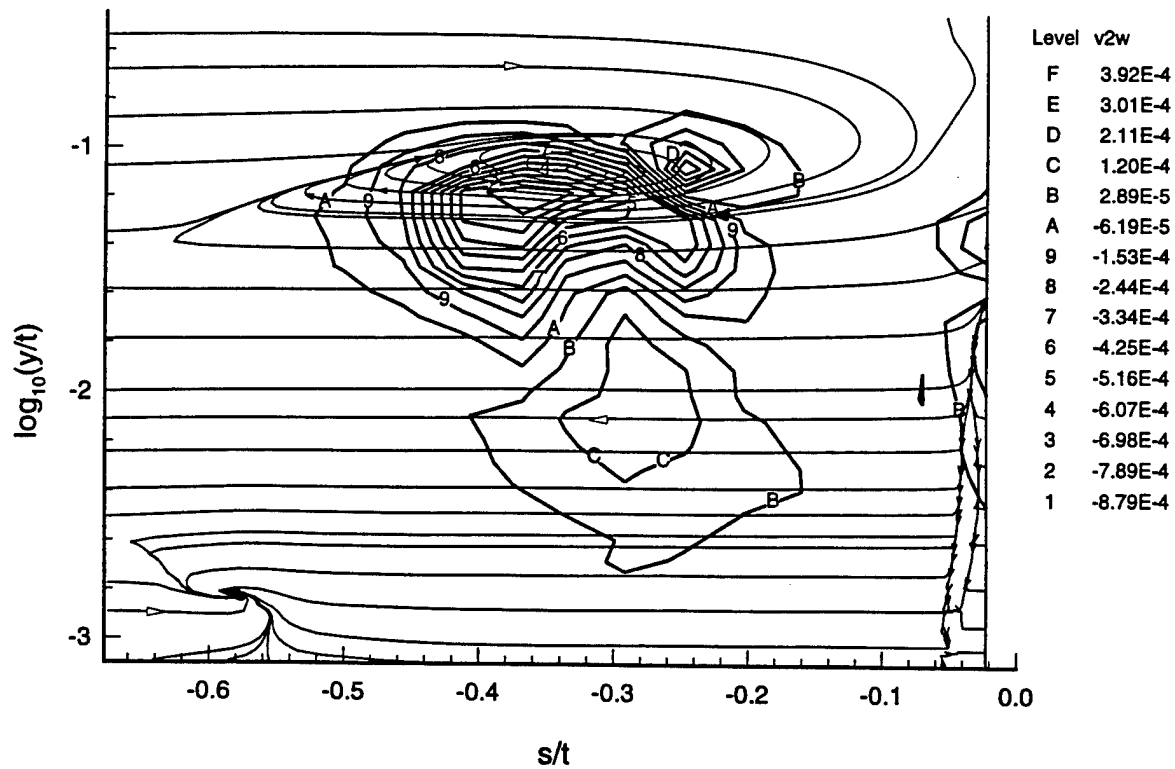


Figure 20. $\overline{v^2 w} / U_{ref}^3$ triple product contours and secondary flow streamlines.

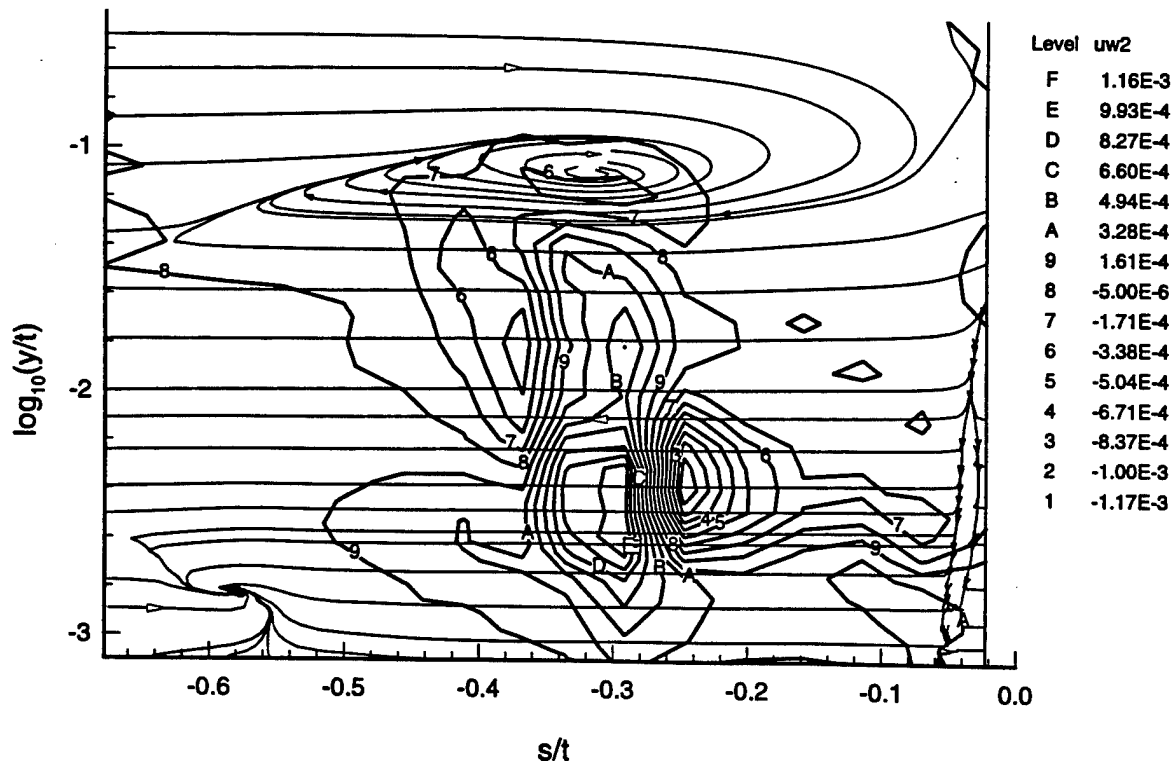


Figure 21. $\overline{u w^2} / U_{ref}^3$ triple product contours and secondary flow streamlines.

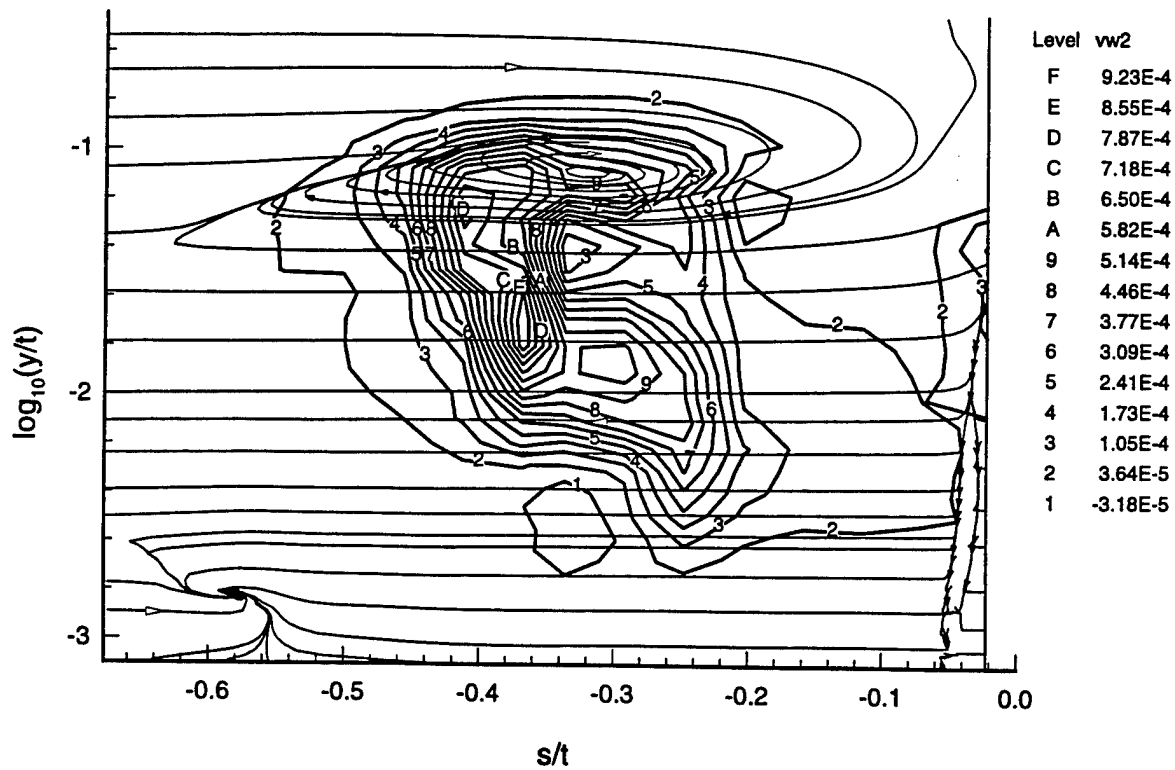


Figure 22. $\overline{vw^2}/U_{ref}^3$ triple product contours and secondary flow streamlines.

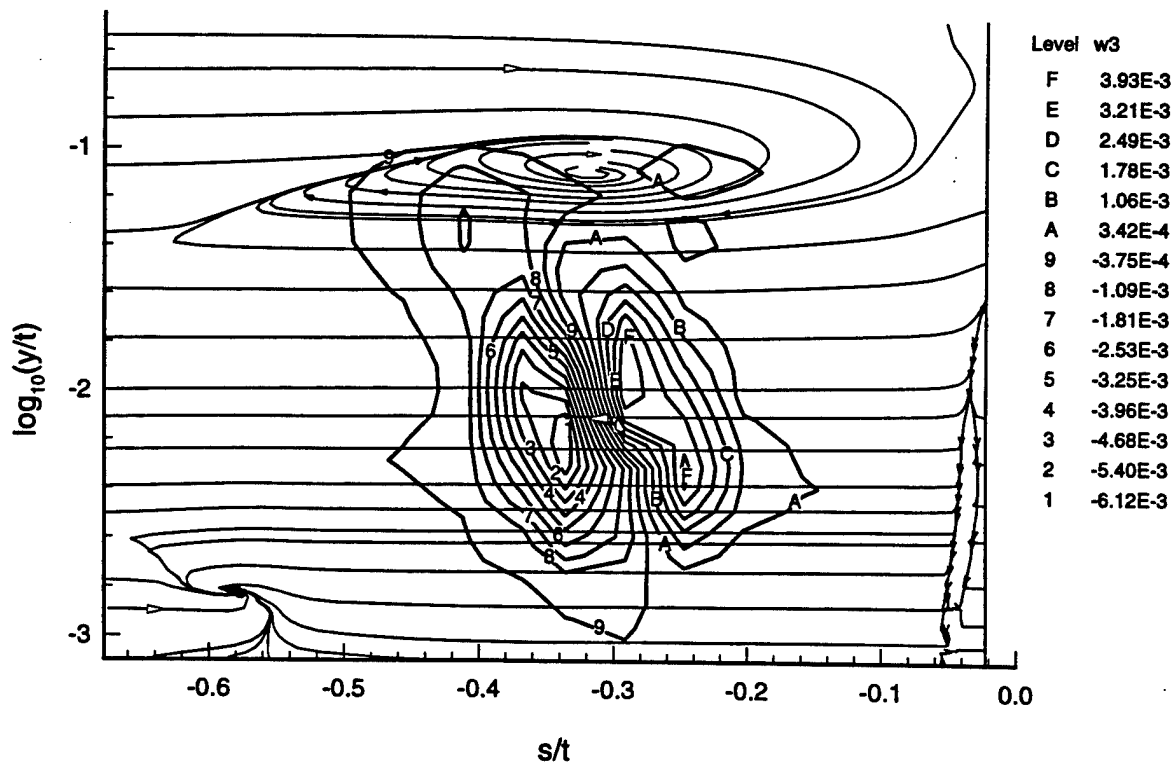


Figure 23. $\overline{w^3}/U_{ref}^3$ triple product contours and secondary flow streamlines.

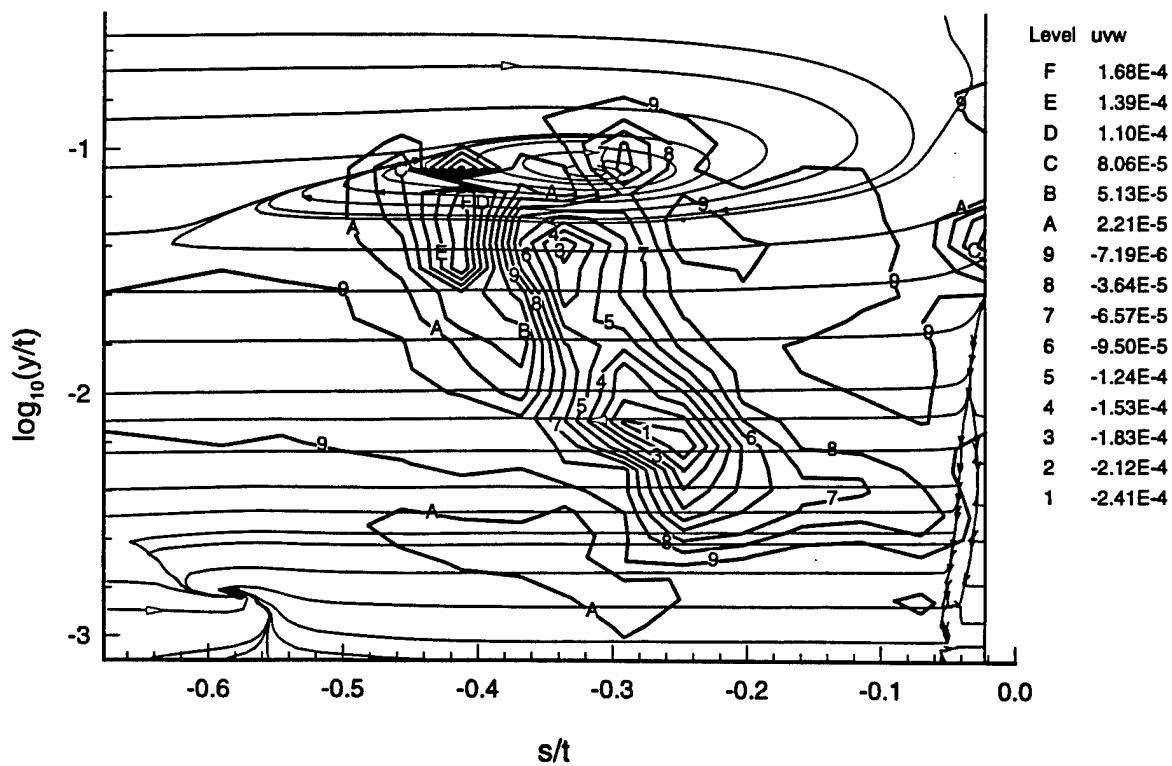


Figure 24. \overline{uvw}/U_{ref}^3 triple product contours and secondary flow streamlines.

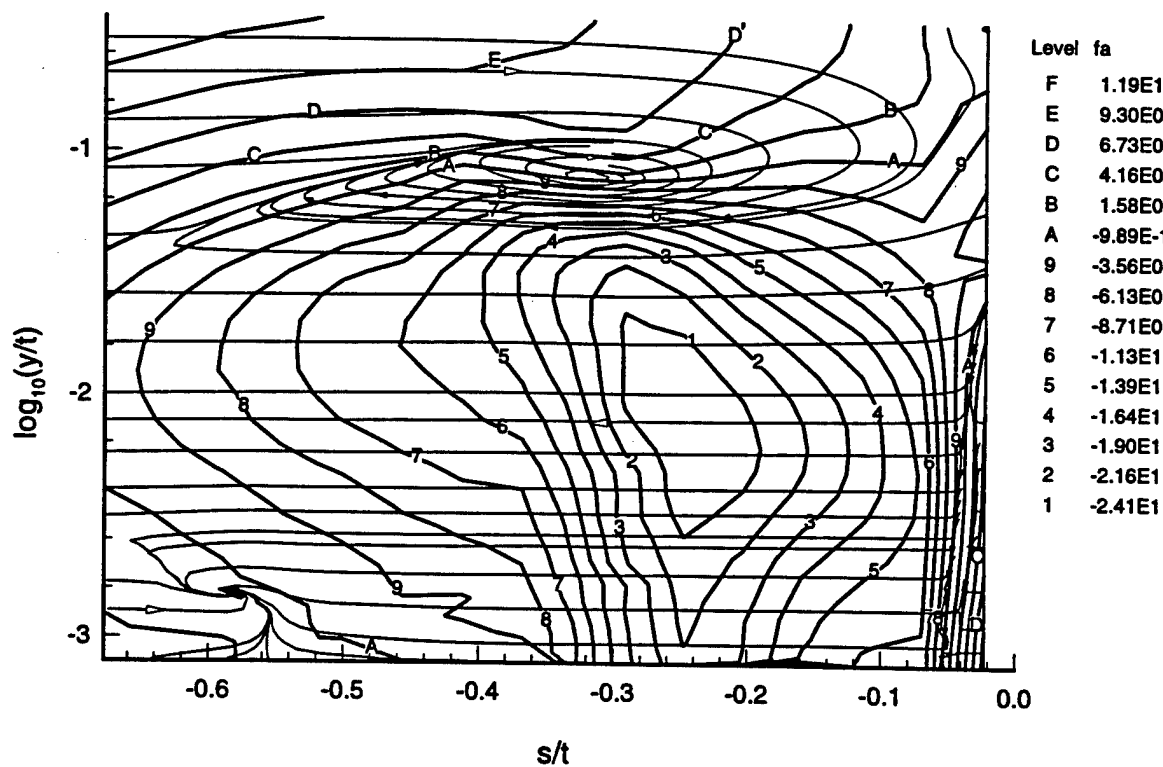


Figure 25. Flow angle (degrees) contours and secondary flow streamlines.

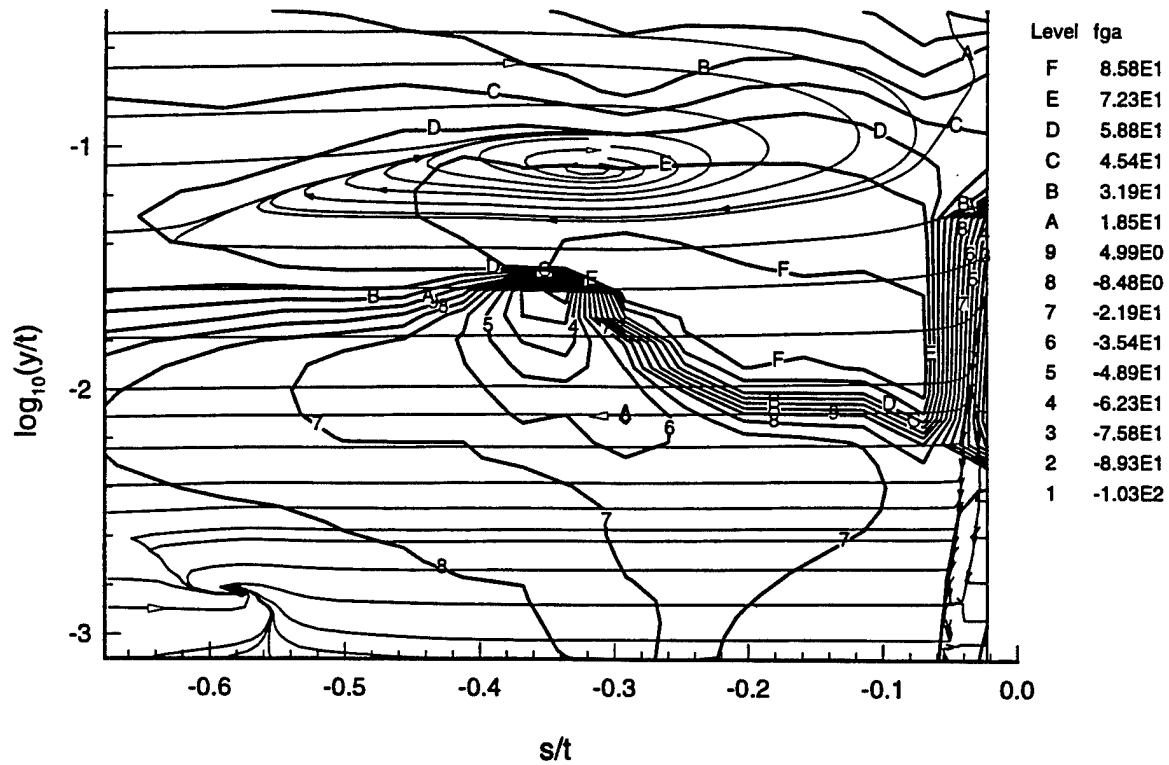


Figure 26. Flow gradient angle (degrees) contours and secondary flow streamlines.

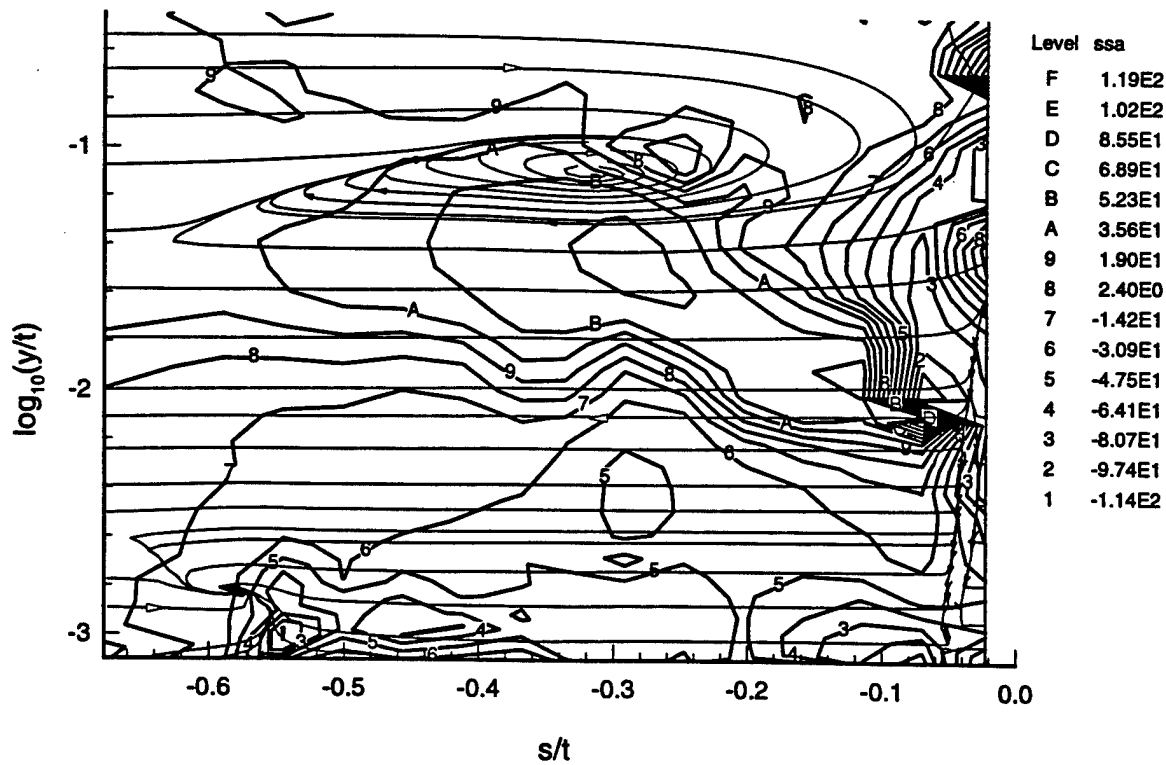


Figure 27. Shear stress angle (degrees) contours and secondary flow streamlines.

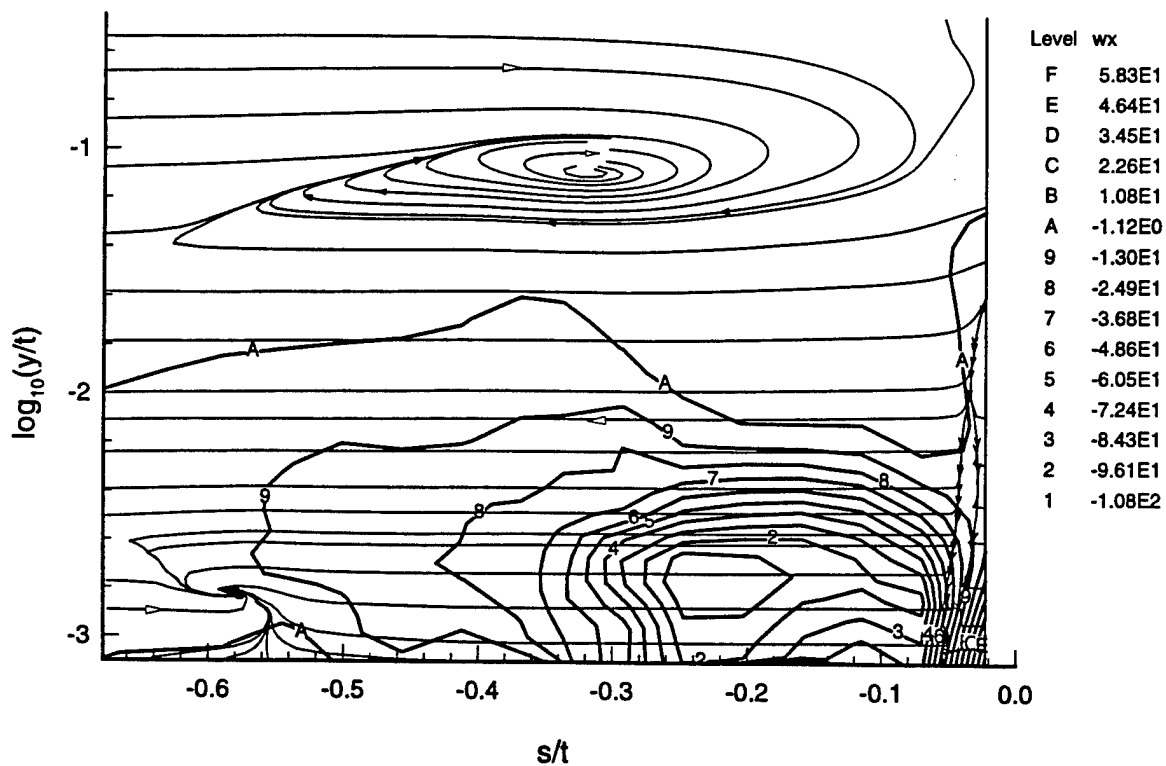


Figure 28. $\omega_x = \frac{\partial W}{\partial y} \frac{t}{U_{ref}}$ vorticity vector component contours and secondary flow streamlines.

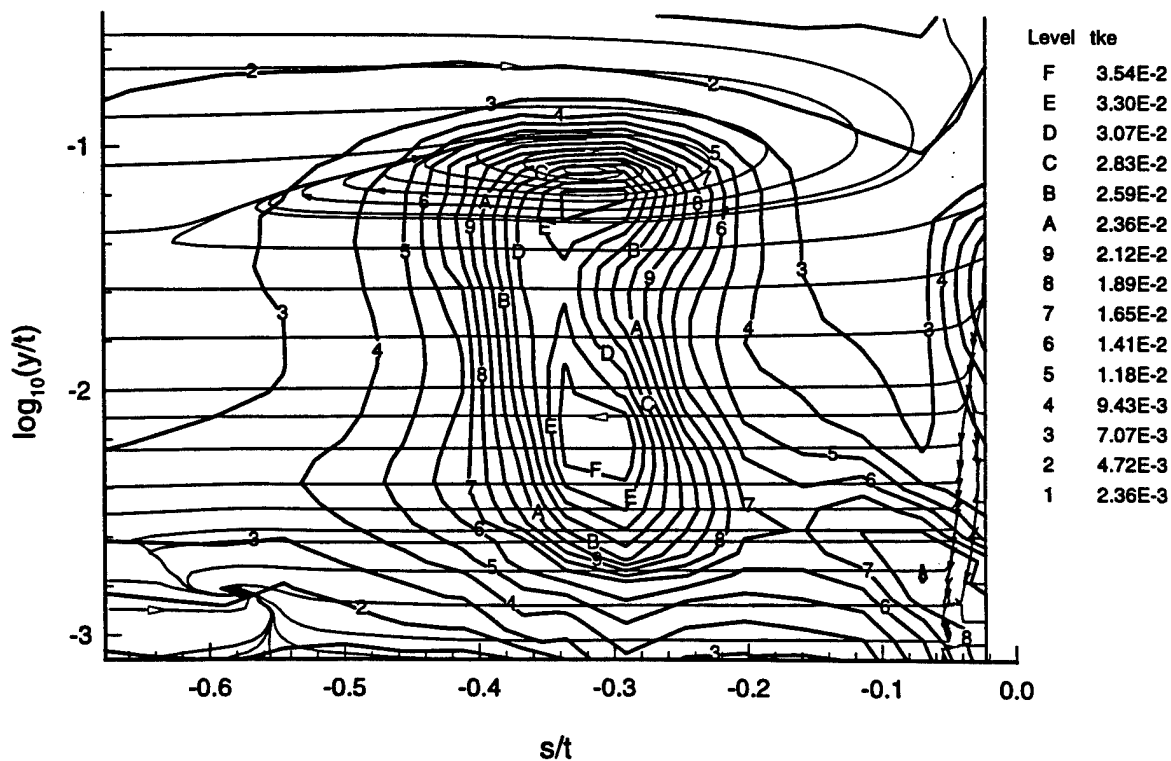


Figure 29. Turbulent kinetic energy/ U_{ref}^2 contours and secondary flow streamlines.

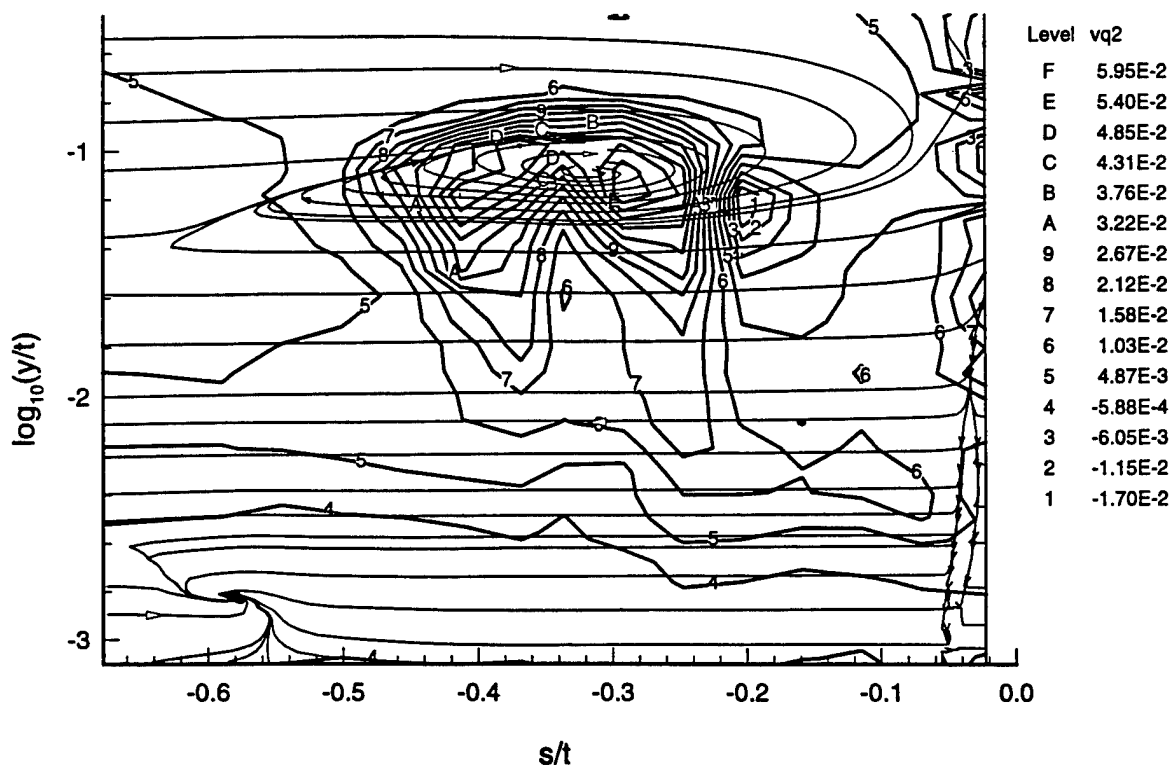


Figure 30. V_{q^2}/U_{ref} transport velocity of turbulent kinetic energy contours and secondary flow streamlines.

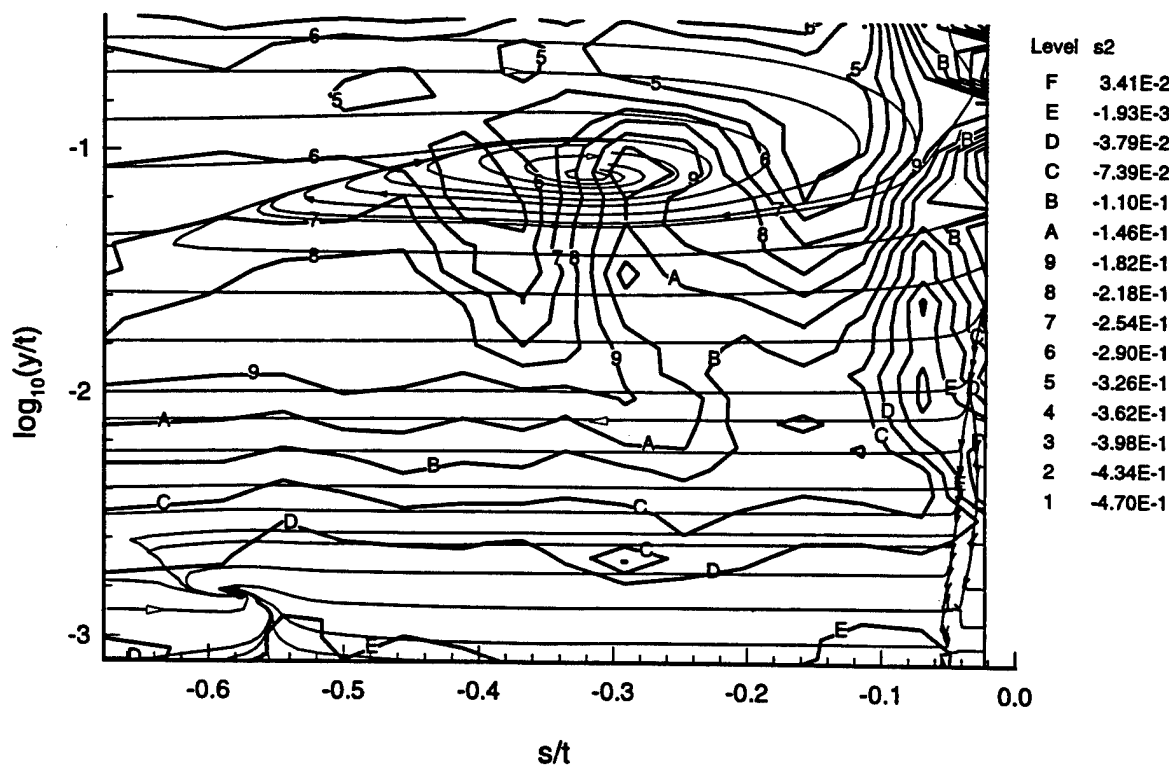


Figure 31. $S_2 = \overline{uv}/\overline{u^2}$ structural parameter contours and secondary flow streamlines.

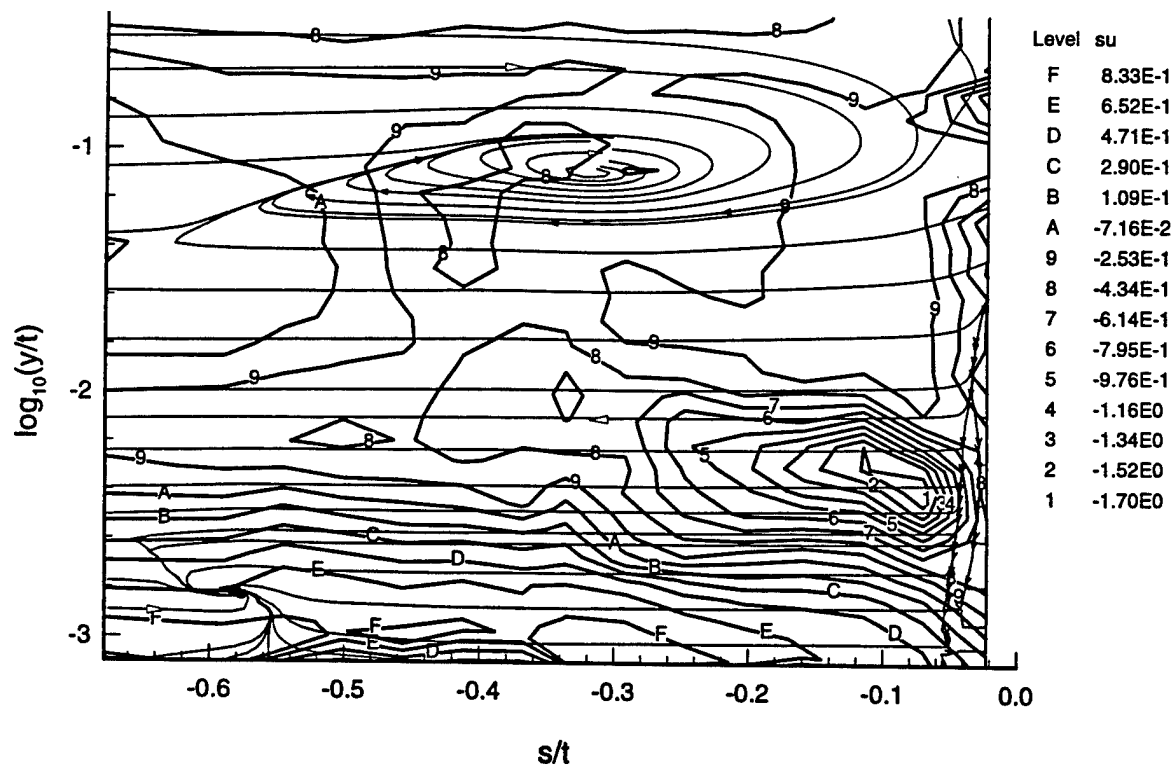


Figure 32. Skewness of u structural parameter contours and secondary flow streamlines.

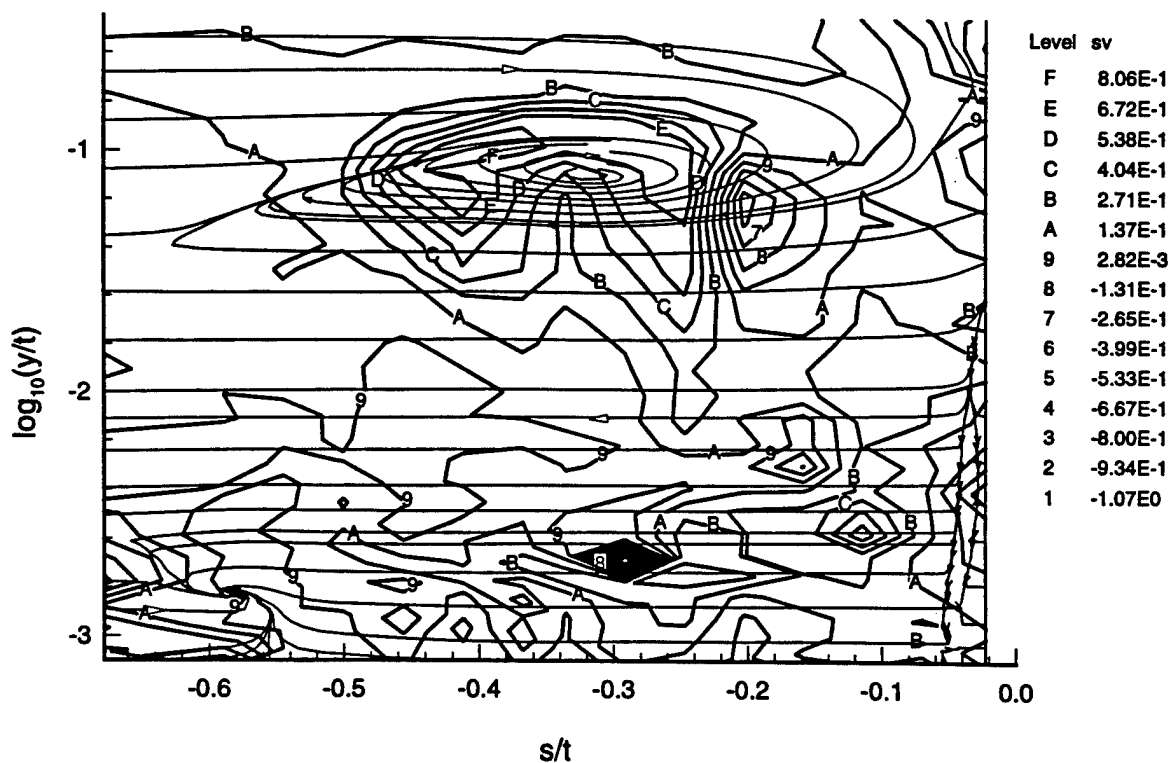


Figure 33. Skewness of v structural parameter contours and secondary flow streamlines.

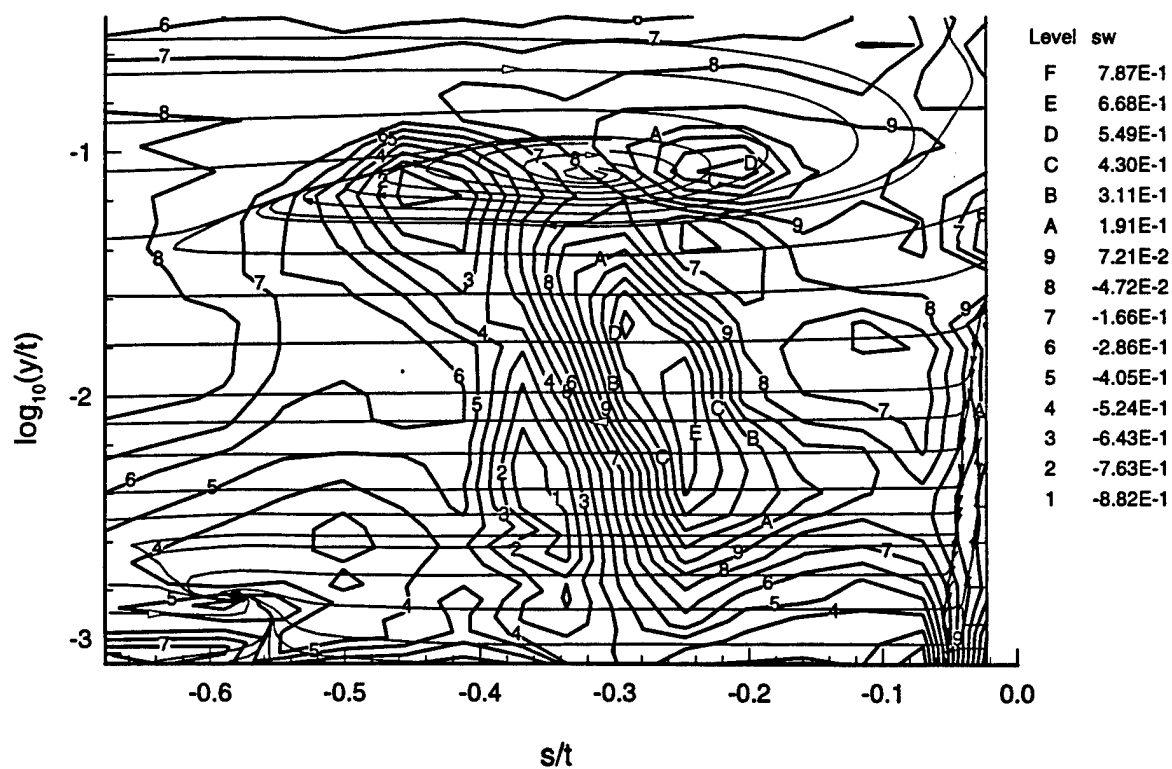


Figure 34. Skewness of w structural parameter contours and secondary flow streamlines.

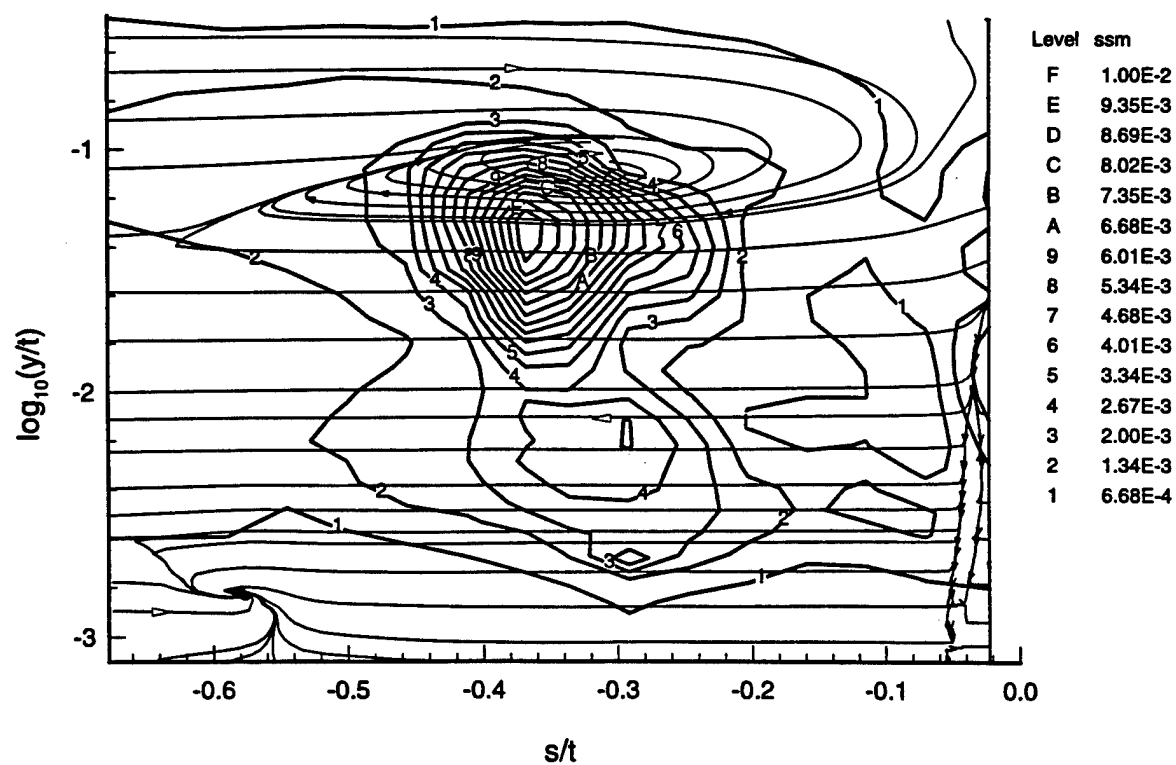


Figure 35. Shear stress magnitude/ U_{ref}^2 contours and secondary flow streamlines.

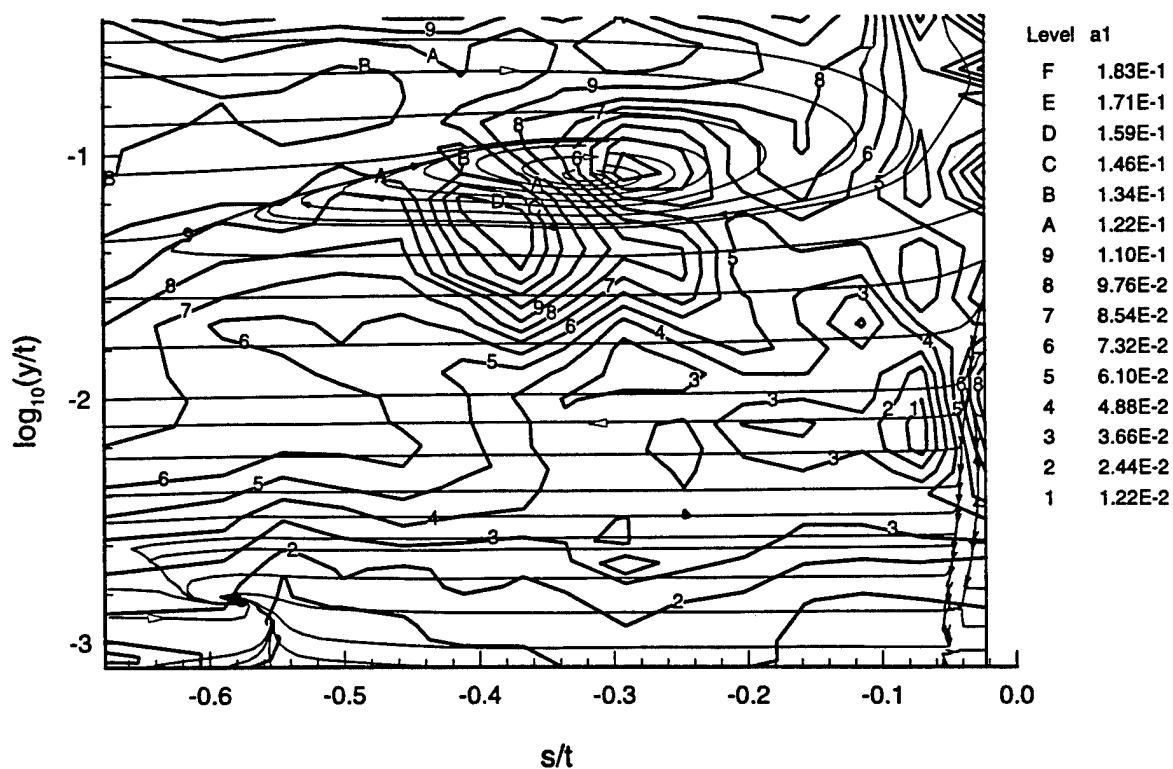


Figure 36. Townsend's structural parameter A , contours and secondary flow streamlines.

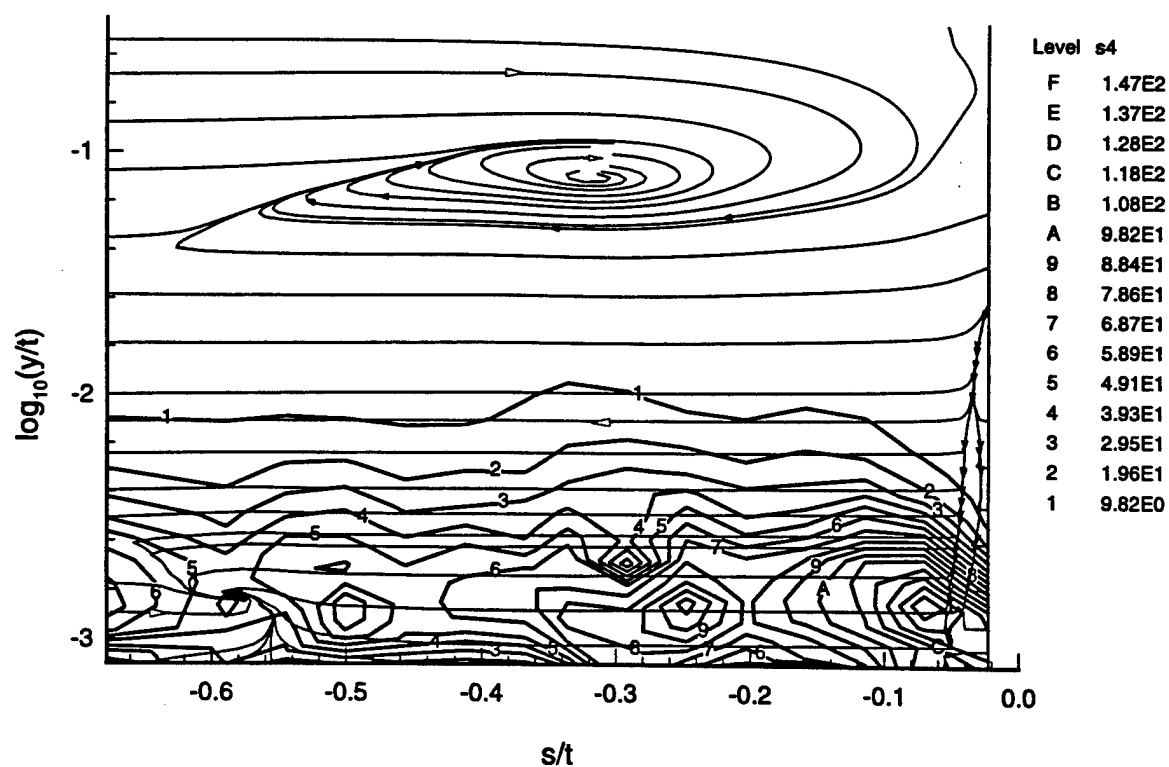


Figure 37. $S_4 = (\overline{u^2} + \overline{w^2}) / \overline{v^2}$ structural parameter contours and secondary flow streamlines.

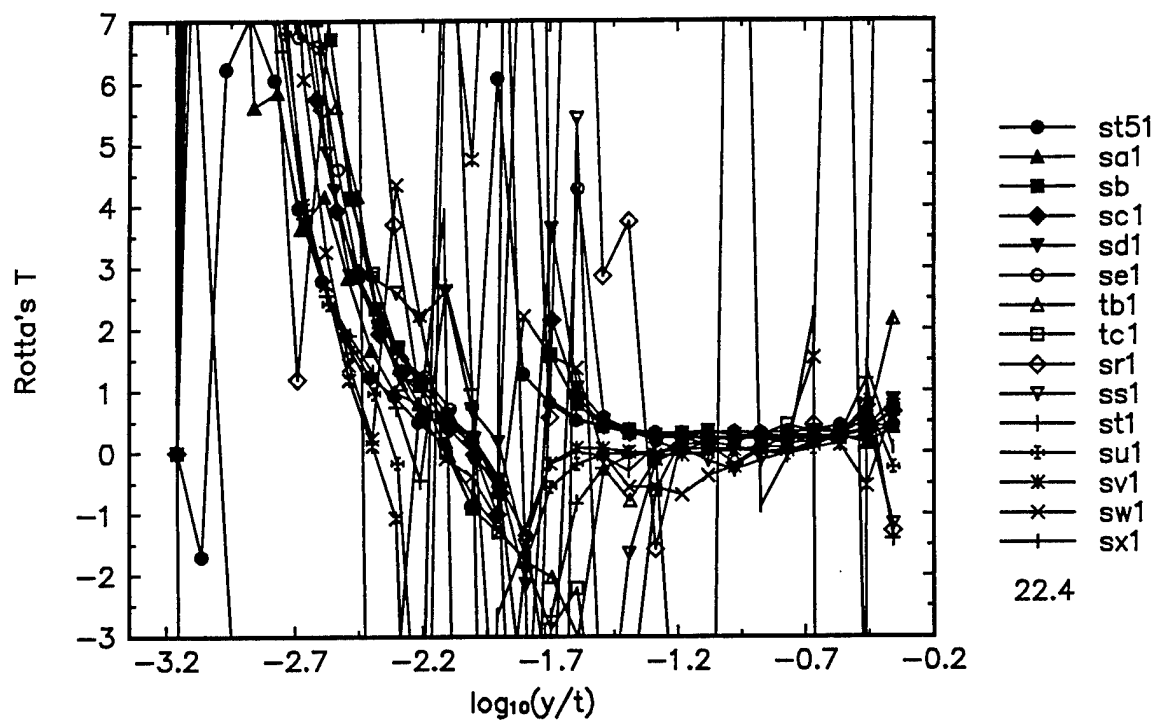


Figure 38. Rotta's T eddy viscosity ratio.

***Appendix A: Line Plots of Flow
Variables and Some Structural
Parameters***

In this Appendix line plots of the flow variables and some structural parameters are given in the 22.4° coordinate system. Mean velocities (pages 53-60) and Reynolds stresses (pages 61-76) are plotted separately for each station. For triple products and derived quantities the stations are marked on the figures. The order of the stations is: station 5, a, b, c, d, e, tb, tc, r, s, t, u, v, w, x. The derived quantity and structural parameter figures are presented on pages 87-104 after the triple product figures (pages 77-86).

The derived quantities and the structural parameters presented are:

Flow angle (FA), page 87;

Flow gradient angle (FGA), page 88;

Shear stress angle (SSA), page 89;

Mean velocity vector magnitude (Q), page 90;

Mixing length (L_m), page 91;

Turbulent kinetic energy (TKE), page 92;

Townsend's structural parameter (A_1), page 93;

$\overline{v^2}/|\tau/\rho|$, page 94;

$\overline{uv}/\overline{u^2}$, page 95;

$(\overline{u^2} + \overline{w^2})/\overline{v^2}$, pages 96-97;

The ratio of \overline{vw} stress production to that of \overline{uw} stress production $C = \frac{\overline{v^2} \tan(FGA)}{\overline{uv} \tan(FGA) + \overline{vw}}$, page 98;

u skewness, page 99;

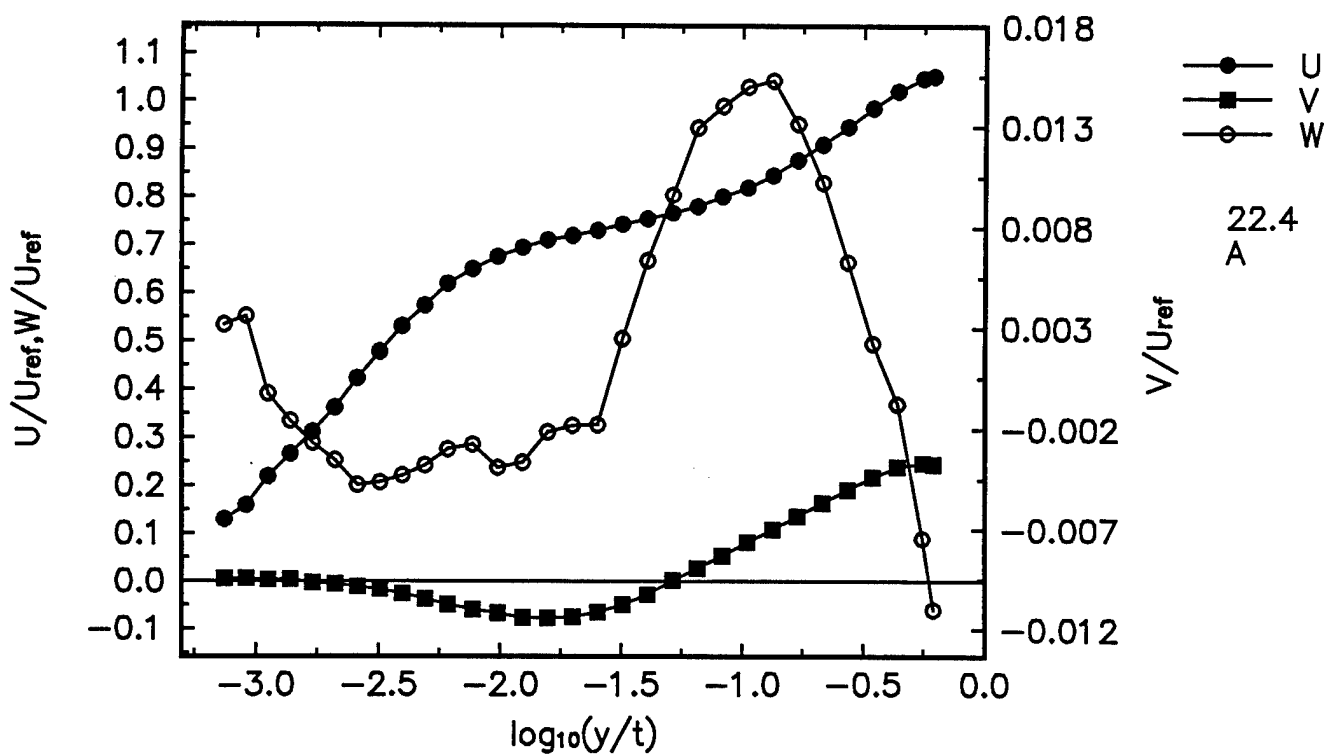
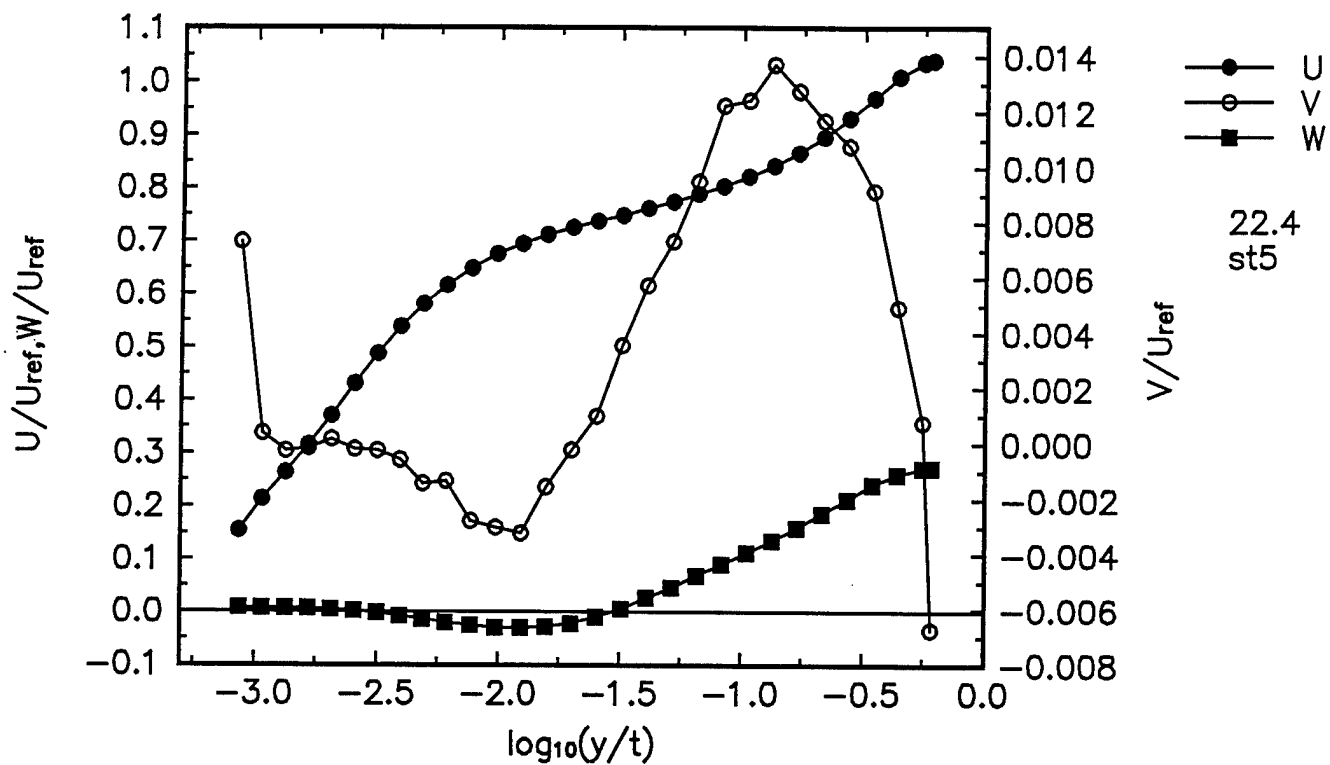
v skewness, page 100;

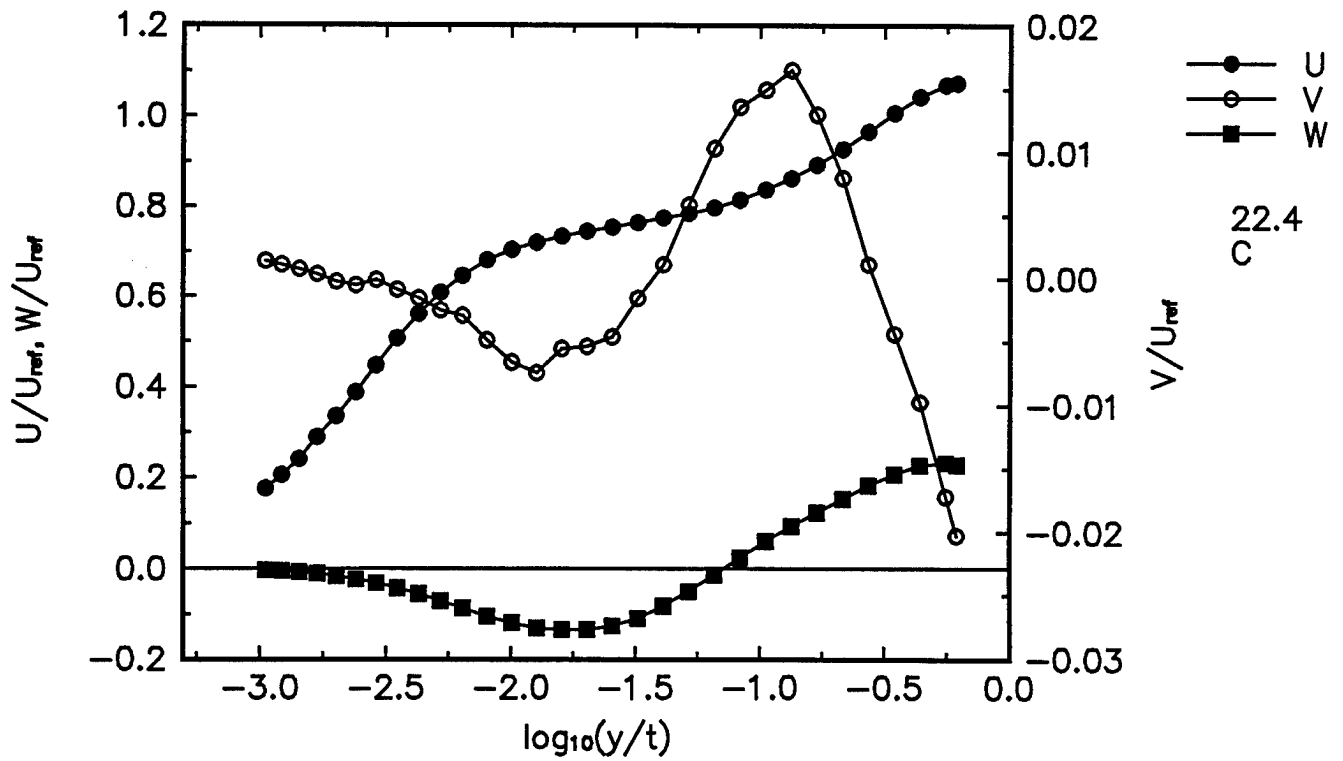
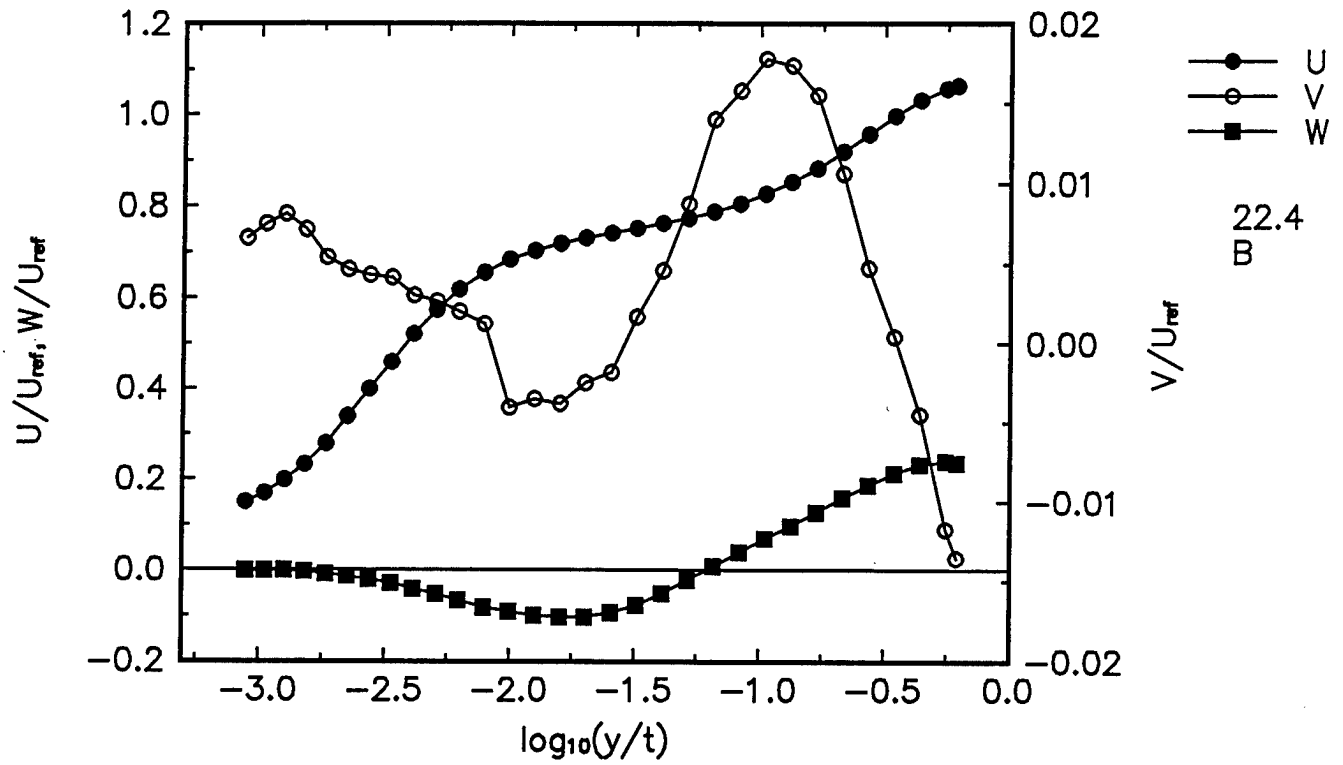
w skewness, page 101;

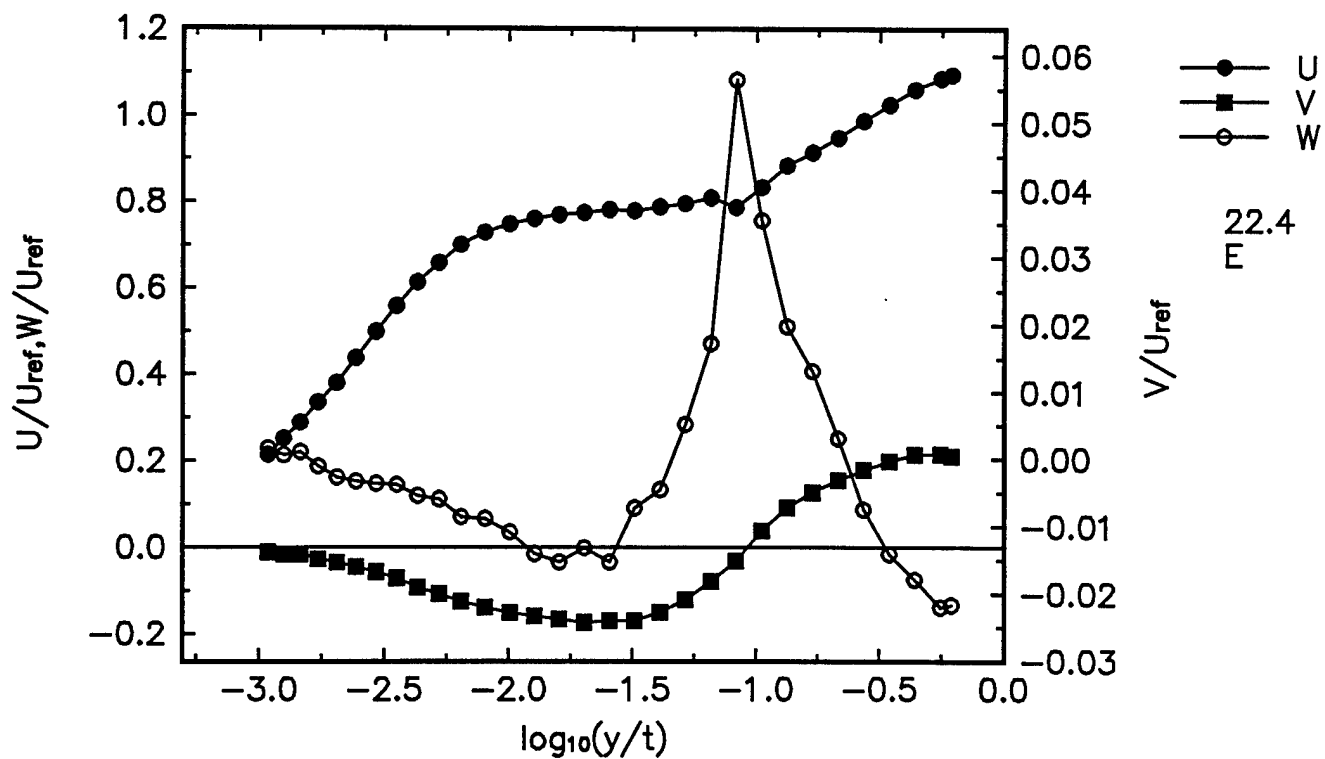
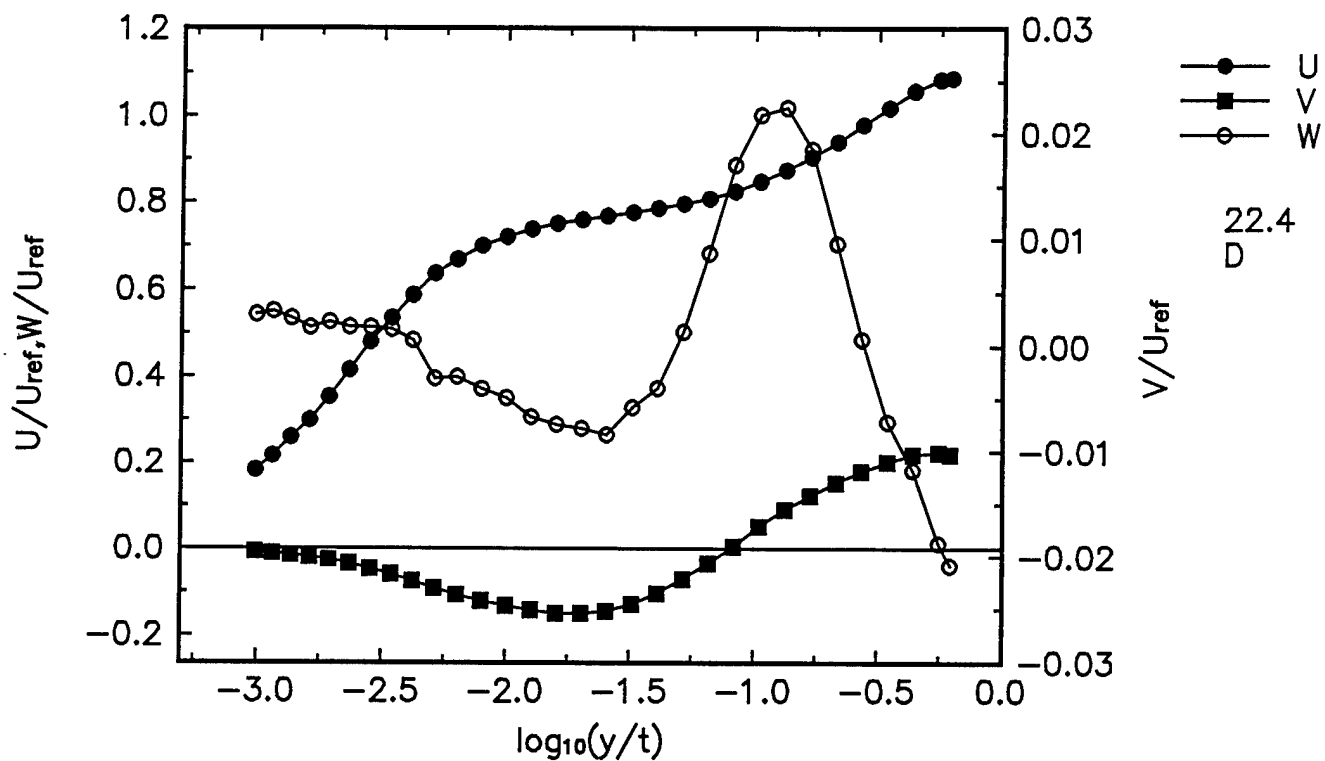
Turbulent kinetic energy transport velocity V_{q^2} , page 102;

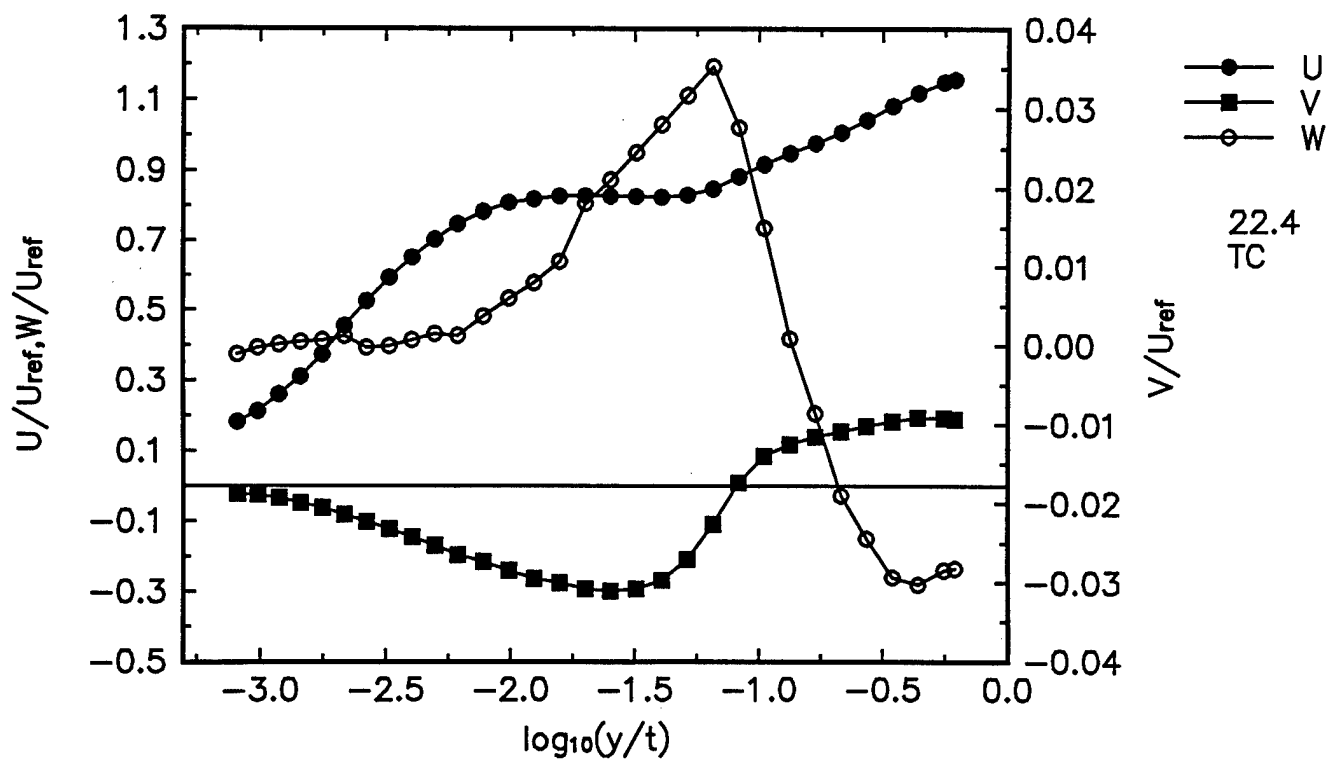
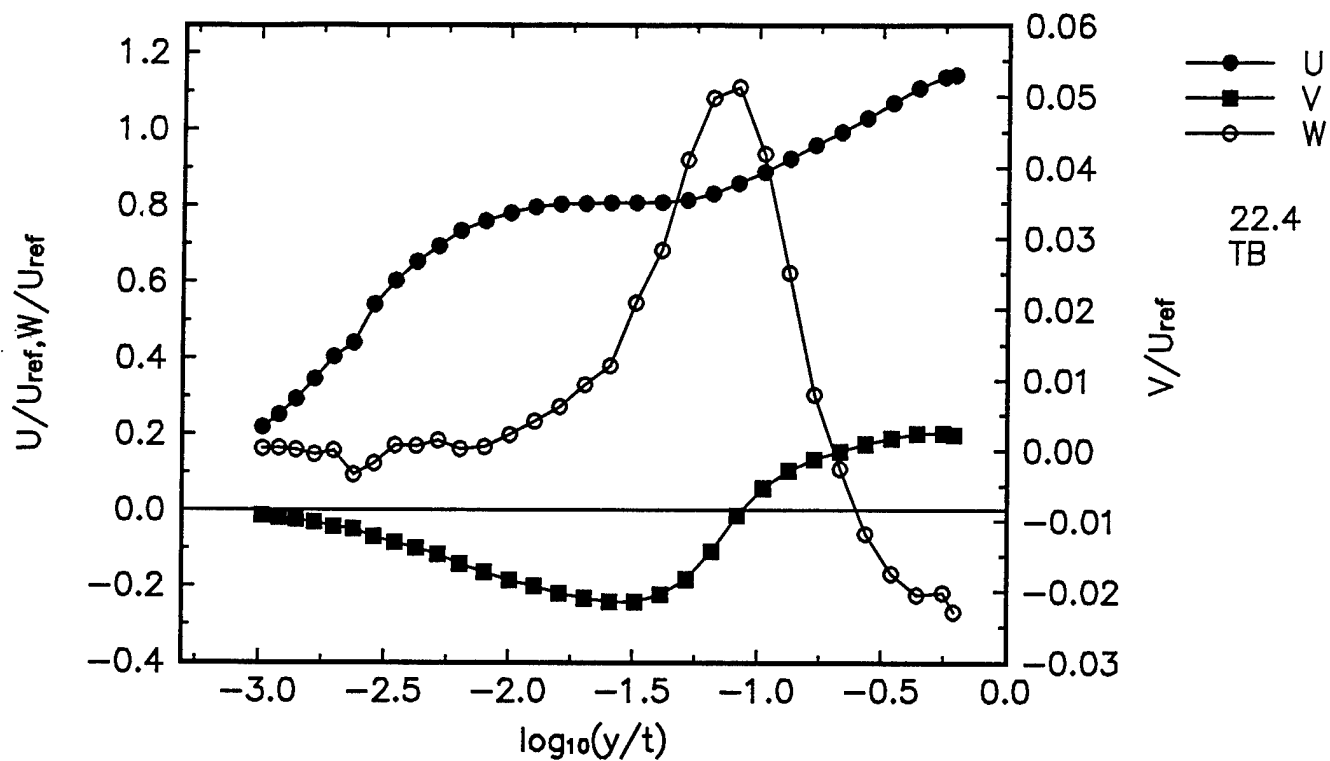
Longitudinal axis vorticity component, page 103;

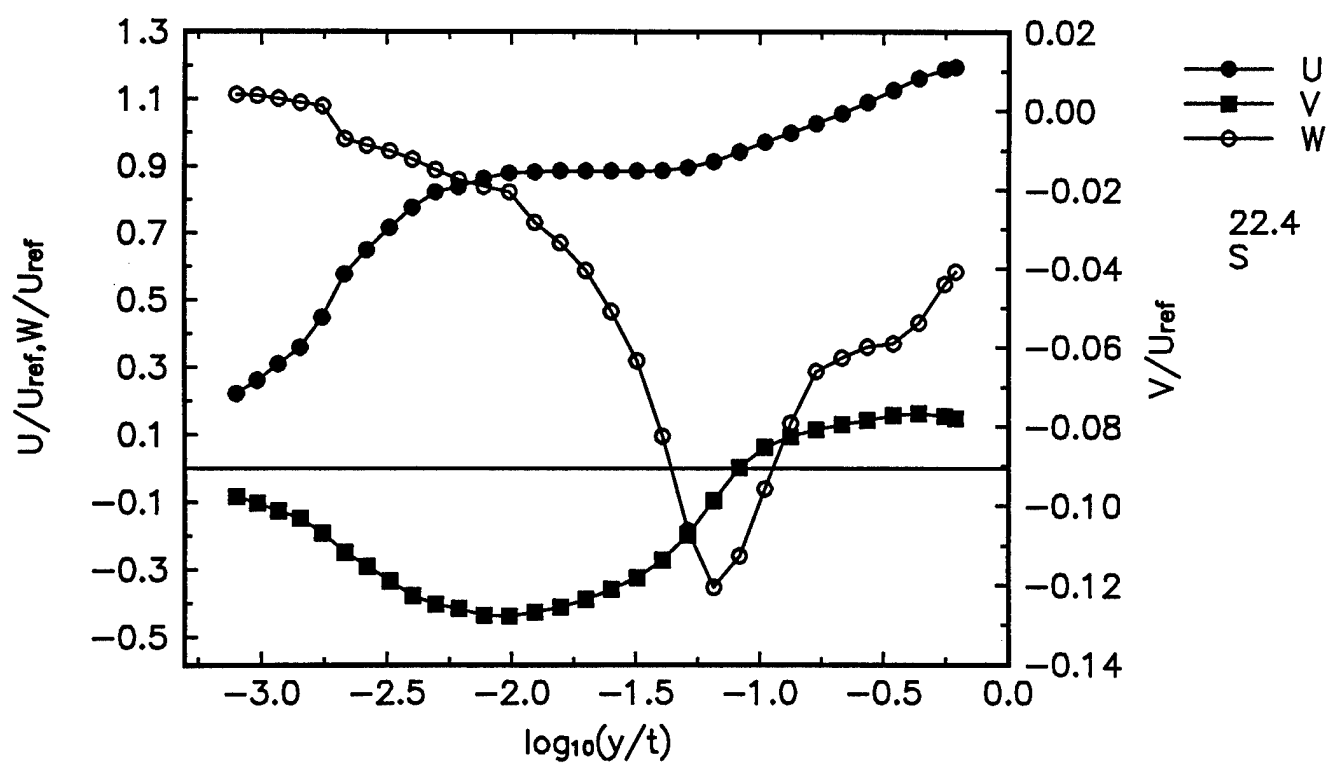
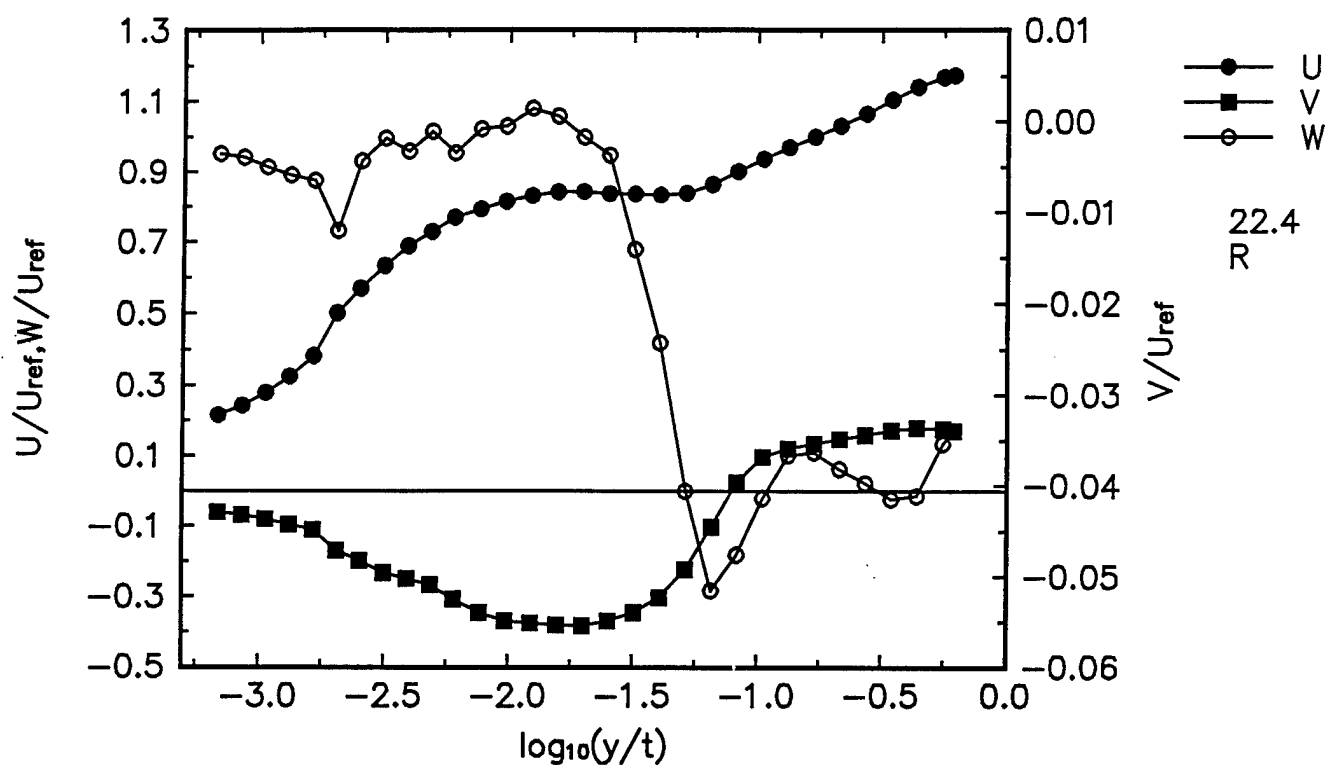
Shear stress magnitude, page 104.

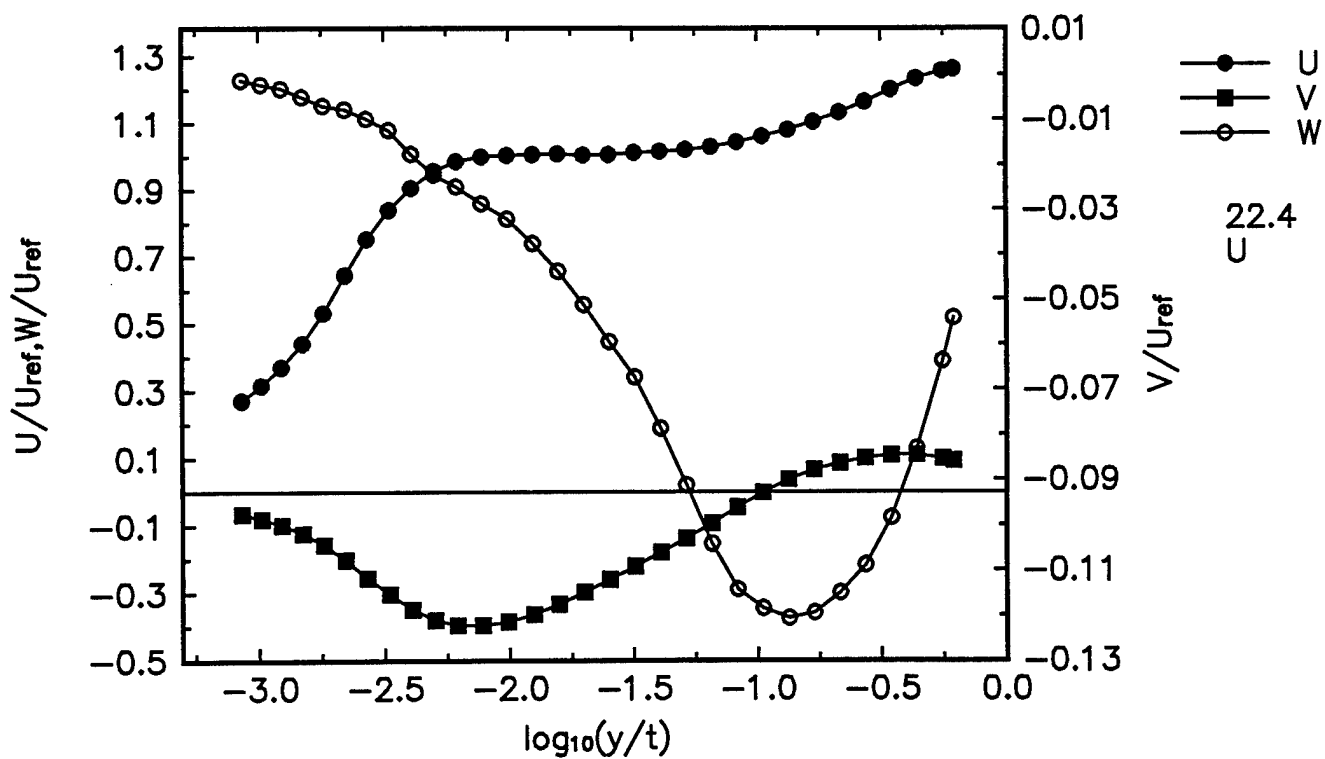
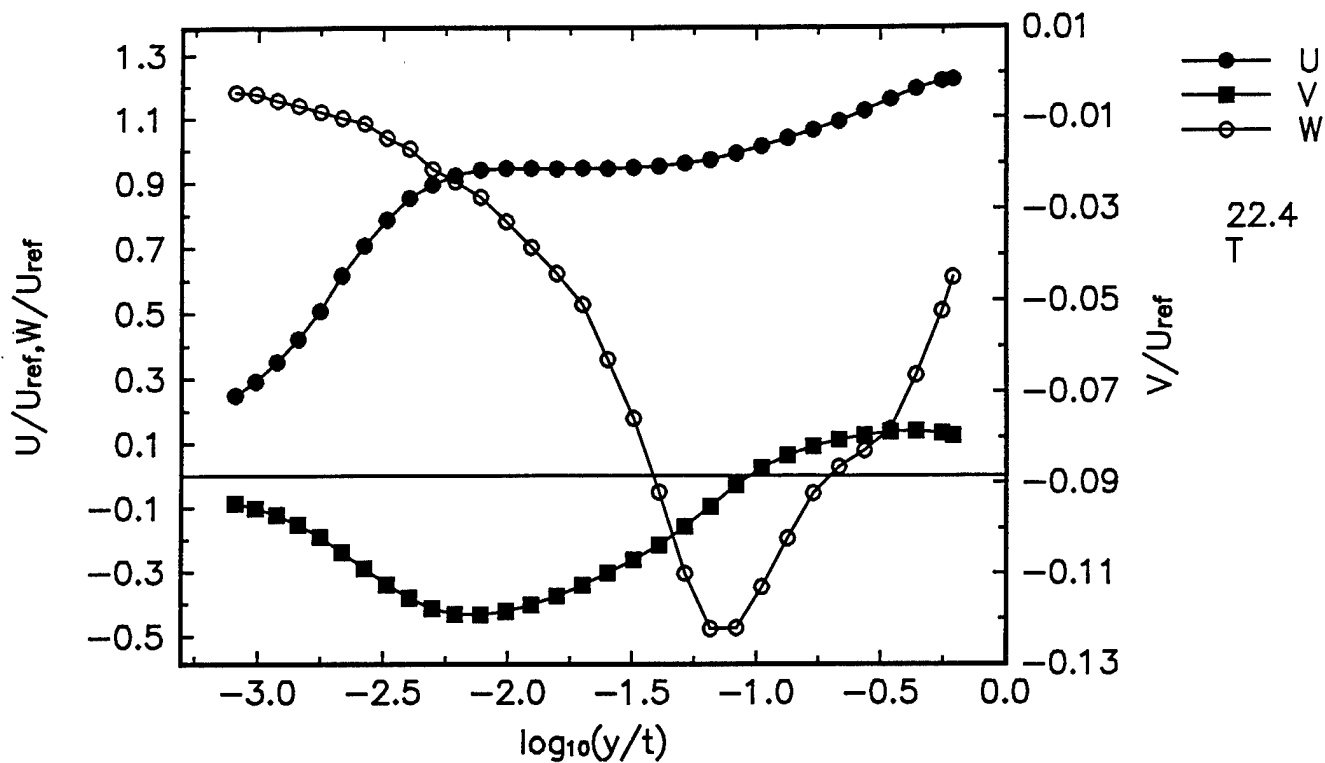


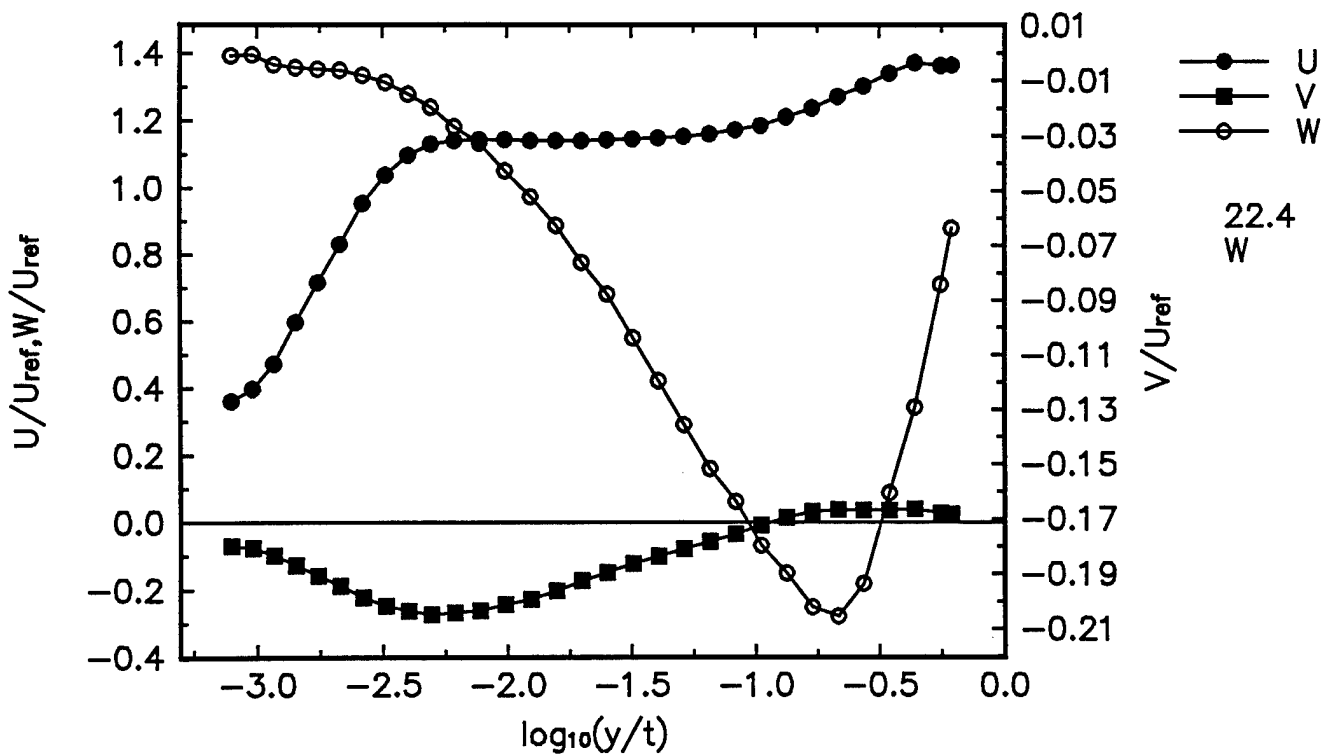
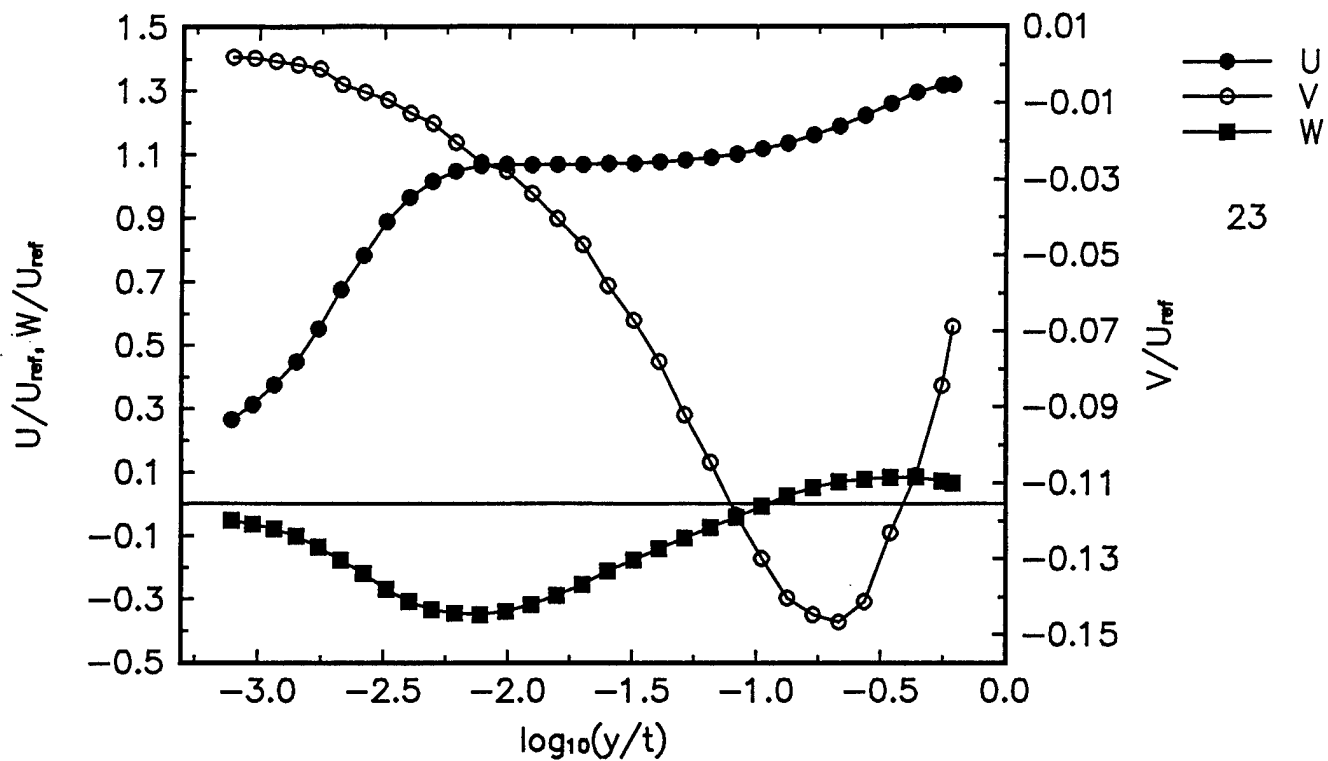


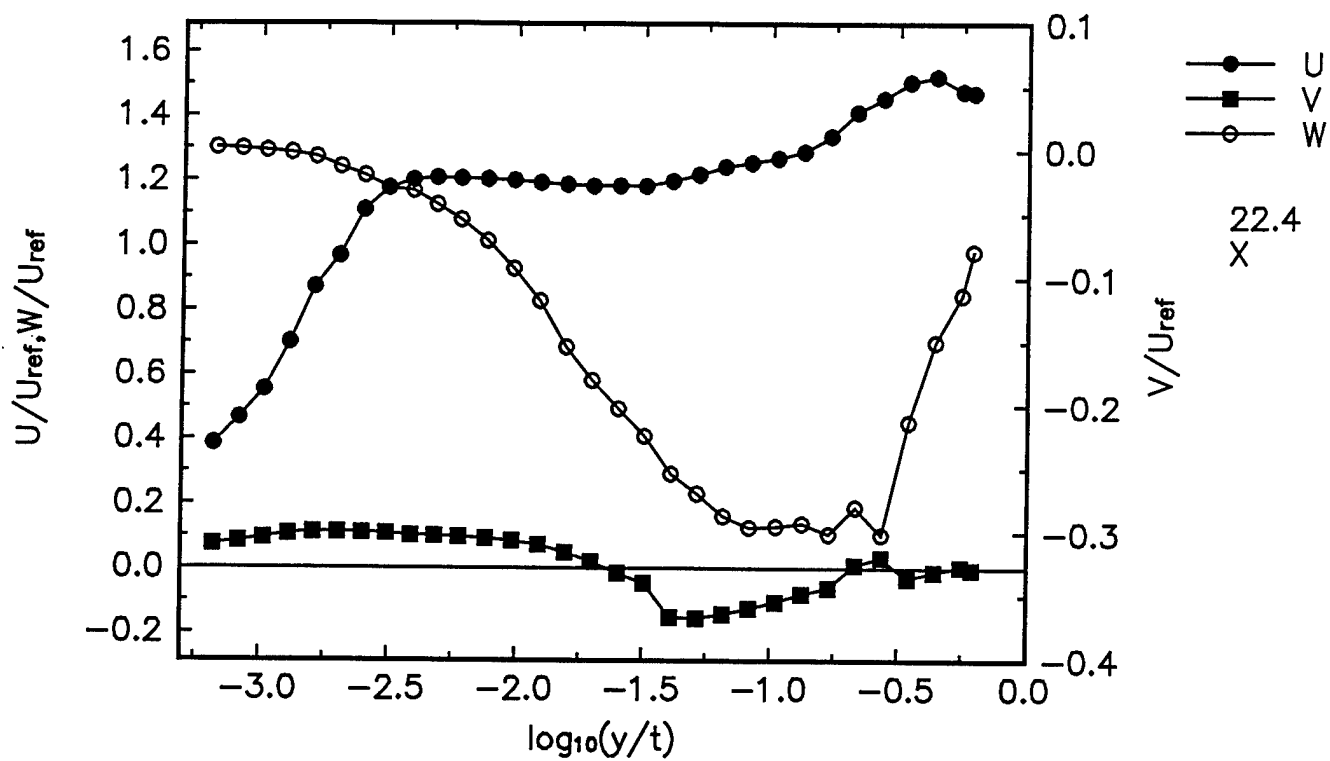


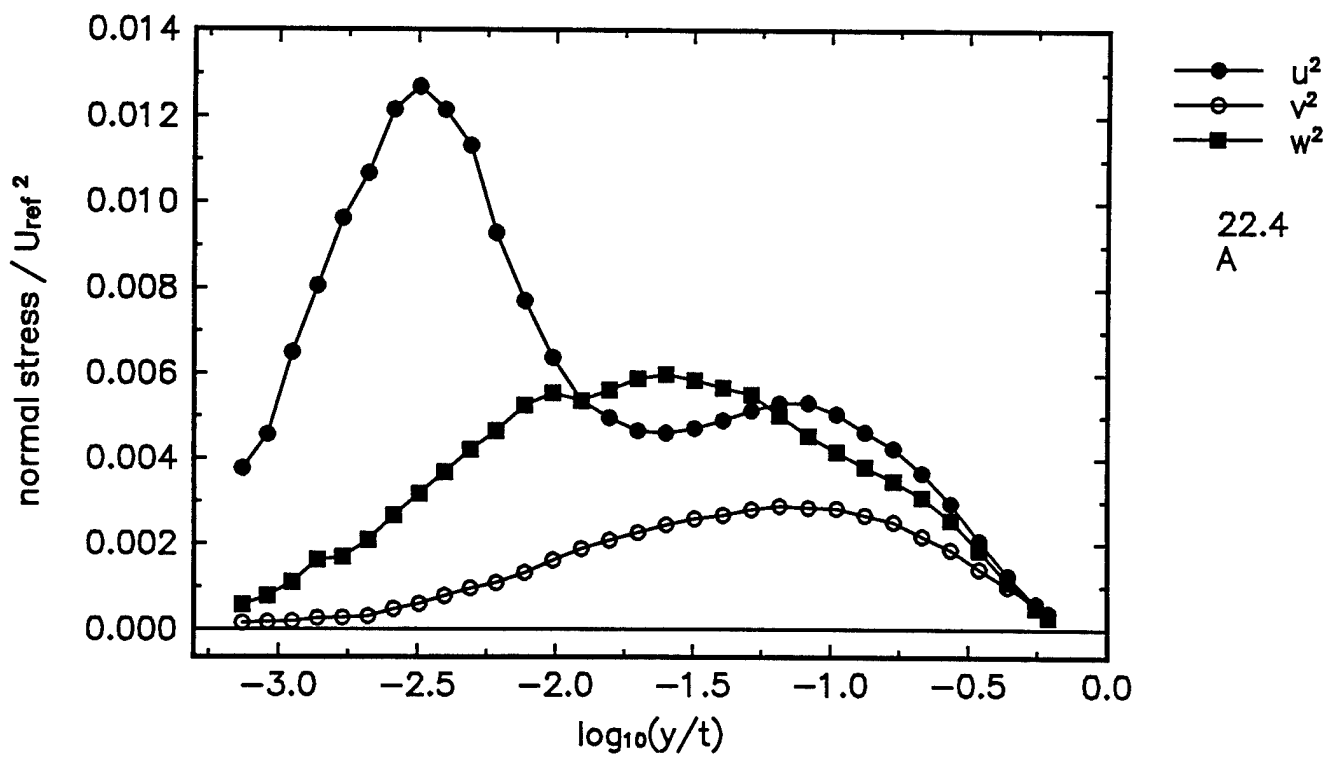
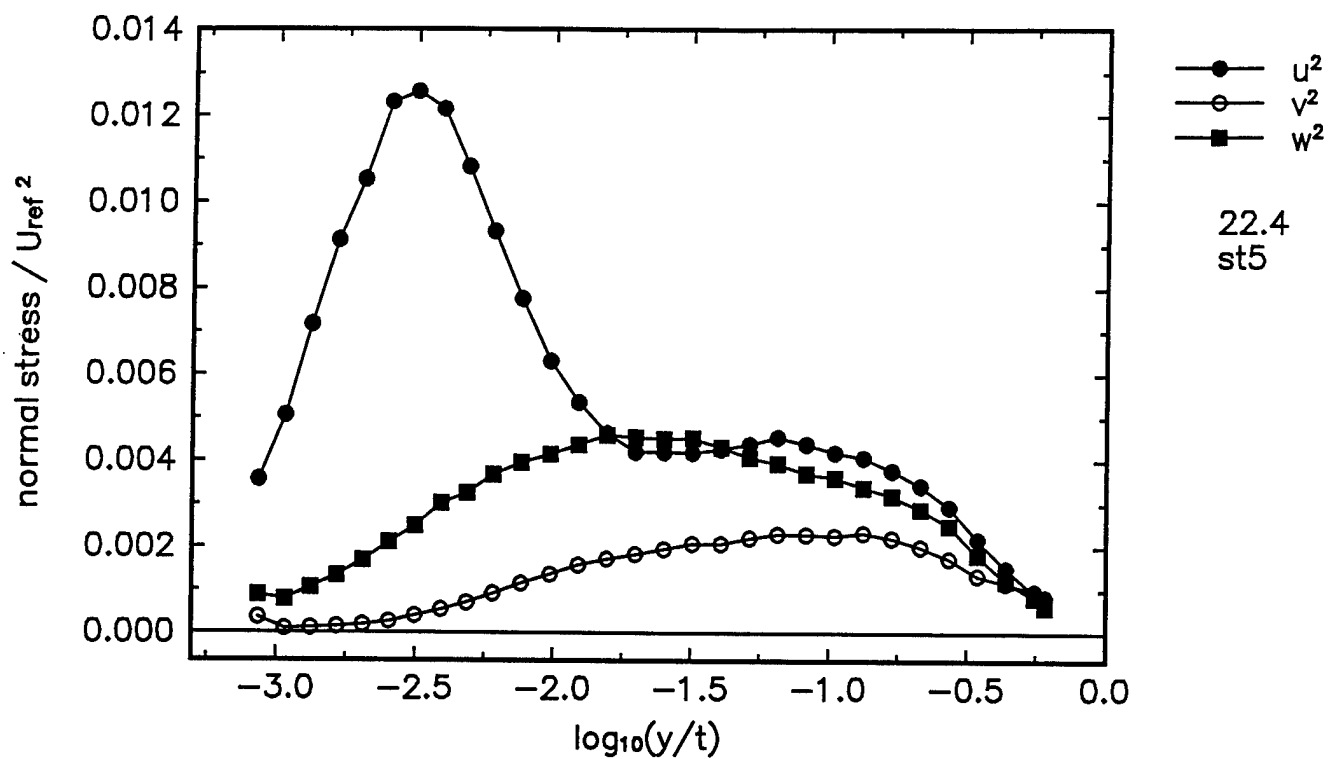


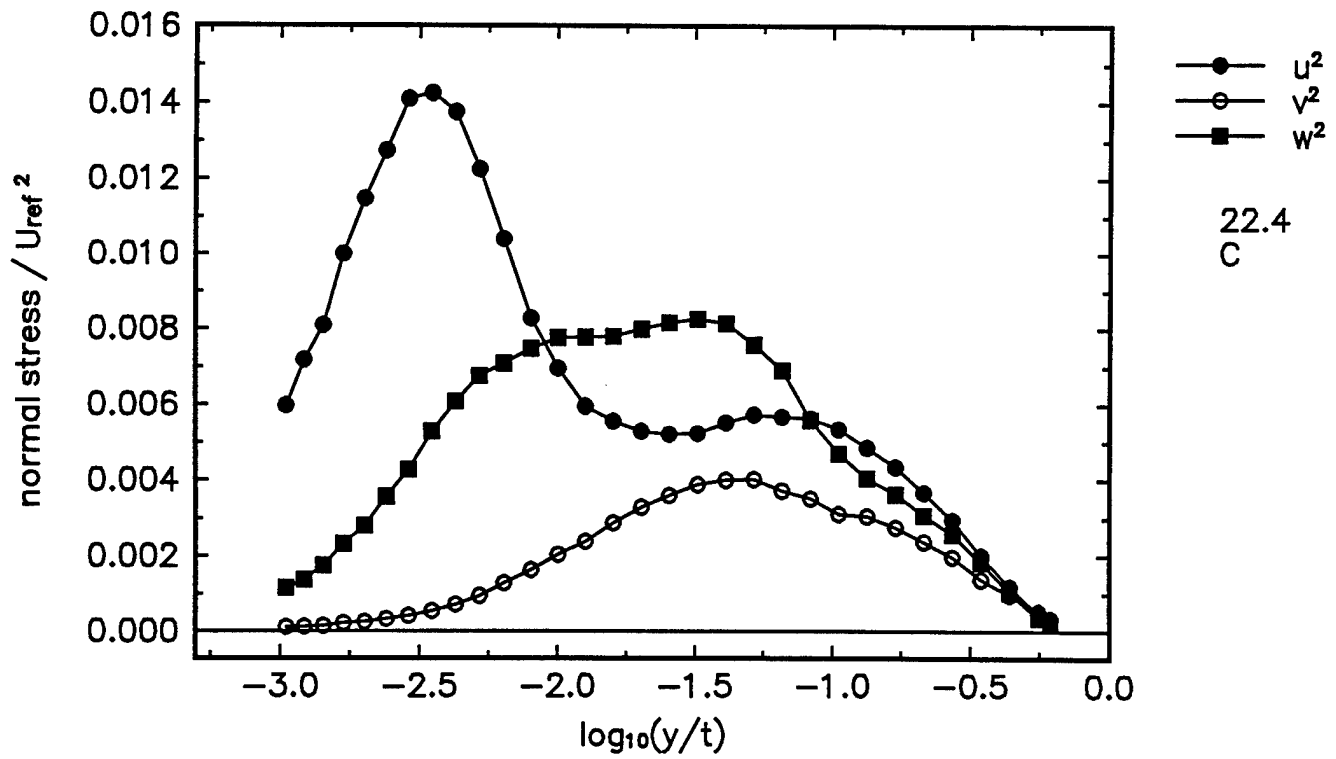
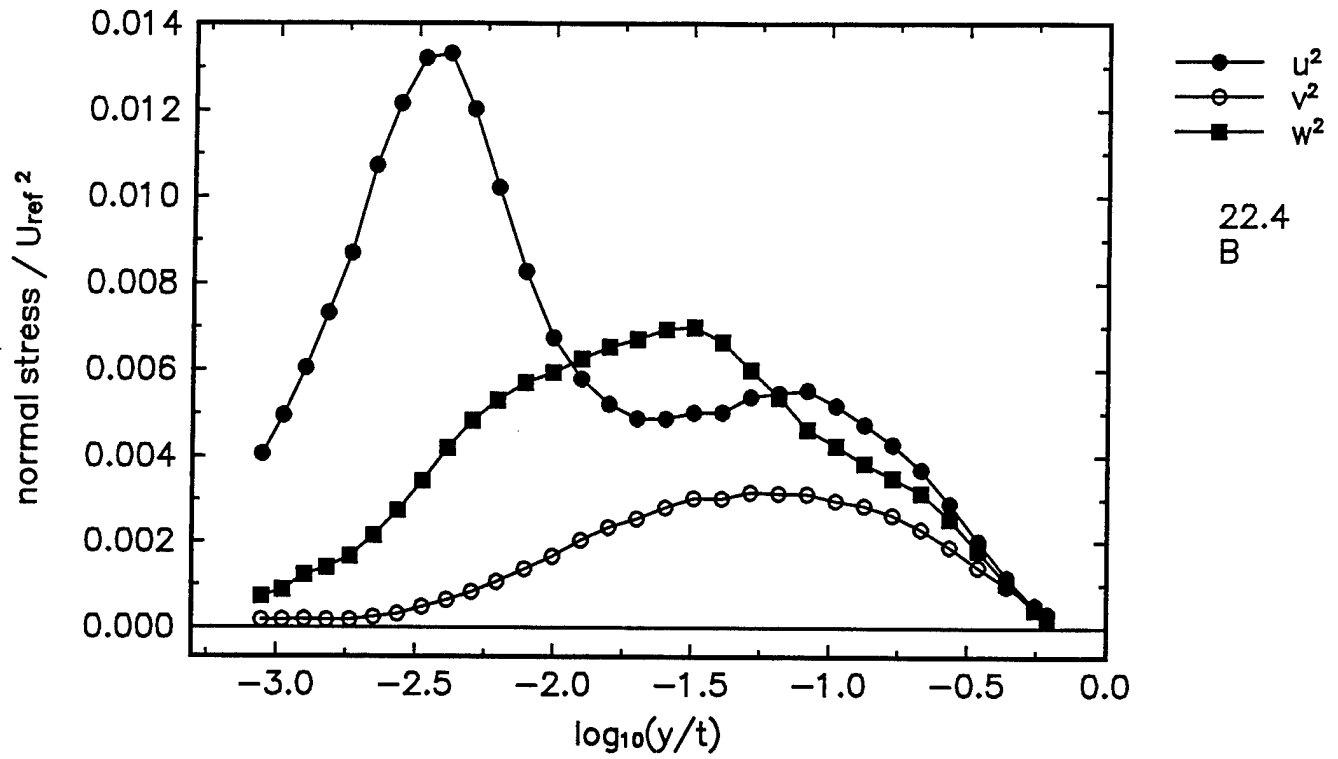


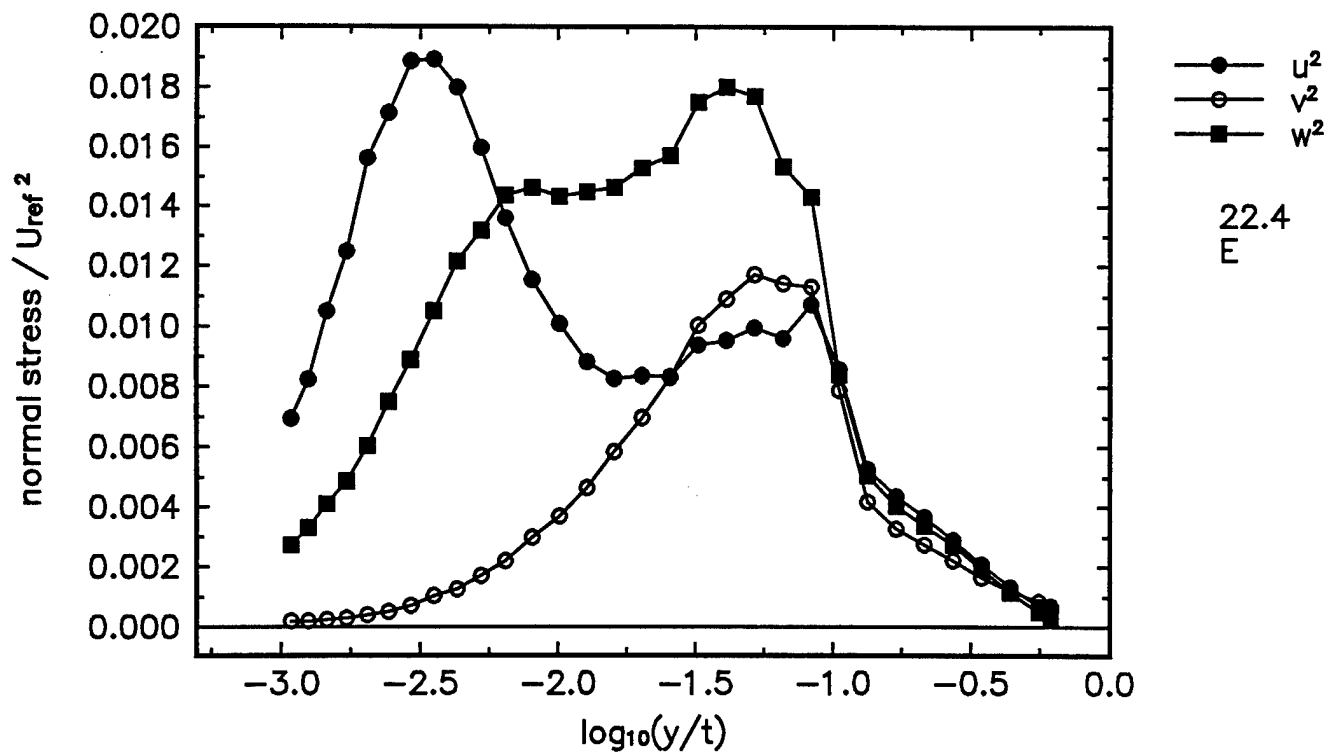
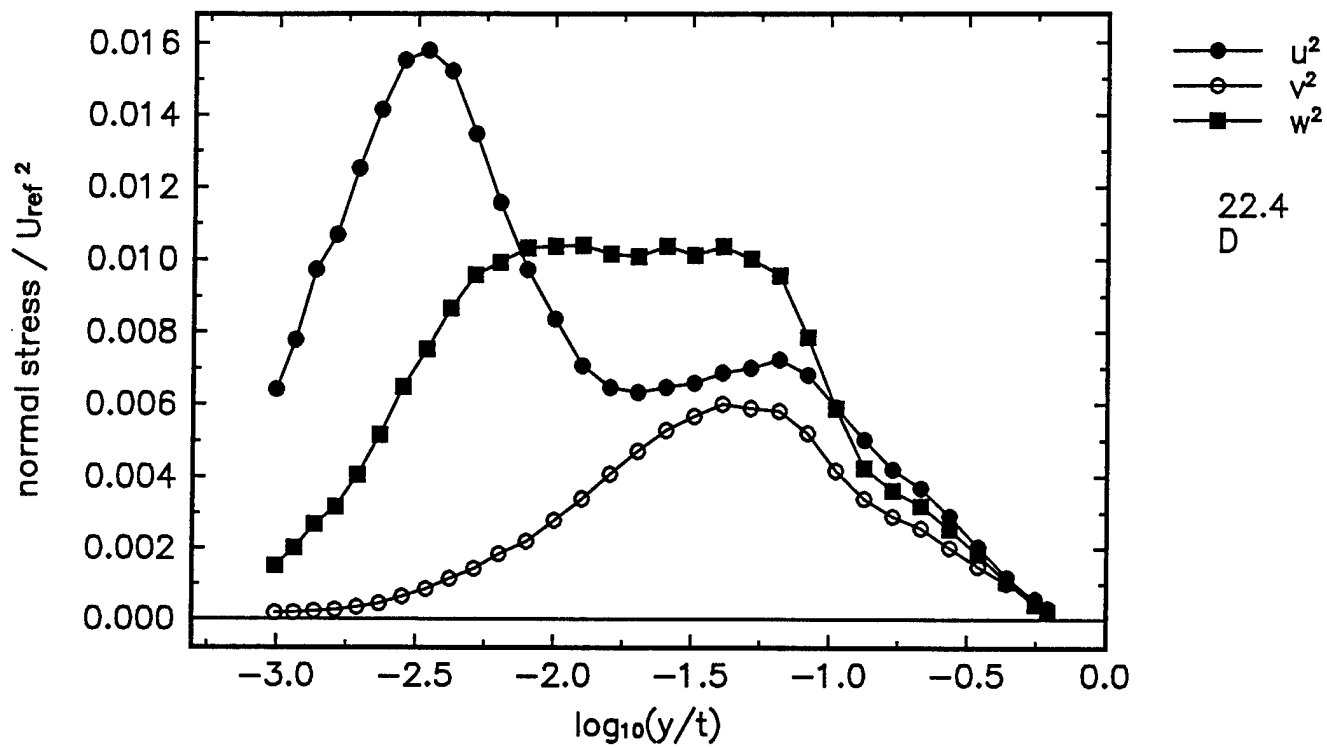


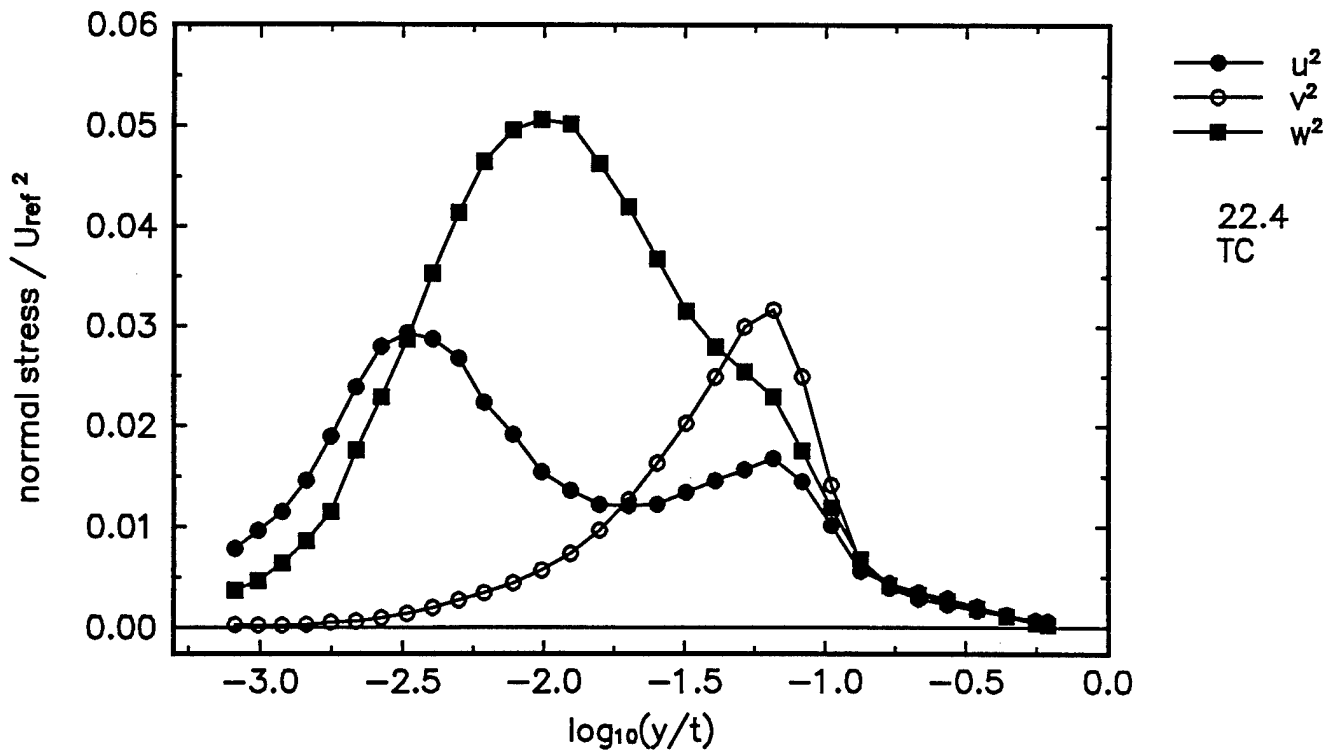
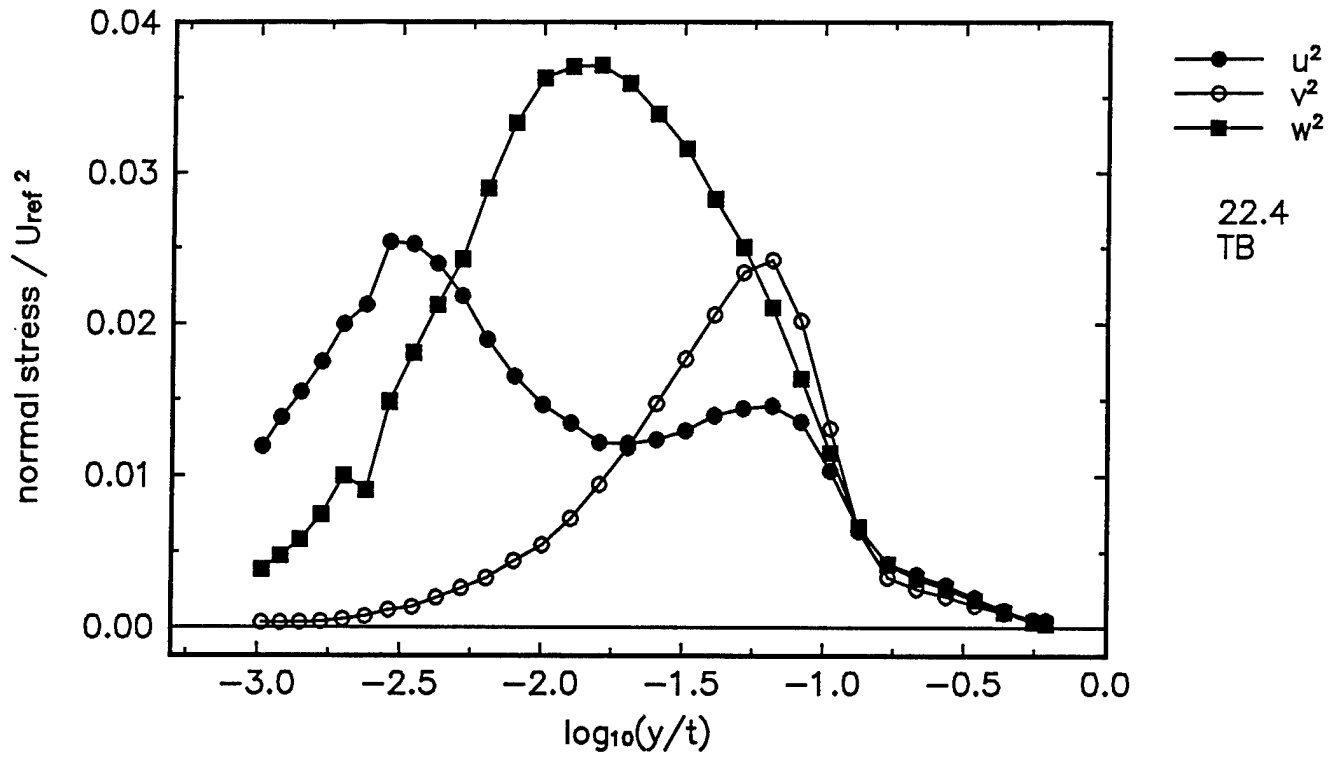


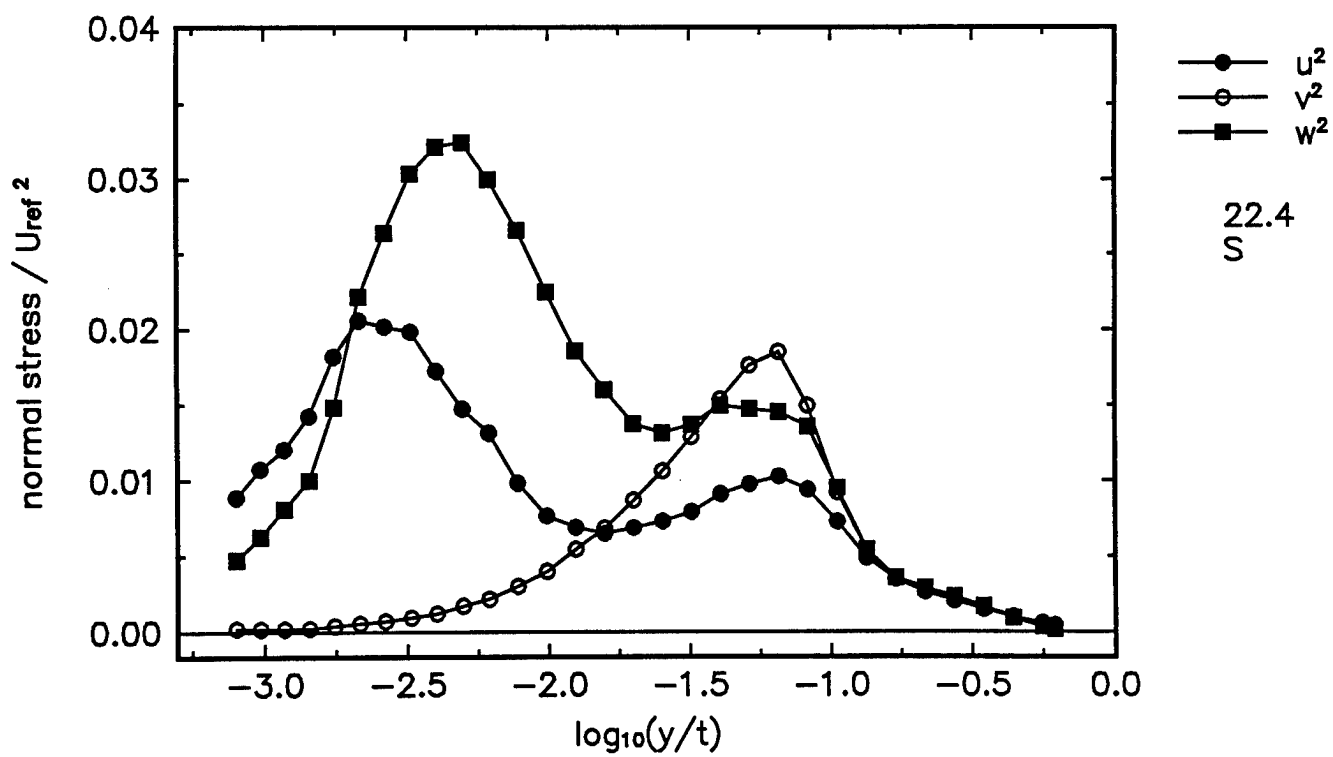
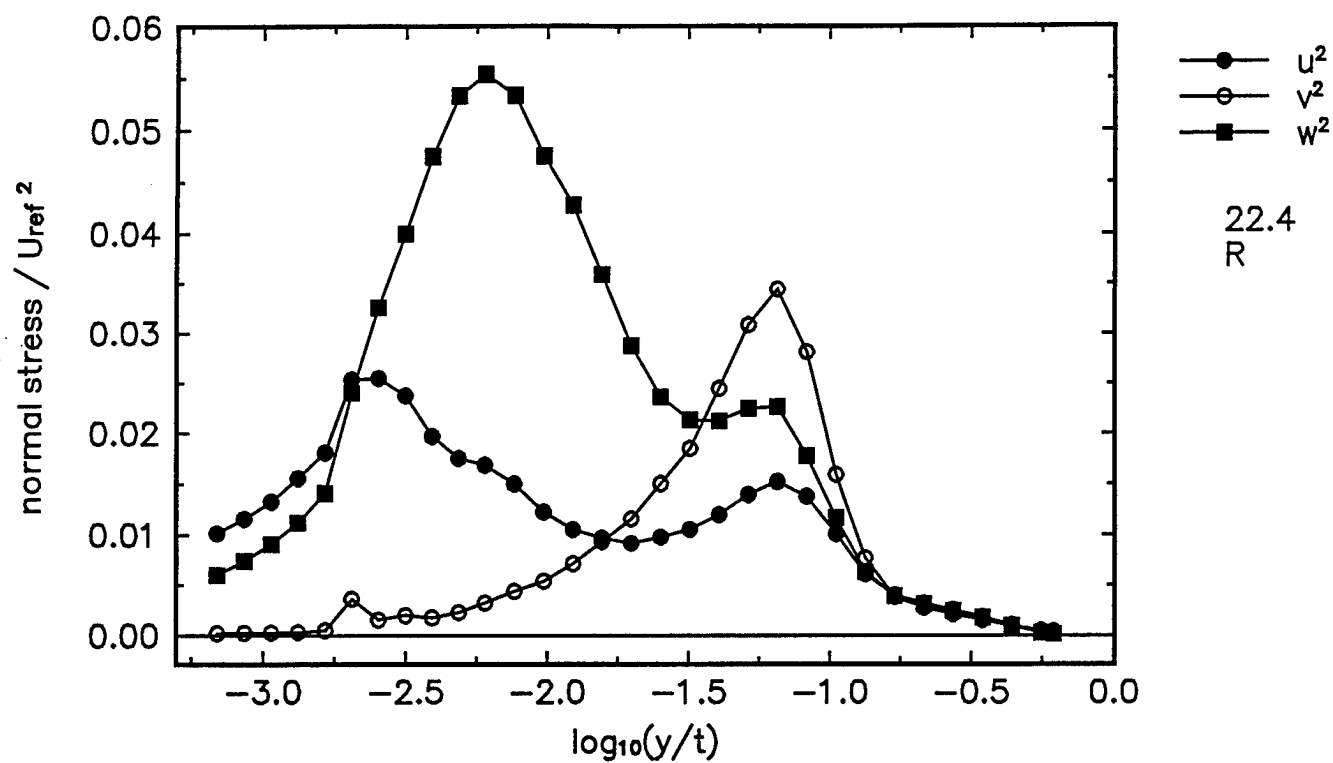


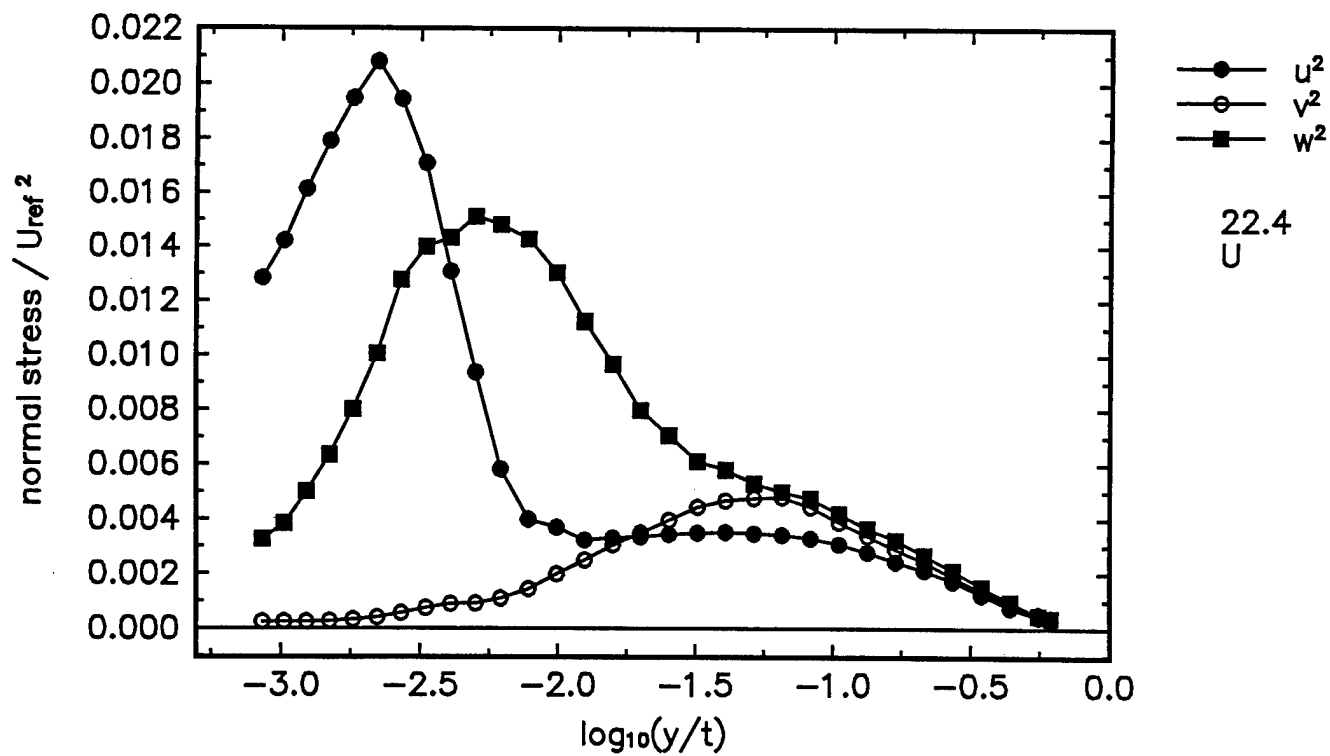
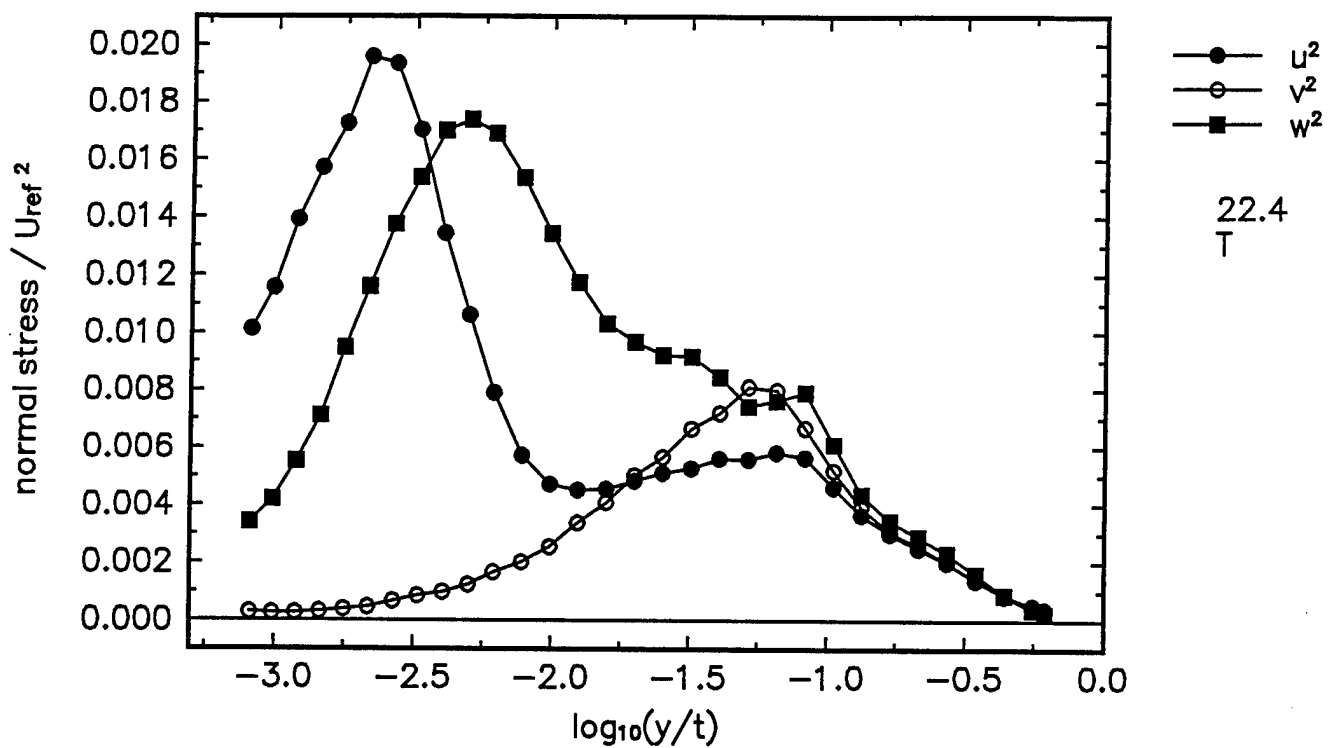


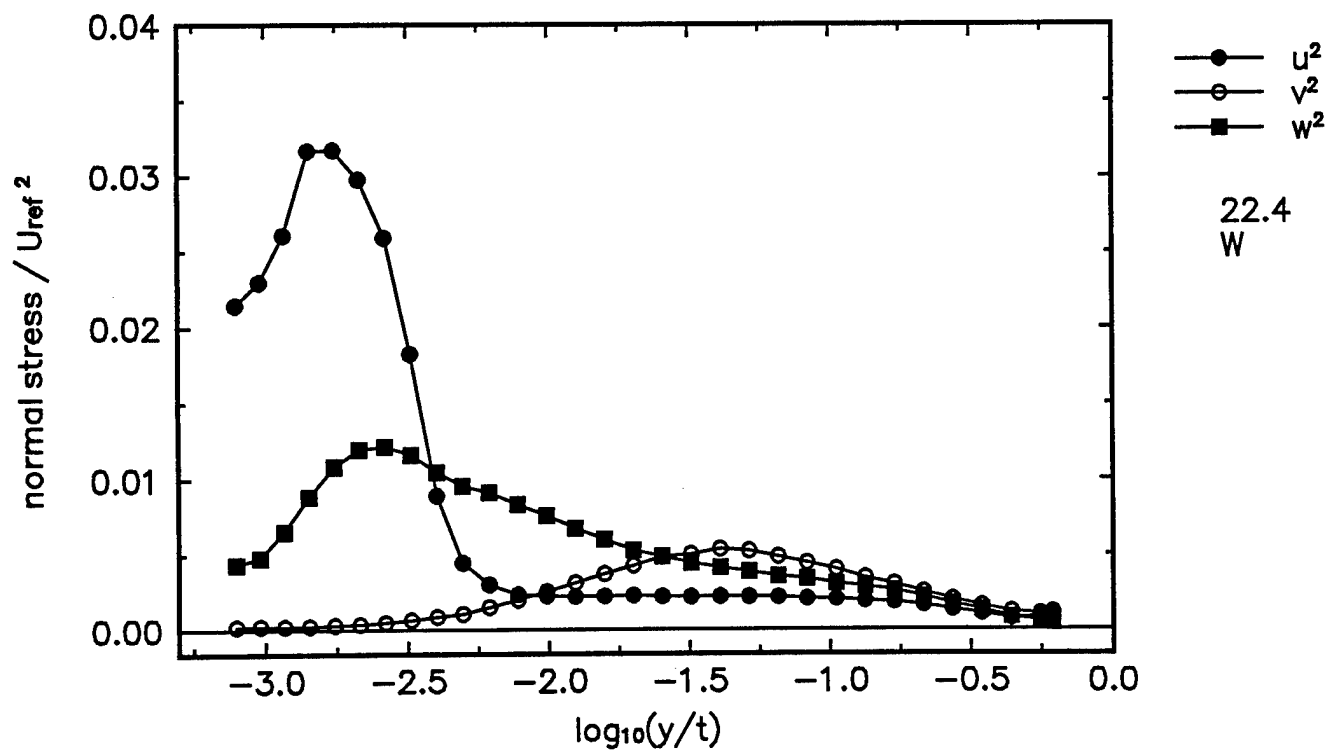
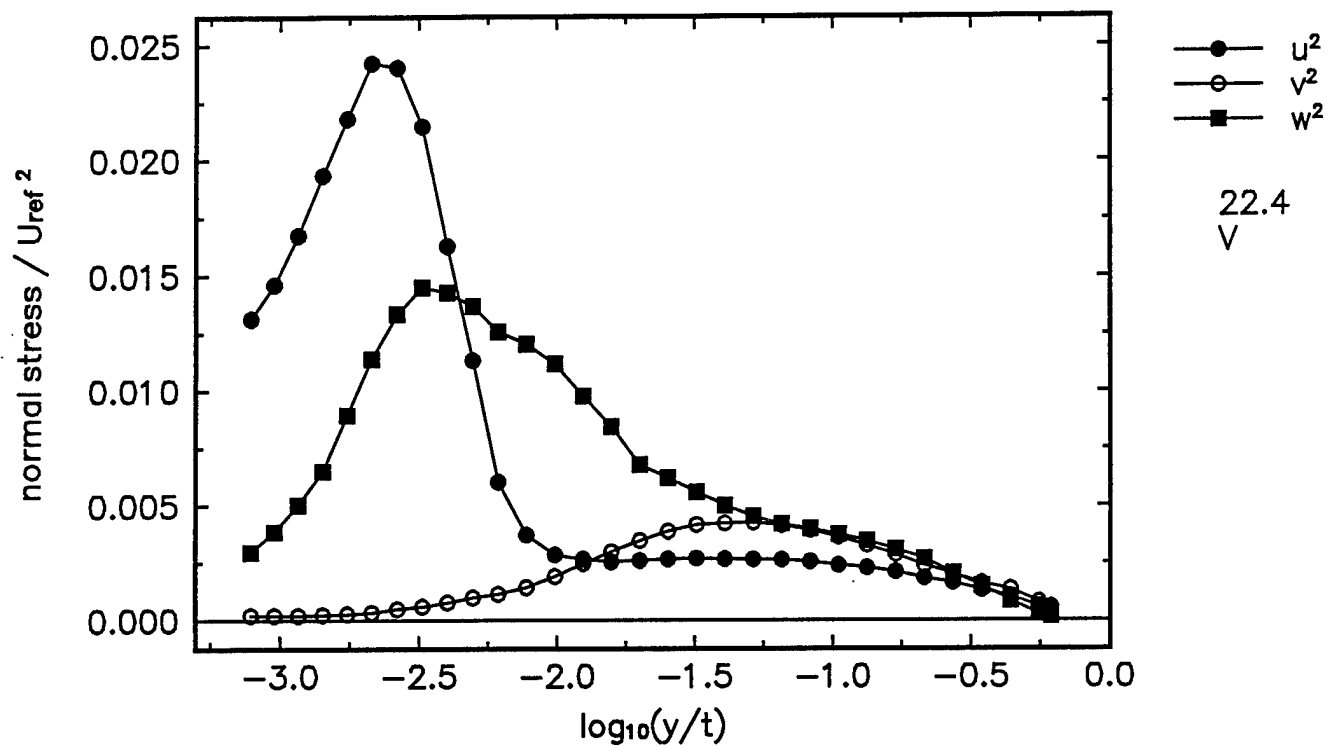


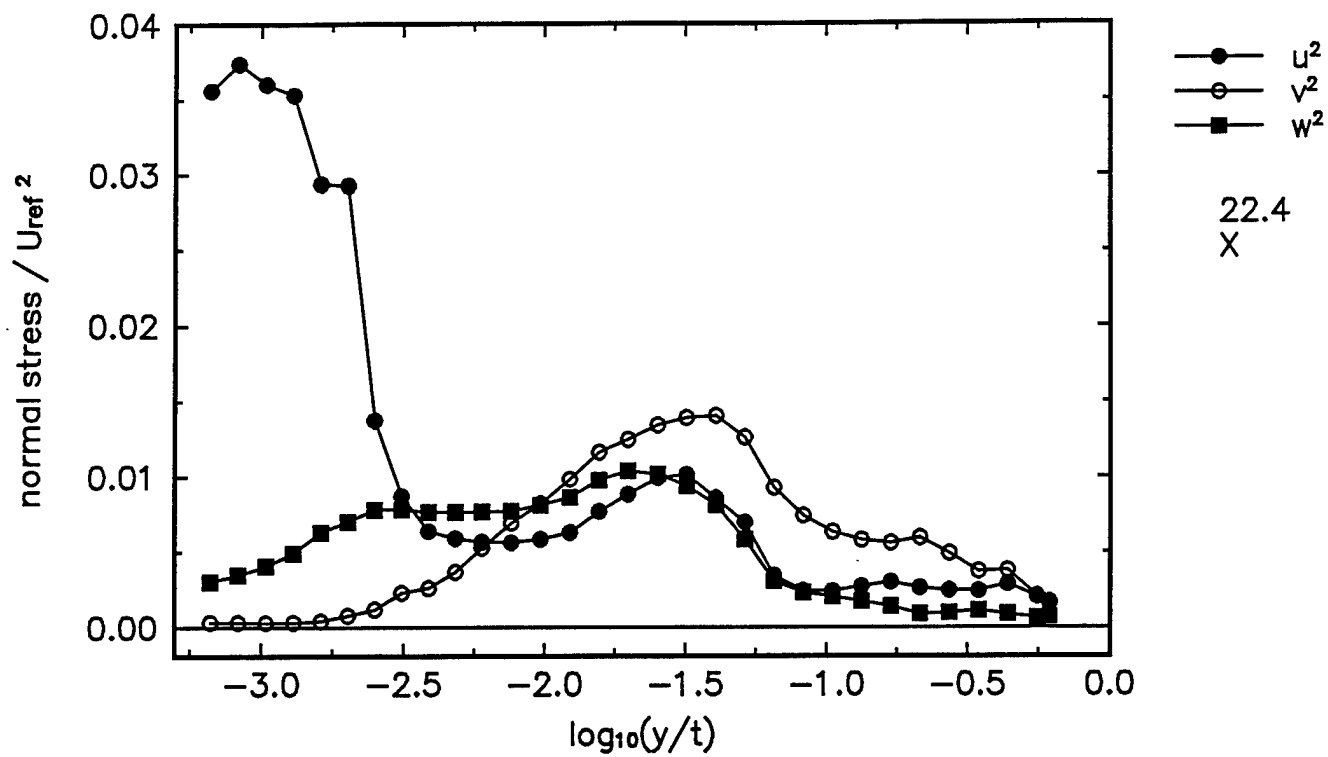


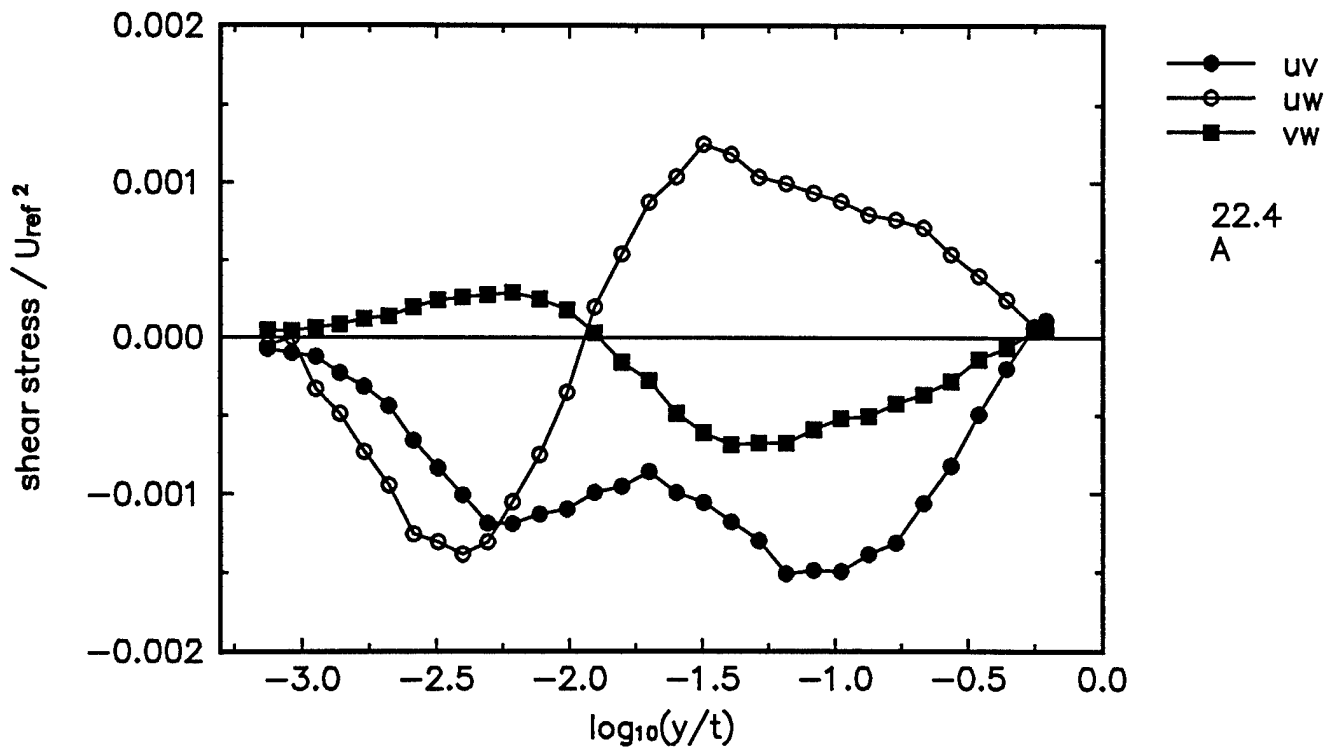
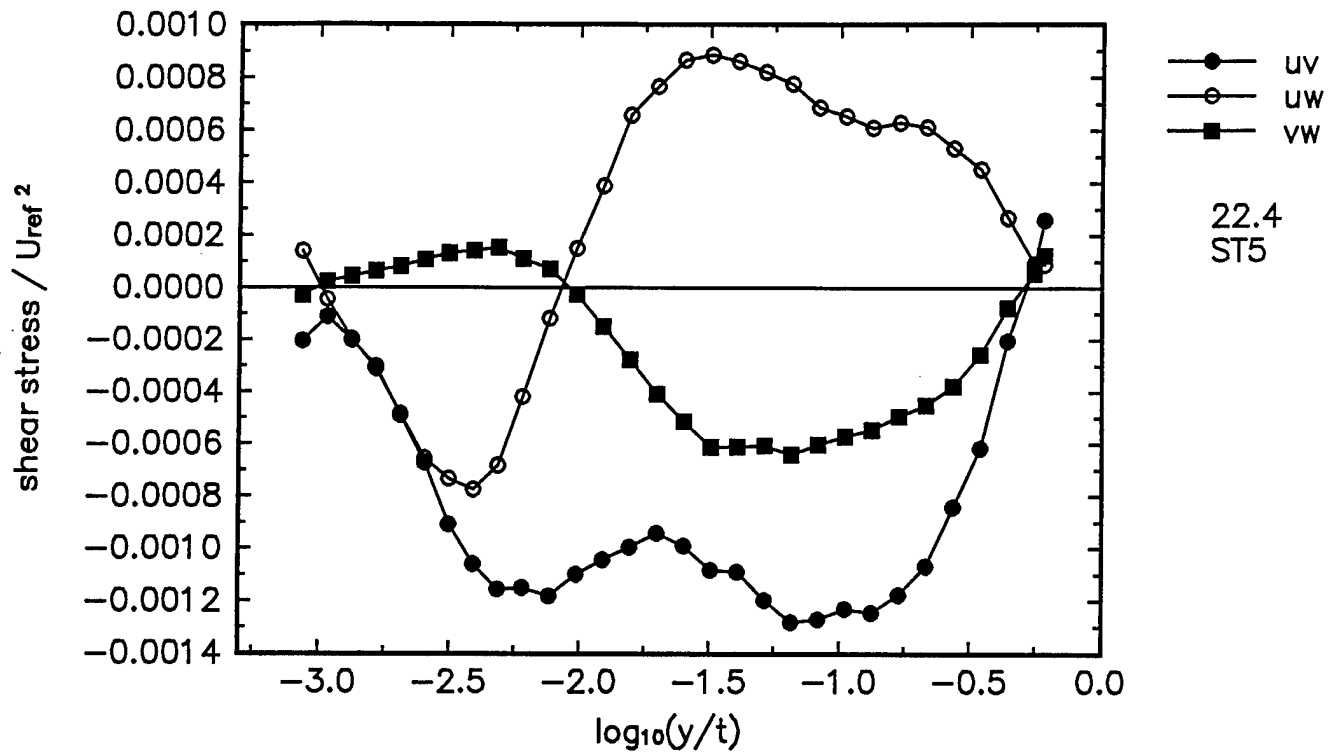


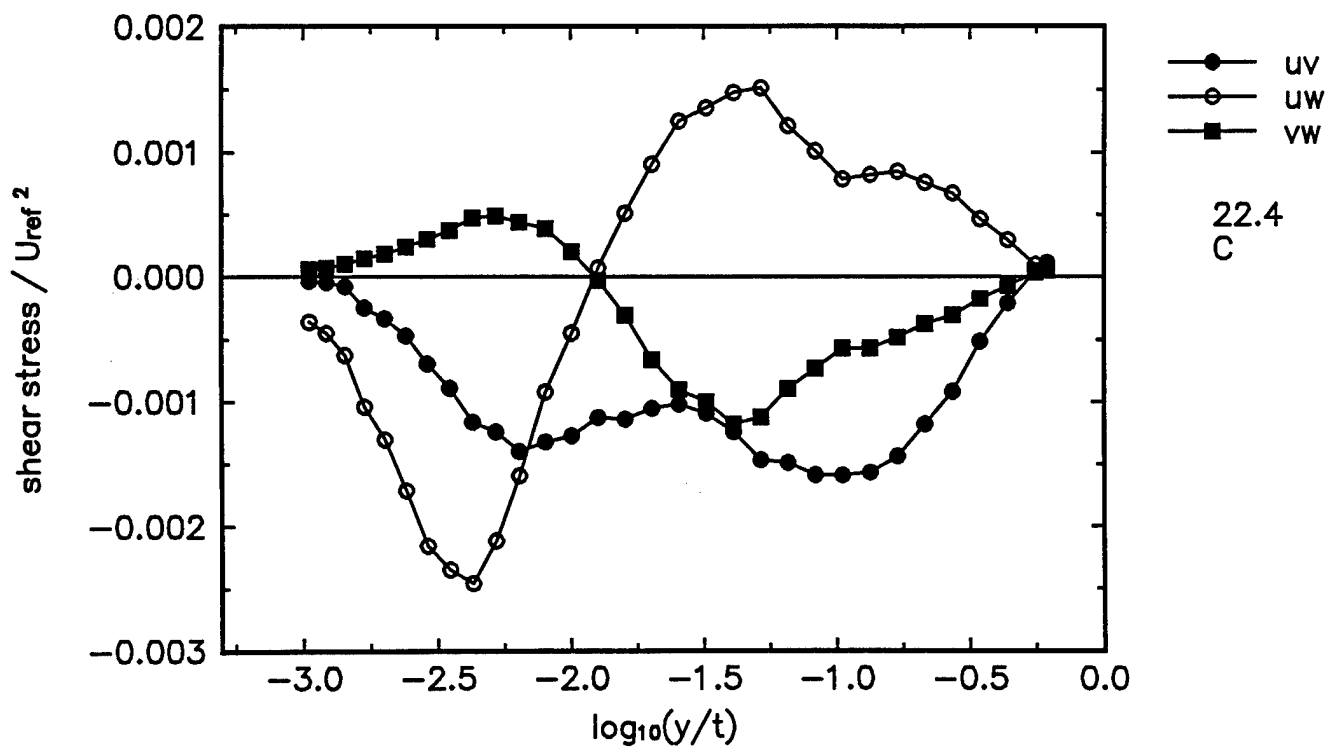
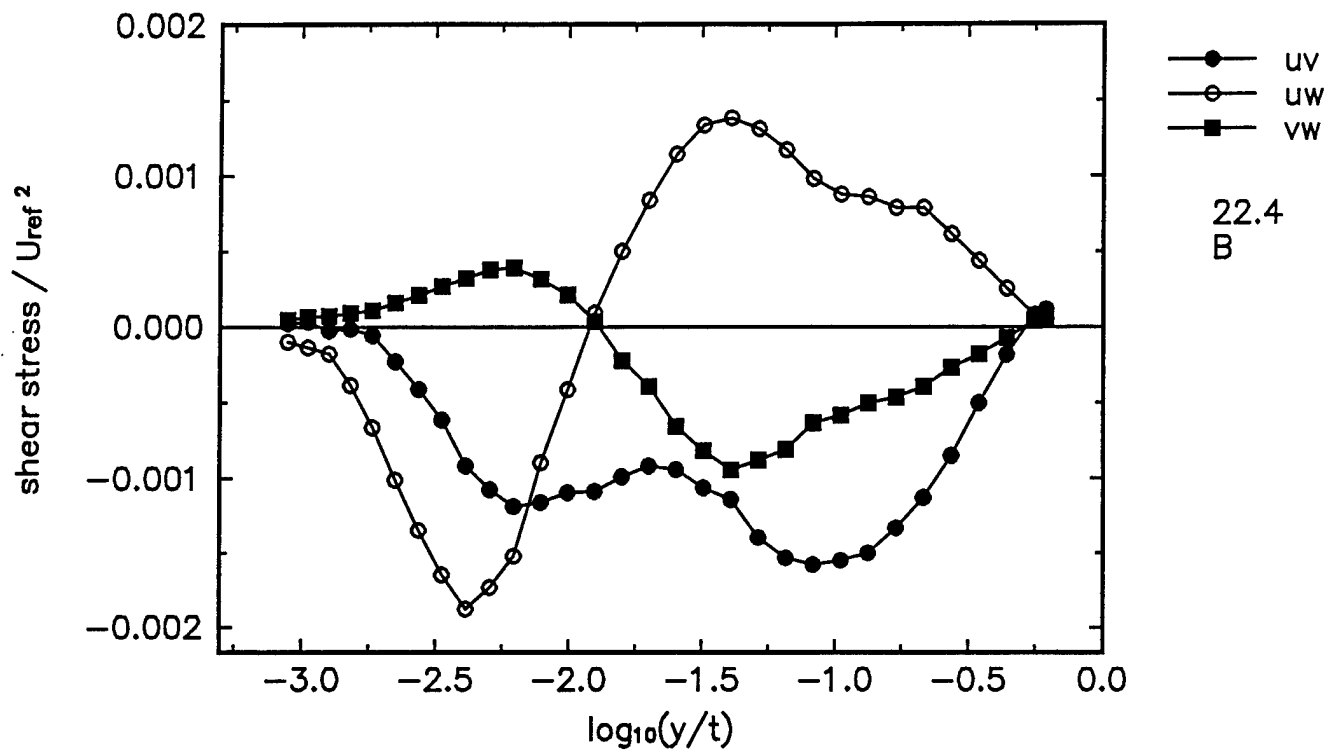


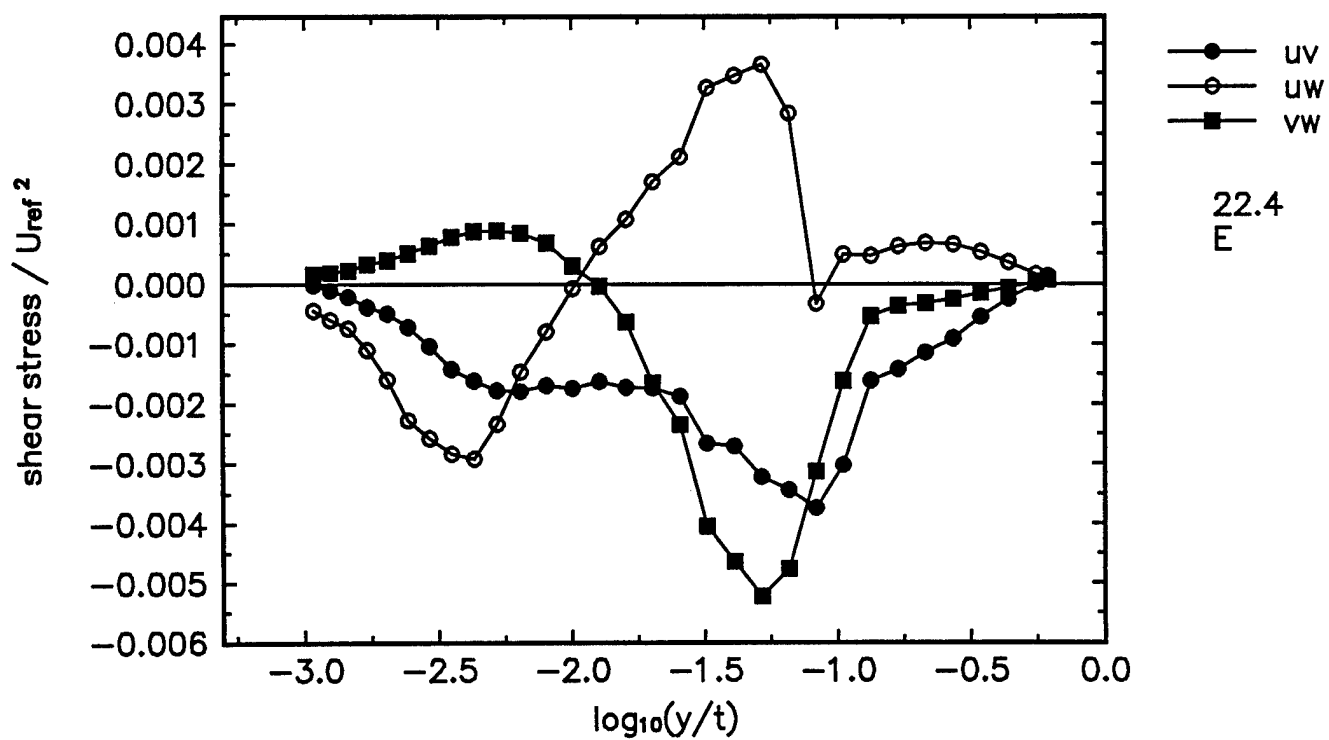
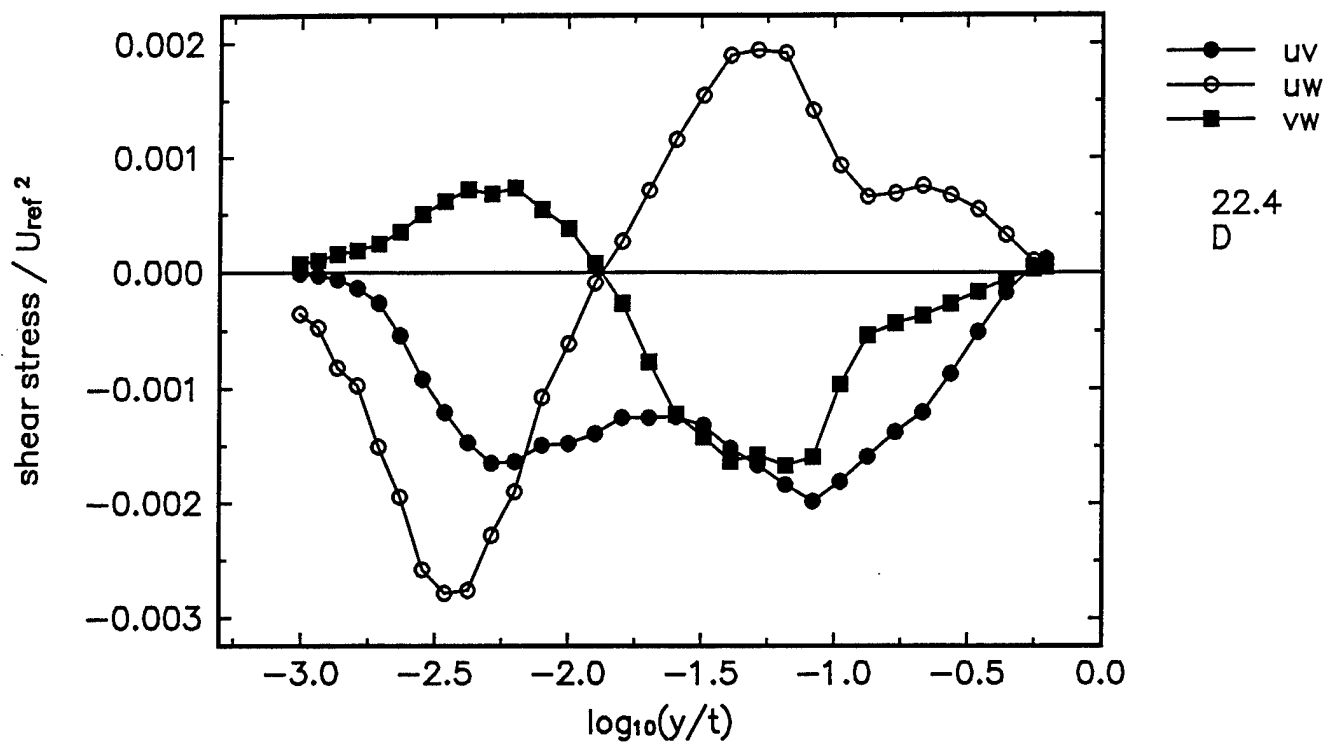


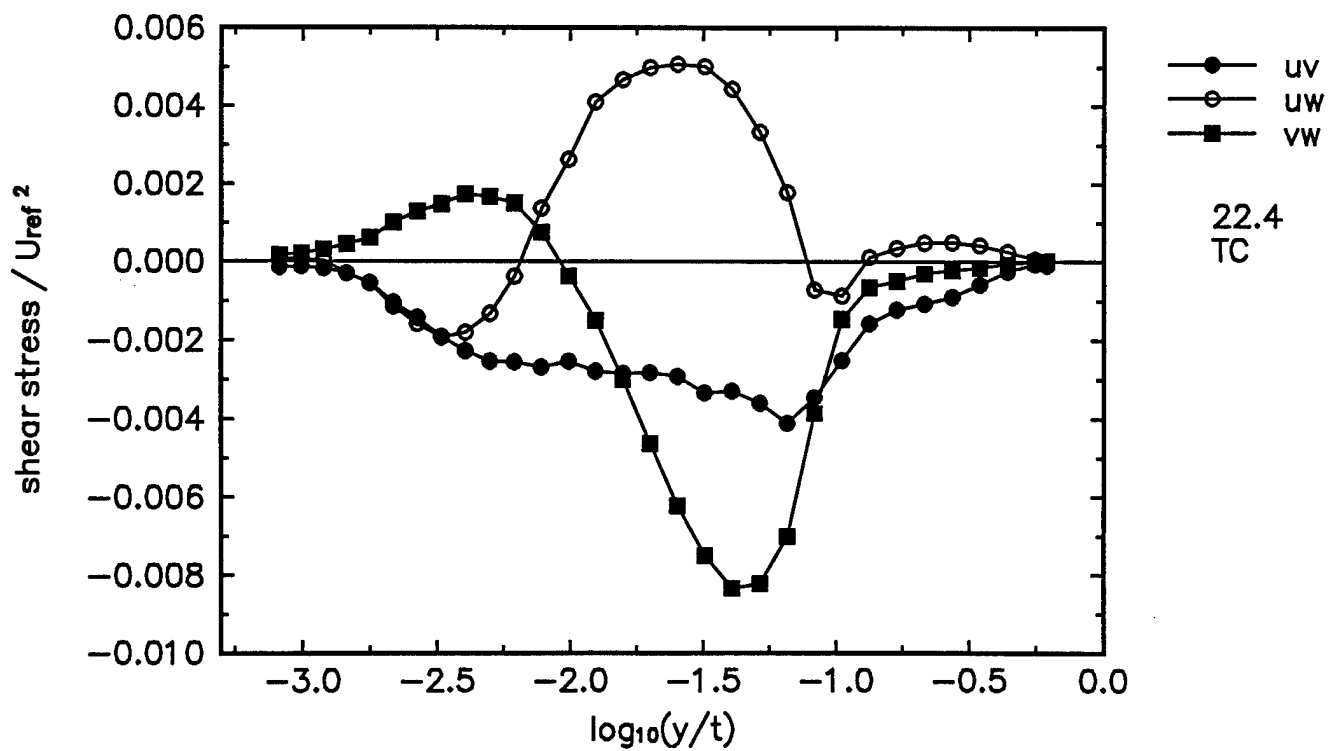
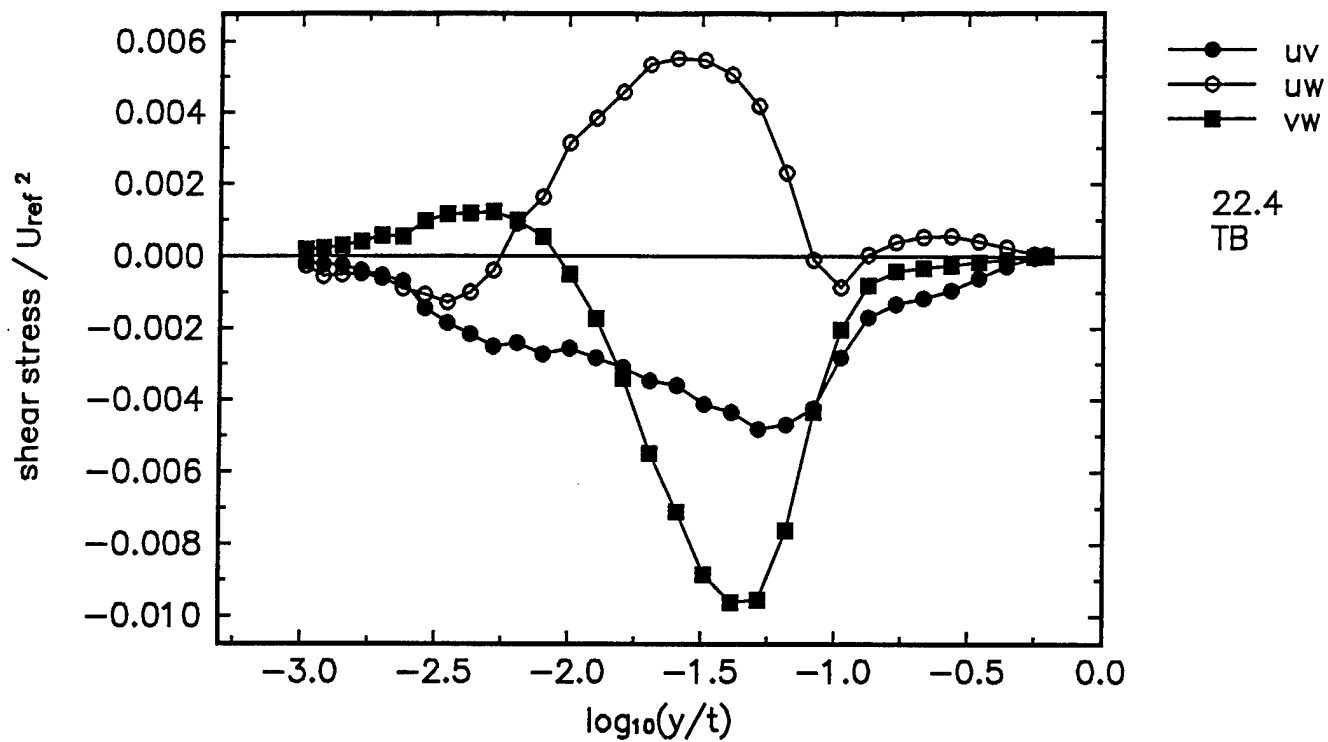


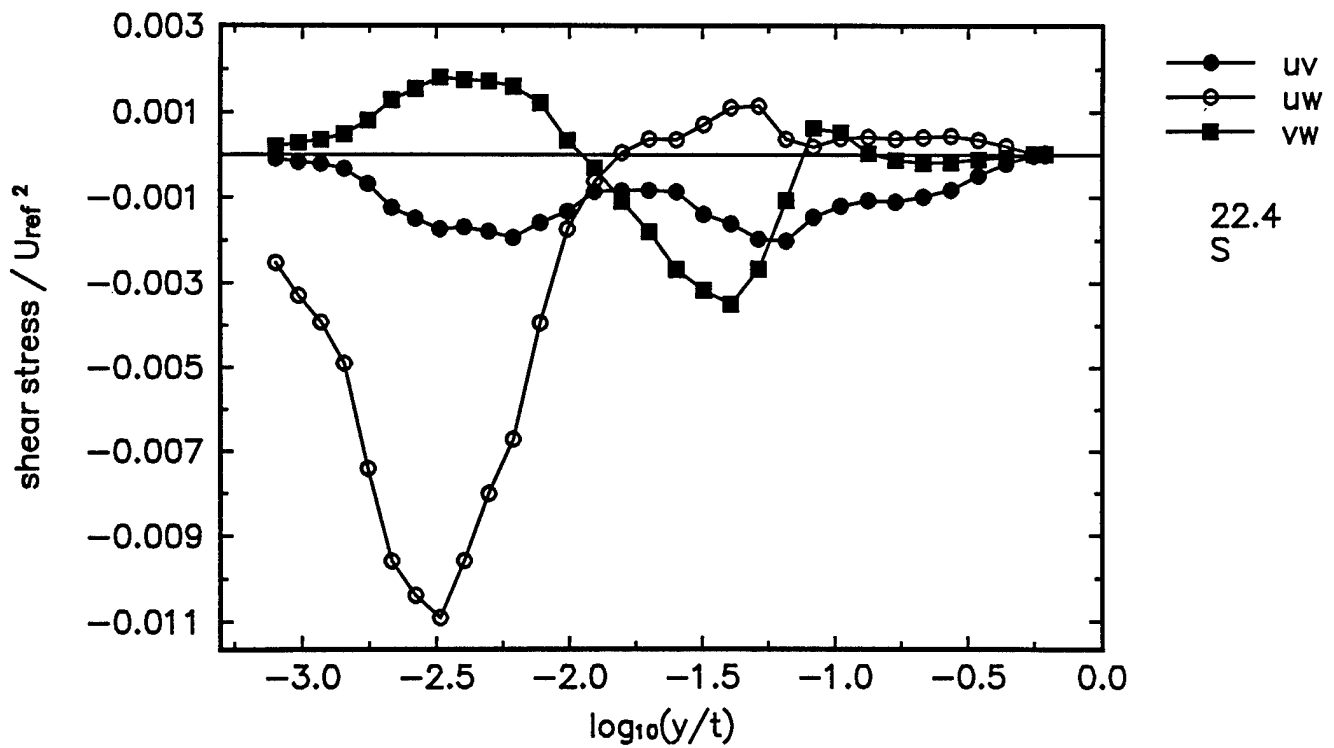
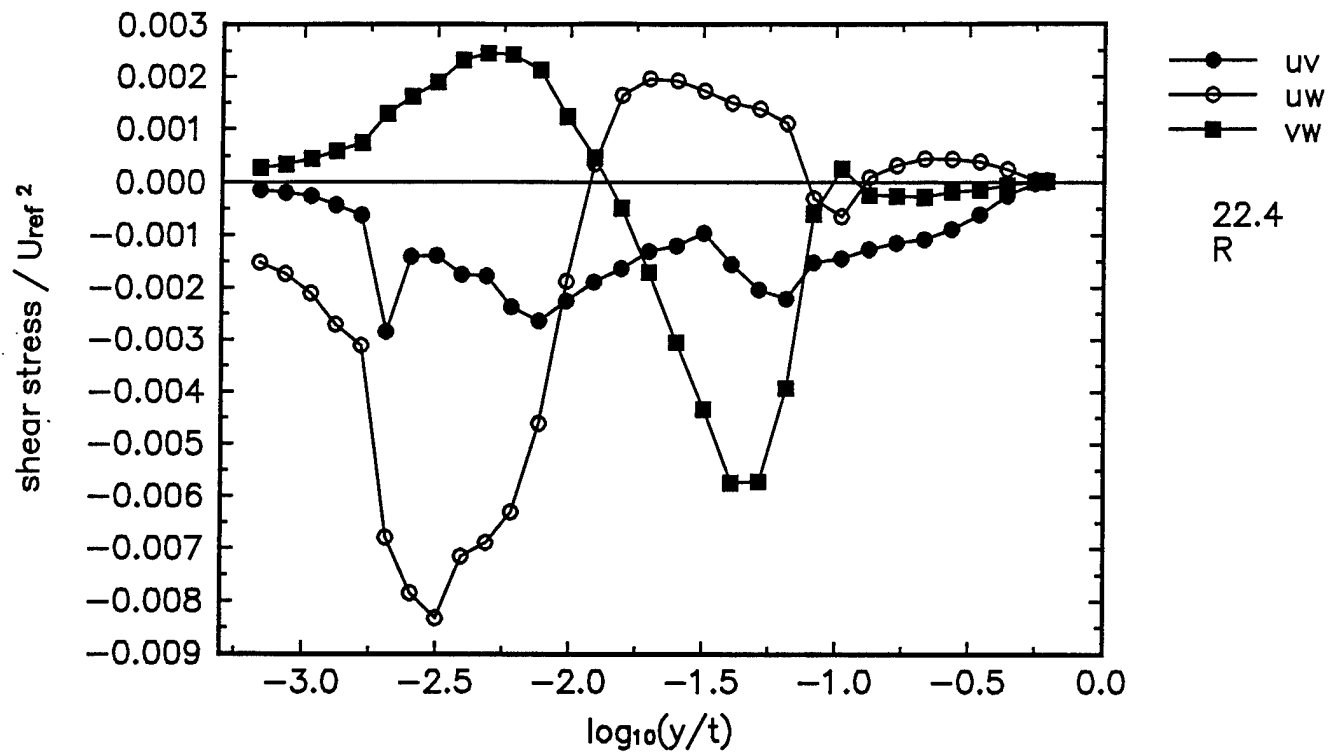


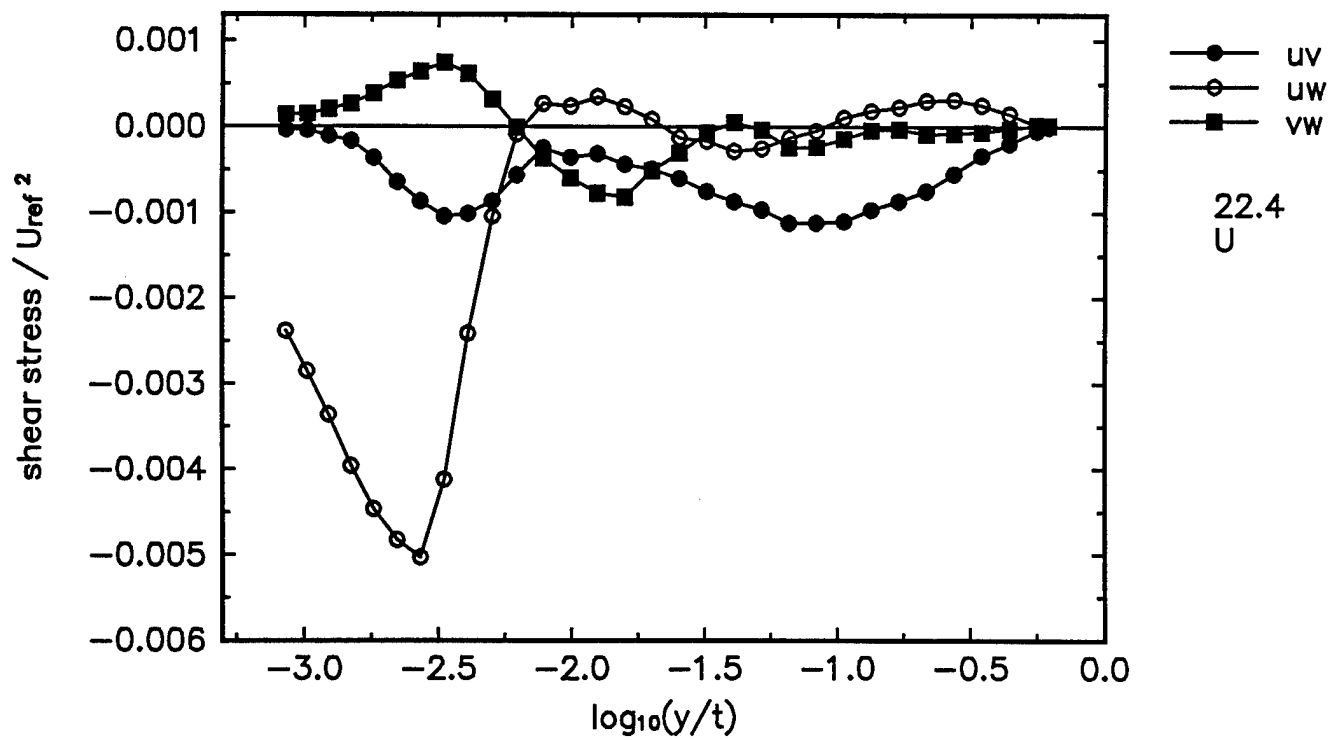
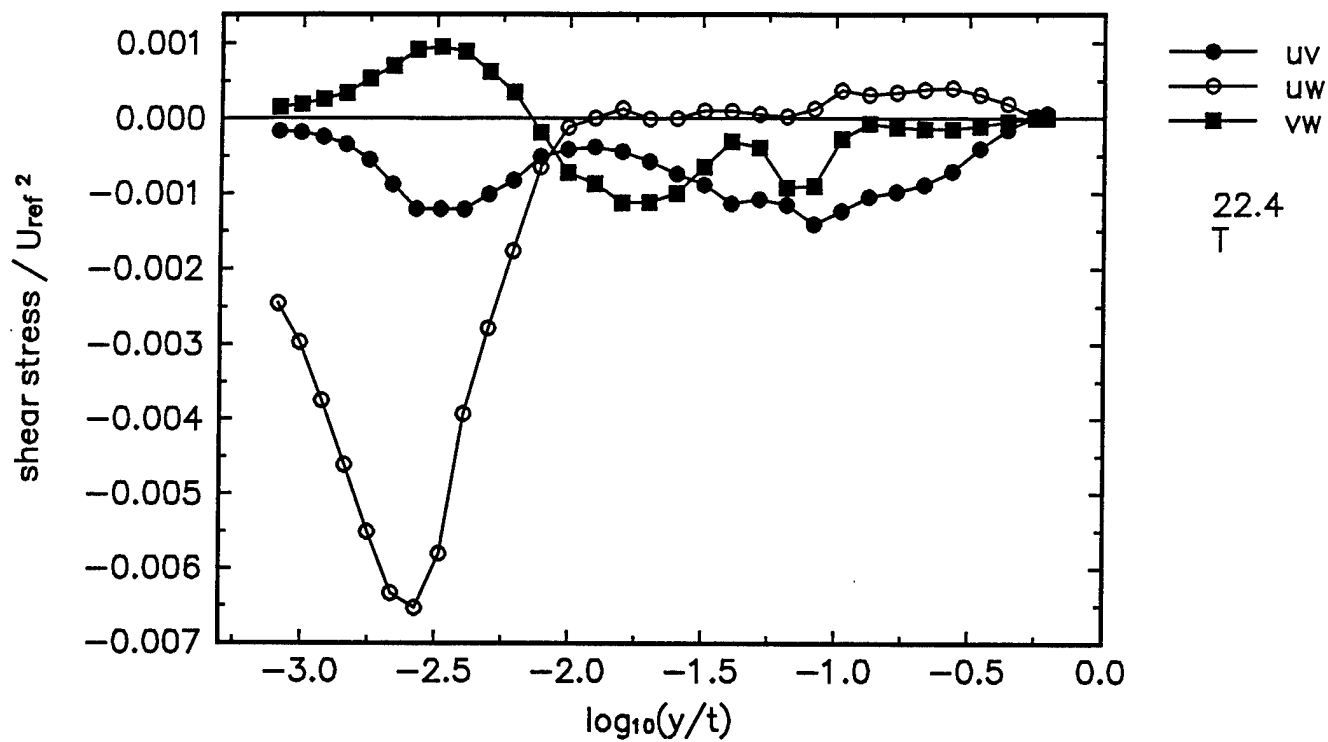


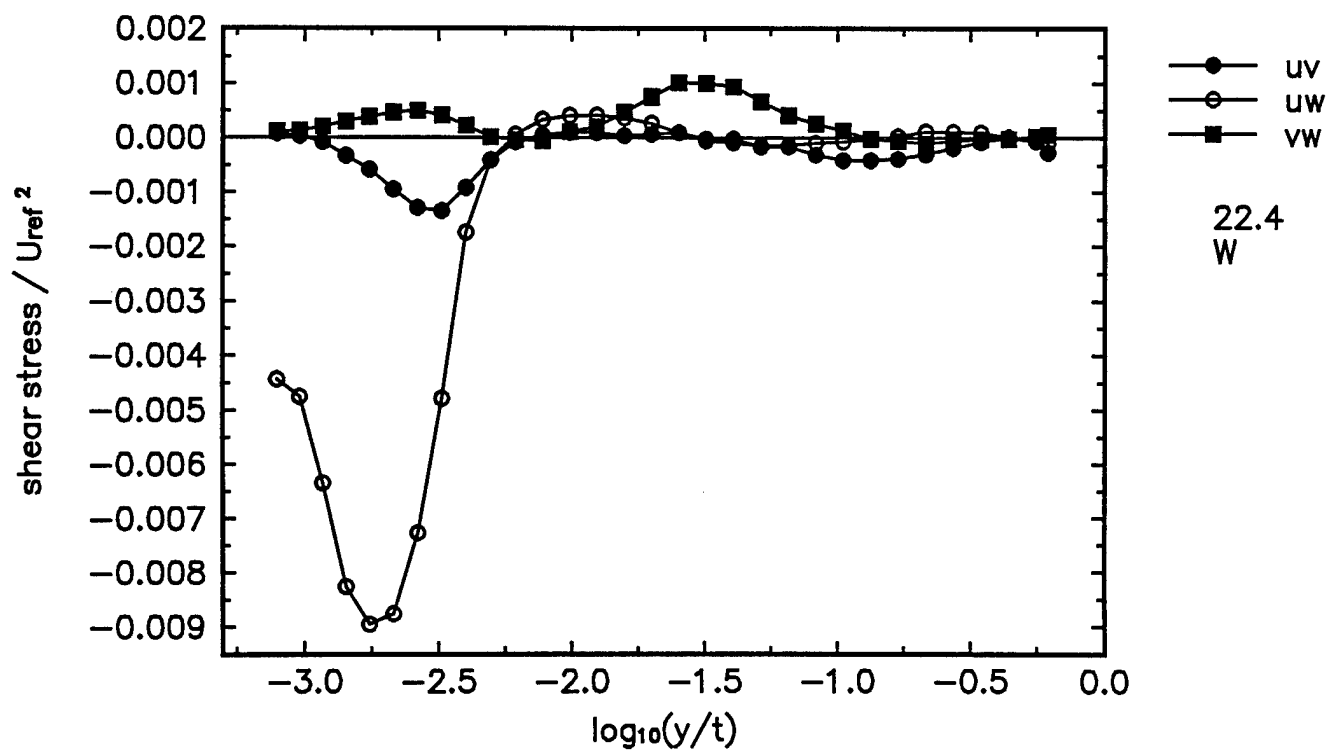
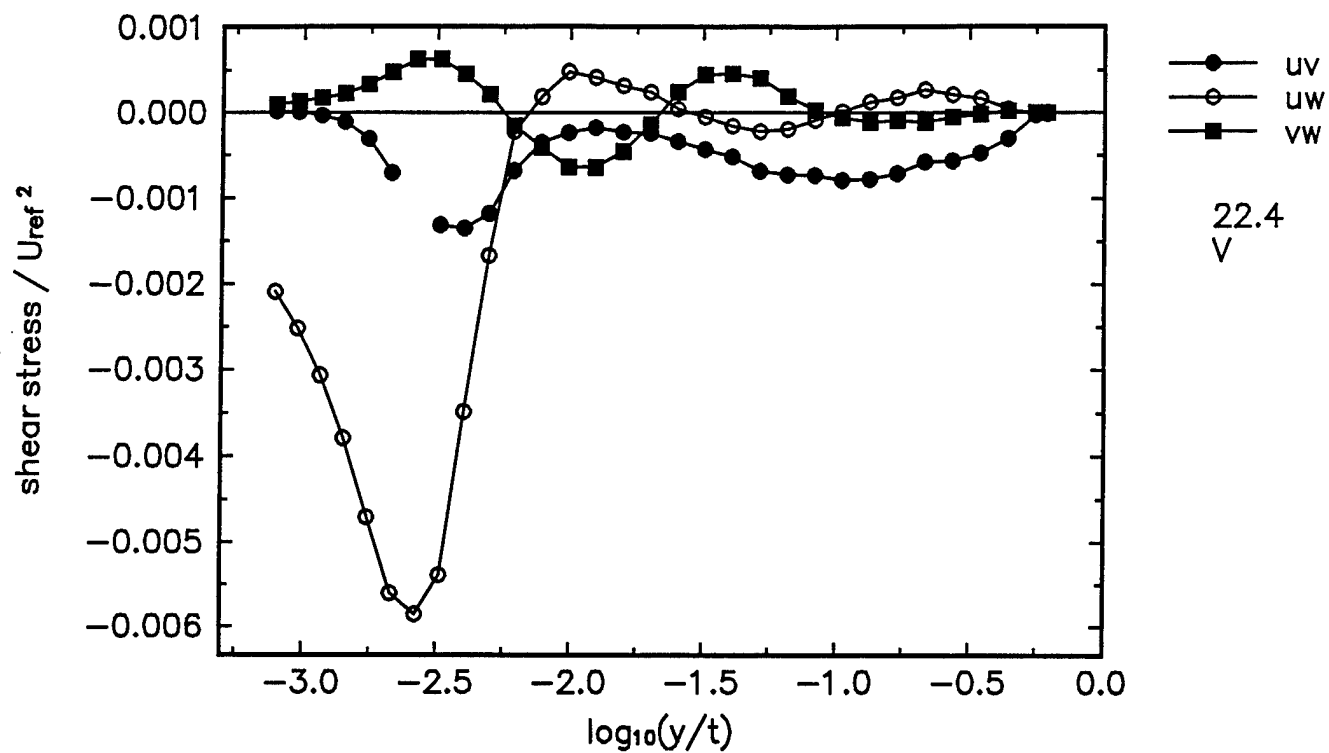


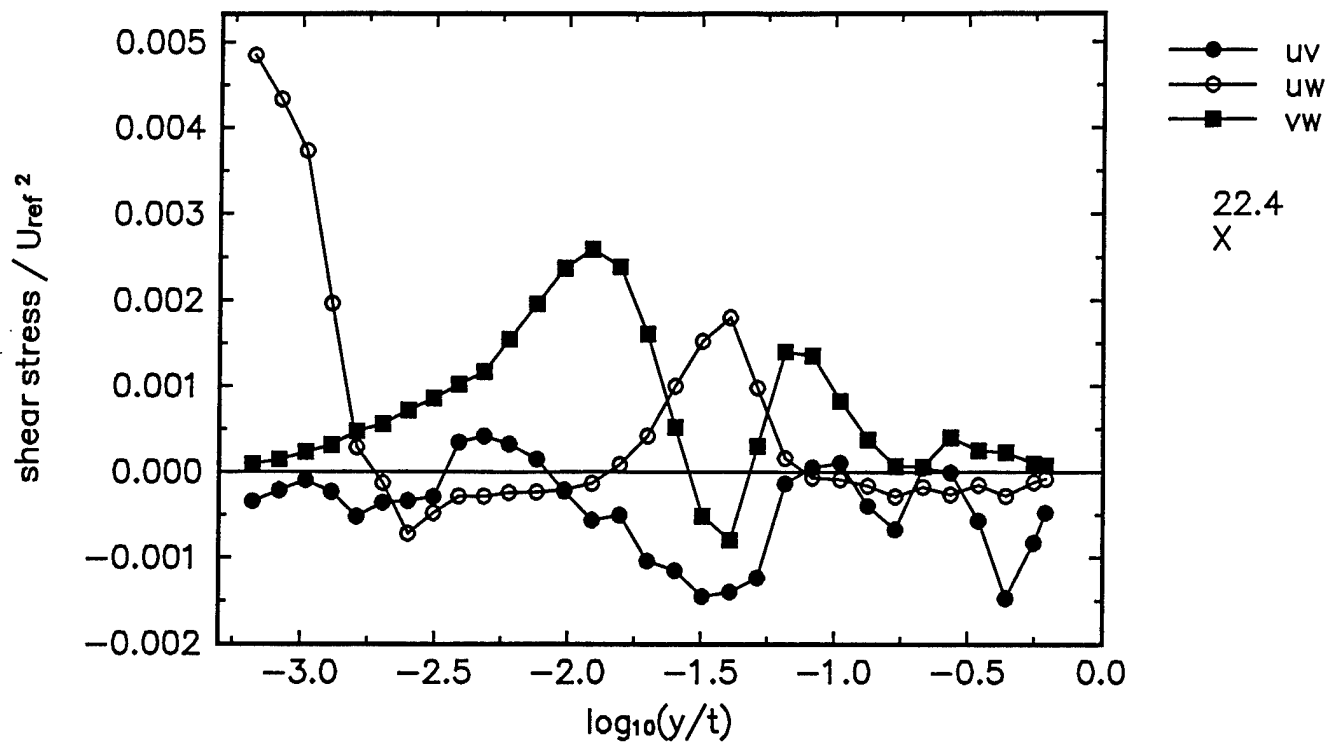


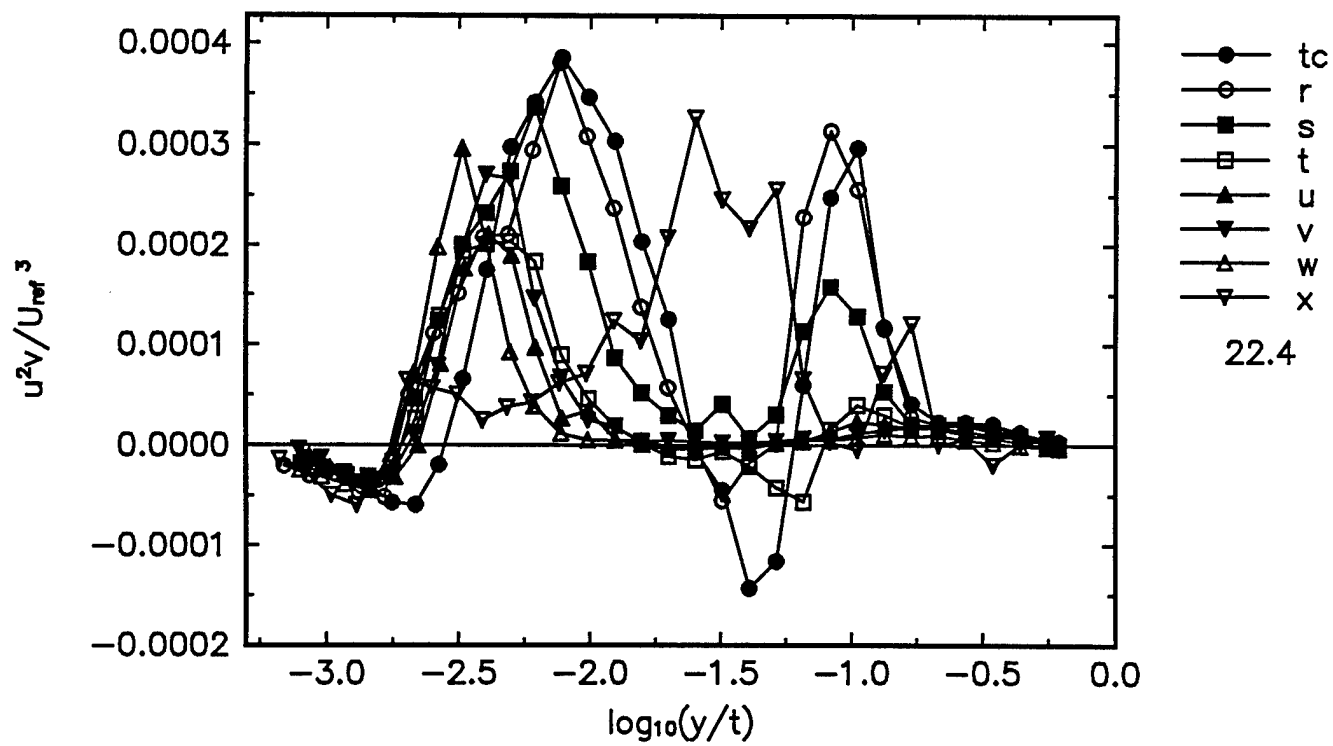
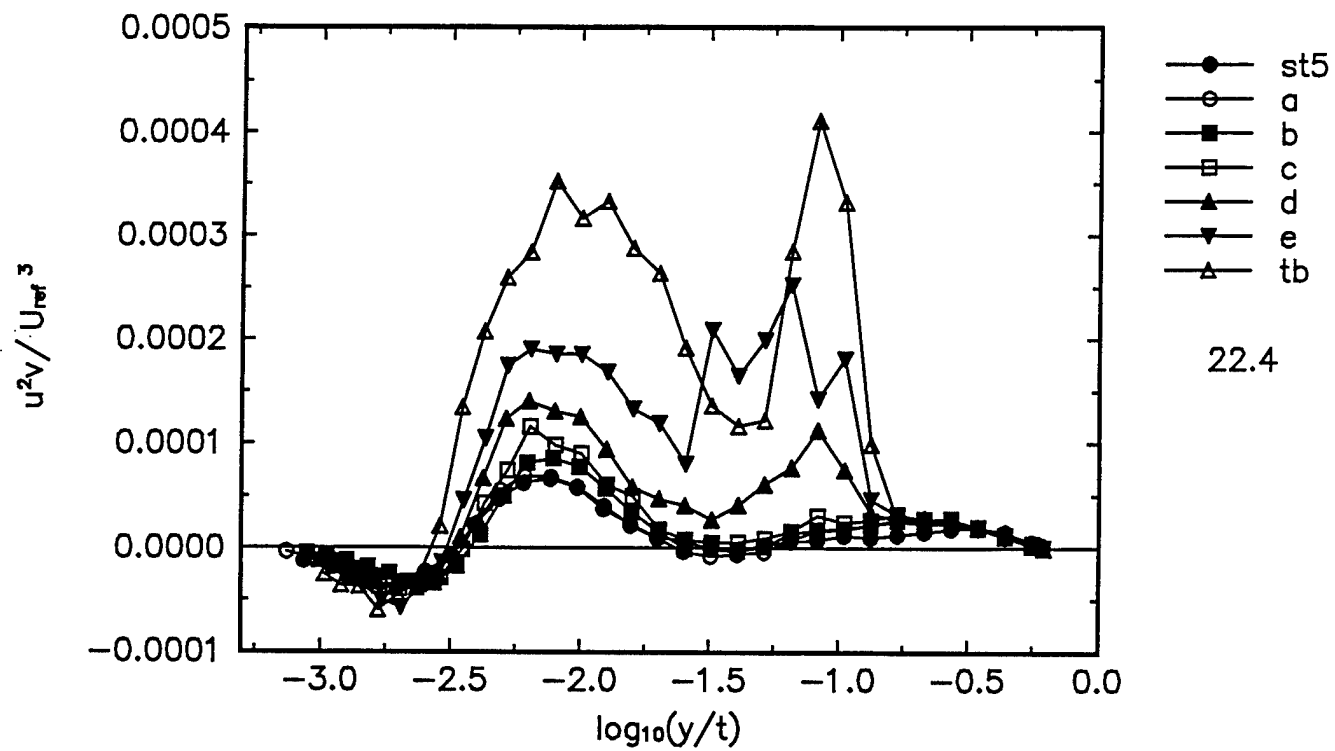


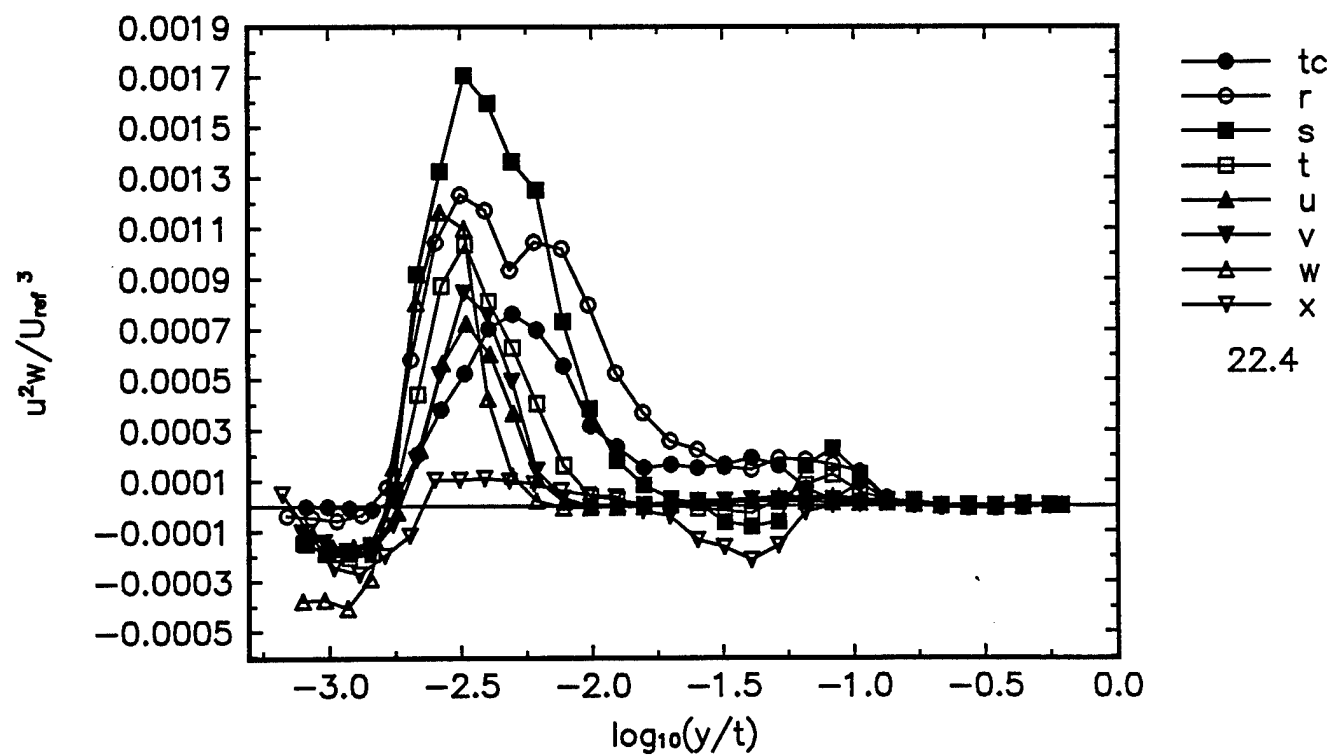
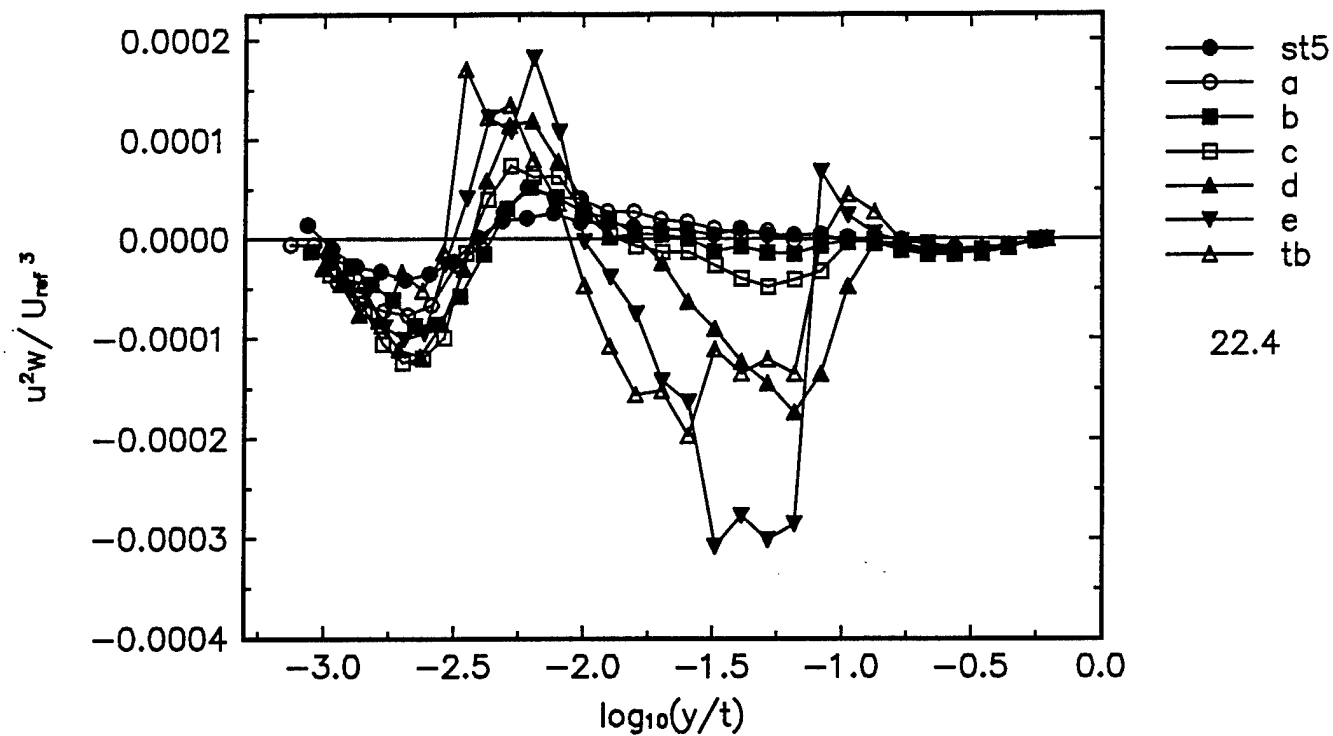


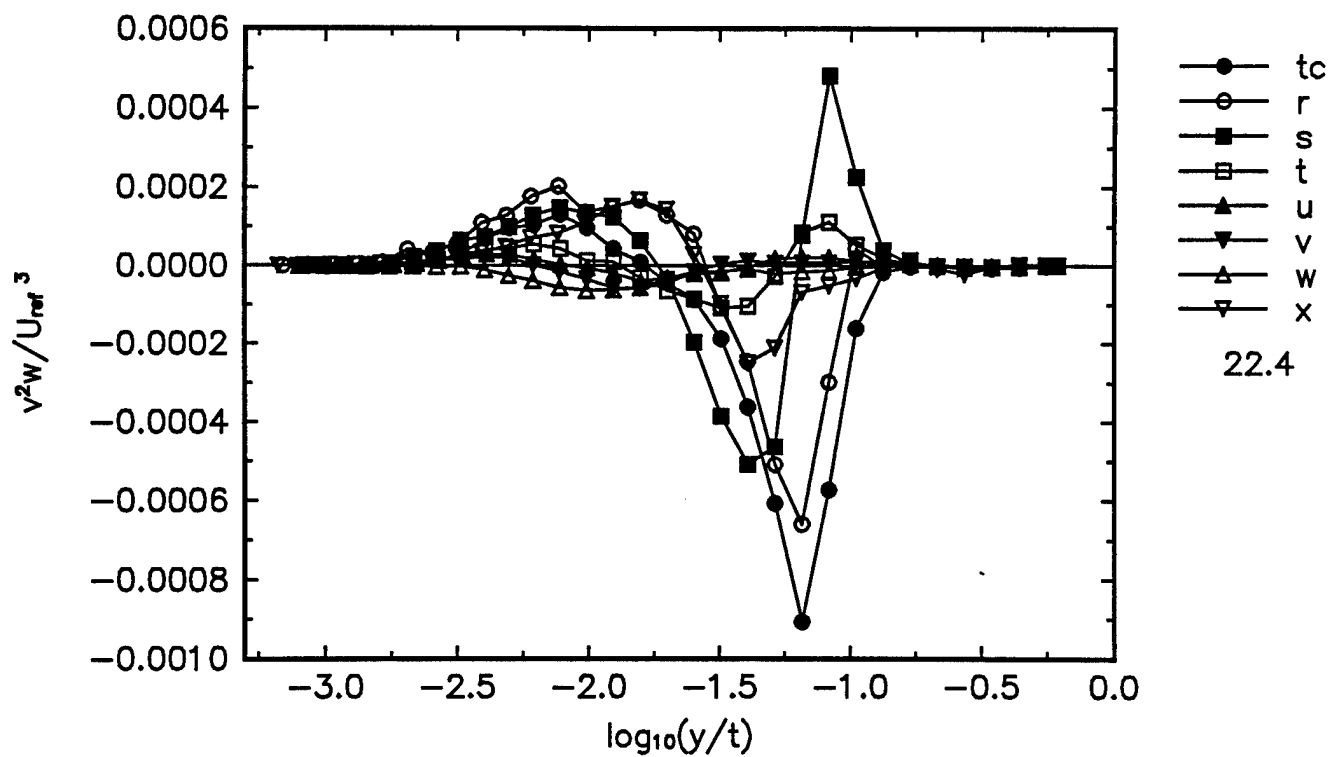
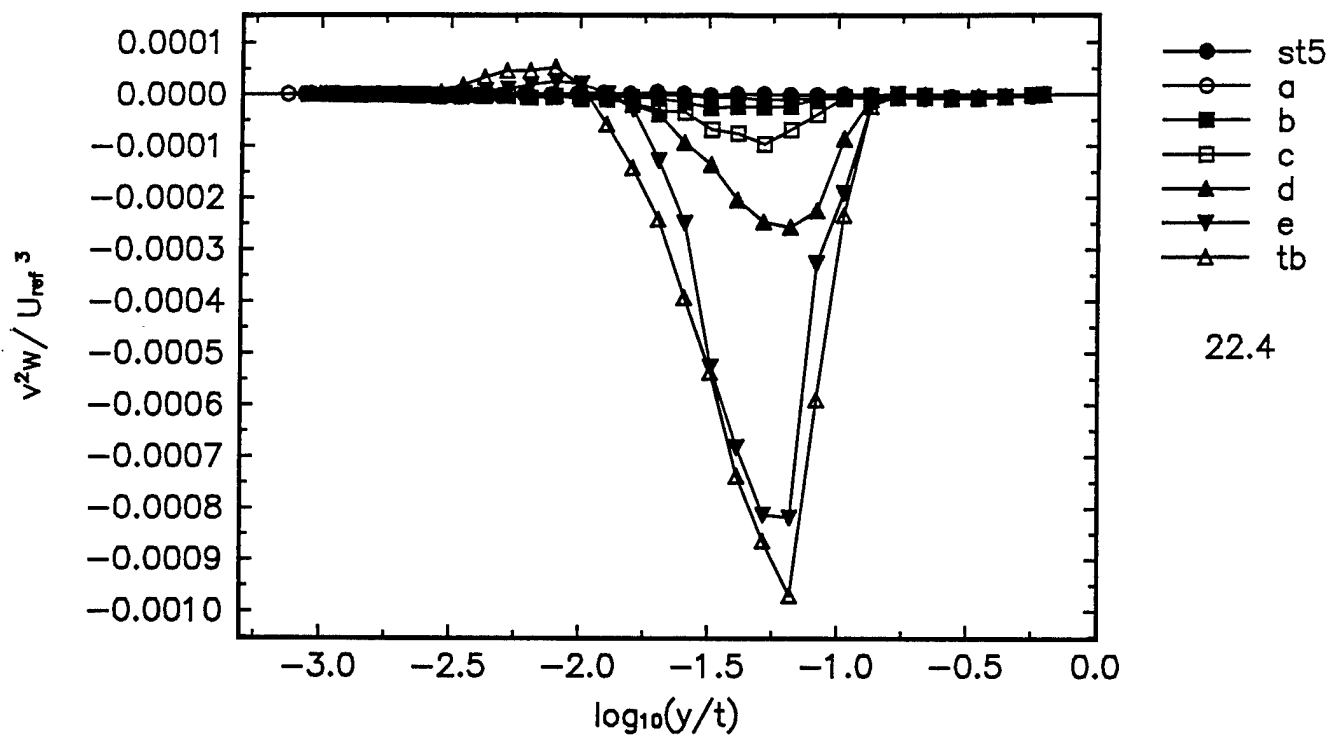


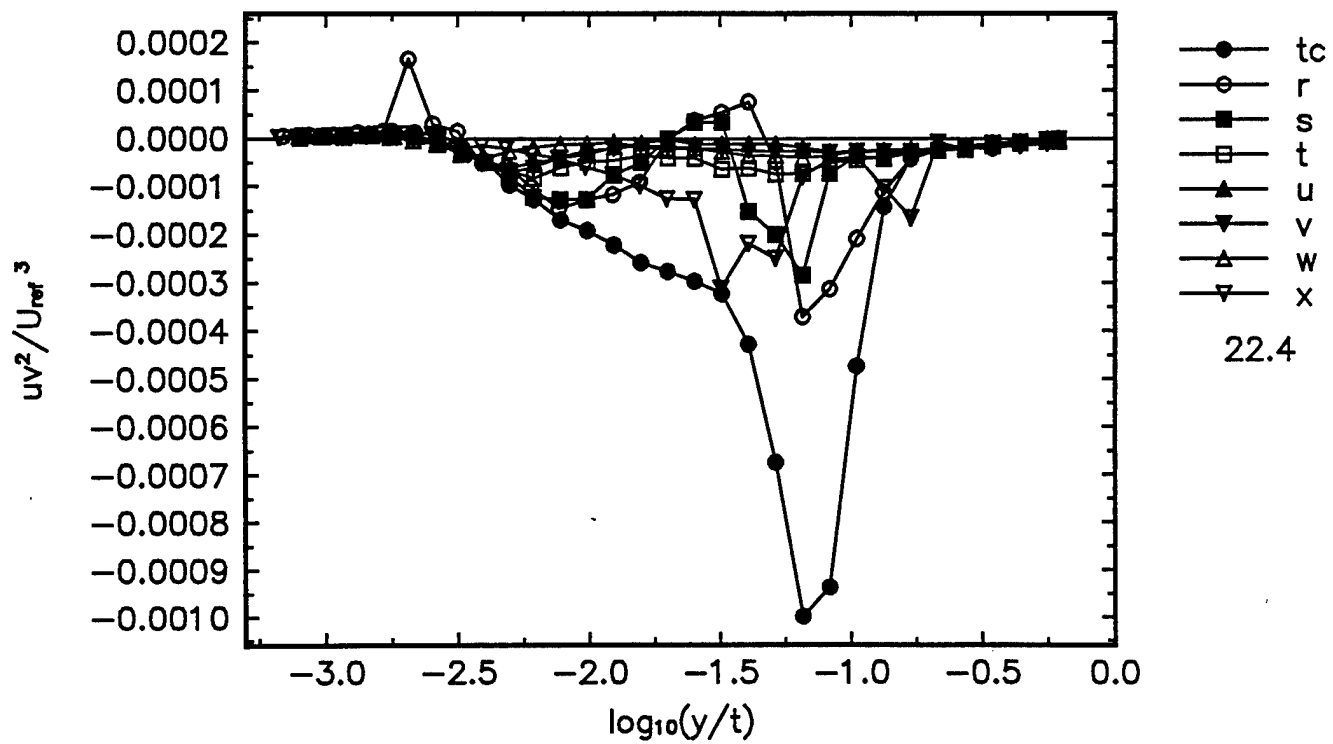
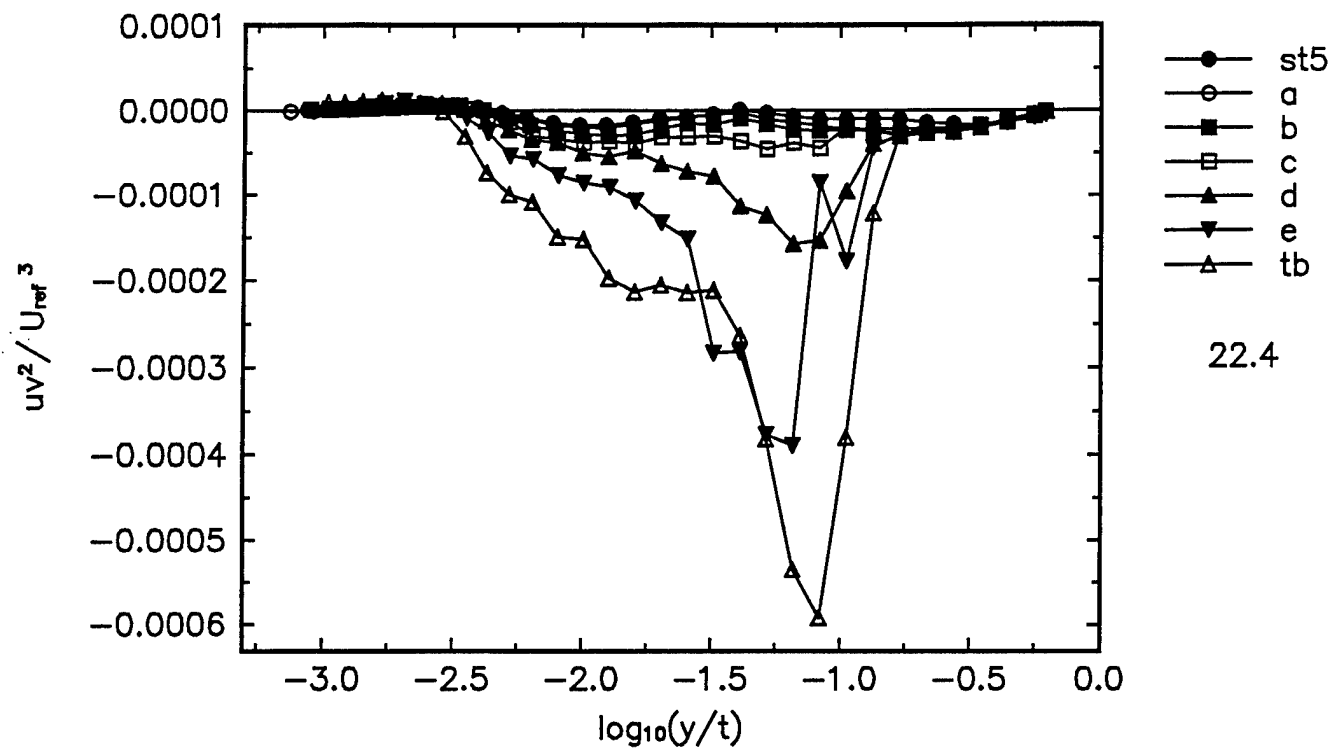


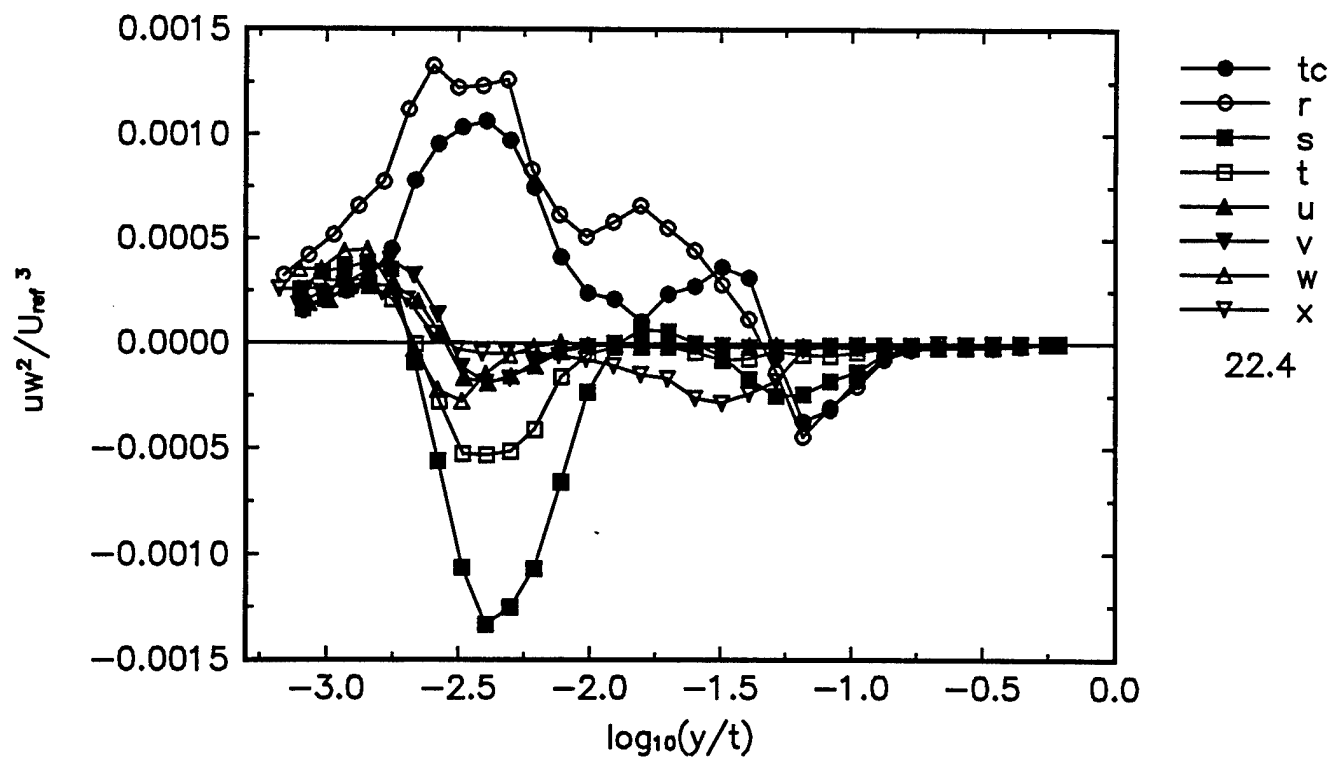
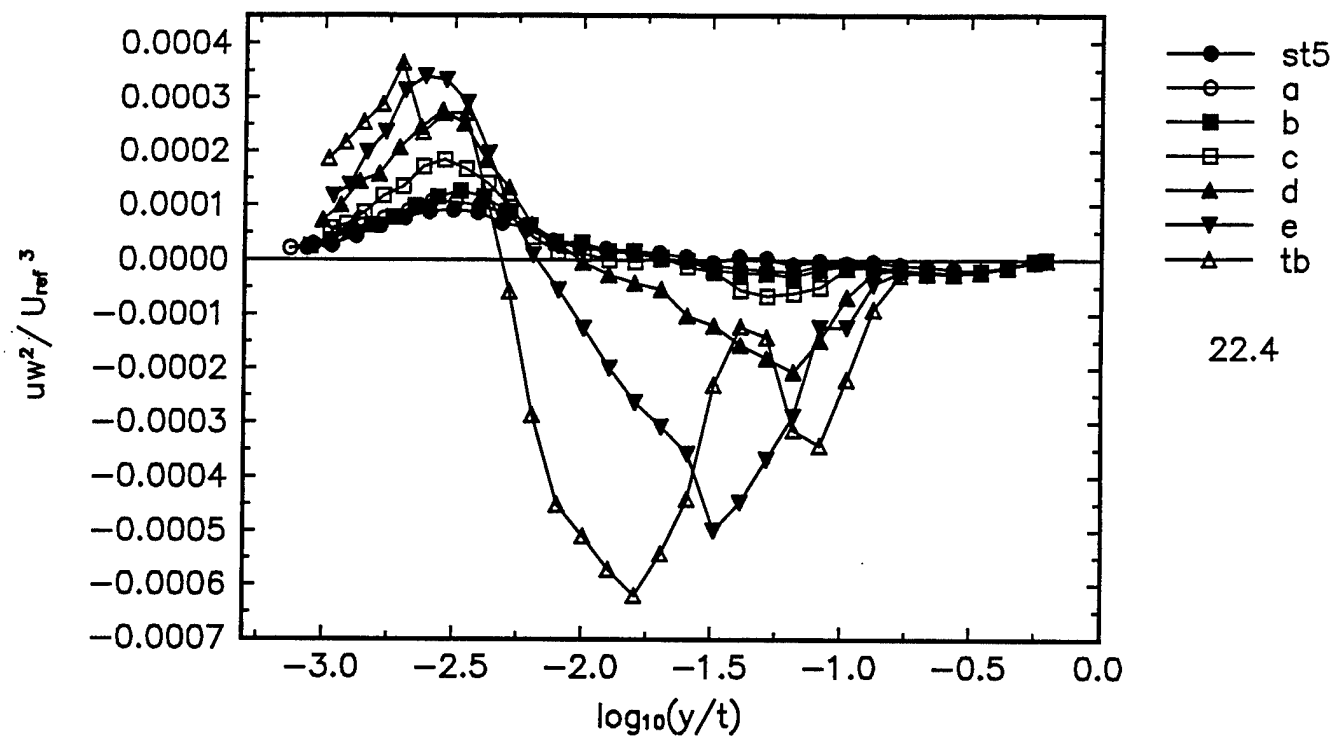


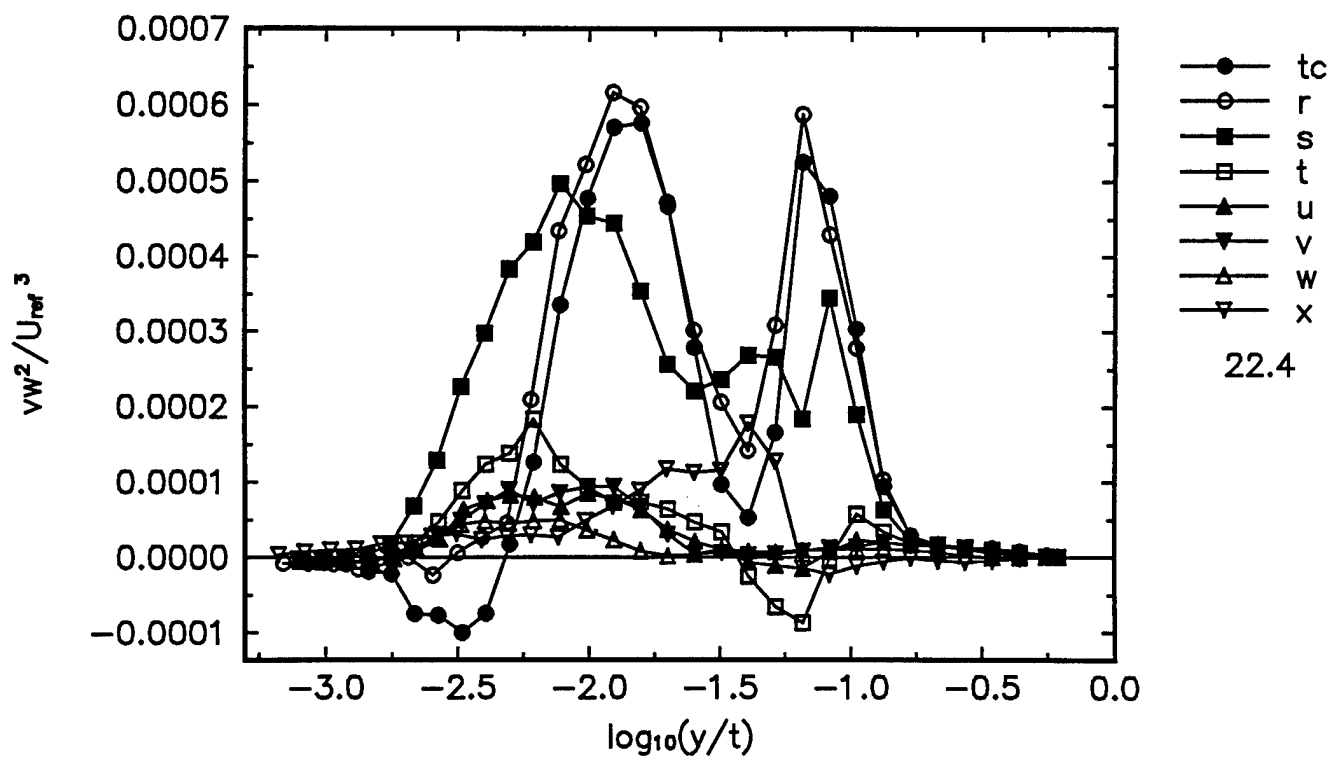
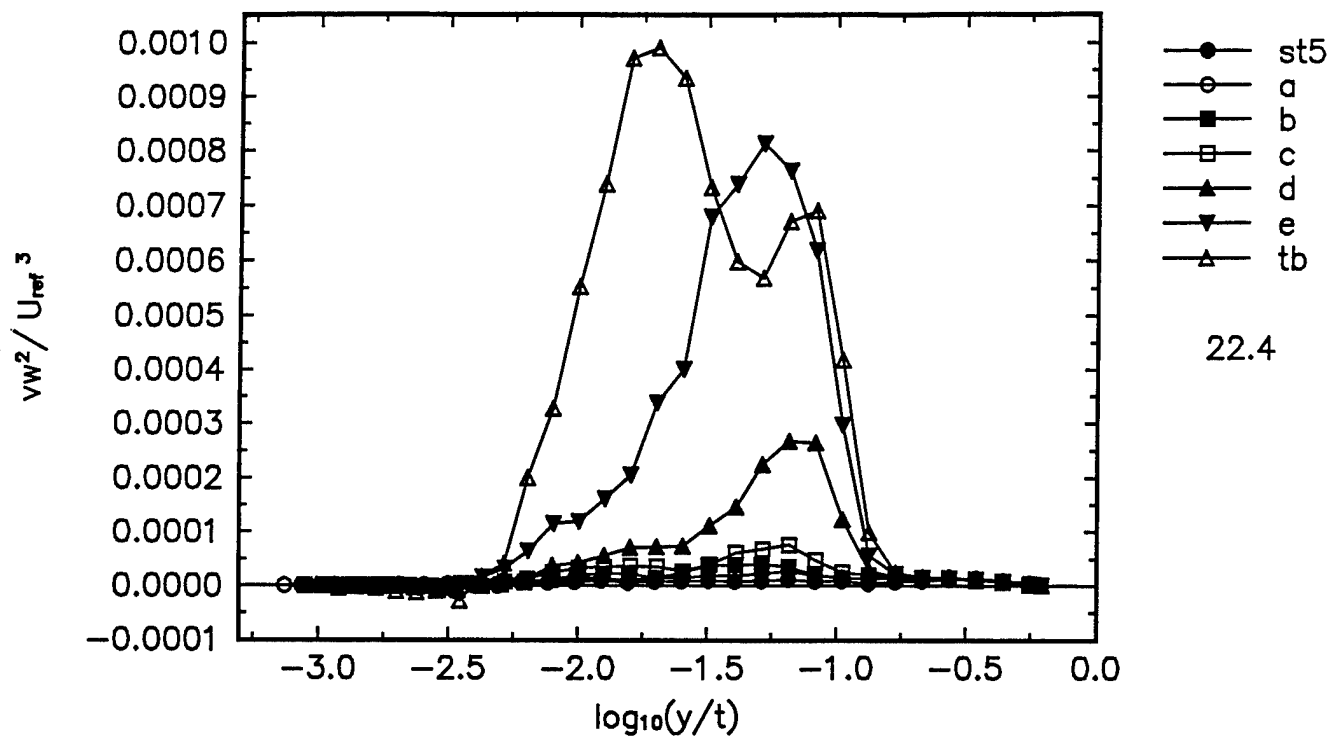


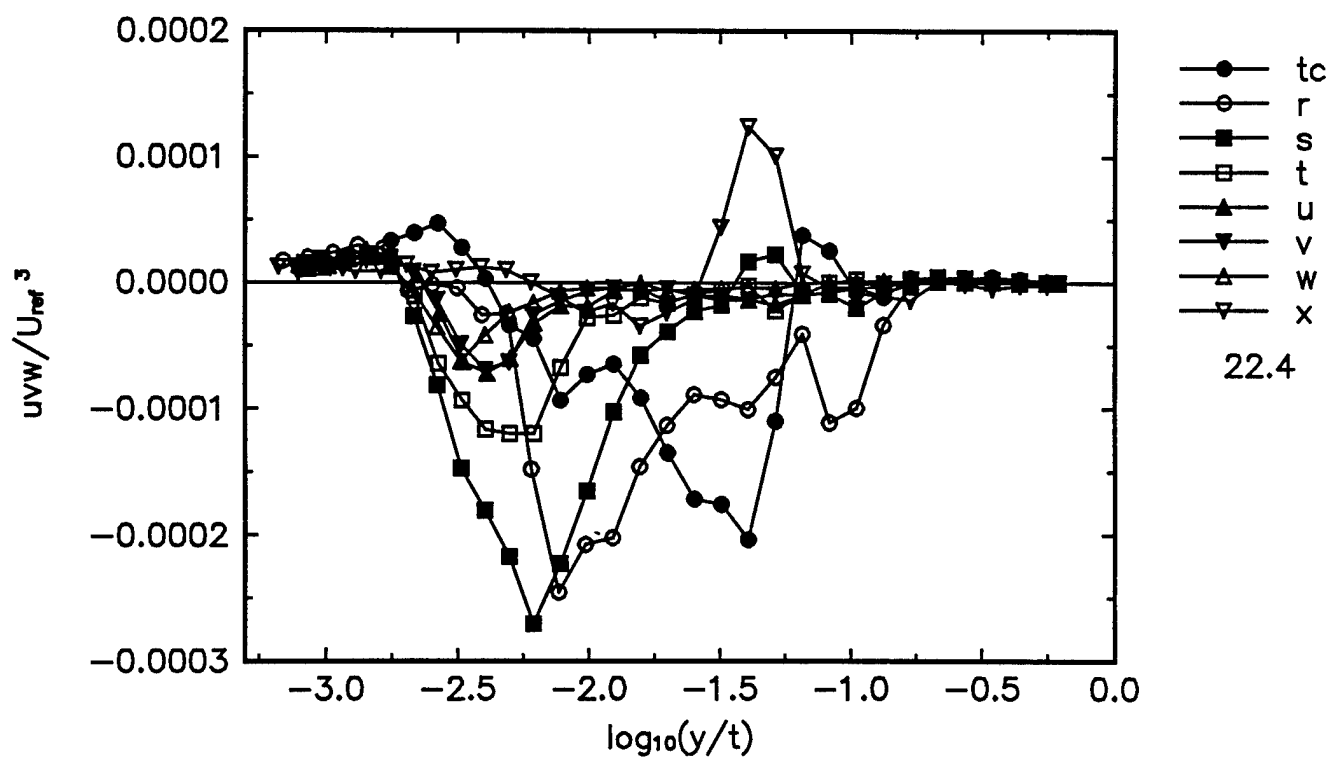
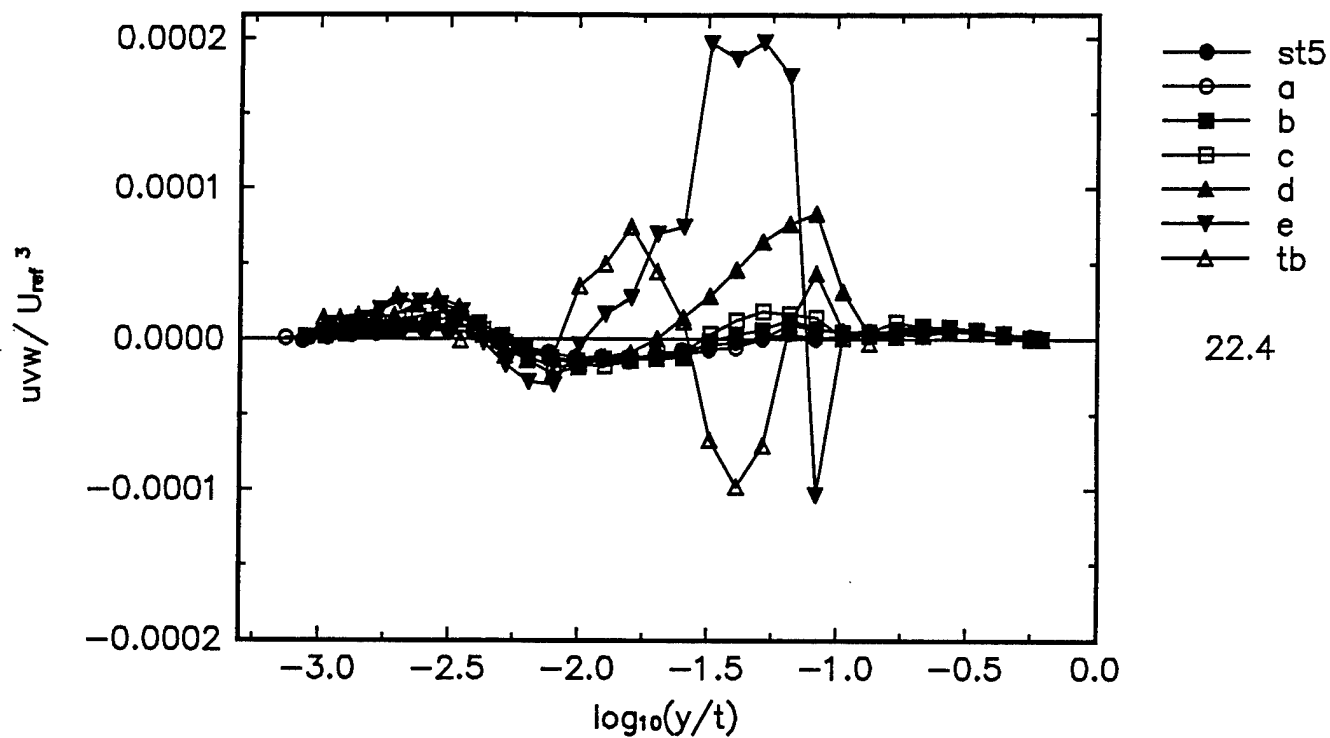


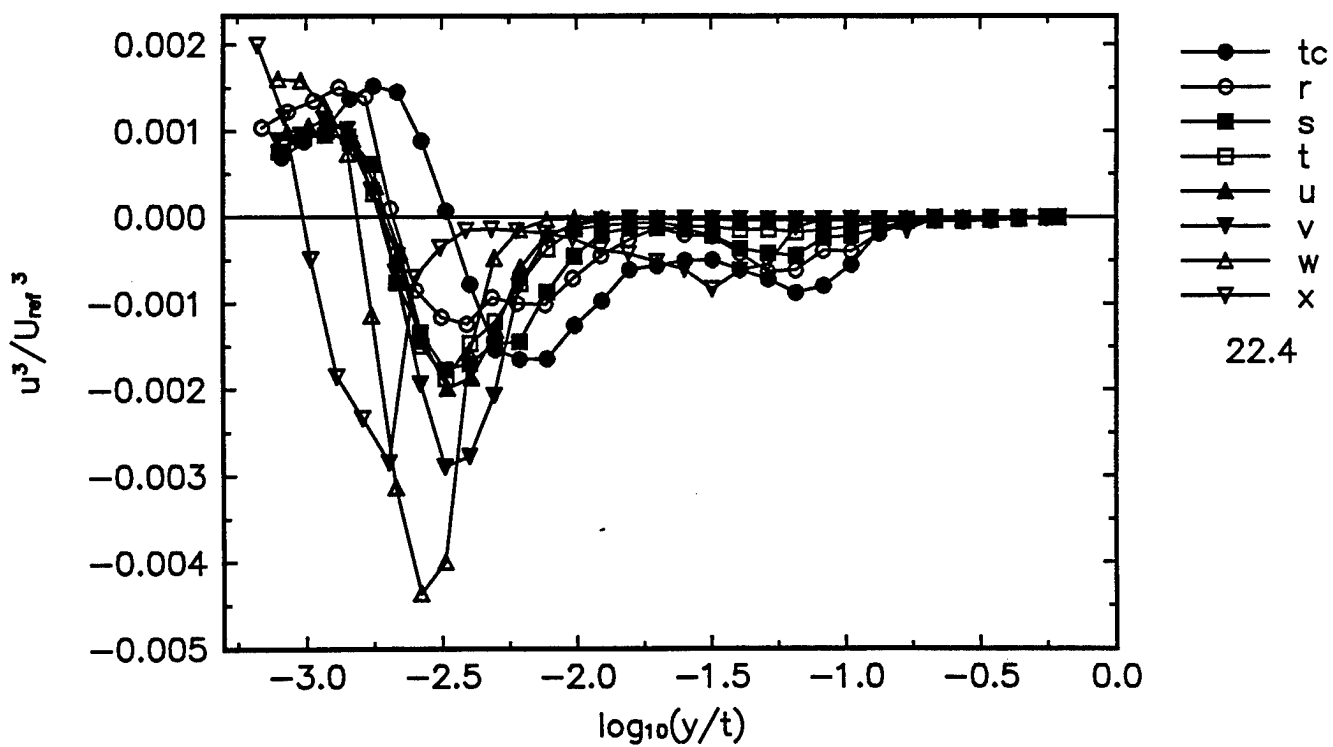
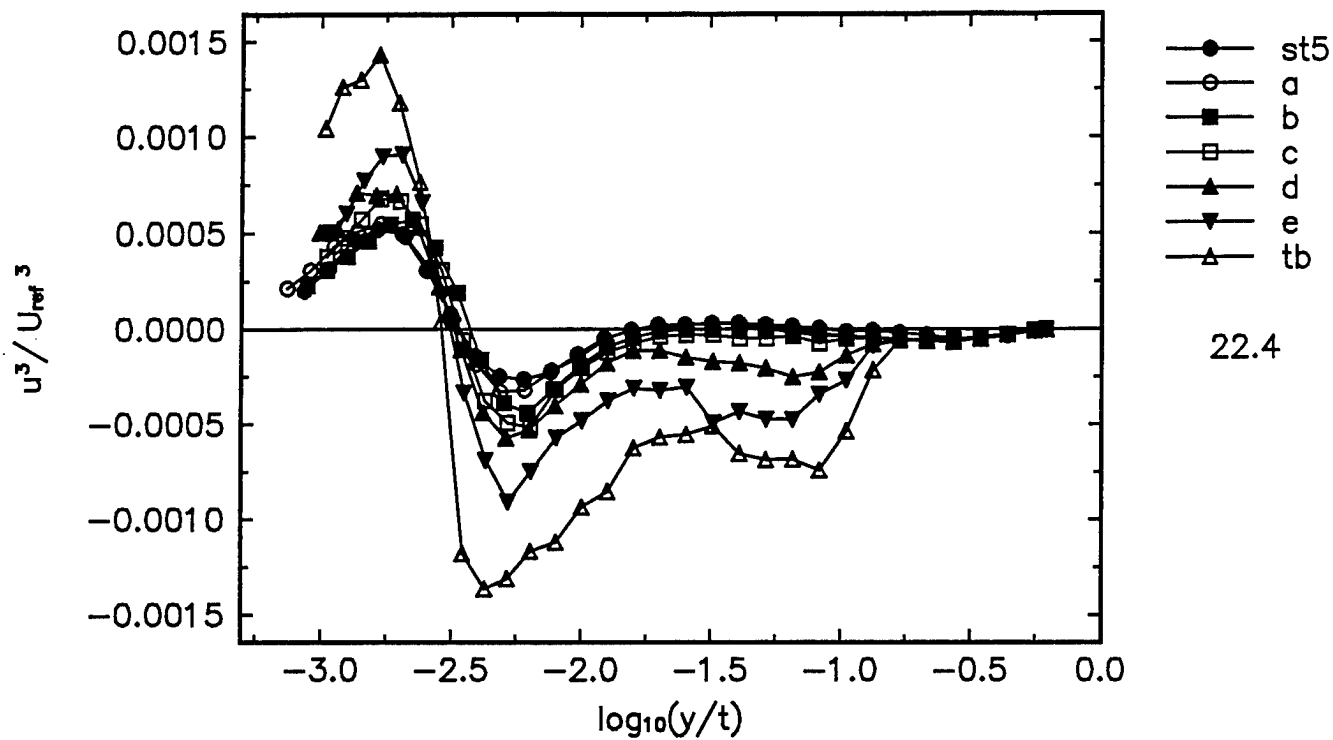


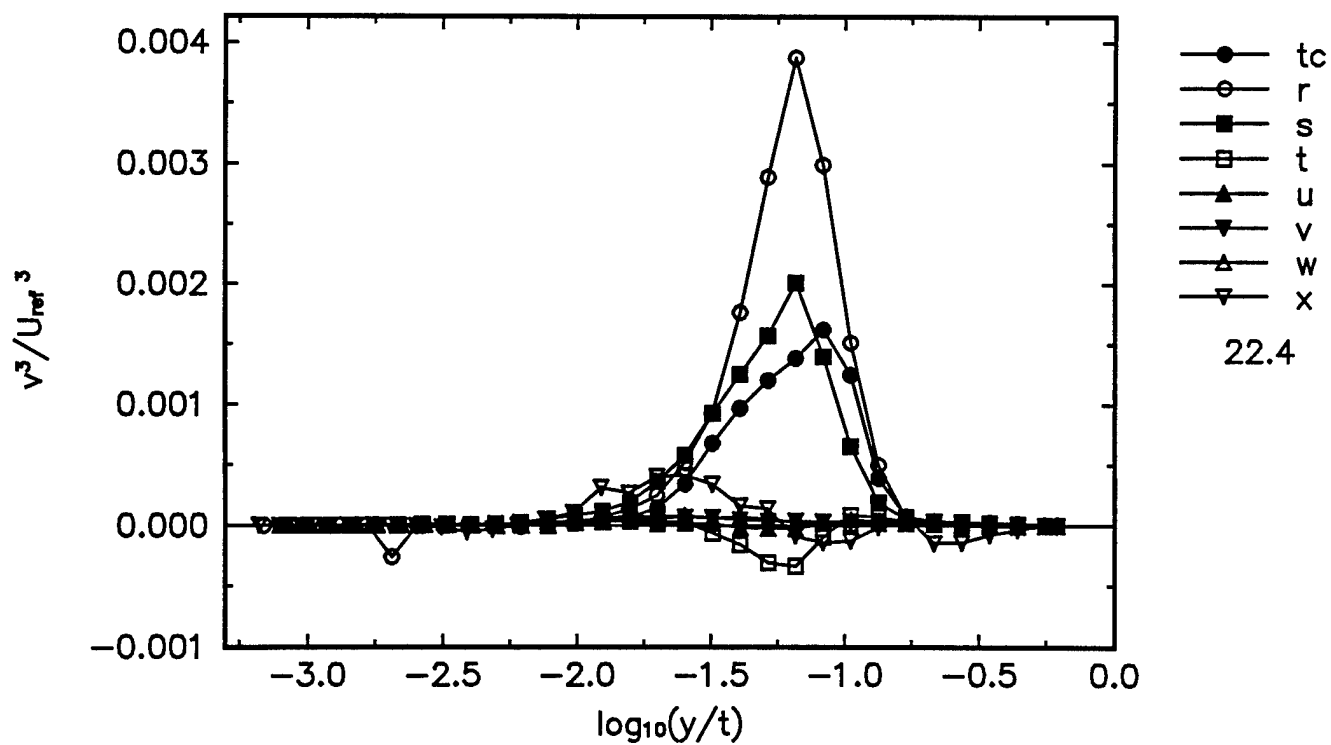
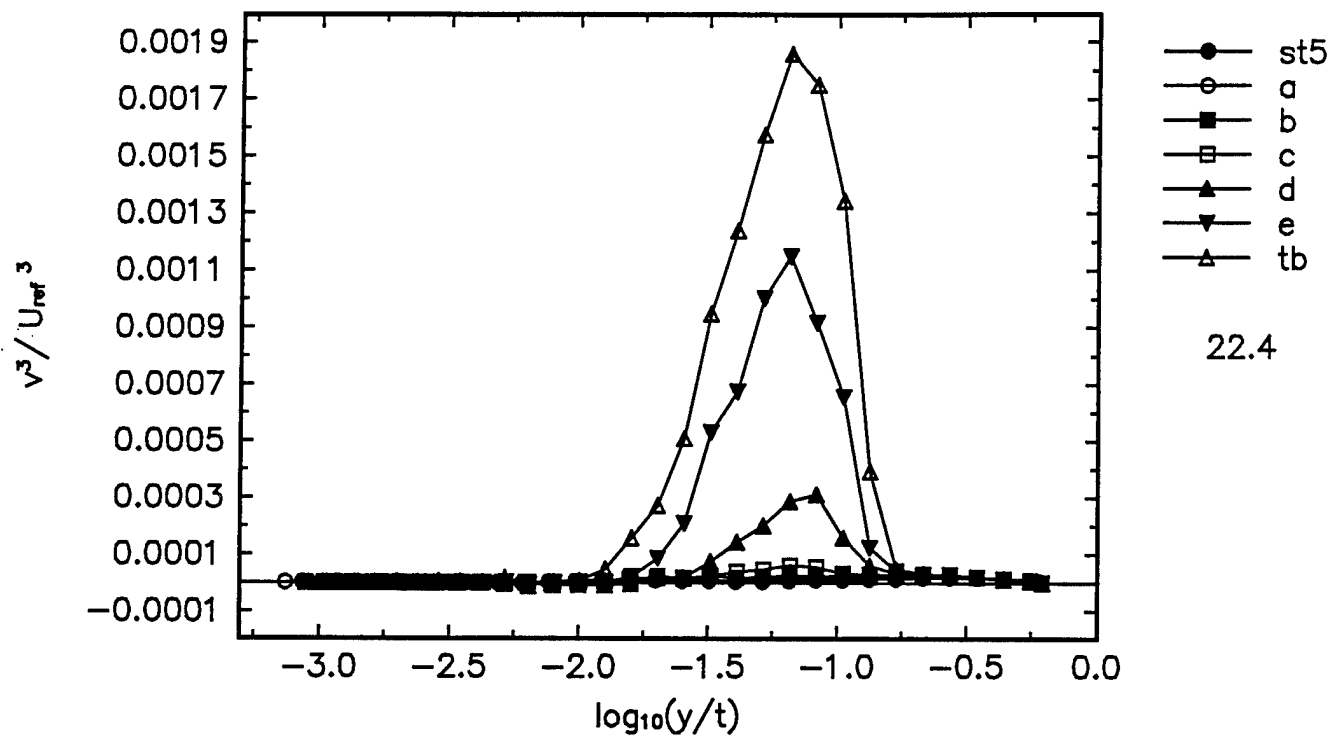


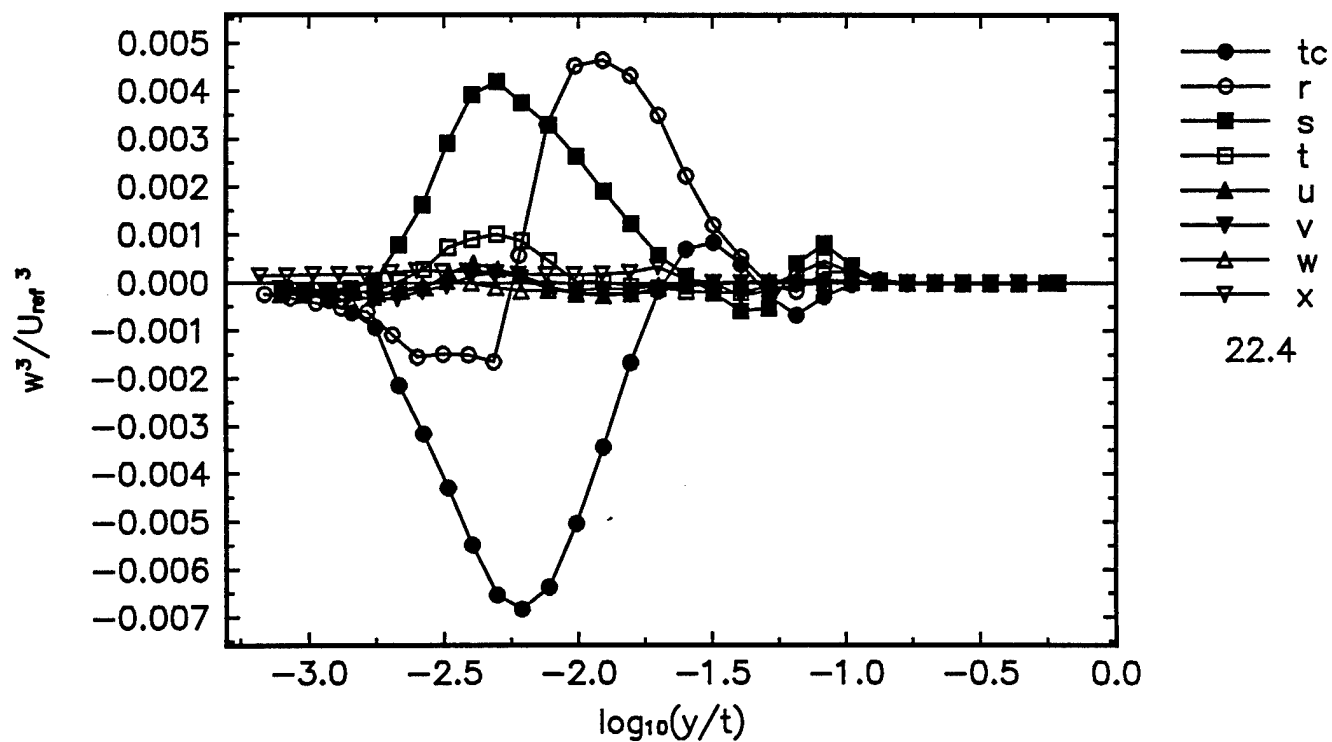
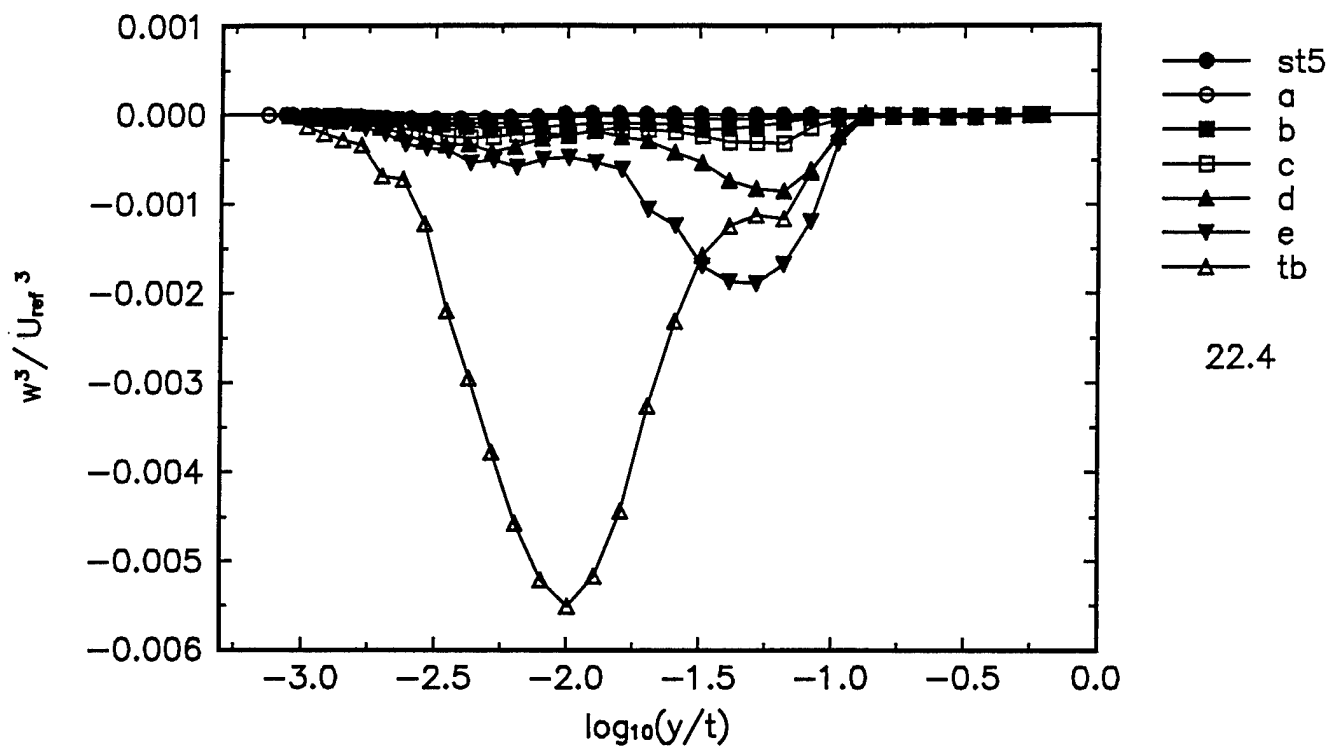


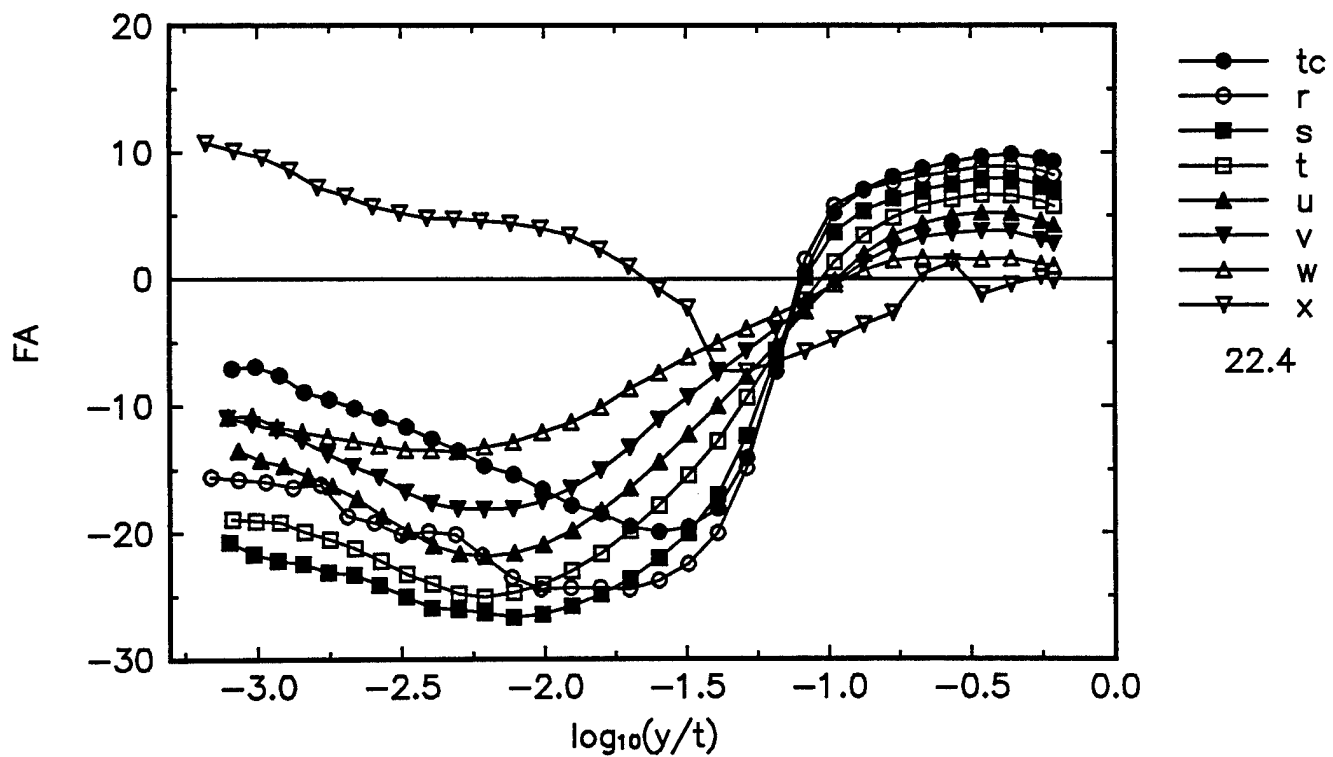
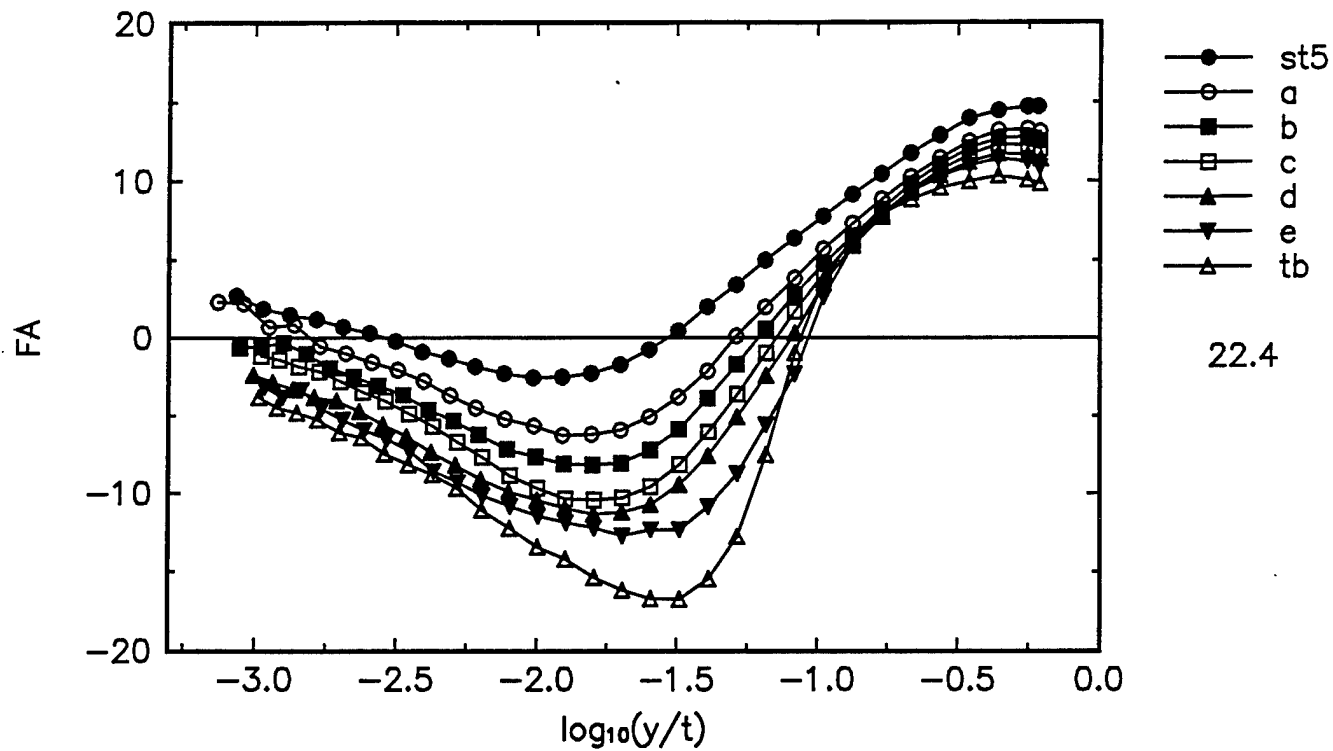


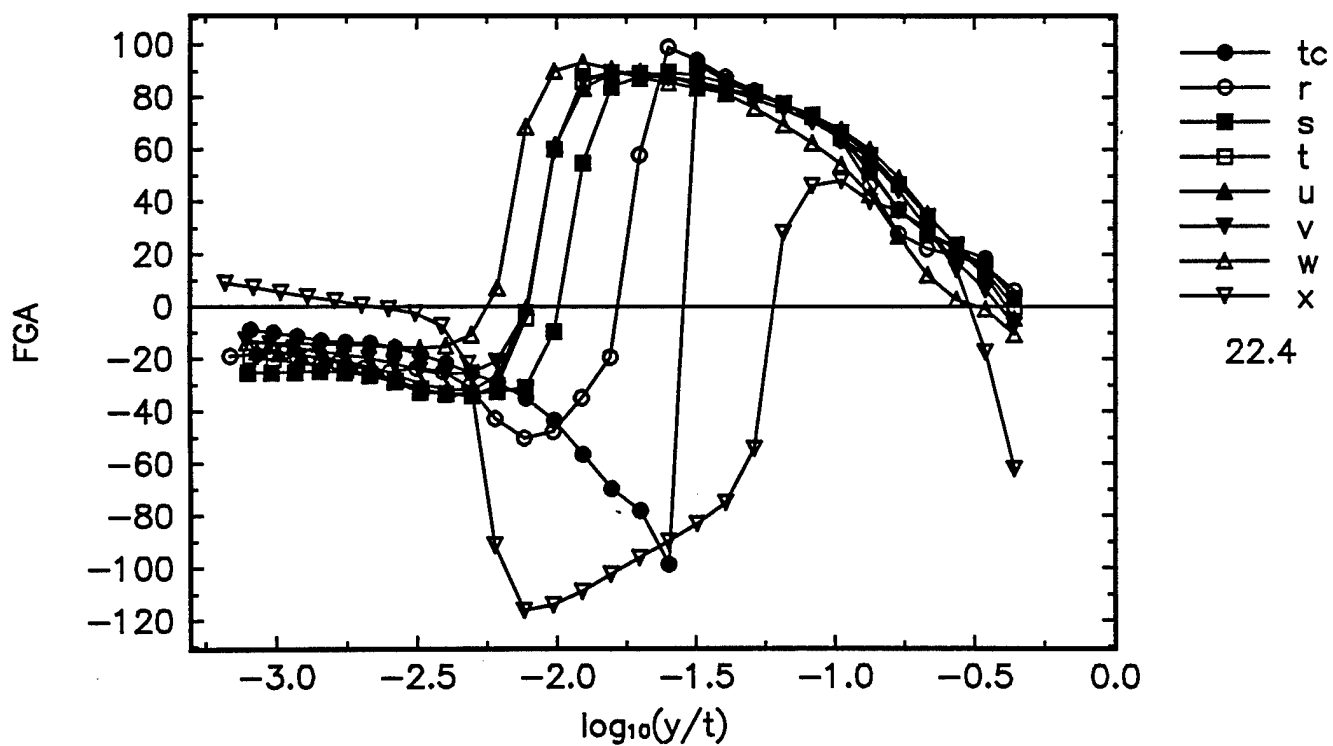
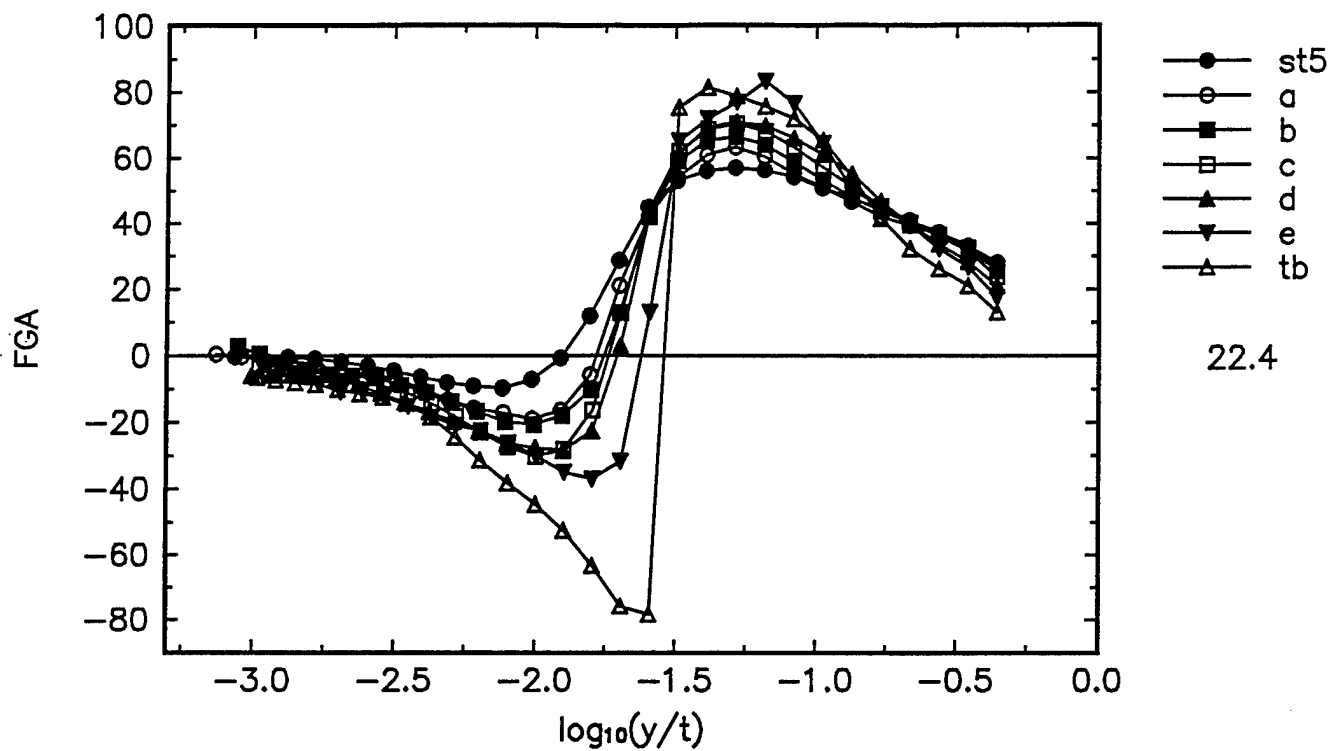


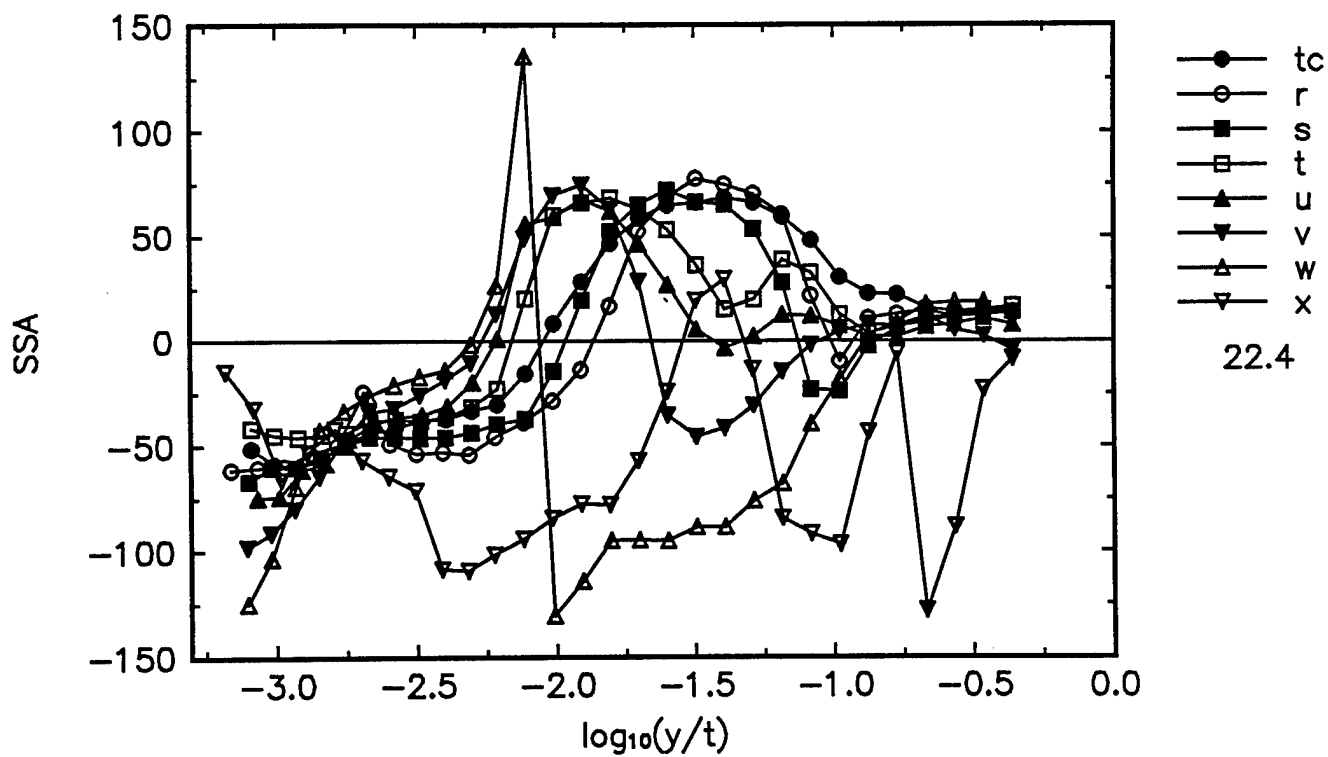
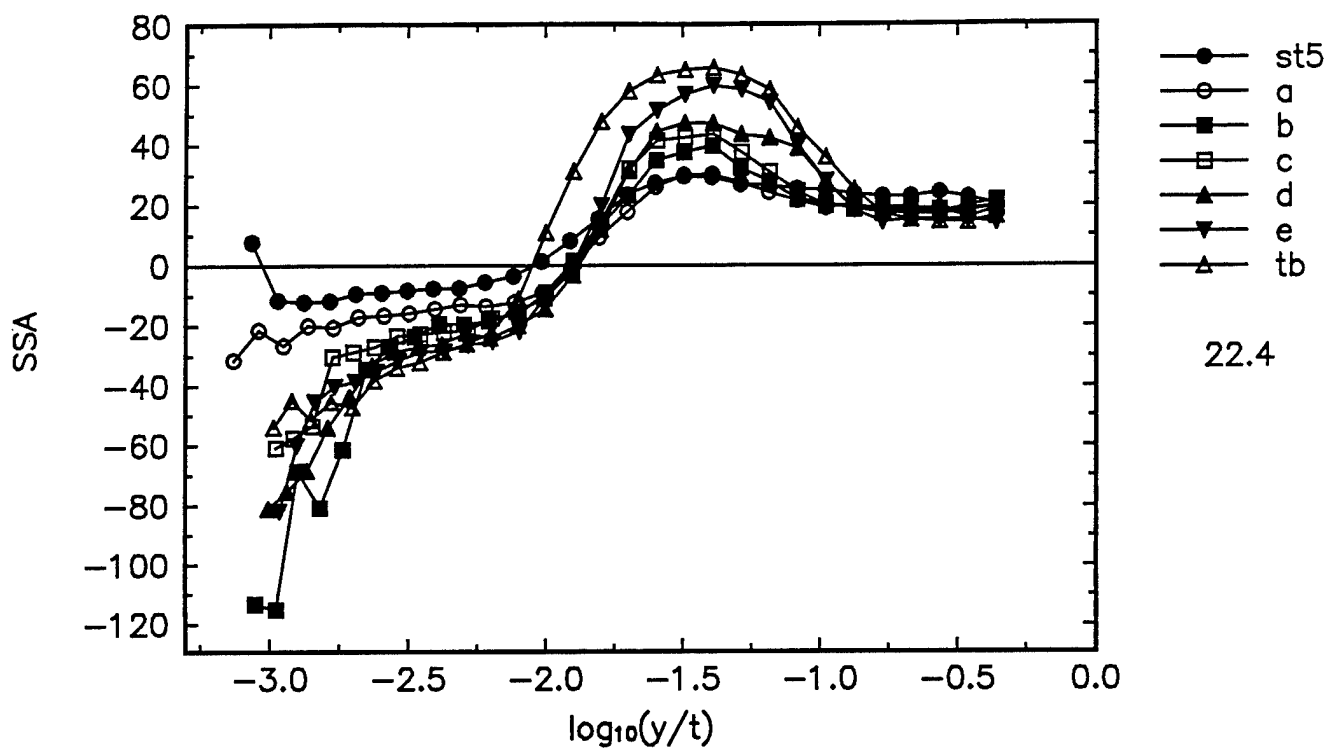


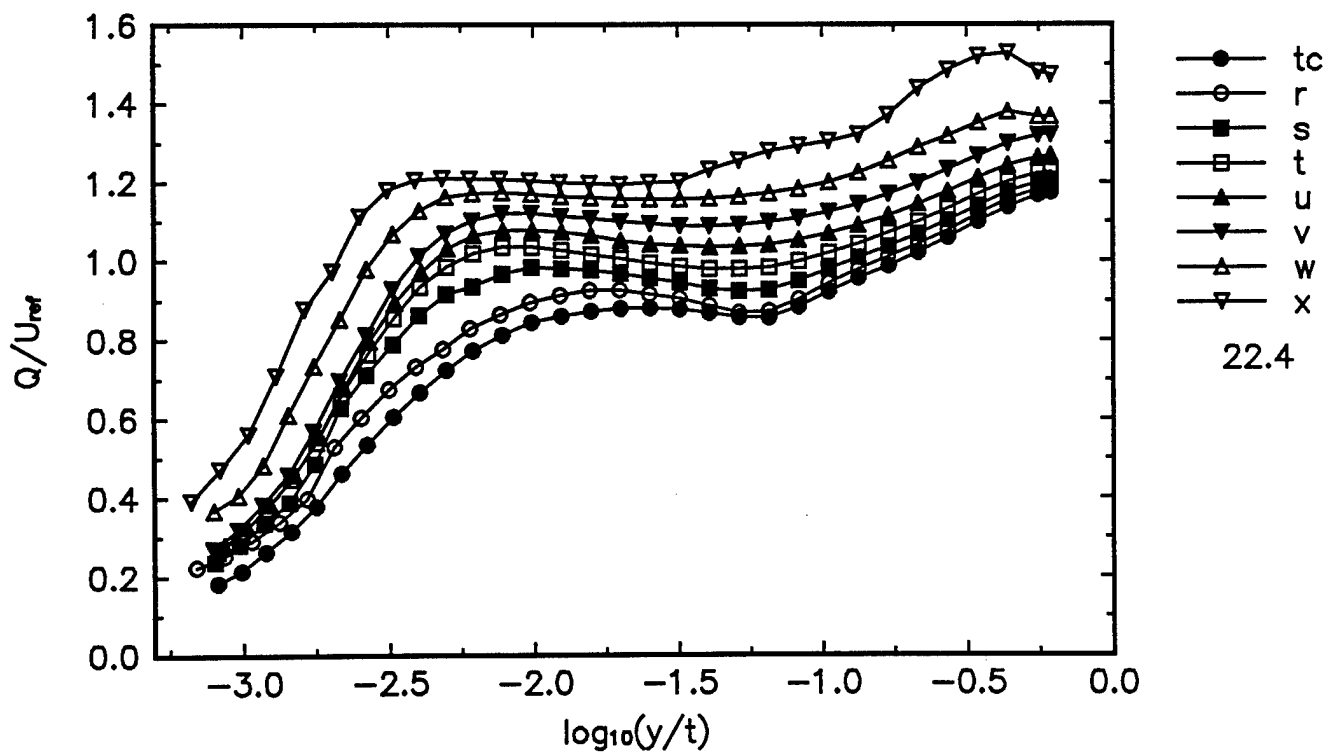
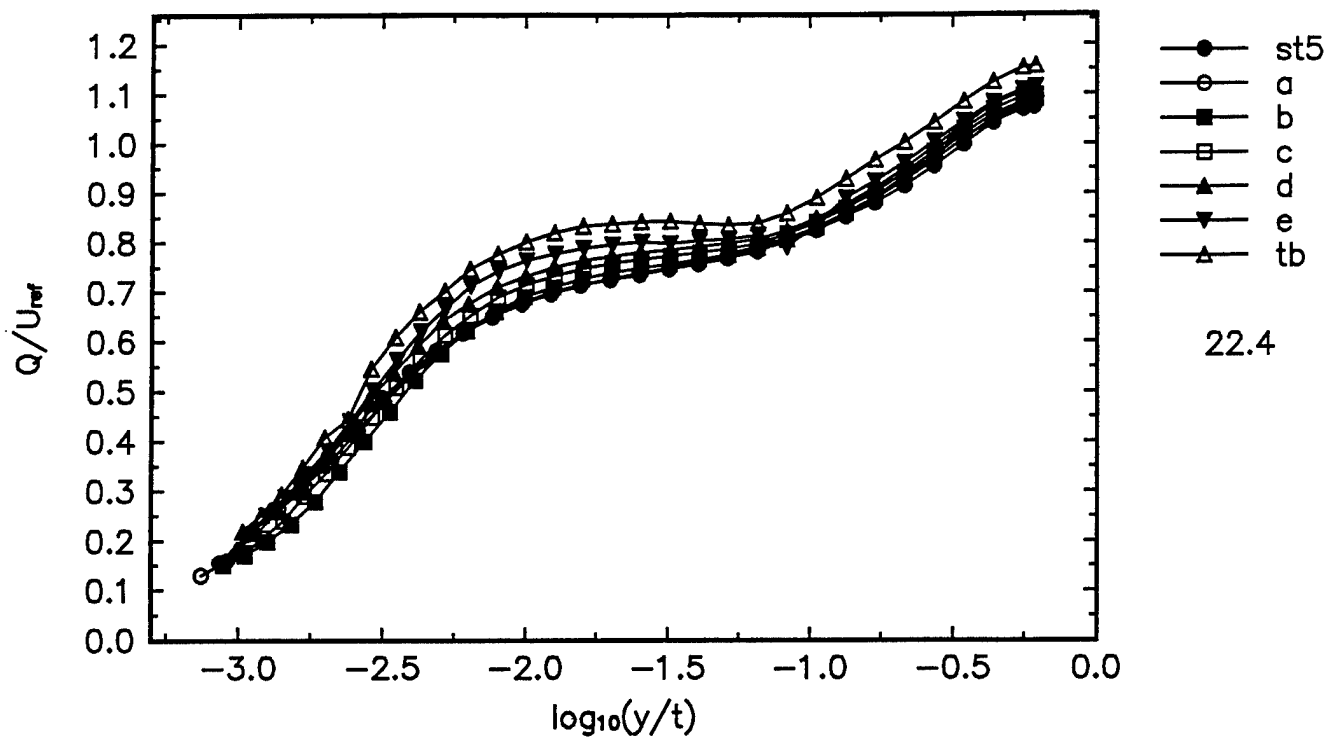


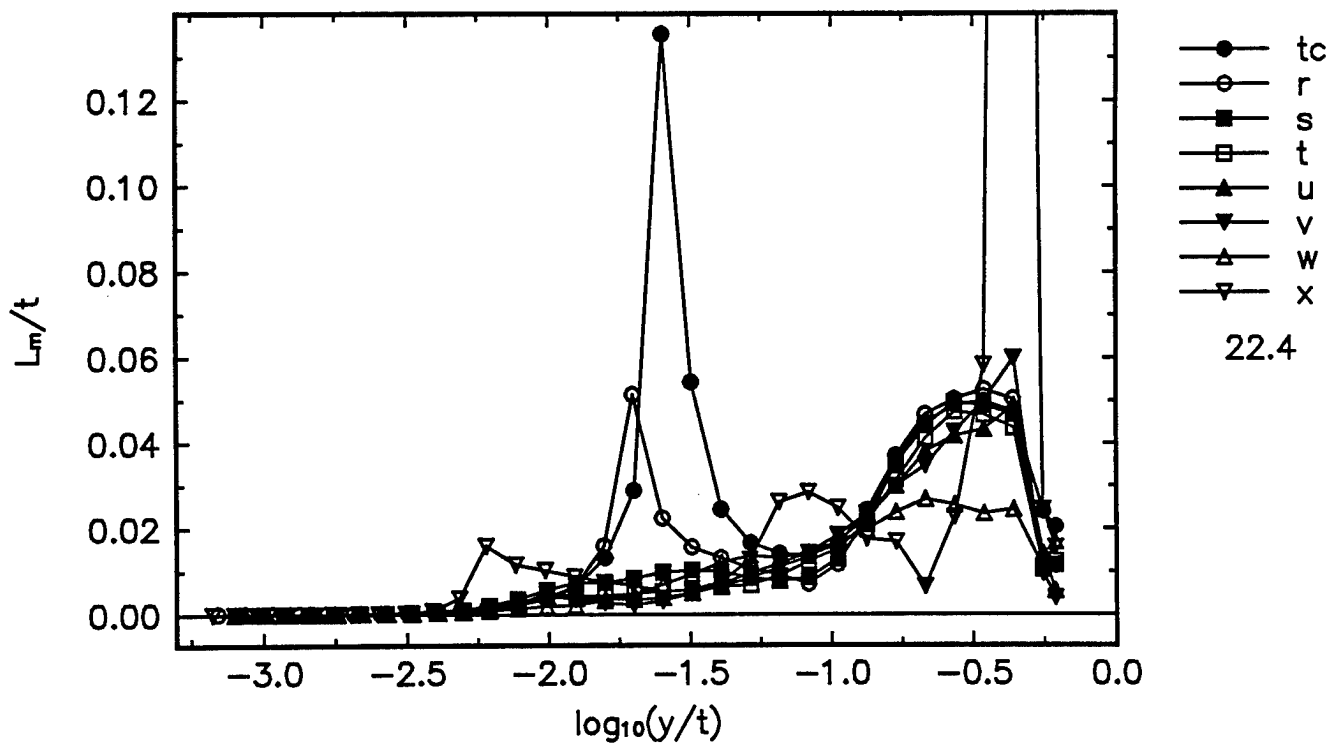
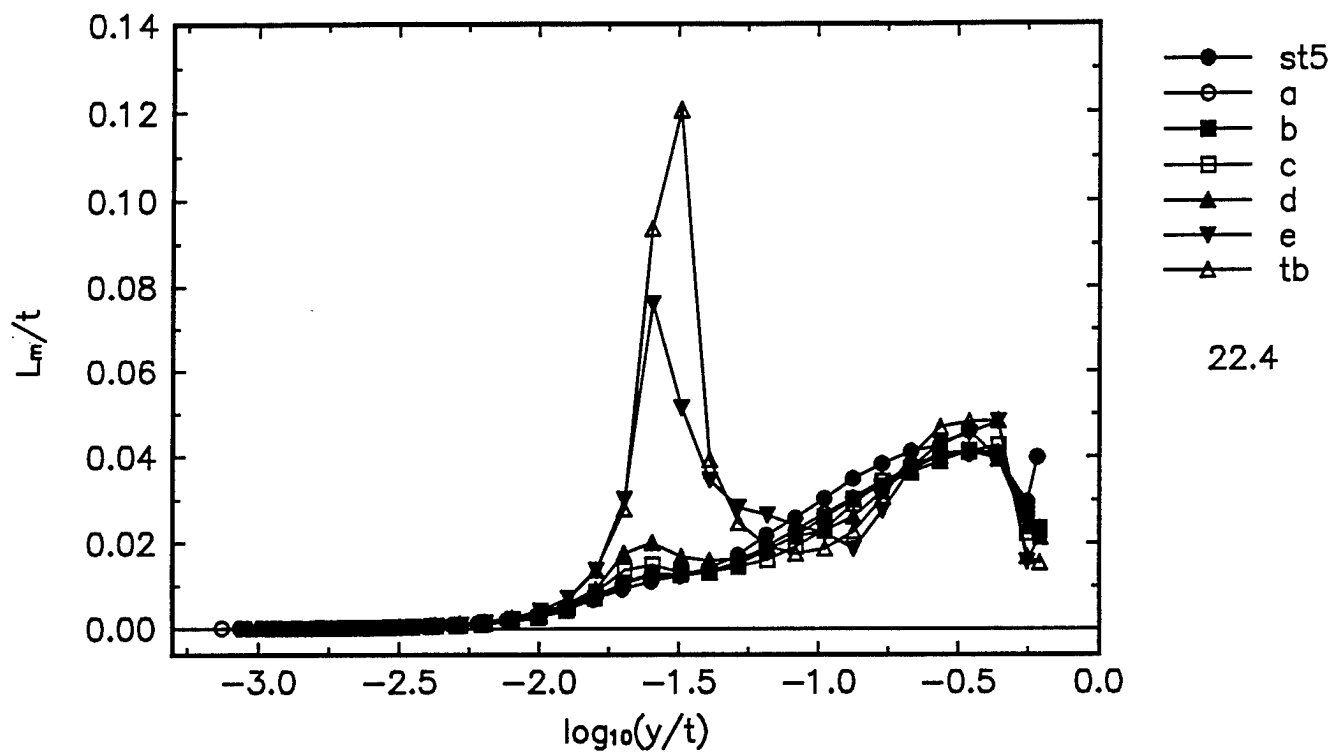


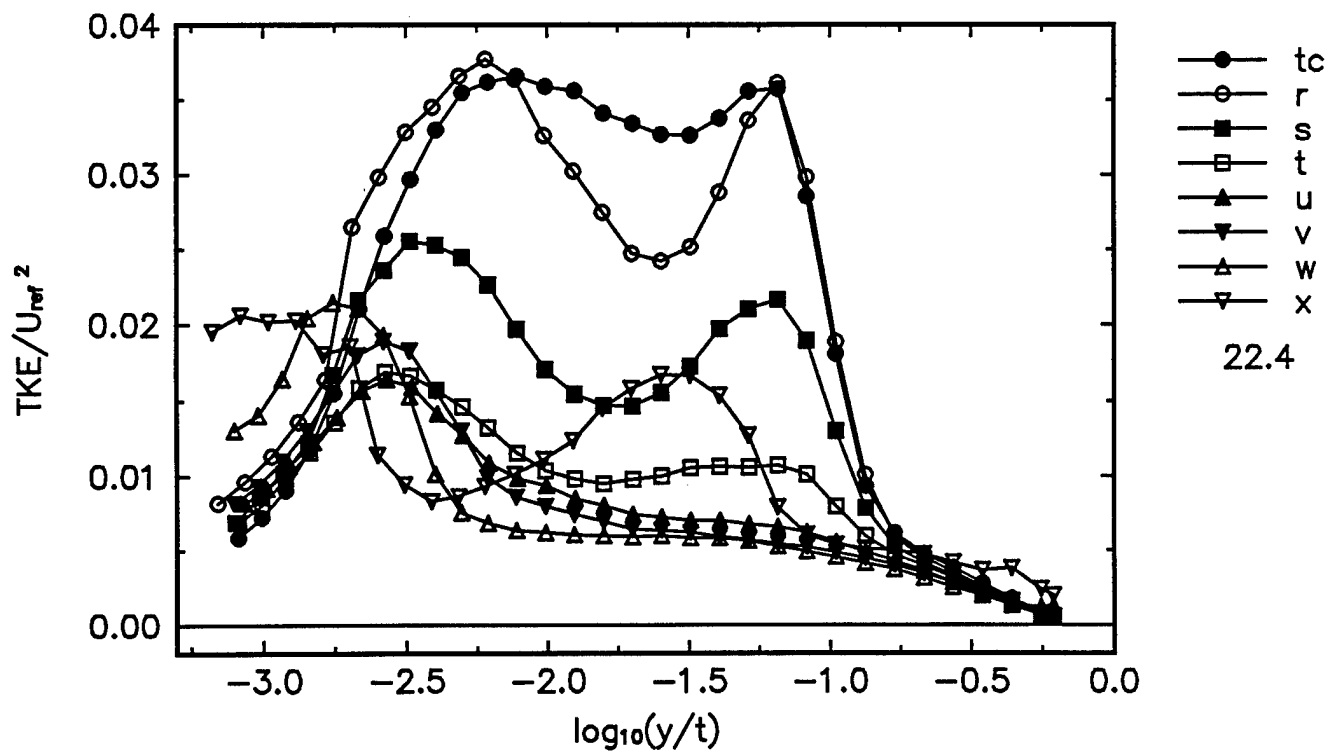
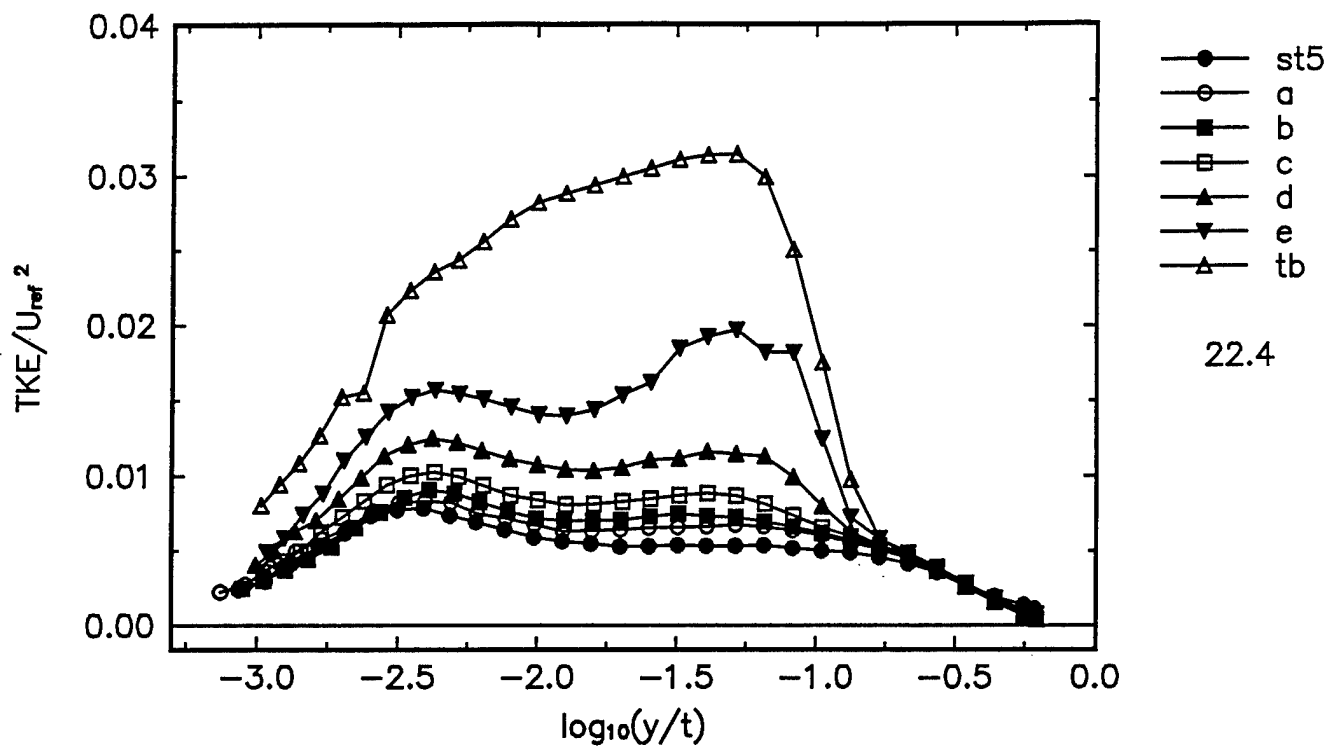


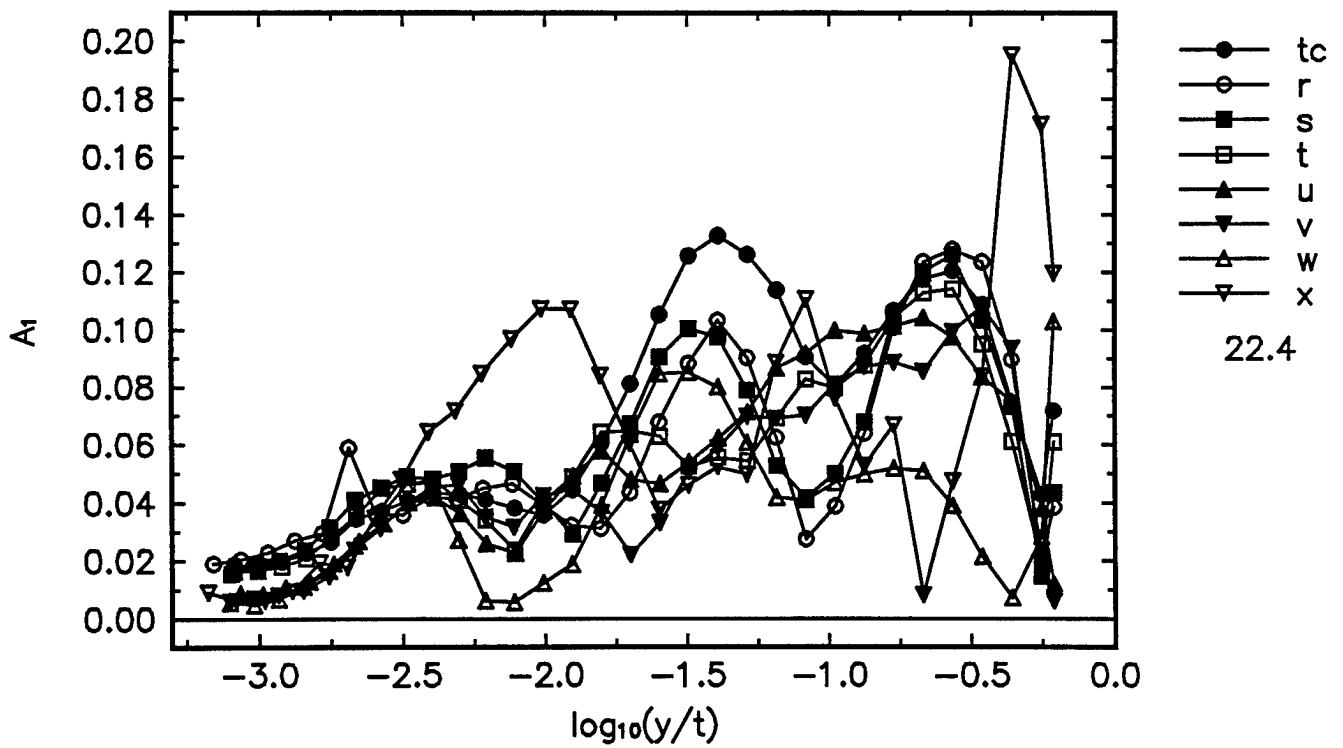
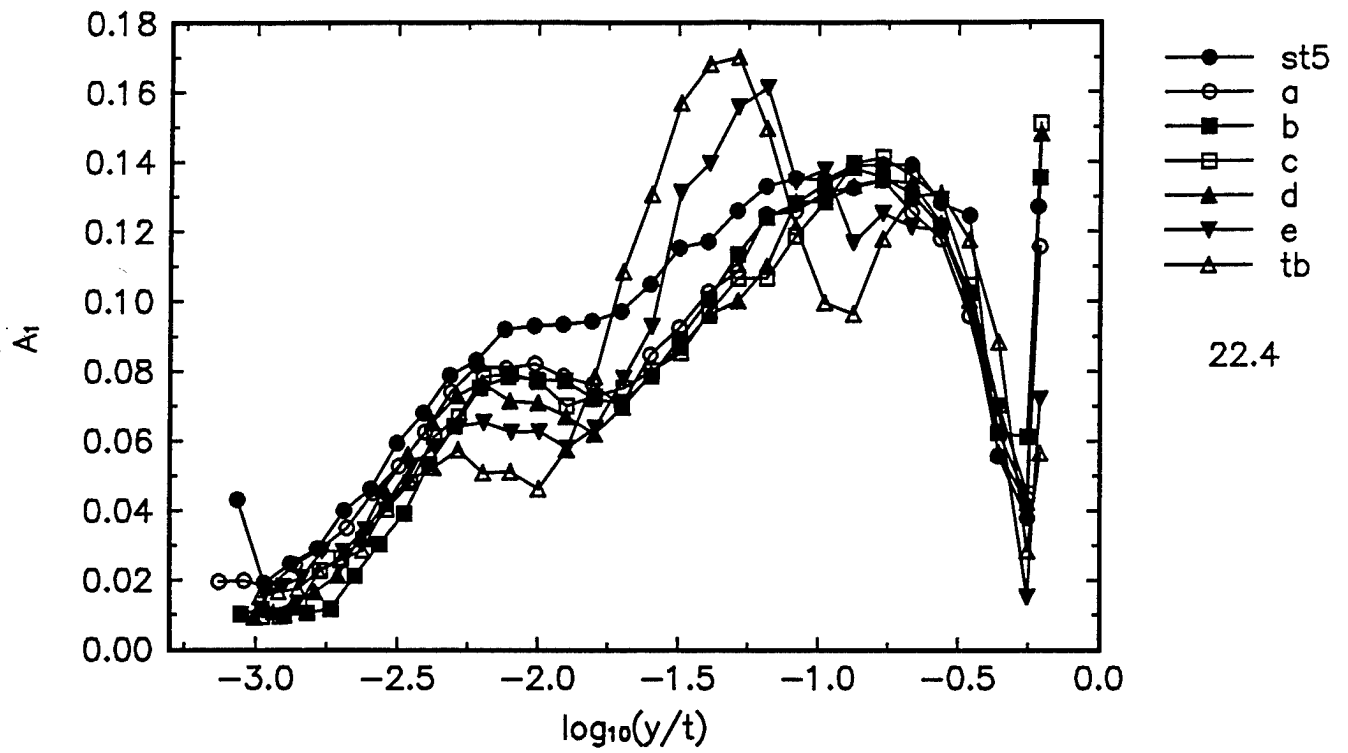


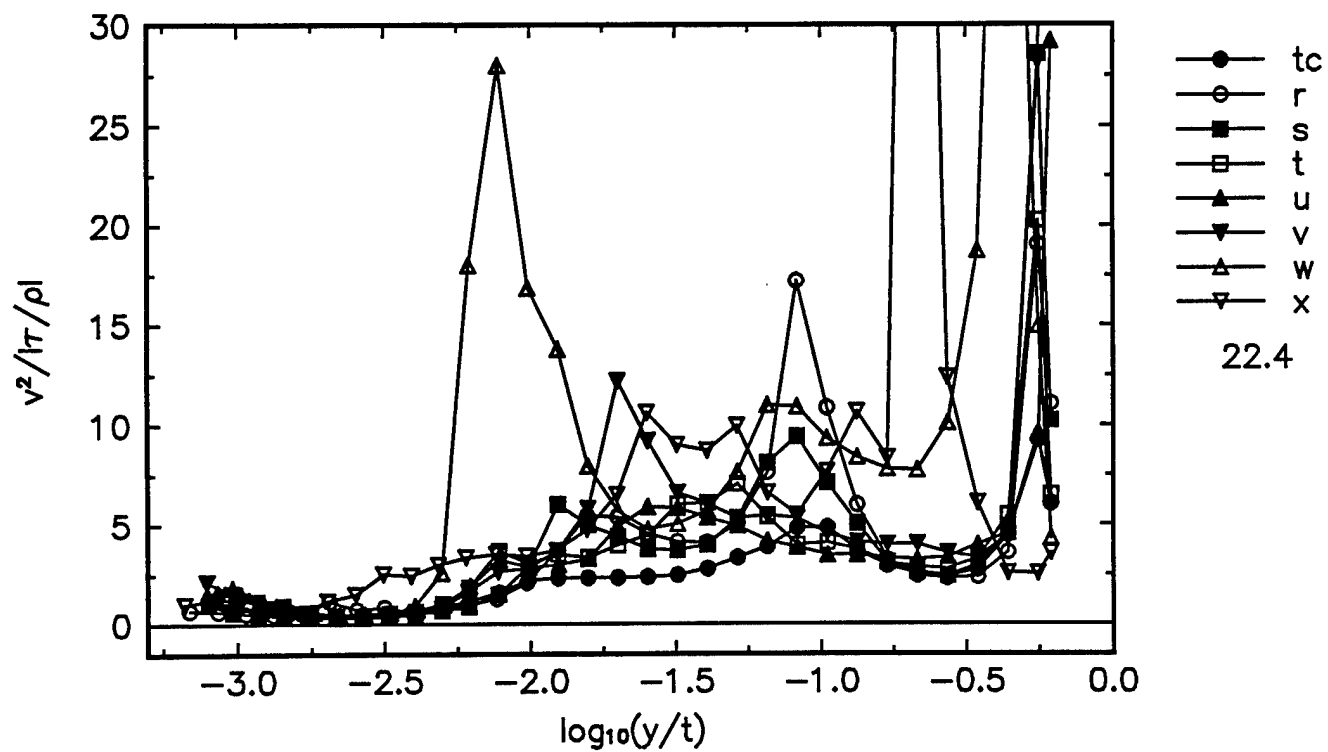
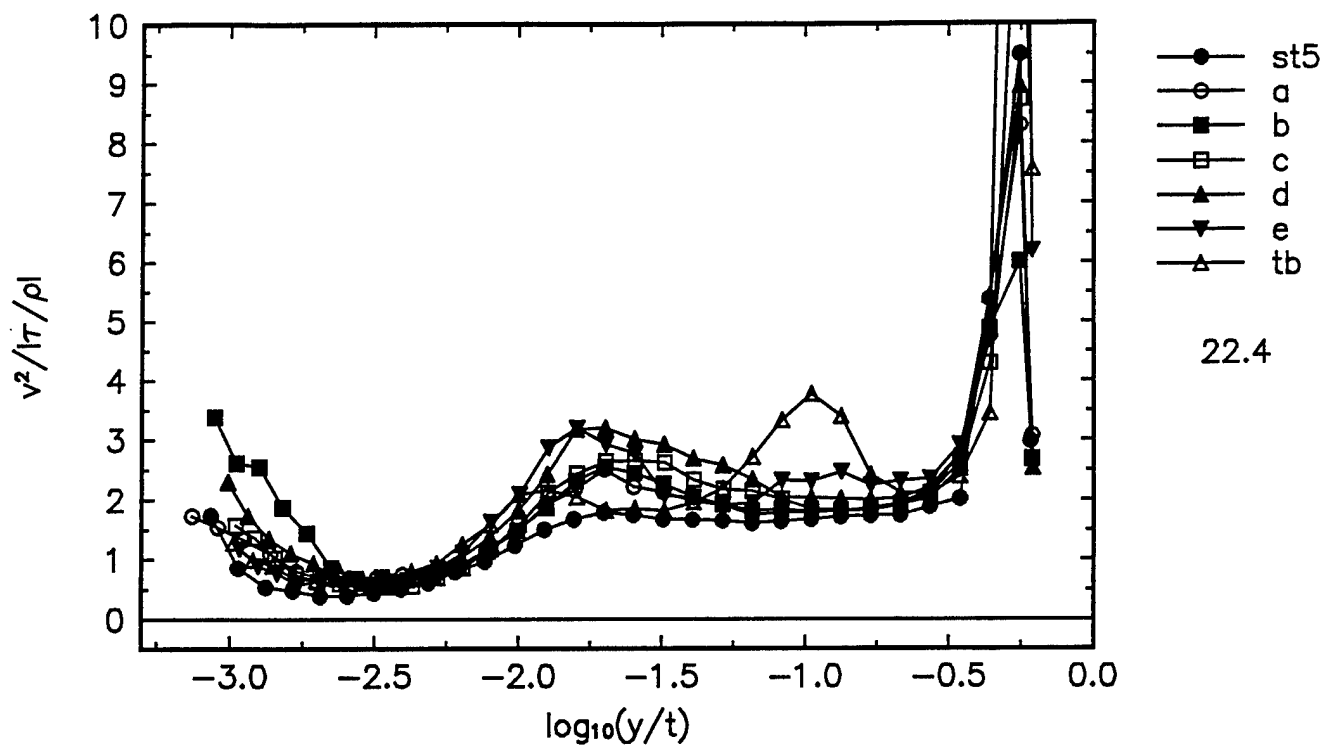


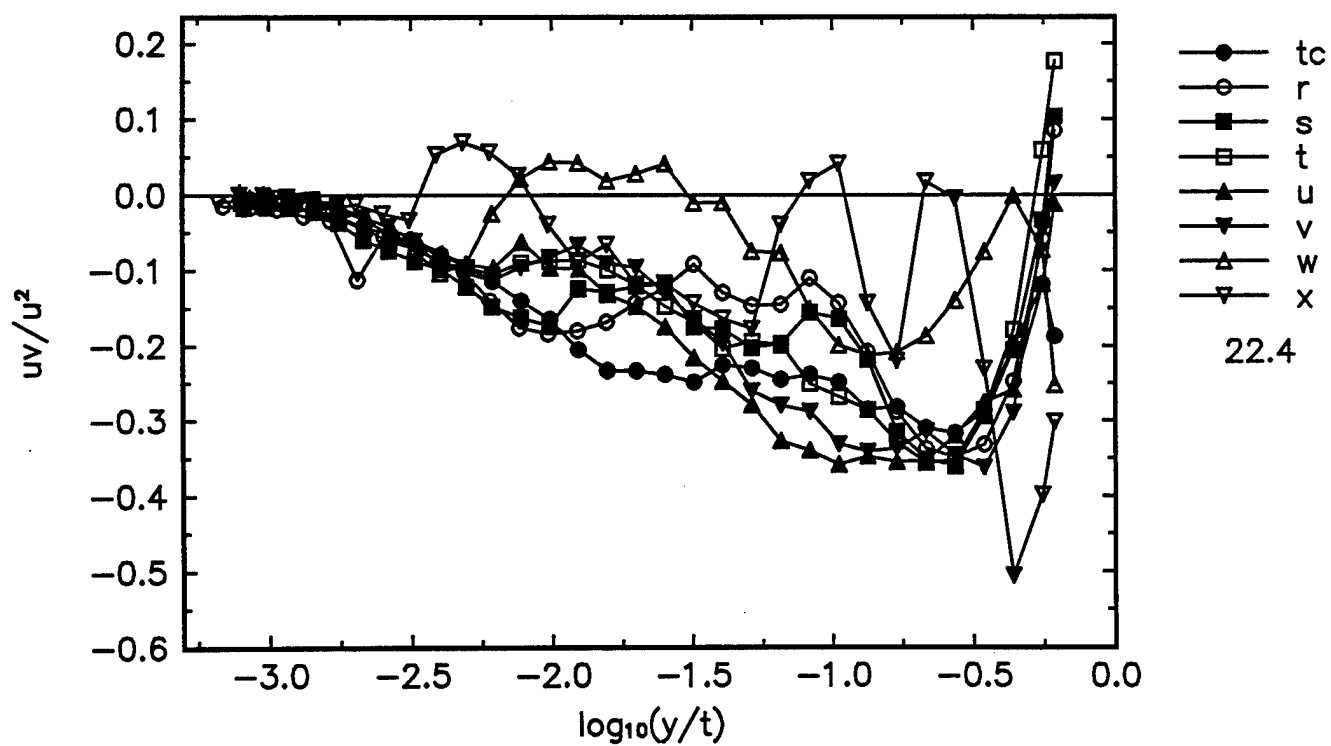
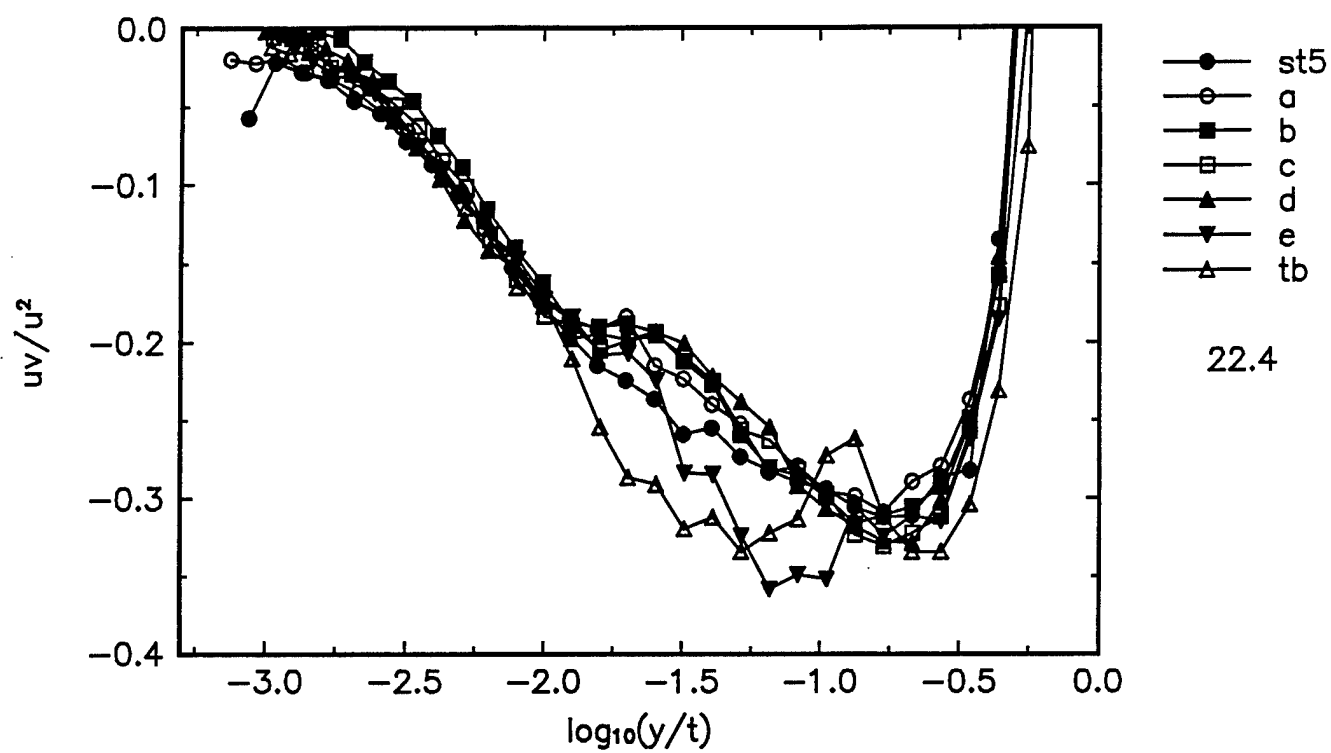


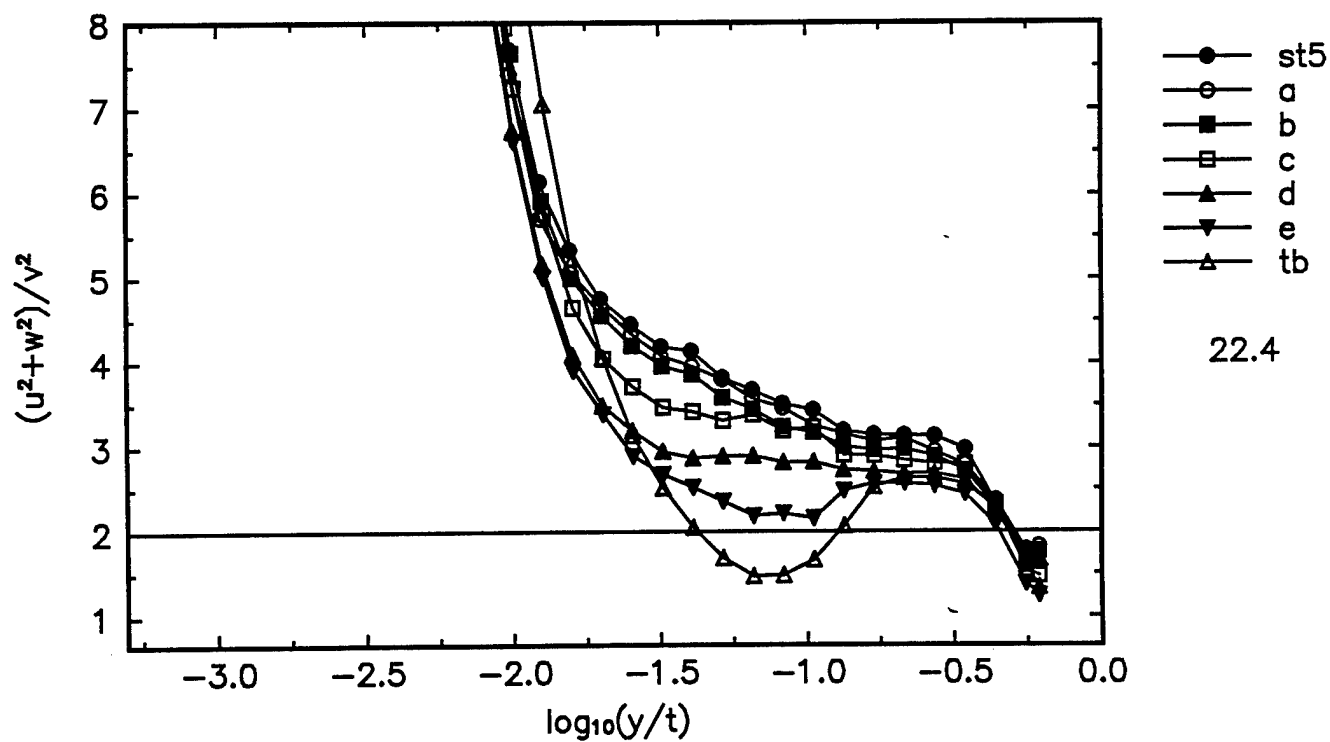
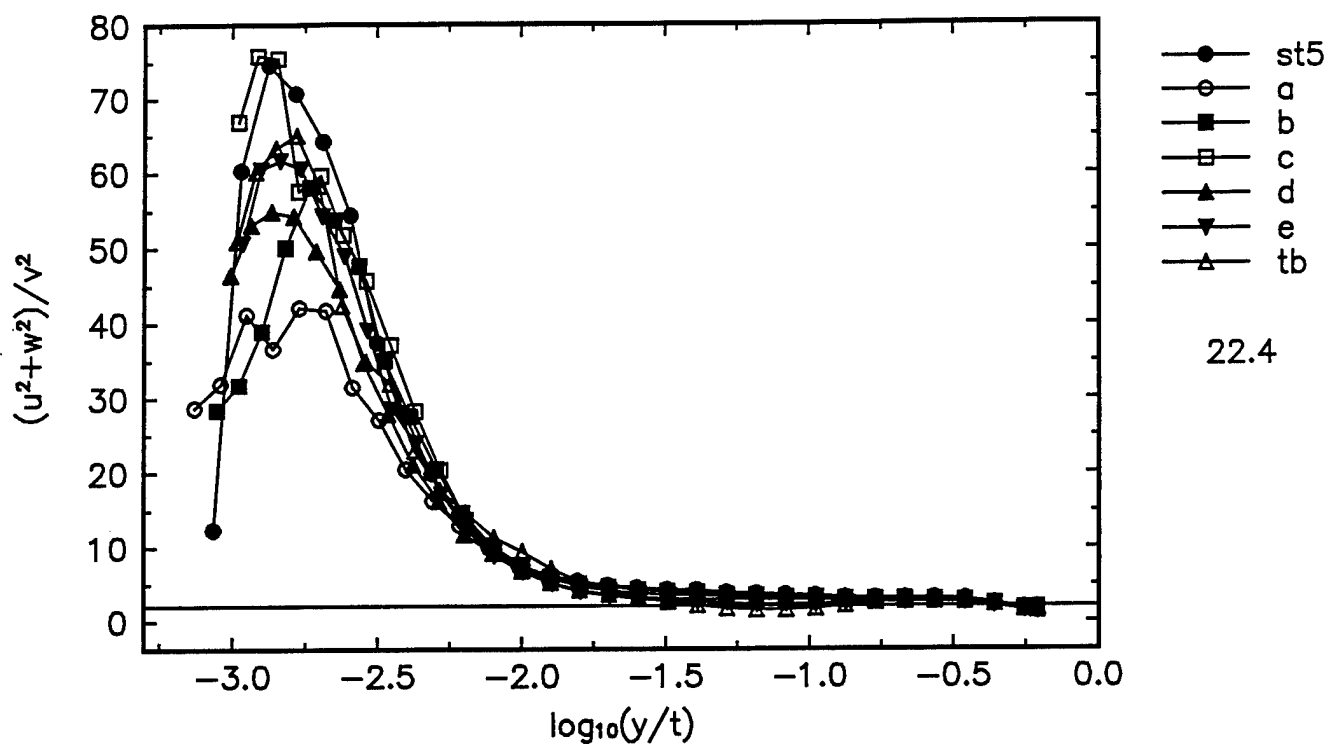


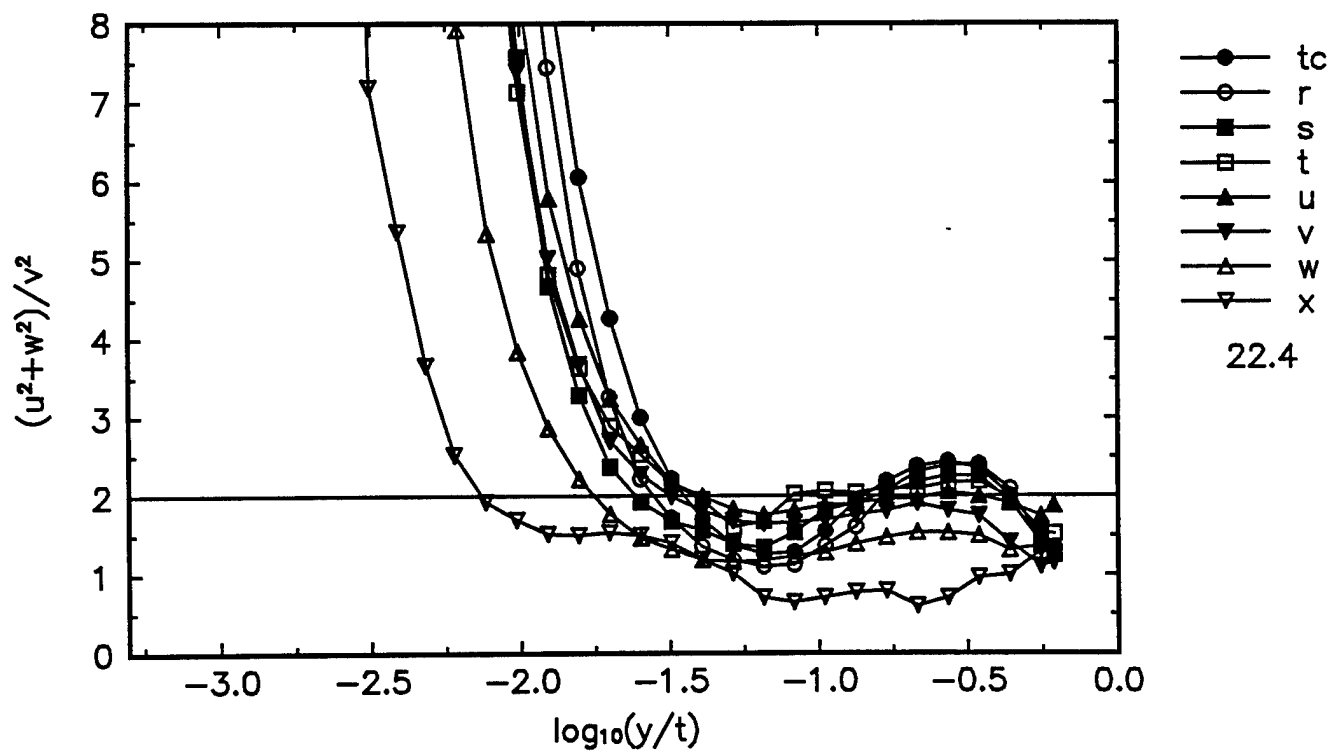
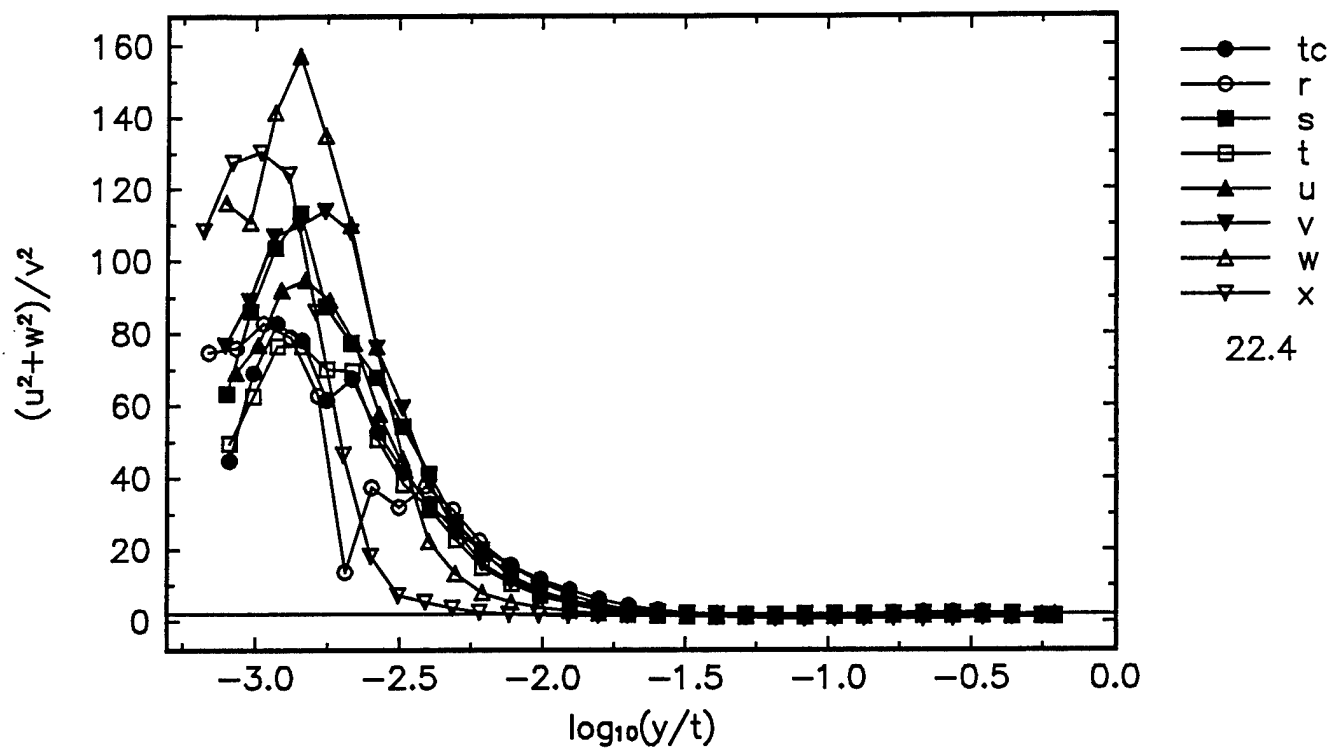


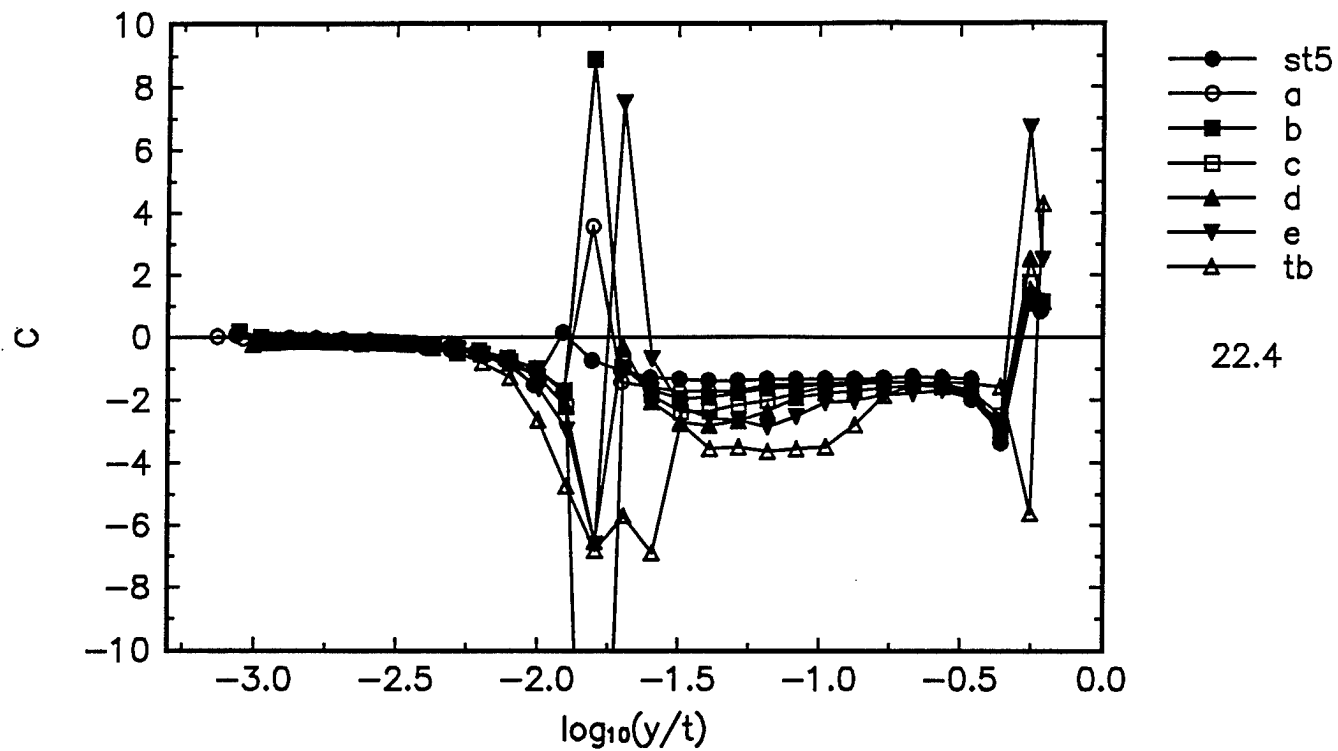




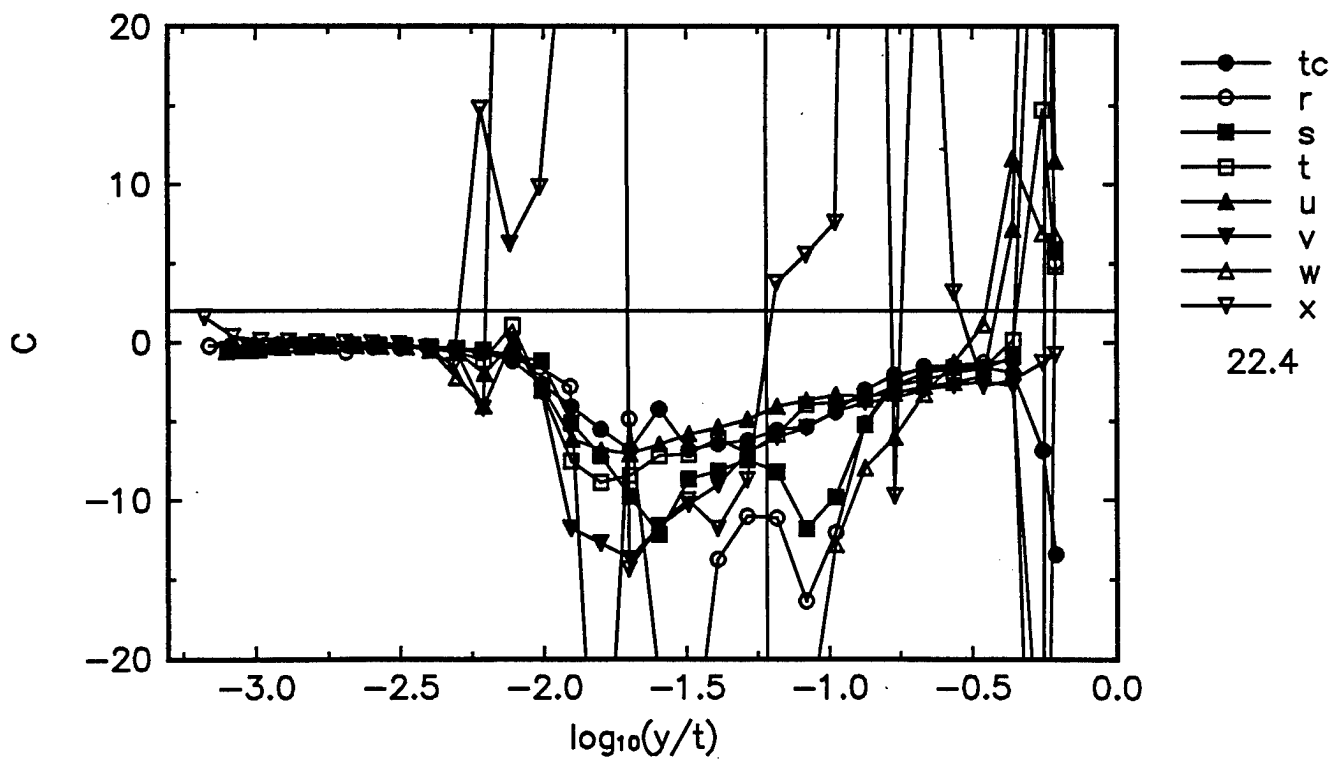


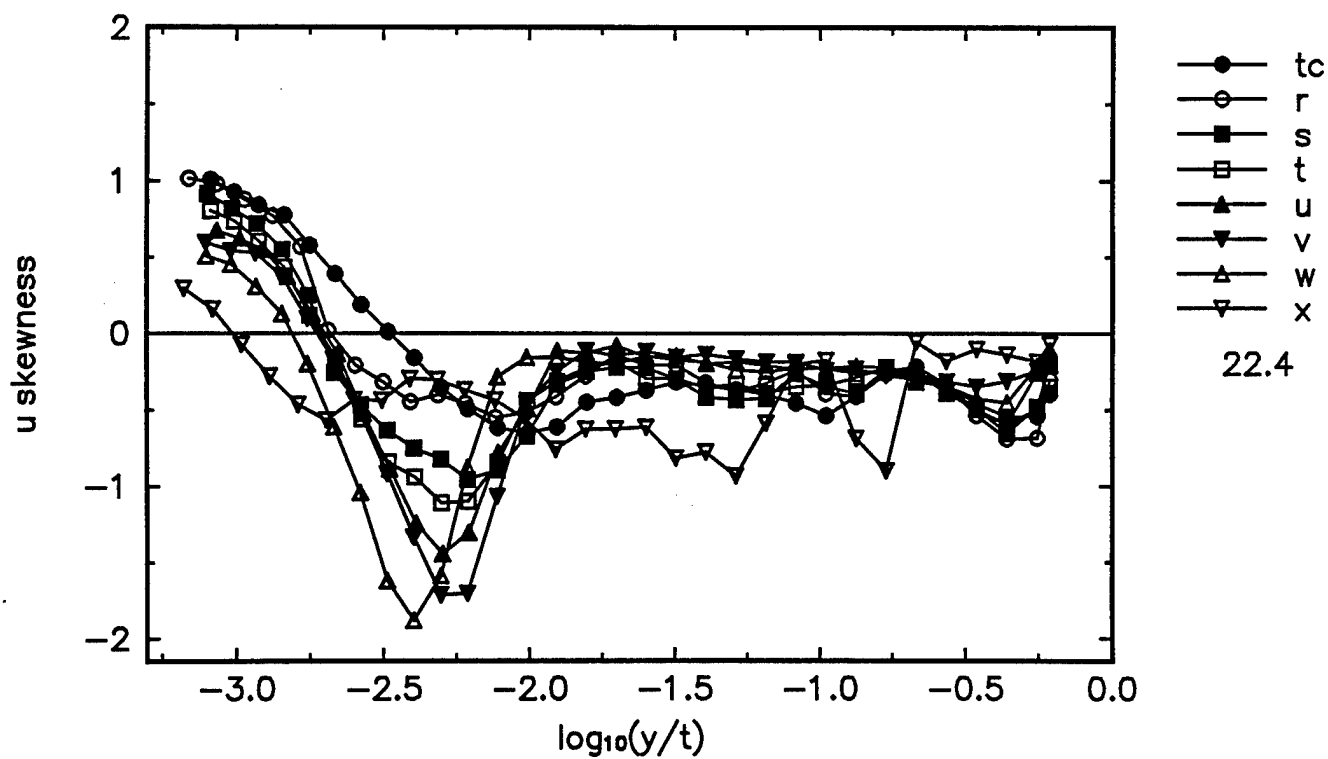
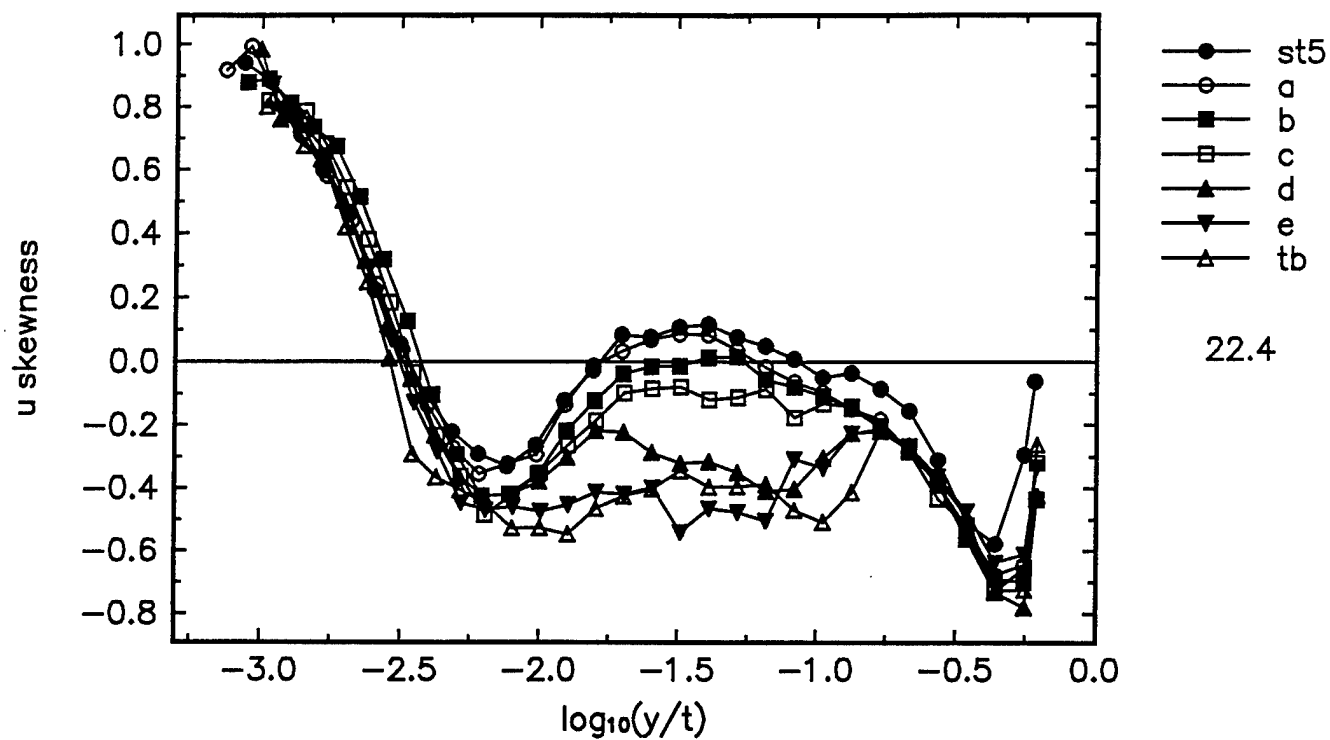


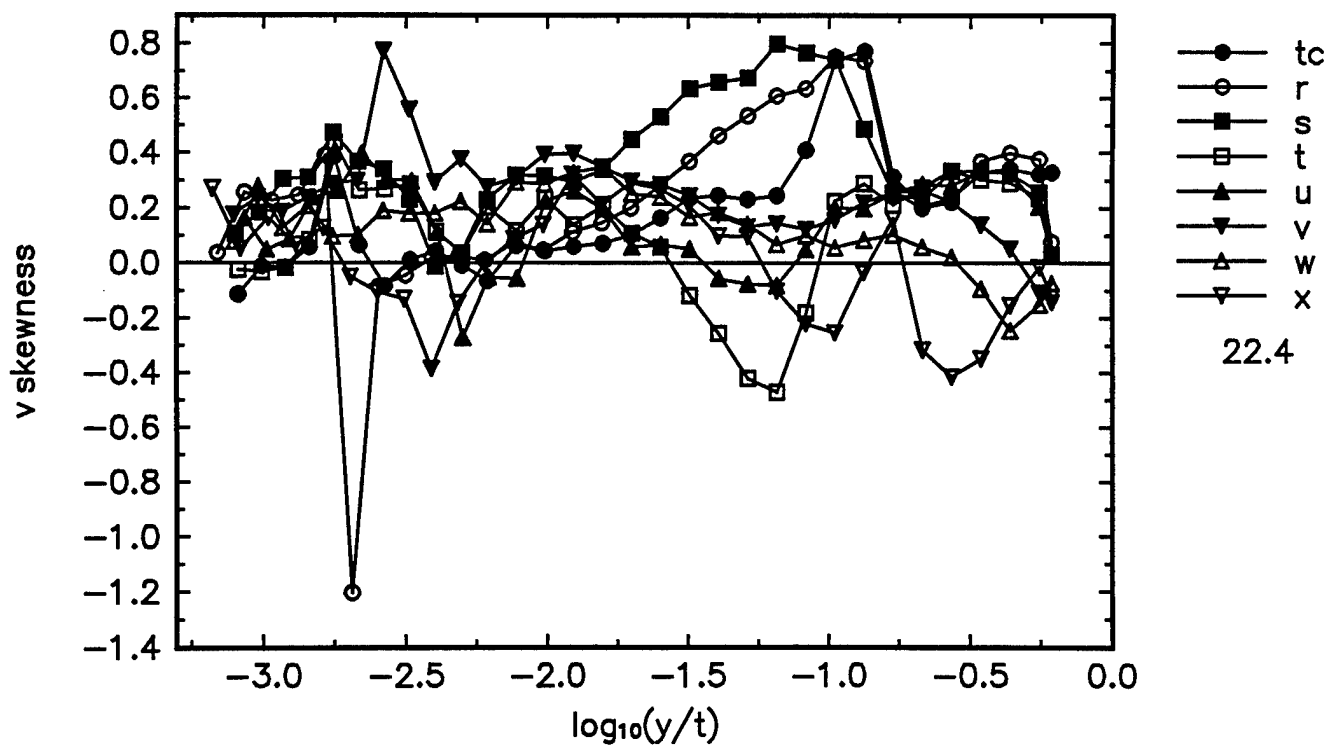
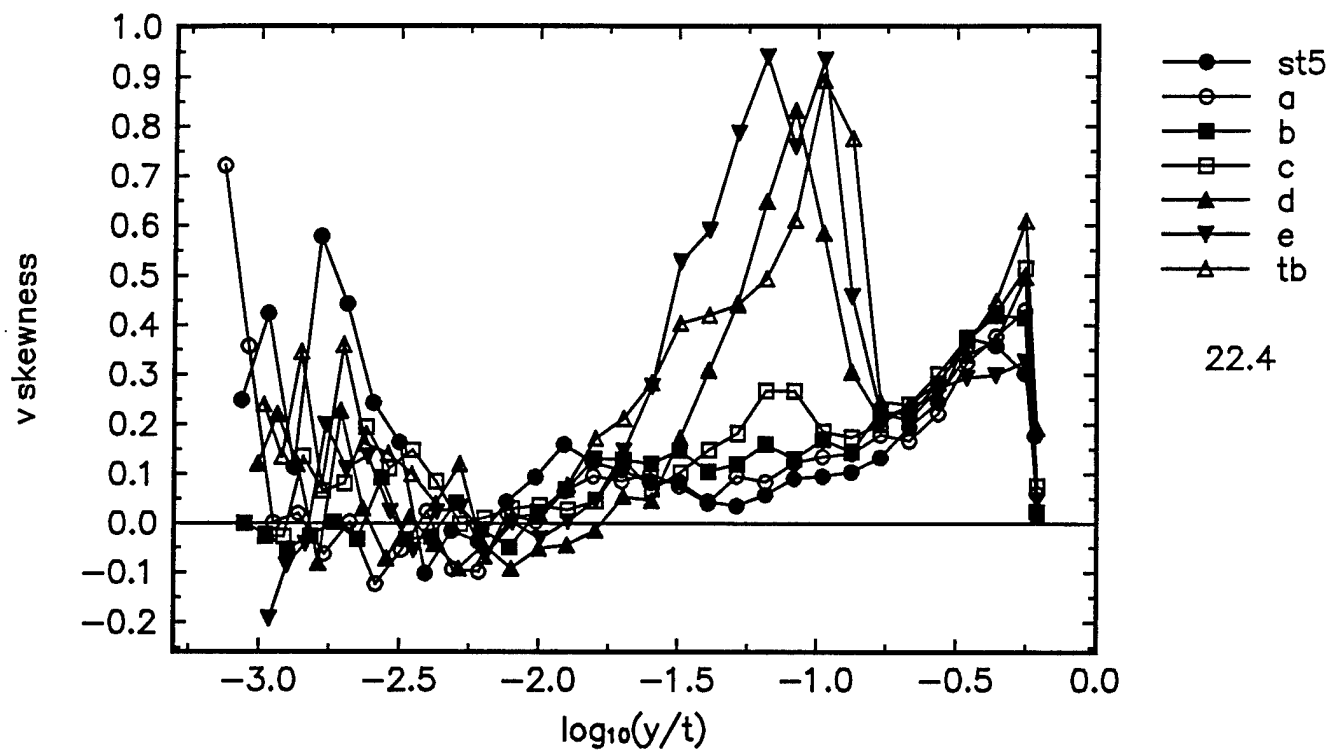


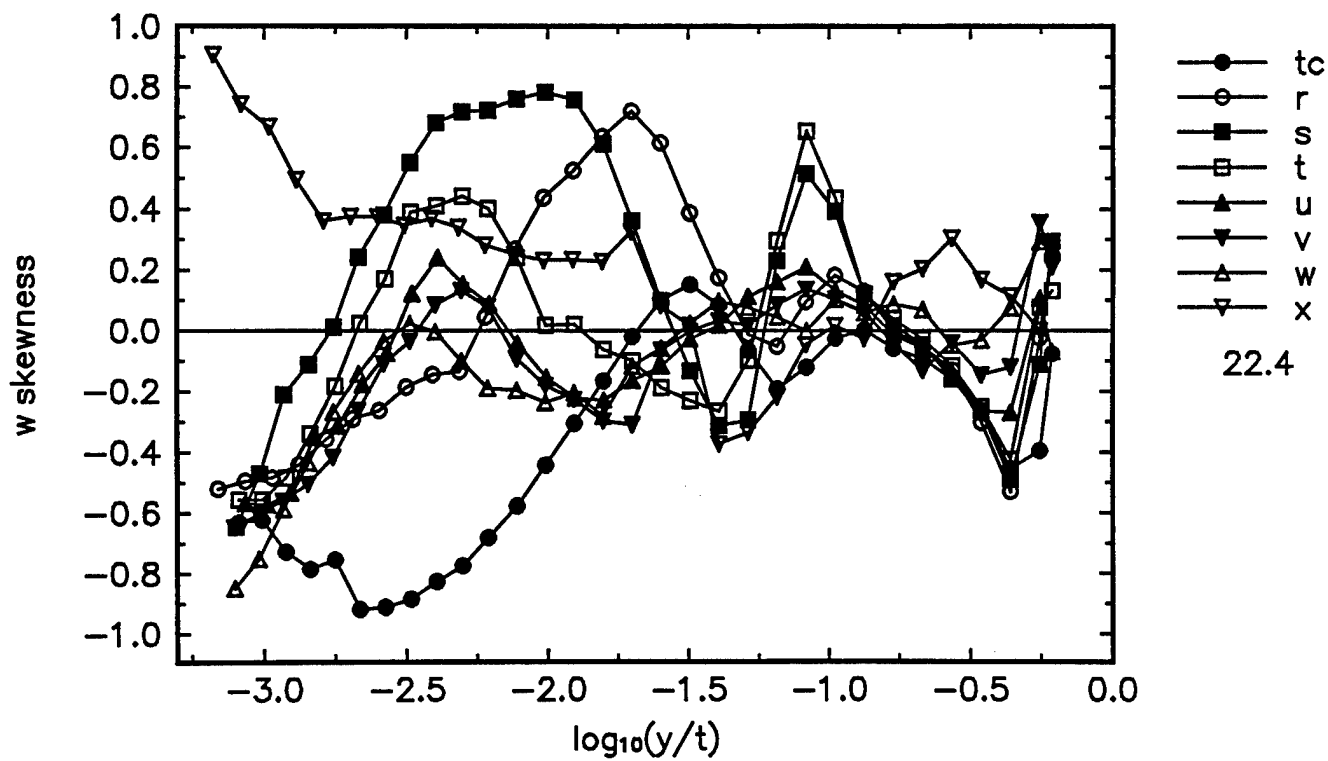
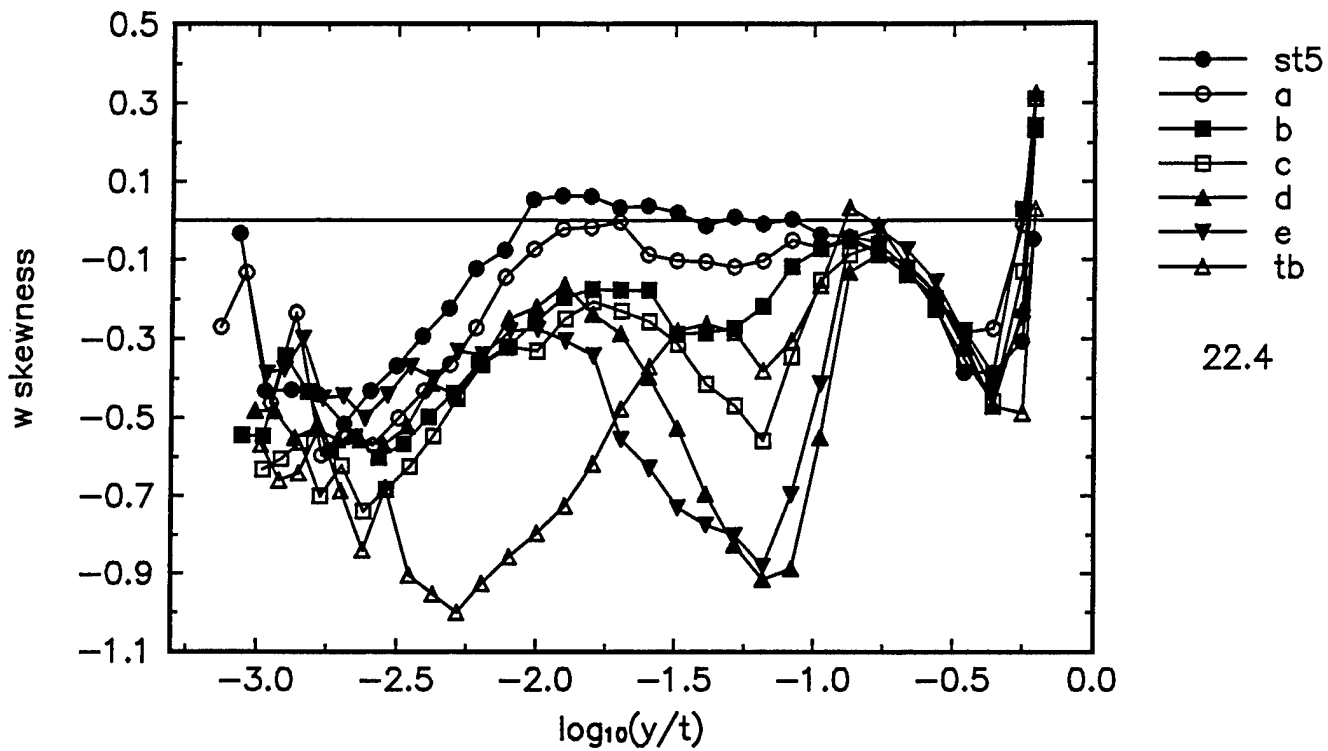


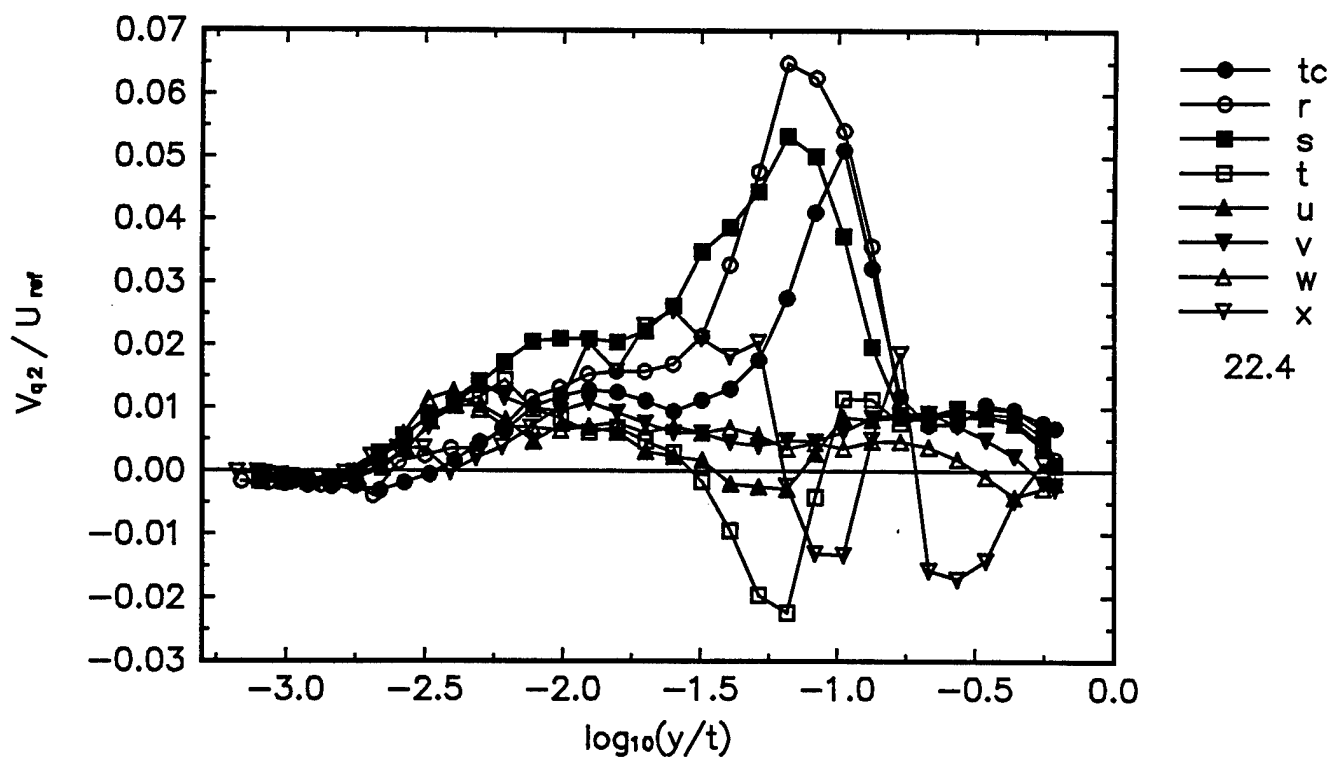
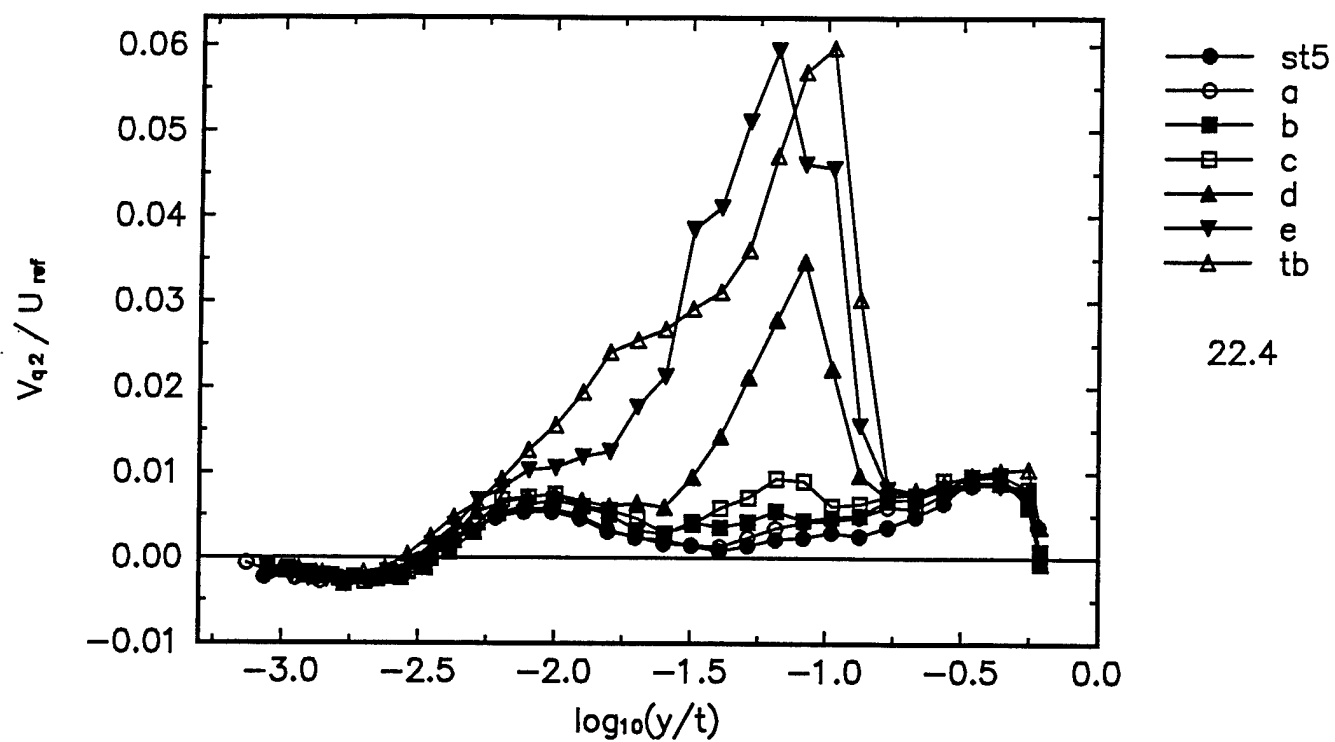
The ordinate of the second figure is also C . $C = \frac{\overline{v^2} \tan(FGA)}{\overline{uv} \tan(FGA) + \overline{vw}}$

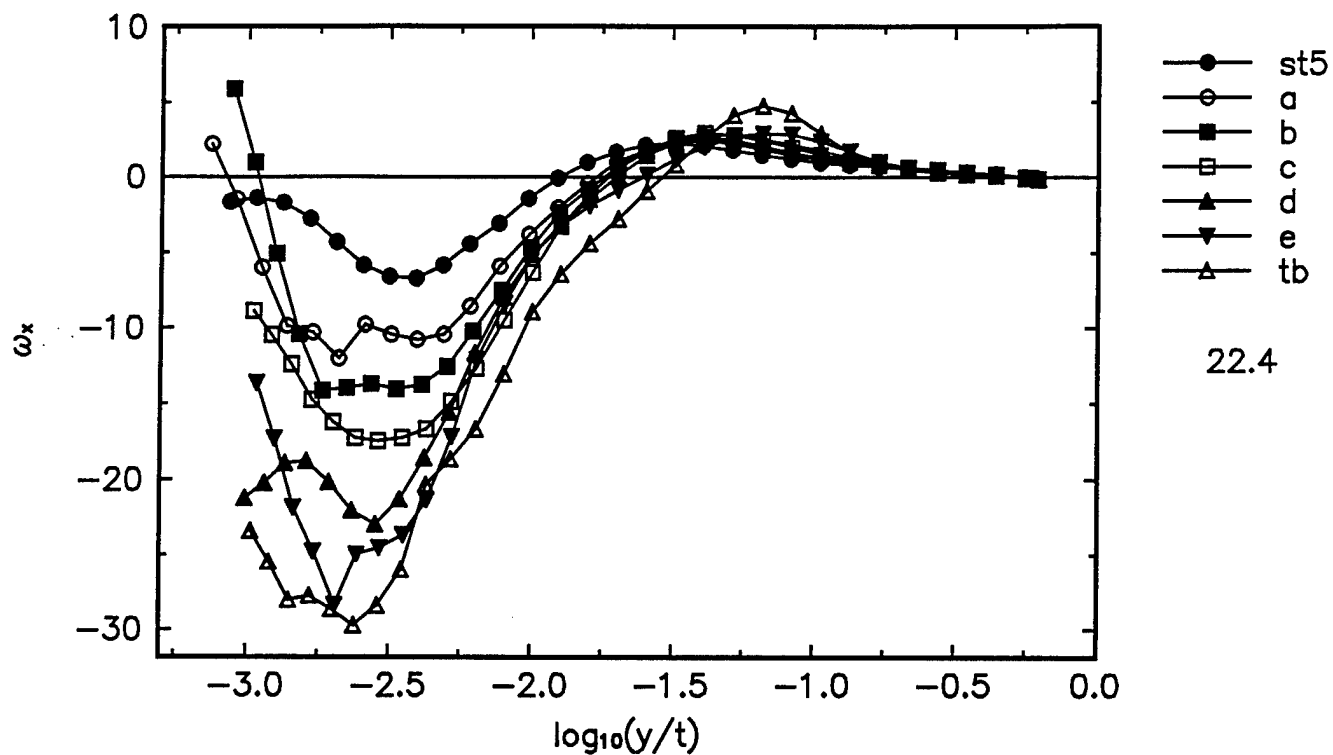












The ordinate of the plot should have been $w_x t / U_{ref}$, where $w_x = \frac{\partial W}{\partial y}$.

